Elucidating the Roles of Wnt-Secretion and β-Catenin's Interaction Partners in Development and Disease

---

Dissertation

zur

Erlangung der naturwissenschaftlichen Doktorwürde
(Dr. sc. nat.)

vorgelegt der

Mathematisch-naturwissenschaftlichen Fakultät

der

Universität Zürich

von

Dario Zimmerli

von

Oftringen, Aargau

Promotionskommission

Prof. Dr. Konrad Basler (Vorsitz und Leitung der Dissertation)

Prof. Dr. Maries van den Broek

Prof. Dr. Sabine Werner

Zürich, 2018

Summary

The discovery of the connection between Wnt/β-catenin signaling, APC and colon cancer two decades ago created fertile ground for research in the field of Wnt/β-catenin signaling. The hope was that by elucidating all the elements of the cascade, one might discover inhibitors of this pathway that help treating cancer patients. This work has revealed a picture of Wnt/β-catenin signaling's pivotal involvement in virtually every developmental process as well as in adult tissue homeostasis; moreover, Wnt-signaling is involved in many forms of cancer. Unfortunately, one aspect that also became clear over the years was that targeting the pathway is not a simple matter. Apart from the fact, that inhibition of the pathway is associated with severe side effects due to its crucial role in gut homeostasis, it is also a notoriously difficult cascade to target. This difficulty arises mainly because there are no pathway specific kinases known against which an inhibitor could be developed. Another problematic aspect is the dual role the main pathway effector β-catenin has in transducing the Wnt signal as well as maintaining adherens junctions. Nevertheless, the last years have shown several possible ways to tackle these issues. Besides the discovery of Porcupine inhibitors, which hinder palmitoylation of the Wnt ligands, thereby blocking secretion and shutting down the pathway, the idea to block β-catenin's interaction with transcriptional co-factors has gained some merit. In this work, we set out to test the advantages and draw-backs of Porcupine inhibitors. Furthermore, we wanted to clarify the tissue specific roles of β-catenin's transcriptional co-factors with regards to their ability to transduce the signal. This information will be crucial to judge the feasibility of using an inhibitor in a specific setting.

Here we show that Porcupine is overexpressed in a murine cutaneous squamous cell carcinoma model (cSCC) model, as well as in human cSCCs. This gave us the incentive to test Porcupine inhibitors in this cSCC model, where we found that this hinders tumor development and reduces the cancer stem cell compartment of established tumors. This leads to increased differentiation and a reduction of markers for tumor invasiveness.

In an effort to further characterize the specific roles of β-catenin's transcriptional co-factors, we used mouse models with specific domain deletions inhibiting the binding of β-catenin to the N-terminal co-factors (Bcl9 and Pygopus) and the co-factors to each other. We found that the integrity of these interactions is specifically needed in the development of the embryonic heart and limbs. Loss of Bcl9-Pygo-β-catenin binding in mouse embryos phenocopies human congenital heart disorders by disrupting a molecular cascade necessary for the correct specification of the heart outflow tract and valves. We thus uncovered a novel role for Wnt/β-catenin signaling in heart development and possibly human congenital heart disorders.

Zusammenfassung

Die Erkenntnis in den Neunzigerjahren, dass zwischen der Wnt/β-catenin Signalkaskade, APC und Darmkrebs ein Zusammenhang besteht, liess die Forschung im Wnt/β-catenin Gebiet aufleben. Das Ziel dieser Forschungstätigkeit war, durch besseres Verständnis aller Elemente der Signalkaskade neue Inhibitoren zu entdecken, um Darmkrebs zu heilen. Die Studien damals haben gezeigt, dass die Wnt/β-catenin Signalkaskade in praktisch allen entwicklungsbiologischen Schritten als auch in der Gewebehomöostase eine Rolle spielt. Unglücklicherweise wurde auch immer klarer, dass es nicht einfach werden würde diese Signalkaskade zu inhibieren. Abgesehen davon, dass die Inhibition der Kaskade schwere Nebenwirkungen hervorrufen kann wegen der wichtigen Rolle, die die Wnt/β-catenin Signalkaskade in der Homöostase des Darmes spielt, ist es generell extrem schwierig diese Kaskade zu inhibieren. Dies kommt vor allem daher, dass keine Kaskaden-spezifischen Kinasen bekannt sind, welche als Ziel eines Inhibitors verwendet werden könnten. Ein anderer sehr problematischer Aspekt der Kaskade ist die Doppelrolle des Haupteffektors β-catenin als Signalgeber sowie als Teil der Adhärenzverbindungen zwischen zwei Zellen. Trotzdem wurden in den letzten Jahren verschiedene Möglichkeiten gezeigt, wie das Problem angegangen werden könnte. Einerseits wäre da die Entdeckung von Porcupine Inhibitoren zu erwähnen, welche die Palmytoylierung der Wnt-Liganden verhindern, was zur kompletten Blockade jeglicher Sekretion der Wnt-Moleküle führt, womit die Kaskade blockiert wird. Des Weiteren wird die Idee in Erwägung gezogen, die Bindung von β-catenin mit transkriptionellen Hilfsfaktoren zu blockieren. In dieser Arbeit wollten wir die Vor- und Nachteile der Inhibierung von Porcupine klären. Zusätzlich versuchten wir klarzustellen, welche gewebsspezifische Aufgabe die β-catenin Hilfsfaktoren haben in Bezug auf ihre Fähigkeit, das Signal zu übermitteln. Diese Informationen werden imminent wichtig sein um zu beurteilen, ob ein Inhibitor in einem spezifischen Fall erfolgsversprechend sein kann.

In dieser Studie konnten wir zeigen, dass Porcupine in einem Plattenepithelkarzinom-Modell von Mäusen überexprimiert ist. Interessanterweise trifft diese Beobachtung auch auf menschliche Tumore zu. Diese Entdeckung gab uns den Anreiz, Porcupine Inhibitoren in einem Mausmodell zu testen. Wir entdeckten dabei, dass diese Inhibitoren die Entstehung

der Tumore behindern und die Stammzell-Nische der schon etablierten Tumore verkleinert. Dies führt zu erhöhter Differenzierung und einer Reduktion von Markern der Tumorinvasion. In einem Versuch, die spezifische Rolle von β-catenin's transkriptionellen Hilfsfaktoren zu charakterisieren, benützten wir Mausmodelle mit spezifischen Deletionen um die Bindung von β-catenin mit den N-terminalen Hilfsfaktoren (Bcl9 und Pygopus) und der Hilfsfaktoren zueinander zu verunmöglichen. Wir entdeckten, dass die Integrität dieser Interaktionen spezifisch während der Entwicklung des embryonalen Herzens und der Extremitäten gebraucht wird. Der Verlust dieser Interaktionen unterbindet molekulare Signalkaskaden, welche für die korrekte Spezifikation des Herzens essentiell sind, was zu Phänotypen führt, welche an häufig auftretende Herzfehler in menschlichen Patienten erinnern. Somit haben wir eine neue Aufgabe der Wnt/β-catenin Signalkaskade in der Herzentwicklung sowie in der Entstehung von humanen Herzfehlern gefunden.

Introduction

In the nineties, the discovery of the connection between Wnt/β-catenin signaling, APC and colon cancer, sparked intense research in the field of Wnt/β-catenin signaling. The hope was that by elucidating all the possible elements of the cascade, one might discover inhibitors of this pathway that could help treating cancer patients (Kahn, 2014). The work has revealed a picture of Wnt/β-catenin signaling's pivotal involvement in virtually every developmental process as well as in adult tissue homeostasis and many forms of cancers.

Depending on which Wnt binds to what Frizzled-co-receptor combination, different downstream cascades are induced. Adding to the complexity there are 19 different Wnts and 10 Frizzled receptors (Kahn, 2014).

In this work, we focus on the Wnt/β-catenin signaling cascade, which is most prominently triggered by Wnt binding to Frizzled and the co-receptors Lrp5/6. This binding event leads to recruitment and inactivation of the destruction complex, a large protein complex containing APC (Adenomatous polyposis coli), Axin and Ck1 (Casein kinase1) among others, to the membrane. When active this multiprotein complex marks β-catenin for degradation via phosphorylation in the absence of a Wnt ligand. Destruction complex inactivation upon Wnt binding leads to β-catenin stabilization, promoting its translocation to the nucleus, where it associates with its transcription factors of the Tcf family. For efficient transcription to occur, several other co-factors binding to β-catenin are needed, such as a Bcl9-Pygo complex at the N-terminal end of β-catenin and at the C-terminus histone modifiers like CREB and p-300, as well as several other transcriptional co-activators (Valenta et al., 2012). The exact requirement for specific co-factors in certain cell types and developmental stages is an open question, which we are trying to address with this work. Many direct target genes of the cascade are negative feedback regulators, ensuring that the pathway activation does not overshoot.

Curiously, in *D. melanogaster*, one of the bona fide Wnt target genes is Frizzled 3, while Arrow (the homologue of Lrp5/6) seems to be a negative target. A Frizzled protein being a positive target was mysterious, since one would associate a positive rather than a negative role for a receptor of the pathway, which would make it a positive feedback regulator.

Therefore, we set out to investigate the specific roles of Frizzled 3 as well as Arrow in *D. melanogaster* development as well as how their regulation by the Wnt/β-catenin signaling cascade works (Schilling et al., 2014), manuscript inserted below.

As noted above, impetus for therapeutic modulation of the Wnt/β-catenin cascade arises from its role as a key player in most epithelial cancer types, foremost among them colon, breast and lung carcinoma, as well as its involvement in other diseases such as osteoporosis, fibrosis and neurological diseases. The task has been herculean because of the lack of kinases to target, as well as the multi-functionality of many of the key pathway components, especially β-catenin. To remedy this, a better understanding of the molecular mechanisms of the cascade as well as of the specific biological consequences of Wnt/β-catenin signaling in different tissues is of utmost importance. Only in recent years, due to a better understanding of the pathway, some promising attempts at inhibiting this cascade have been made (Zimmerli et al., 2017).

One such avenue is inhibiting Porcupine, which is necessary for all Wnts to be secreted. It is also the only known enzyme that is specific to the Wnt cascade (Herr et al., 2012). The usefulness of Porcupine inhibition is unclear in cancers with activating mutations downstream of the ligands, like APC in colon carcinoma. However there are cancers with increased secretion of Wnts like certain SCCs and mammary carcinomas. We investigated this in a study looking at the role of Wnt ligands in the progression of human papilloma-virus-driven cSCCs (Zimmerli et al., 2017, included below), (Manuscript: WNT ligands control initiation and progression of human papilloma-virus-driven squamous cell carcinoma; in revision, attached below).

Another therapeutic target might be β-catenin's N-terminal co-activators Bcl9 and Pygo. They are especially interesting, since a single amino acid mutation in β-catenin can abrogate the binding of β-catenin to these co-factors. The drawback is the relatively scarce knowledge about their exact function in the Wnt/β-catenin cascade in mammals.

A reason for this is, that when Pygo and Bcl9 were discovered in Drosophila as components of the Wnt/β-catenin signaling cascade, crucial for any β-catenin mediated outputs (Kramps et al., 2002), the enthusiasm in the field reached its zenith. But when it became obvious from studies using mouse models, that these factors were not needed to transduce all β-catenin mediated signaling in mammals, the attention paid to these proteins got declined

abruptly. Nevertheless, recent studies take up the cudgels for the validity of N-terminal β-catenin interactors as drug targets. In these studies, it was shown that these N-terminal factors are negligible in normal gut homeostasis, but loss of them reduces colon carcinoma invasiveness (Deka et al., 2010, Moor et al., 2015).

Therefore, we decided to revisit the function of these proteins in mammalian development. Fuel for this idea were the findings, that Pygo as well as Bcl9 loss of function are lethal in developing mouse embryos, despite not being necessary for all Wnt/β-catenin signaling outputs. This led us to question if the cause of this lethality was Wnt/β-catenin signaling related, indicating tissue specificity for a role of these proteins as β-catenin co-factors in mammals, or if they acquired novel, β-catenin independent functions in the mammalian kingdom. A possibility which should not be neglected is that these functions are actually conserved in flies as well, but were so far overlooked, because the Wnt-induced lethality is too early.

In our lab, we have shown that Bcl9 and Pygo indeed do have β-catenin independent functions, specifically in the developing eye as well as teeth (Cantù et al., 2014), (Cantù et al., 2017), but the observed lethality of the embryos upon loss of these β-catenin N-terminal co-factors is most likely β-catenin dependent (Manuscript: Mutations in the Wnt/β-catenin cofactors Bcl9 and Pygo cause congenital heart malformations, below).

Review

Pharmacological interventions in the Wnt pathway: Inhibition of Wnt secretion versus disrupting the protein-protein interfaces of nuclear factors

Dario Zimmerli[1], George Hausmann[1], Claudio Cantù[1], Konrad Basler[1*]

[1]Institute of Molecular Life Sciences, University of Zürich, CH-8057, Zürich, Switzerland

* Corresponding author

British Journal of Pharmacology

REVIEW ARTICLE THEMED ISSUE

Pharmacological interventions in the Wnt pathway: inhibition of Wnt secretion versus disrupting the protein–protein interfaces of nuclear factors

Correspondence Konrad Basler, Institute of Molecular Life Sciences, University of Zürich, CH 8057, Zürich, Switzerland. E-mail: konrad.basler@imls.uzh.ch

Received 2 March 2017; **Revised** 4 May 2017; **Accepted** 11 May 2017

Dario Zimmerli, George Hausmann, Claudio Cantù and Konrad Basler

Institute of Molecular Life Sciences, University of Zürich, Zürich, Switzerland

Mutations in components of the Wnt pathways are a frequent cause of many human diseases, particularly cancer. Despite the fact that a causative link between aberrant Wnt signalling and many types of human cancers was established more than a decade ago, no Wnt signalling inhibitors have made it into the clinic so far. One reason for this is that no pathway-specific kinase is known. Additionally, targeting the protein–protein interactions needed to transduce the signal has not met with success so far. Complicating the search for and use of inhibitors is the complexity of the cascades triggered by the Wnts and their paramount biological importance. Wnt/β-catenin signalling is involved in virtually all aspects of embryonic development and in the control of the homeostasis of adult tissues. Encouragingly, however, in recent years, first successes with Wnt-pathway inhibitors have been reported in mouse models of disease. In this review, we summarize possible roads to follow during the quest to pharmacologically modulate the Wnt signalling pathway in cancer.

Abbreviations

APC, adenomatous polyposis coli; Bcl9/9l, Bcl9 and Bcl9l; CK1, casein kinase; DKK, Dickkopf; FZD, Frizzled; GSK3β, glycogen synthase kinase; LRP5, low-density lipoprotein 5; PORCN, Porcupine; Pygo, Pygopus; SFRPs, secreted FZD-related proteins; WLS, Wntless

DOI:10.1111/bph.13864

Introduction

Wnts activate diverse signalling cascades

Mammalian genomes encode for 19 different **Wnt** molecules, which can bind to 10 different **Frizzled** (FZD) receptors (Koike *et al.,* 1999; Langton *et al.,* 2016). FZDs belong to the family of seven-pass transmembrane GPCRs. When bound by Wnt proteins on their extracellular cysteine rich domain, they activate the cytosolic protein Dishevelled to transduce the signal inside the cell (reviewed in Dijksterhuis *et al.,* 2014). Several independent Wnt signalling cascades are activated in response to Wnts binding to their cognate receptors. The best studied and perhaps the most important is the β-catenin-dependent signalling cascade, mediated by **β-catenin** (Figure 1). The β-catenin-dependent cascade is of foremost importance for normal development and tissue homeostasis. When deregulated, it causes the initiation and progression of a myriad of different tumour types. Besides the β-catenin-mediated cascade, there are other β-catenin-independent outputs, such as the planar cell polarity and the Wnt/Ca^{2+} signalling pathway. The nature of the pathway transduced depends on the receptors/co-receptors present (He *et al.,* 1997; van Amerongen *et al.,* 2008). To transduce the β-catenin-dependent signal, FZD proteins bind the co-receptors low-density lipoprotein 5 (LRP5) or LRP6. Why in each specific context a particular Wnt/receptor combination activates one cascade or another is not entirely clear. However, some Wnts are thought to be preferentially β-catenin dependent (e.g. Wnt3a) or independent (e.g. Wnt5a). Wnt5a normally binds to FZD receptors and Ror/Ryk instead of Lrp5/6 and activates, among others, JNK signalling (Yamanaka, 2002). β-Catenin-independent signalling is often associated with the regulation of cell adhesion, migration and polarity (reviewed in Veeman *et al.,* 2003). Furthermore, it is also thought to suppress β-catenin-dependent signalling (Yuzugullu *et al.,* 2009). The β-catenin-independent cascade has received increasing attention in recent years due to its role in melanoma formation and metastasis (Weeraratna *et al.,* 2002; Chien *et al.,* 2009).

While the search for therapeutic targets has long focused on the transduction of the signal in the receiving cell, it is increasingly evident that an alternative strategy to modulate the Wnt signalling cascade is at the level of the ligands, for example, inhibiting their secretion.

Wnt secretion is dependent on Porcupine and Wntless

To be fully active, Wnts must undergo glycosylation and lipid modification (Figure 2). Whereas Wnt glycosylation enhances but is not essential for secretion and signalling, the lipid modifications are necessary for both functions. Wnts are acylated on two conserved residues, corresponding to cysteine 77 and serine 209 in mouse Wnt3a (Harterink and Korswagen, 2012). The enzyme responsible for these lipid modifications is the O-acyl-transferase Porcupine (PORCN). This is demonstrated by the fact that the genetic loss of PORCN, or the impairment of its activity, leads to Wnt molecules being retained in the endoplasmic reticulum (ER). The acylation of *Drosophila* Wnts in position Ser^{209} (or the mammalian homologue position) is required for the interaction of Wnts with Wntless (Wls), which is another protein critical for Wnt secretion (Herr and Basler, 2012). Wls is a multipass transmembrane protein that is an absolute requirement for the secretion of all Wnts (Bänziger *et al.,* 2006; Bartscherer *et al.,* 2006). The puzzle of how Wls promotes Wnt secretion remains unresolved; however, many pieces have already been put together. These include the unearthing of the role of the retromer complex in the retrieval of Wls, which establishes a trafficking loop from the ER to the plasma membrane via the Golgi (Herr *et al.,* 2012). While our understanding of Wls function is not sufficient to generate small molecule inhibitors, suitable inhibitors for the enzyme PORCN have been discovered. Porcupine is an attractive target because it seems to be exclusively required for Wnt secretion. Moreover, we have also found that PORCN, which is the sole enzyme known to be specific to the Wnt cascade, is up-regulated in murine cancer models. Additionally, elevated PORCN expression is an indicator for a bad prognosis in head and neck squamous cell carcinomas (the cancer genome atlas, unpublished observations by Dario Zimmerli).

Wnt signalling initiated by the Wnt–FZD interaction is highly regulated

Wnt signalling transduction is tightly regulated at the level of the ligand–receptor interaction. This is achieved by titration of the ligands and/or of the receptors.

Ligand availability can be modulated by the production of secreted FZD-related proteins (**SFRPs**). SFRPs are secreted molecules with no direct signalling activity, but they possess a Wnt-binding domain through which they sequester extracellular Wnts (Leyns *et al.,* 1997; Wang *et al.,* 1997). Another way to modulate Wnt signalling is to alter the level and/or availability of the receptors or co-receptors. The four secreted Dickkopf (**DKK**) proteins are a well-studied class of molecules that act in this way. In the Wnt cascade, DKKs act by binding to the FZD co-receptors LRP5/6, thereby inhibiting the binding of the Wnts (Mao *et al.,* 2001). Three of the DKK proteins (DKK1, 2 and 4) appear to be specific for the Wnt pathway and act by binding to LRP5/6 (Mao *et al.,* 2001). Interestingly, DKK2 and DKK4 can act as either activators or as repressors of the pathway, depending on the abundance of the cofactor **Kremen 2** (Mao and Niehrs, 2003). In contrast to the three other members of the DKK family, DKK3 acts in the TGF-β signalling cascade (Pinho and Niehrs, 2007; Nakamura and Hackam, 2010). In addition to above-mentioned mechanisms, there is a variety of other transmembrane or secreted inhibitors with various modes of action, such as WIF, WISE/SOST, CERBERUS, IGFBP, TIKI1, SHISA, WAIF1 and APCDD1 (reviewed in Cruciat and Niehrs, 2013).

Besides LRP proteins, there are other receptor-co-receptor pairs such as Ryk, which can enhance Wnt signalling (Lu *et al.,* 2004). Additionally, there are ancillary receptor complexes, which regulate the levels of available Wnt receptors. Most prominent among them are LGR4/5/6. Those proteins came to fame as Wnt target genes expressed in the intestine and were found to mark various stem cell populations (Barker *et al.,* 2007). Later on, it was revealed that

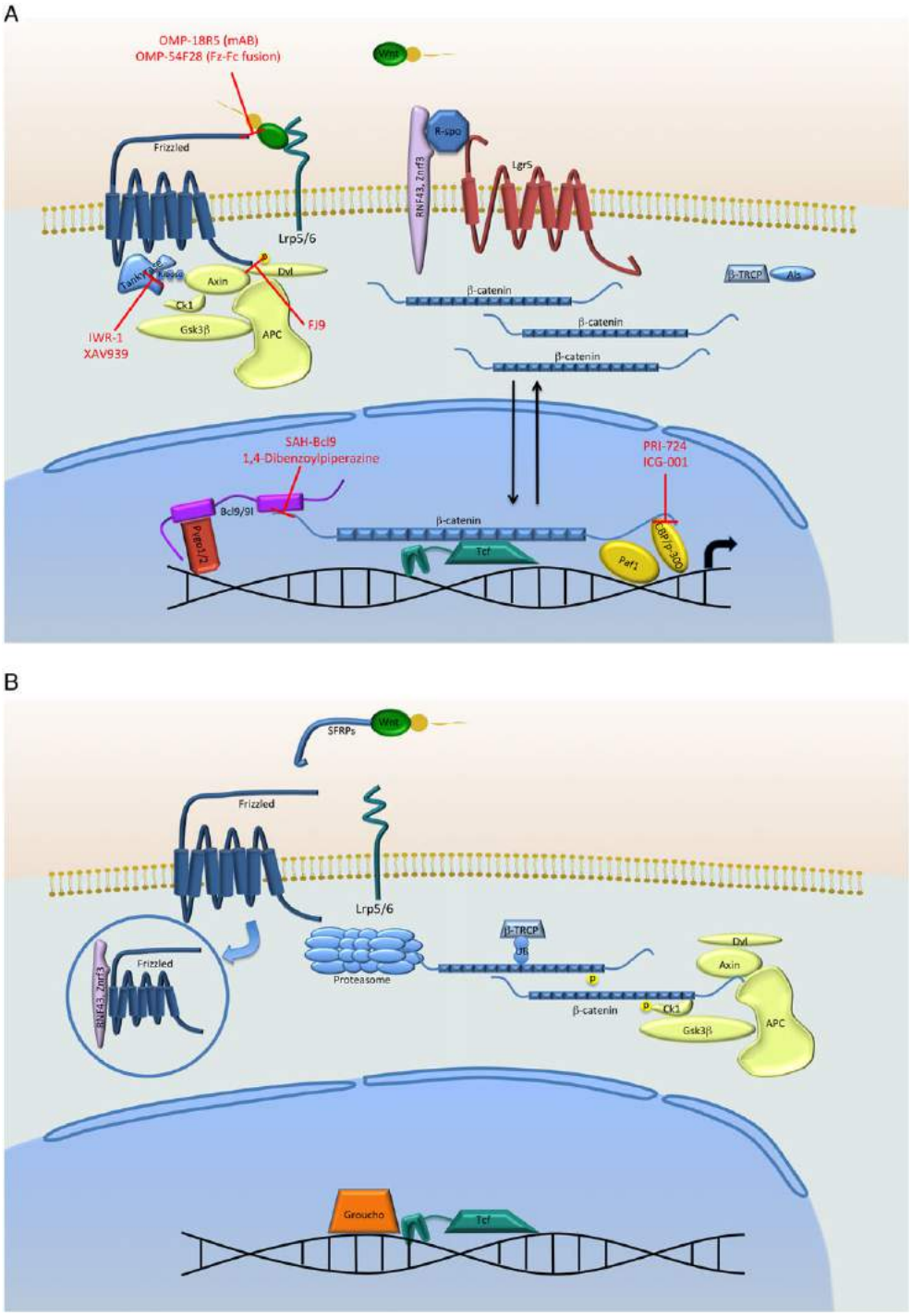

Figure 1

(A) The β-catenin-dependent Wnt signalling cascade in the ON-state. Upon binding of the Wnts to the receptors of the FZD family and the co-receptors LRP5/6, Dishevelled (Dvl) is recruited to the membrane, thus disassembling the destruction complex consisting of Axin, GSK3β, APC and CK1, preventing phosphorylation and thus protecting β-catenin from proteasomal degradation. This allows β-catenin to accumulate and translocate to the nucleus to initiate target gene transcription. Tankyrases can further increase the signal by marking Axin for degradation. Furthermore, when ZNRF3 and RNF43 are bound by R-spondin and LGR5 and, therefore, unable to target FZD receptors for degradation, Wnt signalling is enhanced in the Wnt-ON state. A further step protecting β-catenin from degradation is the inhibition of E3 ubiquitin ligases such as βTRCP by Armless, at least in *D. melanogaster*. A selection of Wnt-pathway inhibitors currently used in research are shown in red; red bars indicate the interaction they inhibit. (B) The Wnt signalling cascade in the OFF-state. Without Wnts binding to the FZD and LRP receptors, the destruction complex is active and phosphorylates β-catenin, thus marking it for proteasomal degradation. In the absence of LGR5, a Wnt target gene, the FZD receptor is also targeted for degradation by ZNRF3 and RNF43. Furthermore, E3 ubiquitin ligases, like βTRCP, promote proteasomal turnover of β-catenin.

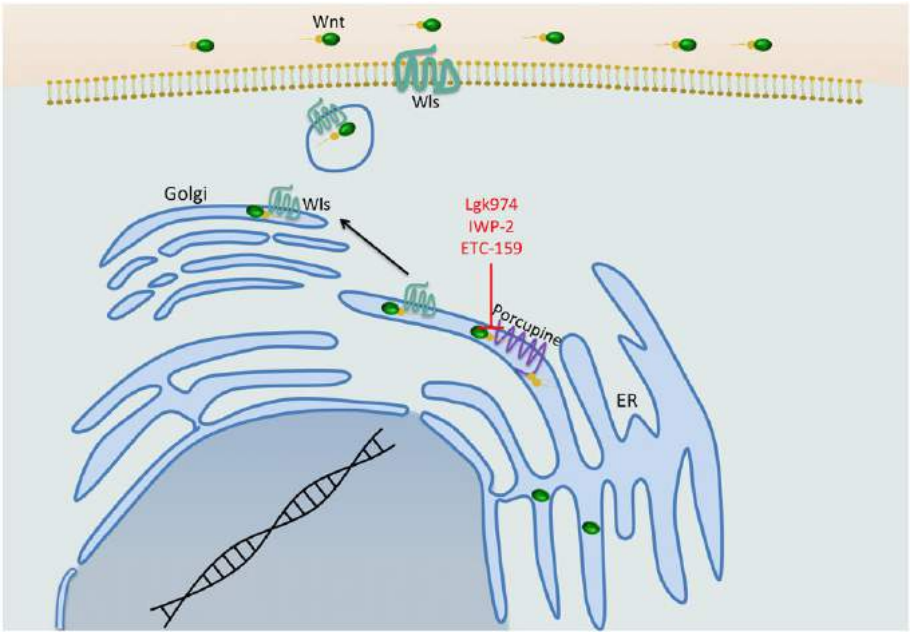

Figure 2

The secretory pathway of the ligands of the Wnt pathway. Wnts need to be coupled to fatty acids to be secreted. This happens in the ER by the acyltransferase Porcupine, which is a prime target for a small molecule inhibitor, since it is the only known enzyme specific to the pathway. Acylation of Wnts allows them to bind to Wntless (Wls) in the Golgi apparatus, which in turn facilitates secretion of the mature Wnts. Wls is a transmembrane protein required for the secretion of all Wnts.

they greatly increase Wnt signal transduction when they are bound by the extracellular R-spondin. They act by inhibiting the ubiquitination of FZD receptors and their subsequent degradation by ZNRF3 and RNF43 (de Lau *et al.*, 2014).

The diversity of mechanisms by which Wnt signalling is initiated by the Wnt-FZD receptor interaction is regulated is both a bane and a boon. There are many potential targets, but their diversity also means that redundancy could affect the efficacy of any intervention.

β-catenin is the central scaffold transducing the β-catenin-dependent Wnt signal

The central node of the β-catenin-dependent pathway is β-catenin. β-Catenin was discovered as a membrane-associated protein that binds E-cadherin (Kemler, 1993). Later, it was found that it regulates Wnt-dependent transcription via the recruitment of different transcriptional cofactors to the regulatory regions of Wnt target genes. In a signalling 'off state', the so-called 'destruction complex' [consisting of adenomatous polyposis coli (APC), Axin and the kinases responsible for the phosphorylation of β-catenin – glycogen synthase kinase (GSK3β) and casein kinase (CK1)] marks cytosolic β-catenin for proteosomal degradation (Stamos and Weis, 2013). Upon activation of this pathway, the rate limiting factor of the destruction complex, Axin, together with GSK3β, is recruited to the so-called Wnt signalosome – consisting of WNT/FZD/LRP and multimer Dishevelled (Bilic *et al.*, 2007). This destabilizes the destruction complex, leaving β-catenin free to accumulate and to translocate into the nucleus, where it binds to the transcription factors of the TCF/LEF family. Acting together with a plethora of N- and C- terminal binding transcriptional co-activators, β-catenin and TCF/LEF facilitate target gene expression.

In the pathway, 'off-state' TCFs are thought to silence target genes by recruiting co-repressors such as Groucho. These co-repressors are displaced by β-catenin and its cohort of transcriptional activators (Clevers, 2006; Städeli *et al.*, 2006; Mosimann *et al.*, 2009; Valenta *et al.*, 2012).

Recently, it was discovered that even if β-catenin escapes degradation by the destruction complex, it can still be degraded by the proteasome unless rescued by Armless, a pathway component recently identified in *Drosophila melanogaster*. Armless protects Arm/β-catenin from degradation by inhibiting the function of Ter^{94} in facilitating protein turnover (Reim *et al.*, 2014). This discovery is interesting in light of this review, as it might represent a so far overlooked mechanism for therapeutic intervention.

The Wnt/β-catenin transcriptional pathway is executed by N- and C- terminal co-activators

β-catenin facilitates transcription by recruiting several N- and C- terminal binding co-activators.

The factors directly binding the N-terminus of β-catenin are Bcl9 and Bcl9l (the two mammalian paralogues of the *Drosophila Legless*); they in turn recruit Pygopus (Pygo1 and 2 in mammals). Bcl9/9l and Pygo are thought to form a 'chain of adaptors' extending from β-catenin. The simple model arising from Drosophila is that Legless and Pygo are essential for the Wnt transcriptional output (Kramps *et al.*, 2002; Thompson *et al.*, 2002; reviewed in Mosimann *et al.*, 2009

and Valenta *et al.,* 2012). In mammals, although also required for a maximal Wnt output, the relative importance of Bcl9/9l and Pygo seems to be context-dependent. In the mouse loss of function mutations in these genes do not replicate loss of β-catenin-dependent Wnt signalling (i.e. by mutations in β-catenin). For example, β-catenin signalling mutants die at E6.5, whereas Bcl9/9l knockout (KO) animals die at E10.5, while Pygo KO animals survive at least to E13.5. Moreover, recent work has demonstrated that the Pygo-Bcl9 complex can also act independently of β-catenin (Cantù *et al.,* 2014; Cantù *et al.,* 2017). We therefore speculate that the role of Bcl9 as well as Pygo is to act as a booster of the signal and facilitate transcription of specific target genes in a subset of cells with active Wnt signalling. As described later, the context-dependent requirement of the so-called N-terminal chain of adaptors for facilitating the Wnt transcriptional output presents an exciting therapeutic target.

Another series of cofactors bind to β-catenin's C-terminus. This ensemble of cofactors comprises a diverse group of proteins, which have a more general role in transcription initiation and progression (reviewed in MacDonald *et al.,* 2009; Mosimann *et al.,* 2009). The most prominent among them are p300 and CBP, members of the basal transcriptional machinery, which were thought to have redundant modes of action in transcriptional activation (Hecht, 2000; Takemaru and Moon, 2000). However, recent studies suggest that although they are redundant in certain tissues, p300 and CBP can play critical roles and determine the nature of the transduced Wnt transcriptional programme. In lung fibrosis, the differential utilization of CBP or p300 seems to determine whether to execute alveolar repair or promote the fibroproliferation associated with fibrosis (Gottardi and Königshoff, 2013; Kahn, 2014).

Wnt signalling in cancer

Since Wnt signalling plays a role in nearly all developmental processes, it does not come as a surprise that it is also implicated in many cancers. There are several possibilities for a cancer cell to hijack this pathway. It can either inactivate/decrease the expression of an inhibitory component or activate/increase the expression of an activating factor. When, in 1991, mutations in the APC gene were discovered in 80% of colorectal cancers, efforts to find a drug acting on this protein were initiated, so far with limited success (Groden *et al.,* 1991; Powell *et al.,* 1992). In addition to mutations in APC, which is a fundamental component of the β-catenin destruction complex, other Wnt pathway mutations have been found: rarely inactivating mutations in Axin and activating mutations in the gene encoding for β-catenin (10%). Whereas in colon cancer APC mutations and β-catenin are prevalent, in other cancer types, such as hepatocellular carcinoma, mutations in Axin predominate. Oncogenic *ctnnb* mutations occur in melanoma and in solid tumours such as thyroid tumours (Kahn, 2014; Mazzoni and Fearon, 2014). The fact that in different tumours, alternate Wnt signalling activating mutations occur means that distinctive strategies may need to be employed in each case. This will be further discussed in the specific sections for the different targets.

As shown in colon cancers, the Wnt pathway is also activated in some tumours through epigenetic silencing of inhibitors of the cascade (Suzuki *et al.,* 2004). Some of these epigenetic changes affect the secreted inhibitors that regulate transduction at the level of the Wnt pathway ligand–receptor interaction: for instance, methylation of *SFRP* genes has been reported in colon, breast, lung, prostate and other cancers (Caldwell *et al.,* 2004; Suzuki *et al.,* 2004; Fukui *et al.,* 2005). Mutations in inhibitory factors like ZNRF43 and RNF43 have also been reported. These proteins act as negative regulators by decreasing FZD protein abundance at the membrane. When they are lost, receptor levels increase, thereby increasing signalling. In fact, mutations in these proteins were found to be common in the extremely aggressive pancreatic ductal adenocarcinomas (Jiang *et al.,* 2013). Another way by which Wnt signalling can be increased is by boosting ligand expression: the discovery of Int1 as a murine mammary tumour oncogene, as well as being a participant of the Wnt signalling field, is a prime example of this (Nusse and Varmus, 1982; Kahn, 2014).

While activating Wnt signalling is often a driver of tumour initiation, the evolution of a tumour to a fully malignant form seems in some cases to correlate with mutations that shut down the β-catenin-dependent Wnt cascade. A prime example of this is melanoma, where increased β-catenin-dependent Wnt signalling actually correlates with a better prognosis (Chien *et al.,* 2009). Therefore, blocking β-catenin-dependent Wnt signalling should not be considered a cure-all and different strategies will have to be applied in different diseases.

Therapeutic inhibitors of the Wnt pathway

Despite the challenges, especially the pivotal role of the pathway in tissue homeostasis, the Wnt pathway can be therapeutically targeted. An example is the targeting of the bone-derived Wnt inhibitor **Sclerostin** to treat osteoporosis. The use of a humanized, anti-sclerostin antibody is currently in phase III clinical trials (Appelman-Dijkstra and Papapoulos, 2016). The approach is successful because of the tissue (bone)-specific function of sclerostin. Discovering and exploiting the tissue- and disease-specific features is likely to be the key to the wider application of Wnt pathway modulators. Below, we describe different targets and their potential usefulness.

Porcupine: a promising target for effective Wnt pathway inhibition

One of the most promising ways for targeting Wnt signalling is to block ligand production. Although, as noted above, many cancers, especially colon carcinomas, have activating mutations in components of the Wnt cascade in the receiving cell, there is a growing body of evidence that additional signalling induced by the presence of Wnts is critical for tumour progression (Lavergne *et al.,* 2011; Koo *et al.,* 2015). Currently, the best way to interfere with Wnt secretion is to inhibit the acyl-transferase Porcupine (Figure 2).

One such inhibitor – Lgk974 – was identified in a high-throughput screen performed on living cells. To achieve this, 2.4 million compounds were tested for their ability to suppress the activity of a transcriptional Wnt reporter in a cell line co-cultured with another cell line overexpressing Wnt3a. Lgk974 binds directly to and inhibits Porcupine (Liu *et al.,*

2013). Currently, it is being tested in a stage 1 dose escalation clinical trial (Lum and Clevers, 2012). Another small-molecule inhibitor of Porcupine, ETC-159, has also just entered the phase of clinical trials (Madan *et al.,* 2016; Nile and Hannoush, 2016).

In mouse tumour models, Porcupine inhibitors (Table 1) showed very promising results in treating various types of cancer. The primary candidates for these studies were cancers known to be dependent on Wnt secretion, for example, due to RNF43 mutations (Liu *et al.,* 2013). Studies were conducted in murine models of mammary carcinomas, basal cell carcinoma, keratoacanthomas, colon cancer and head and neck squamous cell carcinomas (Liu *et al.,* 2013; Proffitt *et al.,* 2013; Zito *et al.,* 2014; Larsimont *et al.,* 2015; Madan *et al.,* 2016). Another scenario where inhibiting the secretion of ligands might be beneficial is when a cancer exploits them to influence the surrounding tissue to create its own niche.

There are several aspects that need to be considered when evaluating the therapeutic potential of globally blocking the secretion of all Wnts. The first is that systemic abolishion of Wnt secretion will result in defects in gut homeostasis (Valenta *et al.,* 2016). It is, therefore, essential to either target inhibitors directly to their site of action or to use smaller doses that do not attenuate Wnt signalling to the extent that tissue homeostasis is affected. The existence of a useful therapeutic window is demonstrated by studies showing that treatment with the Porcupine inhibitor Lgk974 resulted in cancer regression, but gut homeostasis was unaffected (Liu *et al.,* 2013).

The possibility that blocking Wnt secretion will affect both β-catenin-dependent and -independent Wnt signalling also needs to be taken into account. The consequences of applying Porcupine inhibitors will therefore depend on what Wnts are present and what pathways are activated. Since β-catenin-dependent and -independent Wnt signalling seem to influence each other, predicting the outcome is not easy (Yuzugullu *et al.,* 2009; Grumolato *et al.,* 2010). An illustrative example is melanoma, where the relative contribution of β-catenin-dependent and -independent signalling is unclear, particularly in the later stages such as metastases formation. The loss of the β-catenin-independent Wnt5a has been found to inhibit tumour growth and metastasis (Weeraratna *et al.,* 2002; Anastas *et al.,* 2014); however, it also seems to lead to activation of β-catenin-dependent signalling, which in different studies has positive or negative effects on tumour progression (Damsky *et al.,* 2011; Yang *et al.,* 2012; Caramel *et al.,* 2013). While this might seem to restrict the utility of Porcupine inhibitors, it may be an advantage to block all Wnt-dependent outputs, β-catenin-dependent and -independent, and thereby simplify the playing field.

Table 1

Selected Wnt pathway inhibitors and their use in mouse tumour models

Compound name	Mode of action	Tested applications	Publications for *in vivo* inhibitor use if applicable
Lgk974	Inhibits Porcupine	Cell lines, div. murine cancer models, phase 1 clinical trial	Liu *et al.,* 2013 Clinical trial identifier: NCT01351103
ETC-159	Inhibits Porcupine	Rspo3 translocations in CRC xenografts	Madan *et al.,* 2016
Wnt-C59	Inhibits Porcupine	Cell lines, murine cancer models	Proffitt *et al.,* 2013
IWP-2	Inhibits Porcupine	Murine keratoacanthoma model, cell lines	Zito *et al.,* 2014
Xav939	Tankyrase 1 + 2	Cell lines, xenografts	Huang *et al.,* 2009, Arques *et al.,* 2016
ICG-001	Inhibits β-catenin- CBP interaction	Diverse murine tumour models	Emami *et al.,* 2004
PRI-724 (2nd generation of ICG- 001)	Inhibits β-catenin- CBP interaction	Clinical trial phase 1	Clinical trials identifier: NCT01764477, NCT01606579
OMP-18R5 (mAB)	Antibody against FZD receptors	Various xenograft models, clinical trial phase 1	Gurney *et al.,* 2012 Clinical trials identifiers: NCT01973309, NCT01345201
OMP-54F28 (Fzd8-Fc fusion)	Competes with FZDs for Wnts	Various xenograft models, clinical trial phase 1	Wei *et al.* 2011 Clinical trial identifier: NCT02092363
FJ9	Inhibits Dishevelled PDZ domain interaction with FZD	Cell lines, xenograft models	Fujii *et al.* 2007
SAH-BCL9	Inhibits Bcl9-β-catenin interaction	Cell lines, xenograft models	Takada *et al.,* 2012
1,4-Dibenzoylpiperazines	Inhibits Bcl9-β-catenin interaction	Cell lines	Wisniewski *et al.,* 2016

A further critical open question with regard to the therapeutic application of Porcupine inhibitors is their effect on the immune system and how those effects will impinge on the efficacy of treatments. Since the inhibitors are typically applied orally, the possibility that the loss of Wnt secretion will affect the tumour micro-environment or the proliferation and differentiation of the infiltrating immune cells cannot be excluded.

However, the above-mentioned challenges necessitate further work to understand the consequences of globally blocking Wnt production and find solutions in order to circumvent challenges such as the paramount importance of Wnt signalling for tissue homeostasis.

Alternatives to small molecules are neutralizing antibodies or biologicals to inhibit the receptors

The development of small molecule inhibitors against components of the Wnt pathway is a challenging task, especially due to the lack of easily targetable enzymes specific for the pathway. An alternative is to use either antibodies against surface molecules like FZD or LRP, or more simply exploit 'natural' inhibitors of the cascade.

The difficulty of targeting FZDs with antibodies is the sheer number of them with poorly defined roles in transducing the signal. This raises the problem of the specificity of the antibody to specific receptors, as well as possible alternative routes for the cell to transduce the signal if only one specific receptor is blocked. Despite these challenges, promising results have been reported with the use of FZD antibodies: one example is the antibody OMP-18R5 that, even though it targets five different FZDs, appears to specifically hamper tumour growth without affecting normal tissues (Gurney *et al.,* 2012).

Another approach, shown to be promising in mice, is the use of biologically occurring inhibitors. A prime example for this is the injection of SFRP proteins, which are 'natural' inhibitors of the pathway (Polesskaya *et al.,* 2003). Instead of using existing SFRPs, it is also possible to engineer new ones by simply removing the transmembrane domain of an FZD of interest, thus rendering the Wnt binding part soluble. These engineered proteins can then act as an artificial soluble SFRP (Wei *et al.,* 2011). An additional possibility is to use other soluble inhibitors like DKK (Aicher *et al.,* 2008). Surprisingly, antibodies against DKK1 have anti-tumourigenic effects in cancer cell lines and xenograft models, which are thought to be Wnt signalling-dependent (Sato *et al.,* 2010). This has to be carefully evaluated, as it points to a broader role for DKK1 in cancer than simply being a negative feedback regulator of the Wnt pathway. With these results in mind, it might not be advisable to increase the DKK1 dose to inhibit the Wnt pathway, since this might have unexpected effects.

Tankyrase inhibitors

Tankyrase is a member of the PARP superfamily of enzymes that add ADP-ribose onto target proteins. With respect to Wnt signalling, tankyrase PARylates Axin and targets it for proteasomal degradation. Inhibition of tankyrase thus leads to an increased abundance of Axin and consequently to an overactivated destruction complex, the final effect being inhibition of the pathway (Huang *et al.,* 2009).

Initial results with tankyrase inhibitors seemed to be promising: in particular, the combined administration of Akt, PI3K and tankyrase inhibitors to human colon carcinoma cell lines xenografted into mice and rats induced apoptosis in cells escaping the therapy targeting only Akt and PI3K. This combined therapy was particularly effective in those cases where the accumulation of nuclear β-catenin was observed in the tumours (Arques *et al.,* 2016).

An impasse of this strategy is that tankyrase has multiple substrates and is critical for many basic cellular processes, for example, in telomere maintenance, mitosis and insulin-mediated glucose uptake; inhibiting it may therefore lead to severe side effects (Riffell *et al.,* 2012).

The β-catenin – TCF interaction is an attractive but elusive target

Another possibility for modulating the β-catenin-dependent Wnt signalling cascade very downstream is to target the nuclear function of β-catenin, more specifically by inhibiting the TCF-β-catenin interaction (Valenta *et al.,* 2012). This would be especially efficacious in colon carcinoma, where the majority of the mutations affect the destruction complex. However, there are a number of hurdles that to date have proven insurmountable. Firstly, β-catenin plays an important role in cell adhesion where, in association with E-cadherin, it forms the adherens junctions, and the interaction sites of TCF and E-cadherin overlap. Secondly, the binding affinity of β-catenin to TCF is quite high (*ca.* 20 nM). Nevertheless, several screens have been performed with the aim of disrupting this interaction. Although several compounds were identified that reduced Wnt signalling in reporter assays and inhibited the growth of colon cancer cell lines, the mechanisms of action of the molecules remained unclear and their specificity was limited (Kahn, 2014).

However, as mentioned above, β-catenin interacts with various transcriptional cofactors *via* its C- and N-terminus. Targeting these interactions represents an interesting alternative strategy.

Targeting the interaction between β-catenin and its C-terminal cofactors – a difficult case

Various screens have been conducted in order to find suitable inhibitors of β-catenin's interaction with C-terminal cofactors like CBP and p300. Even though some of these screens yielded efficacious inhibitors, none of them seem to specifically inhibit the interaction with β-catenin. ICG-001, which does inhibit Wnt signalling, generally interferes with CBP's activity and does not inhibit the binding of CBP to β-catenin. Interestingly, ICG-001 does not inhibit the very closely related p300. Since the inhibitor is effective in colon cancer mouse xenograft models, there may be a tissue-specific requirement for CBP in the colon (Emami *et al.,* 2004; McMillan and Kahn, 2005). However, because ICG-001 inhibits CBP, which is part of the general transcriptional machinery, administering this compound could result in severe side effects. Several phase 1 clinical trials are currently

being conducted to study the efficacy and side effects of this inhibitor in patients.

Targeting β-catenin's N-terminal interaction partners is the promising alternative

The only known N-terminal binding partners of β-catenin are the paralog proteins Bcl9and Bcl19l and indirectly Pygo1/Pygo2 (Figure 1) (Kramps *et al.,* 2002). While in *D. melanogaster* these proteins seem to be mandatory for all Wnt signalling outputs, in the mouse this appears not to be the case and their function seems to be more restricted (Kramps *et al.,* 2002; Song *et al.,* 2007; Cantù *et al.,* 2014). For example, in the intestinal epithelia, N-terminal co-activators are not needed for normal maintenance of homeostasis, but only during inflammation-induced regeneration. Moreover, colon carcinomas heavily depend on Bcl9/9l to become malignant (Deka *et al.,* 2010). Importantly, preventing the binding between β-catenin and Bcl9/9l has exactly the same effect as the complete deletion of Bcl9/9l; therefore, this genetically very well-defined interaction represents an ideal target for the development of small molecule inhibitors (Moor *et al.,* 2015). In terms of specificity, the context-dependent requirement of the N-terminal activators makes it an exciting therapeutic target. Several studies exploring this possibility have been recently published (Hoggard *et al.,* 2015; Wisniewski *et al.,* 2016).

Also promising seems to be the use of stapled peptides. This technology exploits the fact that the Bcl9-β-catenin interaction is mediated by a helical segment of Bcl9, which binds a large groove of β-catenin's structure. Metabolically stable triazole-stapled Bcl9 α-helical peptides seem to be an effective approach for inhibiting this interaction (Kawamoto *et al.,* 2012; Takada *et al.,* 2012). These stapled peptides appear to be good inhibitors *in vitro* and in mouse xenograft models, but the efficacy of such molecules in the clinic has not yet been tested. A possible drawback of inhibiting Bcl9/Bcl9l functions is suggested by recent findings, which show that a dysfunctional Bcl9l impairs caspase 2 expression, thus permitting higher aneuploidy tolerance in colorectal cancer cells (López-García *et al.,* 2017). Whether this is also the case when Bcl9l-β-catenin binding is inhibited will have to be investigated carefully.

Another attractive target is the Bcl9/9l partner, Pygo2. From a developmental viewpoint, the requirement for Pygo2 seems to be even more restricted than that of Bcl9/9l: for example, mouse embryos lacking Pygo2 die at E13.5, while Bcl9/9l loss of function is lethal at earlier stages, between E9.5 and E10.5 (Cantù *et al.,* 2014). Pygo1 seems to be negligible; so far, no phenotype could be observed upon its loss. Interestingly, Pygo2 plays crucial roles in mammary gland outgrowth as well as in mammary cancer stem cells. Furthermore, it may also play a role in some models of intestinal tumour initiation and progression (Talla and Brembeck, 2016). Additionally, there is evidence that Pygo's chromatin binding ability is required for mammary gland outgrowth (Watanabe *et al.,* 2014). Chromatin binding is not essential for Wnt signal transduction in the development and normal homeostasis of mice, suggesting that targeting this interaction will have few side effects (Cantu *et al.,* 2013). Therefore, Pygo's chromatin binding capability is a promising target for drug development. The therapeutic potential of targeting the binding of Pygo to Bcl9/91 requires further exploration of when and where this interaction is required; the interaction is also relevant in Wnt-independent contexts (Cantù *et al.,* 2014).

Delivering inhibitors directly to malignant cells via carrier molecules

In the adult organism Wnt signalling is critical for stem cell maintenance and tissue homeostasis, systemically blocking Wnt signalling will therefore be problematic (Valenta *et al.,* 2016). One way of circumventing this is to use the inhibitors at sub-lethal doses, where only the Wnt signalling-dependent cancer cells are affected. An alternative is to develop strategies to deliver the inhibitors directly and exclusively to the tumour tissue. This could be done by linking an inhibitor/toxin to a compound, which is attracted by the tumour, as for example was described by Krall *et al.,* 2014 (Wichert *et al.,* 2015) for acetazolamide, a ligand with specific receptors in cancerous lesions in clear-cell renal cell carcinomas. If such molecules also exist in Wnt driven tumours, these would be needed to be established. Other strategies to deliver the drug via nanoparticles to a specific tissue/cancer have also been proposed: one method would be to exploit chemical gradients, such as differences in pH or in oxygen concentration. Tumours are often hypoxic, thus the redox potential in the vicinity of the tumours is altered. Additionally, liposomes could be used to deliver the inhibitors (Muller and Keck, 2004; Allen and Cullis, 2013). All these methods have potential, but testing their practical implementation will be an important step in modulating the Wnt-pathway in disease.

Round up and looking forward

Wnt signalling is of paramount importance both in disease and in tissue maintenance; therefore, any therapeutic intervention involving Wnt signalling must solve this conundrum. Targeting inhibitors to the afflicted tissue is a promising but underexplored option. Other possible solutions have emerged and will continue to emerge, as our understanding of the complexities of Wnt signalling in cancer improves.

An exciting target is the Bcl9/9l-Pygo branch of β-catenin-dependent Wnt signalling, since it is not essential for adult tissue homeostasis but, in the case of colorectal cancer, is required for tumour progression. Blocking the β-catenin-Bcl9/9l interaction is one targetable interface. Although targeting a protein–protein interaction is challenging, recently, there have been some very promising results using stapled peptides as well as small molecule inhibitors. Further work is needed to determine other cancer types where impinging on the chain of adaptors could be harnessed. Therefore, further scrutiny of the developmental and disease relevance of the chain of adaptors is important. Basic research that refines our understanding of the intricacies of β-catenin-dependent Wnt signalling will reveal other opportunities – the identification of additional context- and tissue-specific factors is critical.

Another promising avenue is to target Wnt production by inhibiting Porcupine, which is specifically required for the

production and secretion of active Wnts. In cancers where Wnt secretion or receptor turnover is over-activated, Porcupine inhibition can be effective, for example, in head and neck squamous cell carcinoma with Notch mutations (Liu *et al.,* 2013). One future challenge to this is to gauge the consequences of the combined effect of blocking β-catenin-dependent and -independent Wnt signalling. More work is needed to understand the interplay of these signalling cascades. In tumours with downstream mutations in the Wnt cascade, the utility of treatment with Porcupine inhibitors is less obvious; however, as mentioned earlier in such cases, ligand-mediated augmentation of the signalling also probably plays a role in the later stages of tumour progression. Furthermore, β-catenin-independent Wnt signalling, which is also blocked by Porcupine inhibition, is known to play a role in the later stages of tumourigenesis, for example, Wnt5a signalling in melanoma metastases. It is critical to get a better understanding of the biology and the genetics of the tumours that we aim to treat. Given the diversity of the mutational landscapes found in different tumours, a therapy, which does not work in colorectal cancer or melanoma, might well work in mammary tumours.

The practical solution for effective inhibition of Wnt signalling is probably going to be to combine the above-mentioned approaches and, thereby, gain a decisive advantage over the tumour. One would need to carefully weigh the effect of a multifarious approach on homeostasis against the potential enhanced efficacy in killing cancer cells. An additional advantage of a varied strategy would be that it takes away alternative routes for the cancer to escape therapy. Further efficacy from a treatment point of view could also be achieved by using Wnt signalling inhibition as an adjunct therapy to other molecular medicine approaches, chemotherapy, radiology and/or surgery.

Nomenclature of targets and ligands

Key protein targets and ligands in this article are hyperlinked to corresponding entries in http://www.guidetopharmacology.org, the common portal for data from the IUPHAR/BPS Guide to PHARMACOLOGY (Southan *et al.,* 2016), and are permanently archived in the Concise Guide to PHARMACOLOGY 2015/16 (Alexander *et al.,* 2015a,b).

Conflict of interest

The authors declare no conflicts of interest.

References

Aicher A, Kollet O, Heeschen C, Liebner S, Urbich C, Ihling C *et al.* (2008). The Wnt antagonist Dickkopf-1 mobilizes vasculogenic progenitor cells via activation of the bone marrow endosteal stem cell niche. Circ Res 103: 796–803.

Alexander SP, Kelly E, Marrion N, Peters JA, Benson HE, Faccenda E *et al.* (2015a). The concise guide to PHARMACOLOGY 2015/16: Overview. Br J Pharmacol 172: 5729–5743.

Alexander SPH, Davenport AP, Kelly E, Marrion N, Peters JA, Benson HE *et al.* (2015b). The concise guide to PHARMACOLOGY 2015/16: G protein-coupled receptors. Br J Pharmacol 172: 5744–5869.

Allen TM, Cullis PR (2013). Liposomal drug delivery systems: from concept to clinical applications. Adv Drug Deliv Rev 65: 36–48.

van Amerongen R, Mikels A, Nusse R (2008). Alternative Wnt signaling is initiated by distinct receptors. Sci Signal 1: re9–re9.

Anastas JN, Kulikauskas RM, Tamir T, Rizos H, Long GV, von Euw EM *et al.* (2014). WNT5A enhances resistance of melanoma cells to targeted BRAF inhibitors. J Clin Invest 124: 2877–2890.

Appelman-Dijkstra NM, Papapoulos SE (2016). Sclerostin Inhibition in the Management of Osteoporosis. Calcif Tissue Int 98: 370–380.

Arques O, Chicote I, Puig I, Tenbaum SP, Argiles G, Dienstmann R *et al.* (2016). Tankyrase inhibition blocks Wnt/ -catenin pathway and reverts resistance to PI3K and AKT inhibitors in the treatment of colorectal cancer. Clin Cancer Res 22: 644–656.

Bänziger C, Soldini D, Schütt C, Zipperlen P, Hausmann G, Basler K (2006). Wntless, a conserved membrane protein dedicated to the secretion of Wnt proteins from signaling cells. Cell 125: 509–522.

Barker N, van Es JH, Kuipers J, Kujala P, van den Born M, Cozijnsen M *et al.* (2007). Identification of stem cells in small intestine and colon by marker gene Lgr5. Nature 449: 1003–1007.

Bartscherer K, Pelte N, Ingelfinger D, Boutros M (2006). Secretion of Wnt ligands requires Evi, a conserved transmembrane protein. Cell 125: 523–533.

Bilic J, Huang Y-L, Davidson G, Zimmermann T, Cruciat C-M, Bienz M *et al.* (2007). Wnt induces LRP6 signalosomes and promotes dishevelled-dependent LRP6 phosphorylation. Science 316: 1619–1622.

Caldwell GM, Jones C, Gensberg K, Jan S, Hardy RG, Byrd P *et al.* (2004). The Wnt antagonist sFRP1 in colorectal tumorigenesis. Cancer Res 64: 883–888.

Cantu C, Valenta T, Hausmann G, Vilain N, Aguet M, Basler K (2013). The Pygo2-H3K4me2/3 interaction is dispensable for mouse development and Wnt signaling-dependent transcription. Development 140: 2377–2386.

Cantù C, Zimmerli D, Hausmann G, Valenta T, Moor A, Aguet M *et al.* (2014). Pax6-dependent, but β-catenin-independent, function of Bcl9 proteins in mouse lens development. Genes Dev 28: 1879–1884.

Cantù C, Pagella P, Shajiei TD, Zimmerli D, Valenta T, Hausmann G *et al.* (2017). A cytoplasmic role of Wnt/β-catenin transcriptional cofactors Bcl9, Bcl9l, and Pygopus in tooth enamel formation. Sci Signal 10 eaah4598.

Caramel J, Papadogeorgakis E, Hill L, Browne GJ, Richard G, Wierinckx A *et al.* (2013). A switch in the expression of embryonic EMT-inducers drives the development of malignant melanoma. Cancer Cell 24: 466–480.

Chien AJ, Moore EC, Lonsdorf AS, Kulikauskas RM, Rothberg BG, Berger AJ *et al.* (2009). Activated Wnt/ss-catenin signaling in melanoma is associated with decreased proliferation in patient tumors and a murine melanoma model. Proc Natl Acad Sci 106: 1193–1198.

Clevers H (2006). Wnt/beta-catenin signaling in development and disease. Cell 127: 469–480.

Cruciat C-M, Niehrs C (2013). Secreted and transmembrane Wnt inhibitors and activators. Cold Spring Harb Perspect Biol 5: a015081–a015081.

Damsky WE, Curley DP, Santhanakrishnan M, Rosenbaum LE, Platt JT, Gould Rothberg BE *et al.* (2011). β-catenin signaling controls

metastasis in Braf-activated Pten-deficient melanomas. Cancer Cell 20: 741–754.

Deka J, Wiedemann N, Anderle P, Murphy-Seiler F, Bultinck J, Eyckerman S *et al.* (2010). Bcl9/Bcl9l are critical for Wnt-mediated regulation of stem cell traits in colon epithelium and adenocarcinomas. Cancer Res 70: 6619–6628.

Dijksterhuis JP, Petersen J, Schulte G (2014). WNT/Frizzled signalling: receptor-ligand selectivity with focus on FZD-G protein signalling and its physiological relevance: IUPHAR Review 3: Frizzleds as GPCRs. Br J Pharmacol 171: 1195–1209.

Emami KH, Nguyen C, Ma H, Kim DH, Jeong KW, Eguchi M *et al.* (2004). A small molecule inhibitor of -catenin/CREB-binding protein transcription. Proc Natl Acad Sci 101: 12682–12687.

Fujii N, You L, Xu Z, Uematsu K, Shan J, He B et al. (2007). An antagonist of dishevelled protein-protein interaction suppresses -catenin-dependent tumor cell growth. Cancer Res 67: 573–579.

Fukui T, Kondo M, Ito G, Maeda O, Sato N, Yoshioka H *et al.* (2005). Transcriptional silencing of secreted frizzled related protein 1 (SFRP1) by promoter hypermethylation in non-small-cell lung cancer. Oncogene 24: 6323–6327.

Gottardi CJ, Königshoff M (2013). Considerations for targeting β-catenin signaling in fibrosis. Am J Respir Crit Care Med 187: 566–568.

Groden J, Thliveris A, Samowitz W, Carlson M, Gelbert L, Albertsen H *et al.* (1991). Identification and characterization of the familial adenomatous polyposis coli gene. Cell 66: 589–600.

Grumolato L, Liu G, Mong P, Mudbhary R, Biswas R, Arroyave R *et al.* (2010). Canonical and noncanonical Wnts use a common mechanism to activate completely unrelated coreceptors. Genes Dev 24: 2517–2530.

Gurney A, Axelrod F, Bond CJ, Cain J, Chartier C, Donigan L *et al.* (2012). Wnt pathway inhibition via the targeting of Frizzled receptors results in decreased growth and tumorigenicity of human tumors. Proc Natl Acad Sci 109: 11717–11722.

Harterink M, Korswagen HC (2012). Dissecting the Wnt secretion pathway: key questions on the modification and intracellular trafficking of Wnt proteins. Acta Physiol 204: 8–16.

He X, Saint-Jeannet J-P, Wang Y, Nathans J, Dawid I, Varmus H (1997). A member of the Frizzled protein family mediating axis induction by Wnt-5A. Science 275: 1652–1654.

Hecht A (2000). The p300/CBP acetyltransferases function as transcriptional coactivators of beta-catenin in vertebrates. EMBO J 19: 1839–1850.

Herr P, Basler K (2012). Porcupine-mediated lipidation is required for Wnt recognition by Wls. Dev Biol 361: 392–402.

Herr P, Hausmann G, Basler K (2012). WNT secretion and signalling in human disease. Trends Mol Med 18: 483–493.

Hoggard LR, Zhang Y, Zhang M, Panic V, Wisniewski JA, Ji H (2015). Rational design of selective small-molecule inhibitors for β-catenin/B-cell lymphoma 9 protein–protein interactions. J Am Chem Soc 137: 12249–12260.

Huang S-MA, Mishina YM, Liu S, Cheung A, Stegmeier F, Michaud GA *et al.* (2009). Tankyrase inhibition stabilizes axin and antagonizes Wnt signalling. Nature 461: 614–620.

Jiang X, Hao H-X, Growney JD, Woolfenden S, Bottiglio C, Ng N *et al.* (2013). Inactivating mutations of RNF43 confer Wnt dependency in pancreatic ductal adenocarcinoma. Proc Natl Acad Sci 110: 12649–12654.

Kahn M (2014). Can we safely target the WNT pathway? Nat Rev Drug Discov 13: 513–532.

Kawamoto SA, Coleska A, Ran X, Yi H, Yang C-Y, Wang S (2012). Design of triazole-stapled BCL9 α-helical peptides to target the β-catenin/B-cell CLL/lymphoma 9 (BCL9) protein–protein interaction. J Med Chem 55: 1137–1146.

Kemler R (1993). From cadherins to catenins: cytoplasmic protein interactions and regulation of cell adhesion. Trends Genet 9: 317–321.

Koike J, Takagi A, Miwa T, Hirai M, Terada M, Katoh M (1999). Molecular cloning of Frizzled-10, a novel member of the Frizzled gene family. Biochem Biophys Res Commun 262: 39–43.

Koo B-K, van Es JH, van den Born M, Clevers H (2015). Porcupine inhibitor suppresses paracrine Wnt-driven growth of *Rnf43;Znrf3* -mutant neoplasia. Proc Natl Acad Sci 112: 7548–7550.

Krall N, Pretto F, Decurtins W, Bernardes GJL, Supuran CT, Neri D (2014). A small-molecule drug conjugate for the treatment of carbonic anhydrase IX expressing tumors. Angew Chem Int Ed 53: 4231–4235.

Kramps T, Peter O, Brunner E, Nellen D, Froesch B, Chatterjee S *et al.* (2002). Wnt/wingless signaling requires BCL9/legless-mediated recruitment of pygopus to the nuclear beta-catenin-TCF complex. Cell 109: 47–60.

Langton PF, Kakugawa S, Vincent J-P (2016). Making, exporting, and modulating Wnts. Trends Cell Biol 26: 756–765.

Larsimont J-C, Youssef KK, Sánchez-Danés A, Sukumaran V, Defrance M, Delatte B *et al.* (2015). Sox9 controls self-renewal of oncogene targeted cells and links tumor initiation and invasion. Cell Stem Cell 17: 60–73.

de Lau W, Peng WC, Gros P, Clevers H (2014). The R-spondin/Lgr5/Rnf43 module: regulator of Wnt signal strength. Genes Dev 28: 305–316.

Lavergne E, Hendaoui I, Coulouarn C, Ribault C, Leseur J, Eliat P-A *et al.* (2011). Blocking Wnt signaling by SFRP-like molecules inhibits in vivo cell proliferation and tumor growth in cells carrying active β-catenin. Oncogene 30: 423–433.

Leyns L, Bouwmeester T, Kim S-H, Piccolo S, Robertis EMD (1997). Frzb-1 is a secreted antagonist of Wnt signaling expressed in the spemann organizer. Cell 88: 747–756.

Liu J, Pan S, Hsieh MH, Ng N, Sun F, Wang T *et al.* (2013). Targeting Wnt-driven cancer through the inhibition of Porcupine by LGK974. Proc Natl Acad Sci 110: 20224–20229.

López-García C, Sansregret L, Domingo E, McGranahan N, Hobor S, Birkbak NJ *et al.* (2017). BCL9L dysfunction impairs caspase-2 expression permitting aneuploidy tolerance in colorectal cancer. Cancer Cell 31: 79–93.

Lu W, Yamamoto V, Ortega B, Baltimore D (2004). Mammalian Ryk is a Wnt coreceptor required for stimulation of neurite outgrowth. Cell 119: 97–108.

Lum L, Clevers H (2012). The unusual case of Porcupine. Science 337: 922–923.

MacDonald BT, Tamai K, He X (2009). Wnt/β-catenin signaling: components, mechanisms, and diseases. Dev Cell 17: 9–26.

Madan B, Ke Z, Harmston N, Ho SY, Frois AO, Alam J *et al.* (2016). Wnt addiction of genetically defined cancers reversed by PORCN inhibition. Oncogene 35: 2197–2207.

Mao B, Niehrs C (2003). Kremen2 modulates Dickkopf2 activity during Wnt/LRP6 signaling. Gene 302: 179–183.

Mao B, Wu W, Li Y, Hoppe D, Stannek P, Glinka A *et al.* (2001). LDL-receptor-related protein 6 is a receptor for Dickkopf proteins. Nature 411: 321–325.

Mazzoni SM, Fearon ER (2014). AXIN1 and AXIN2 variants in gastrointestinal cancers. Cancer Lett 355: 1–8.

McMillan M, Kahn M (2005). Investigating Wnt signaling: a chemogenomic safari. Drug Discov Today 10: 1467–1474.

Moor AE, Anderle P, Cantù C, Rodriguez P, Wiedemann N, Baruthio F *et al.* (2015). BCL9/9L-β-catenin signaling is associated with poor outcome in colorectal cancer. EBioMedicine 2: 1932–1943.

Mosimann C, Hausmann G, Basler K (2009). Beta-catenin hits chromatin: regulation of Wnt target gene activation. Nat Rev Mol Cell Biol 10: 276–286.

Muller RH, Keck CM (2004). Challenges and solutions for the delivery of biotech drugs – a review of drug nanocrystal technology and lipid nanoparticles. J Biotechnol 113: 151–170.

Nakamura REI, Hackam AS (2010). Analysis of Dickkopf3 interactions with Wnt signaling receptors. Growth Factors 28: 232–242.

Nile AH, Hannoush RN (2016). Fatty acylation of Wnt proteins. Nat Chem Biol 12: 60–69.

Nusse R, Varmus HE (1982). Many tumors induced by the mouse mammary tumor virus contain a provirus integrated in the same region of the host genome. Cell 31: 99–109.

Pinho S, Niehrs C (2007). Dkk3 is required for TGF-β signaling during Xenopus mesoderm induction. Differentiation 75: 957–967.

Polesskaya A, Seale P, Rudnicki MA (2003). Wnt signaling induces the myogenic specification of resident CD45+ adult stem cells during muscle regeneration. Cell 113: 841–852.

Powell SM, Zilz N, Beazer-Barclay Y, Bryan TM, Hamilton SR, Thibodeau SN *et al.* (1992). APC mutations occur early during colorectal tumorigenesis. Nature 359: 235–237.

Proffitt KD, Madan B, Ke Z, Pendharkar V, Ding L, Lee MA *et al.* (2013). Pharmacological inhibition of the Wnt acyltransferase PORCN prevents growth of WNT-driven mammary cancer. Cancer Res 73: 502–507.

Reim G, Hruzova M, Goetze S, Basler K (2014). Protection of armadillo/β-catenin by armless, a novel positive regulator of wingless signaling. PLoS Biol 12: e1001988.

Riffell JL, Lord CJ, Ashworth A (2012). Tankyrase-targeted therapeutics: expanding opportunities in the PARP family. Nat Rev Drug Discov 11: 923–936.

Sato N, Yamabuki T, Takano A, Koinuma J, Aragaki M, Masuda K *et al.* (2010). Wnt inhibitor Dickkopf-1 as a target for passive cancer immunotherapy. Cancer Res 70: 5326–5336.

Song N, Schwab KR, Patterson LT, Yamaguchi T, Lin X, Potter SS *et al.* (2007). Pygopus 2 has a crucial, Wnt pathway-independent function in lens induction. Development 134: 1873–1885.

Southan C, Sharman JL, Benson HE, Faccenda E, Pawson AJ, Alexander SPH *et al.* (2016). The IUPHAR/BPS guide to PHARMACOLOGY in 2016: towards curated quantitative interactions between 1300 protein targets and 6000 ligands. Nucleic Acids Res 44: D1054–D1068.

Städeli R, Hoffmans R, Basler K (2006). Transcription under the control of nuclear Arm/beta-catenin. Curr Biol 16: R378–R385.

Stamos JL, Weis WI (2013). The -catenin destruction complex. Cold Spring Harb Perspect Biol 5: a007898–a007898.

Suzuki H, Watkins DN, Jair K-W, Schuebel KE, Markowitz SD, Dong Chen W*et al.* (2004). Epigenetic inactivation of SFRP genes allows constitutive WNT signaling in colorectal cancer. Nat Genet 36: 417–422.

Takada K, Zhu D, Bird GH, Sukhdeo K, Zhao J-J, Mani M *et al.* (2012). Targeted disruption of the BCL9/β-catenin complex inhibits oncogenic Wnt signaling. Sci Transl Med 4 148ra117.

Takemaru KI, Moon RT (2000). The transcriptional coactivator CBP interacts with beta-catenin to activate gene expression. J Cell Biol 149: 249–254.

Talla SB, Brembeck FH (2016). The role of *Pygo2* for Wnt/ß-catenin signaling activity during intestinal tumor initiation and progression. Oncotarget 7: 80612–80632.

Thompson B, Townsley F, Rosin-Arbesfeld R, Musisi H, Bienz M (2002). A new nuclear component of the Wnt signalling pathway. Nat Cell Biol 4: 367–373.

Valenta T, Hausmann G, Basler K (2012). The many faces and functions of β-catenin. EMBO J 31: 2714–2736.

Valenta T, Degirmenci B, Moor AE, Herr P, Zimmerli D, Moor MB *et al.* (2016). Wnt ligands secreted by subepithelial mesenchymal cells are essential for the survival of intestinal stem cells and gut homeostasis. Cell Rep 15: 911–918.

Veeman MT, Axelrod JD, Moon RT (2003). A second canon. Functions and mechanisms of beta-catenin-independent Wnt signaling. Dev Cell 5: 367–377.

Wang S, Krinks M, Lin K, Luyten FP, Moos M (1997). Frzb, a secreted protein expressed in the Spemann organizer, binds and inhibits Wnt-8. Cell 88: 757–766.

Watanabe K, Fallahi M, Dai X (2014). Chromatin effector Pygo2 regulates mammary tumor initiation and heterogeneity in MMTV-Wnt1 mice. Oncogene 33: 632–642.

Weeraratna AT, Jiang Y, Hostetter G, Rosenblatt K, Duray P, Bittner M *et al.* (2002). Wnt5a signaling directly affects cell motility and invasion of metastatic melanoma. Cancer Cell 1: 279–288.

Wei W, Chua M-S, Grepper S, So SK (2011). Soluble Frizzled-7 receptor inhibits Wnt signaling and sensitizes hepatocellular carcinoma cells towards doxorubicin. Mol Cancer 10: 16.

Wichert M, Krall N, Decurtins W, Franzini RM, Pretto F, Schneider P *et al.* (2015). Dual-display of small molecules enables the discovery of ligand pairs and facilitates affinity maturation. Nat Chem 7: 241–249.

Wisniewski JA, Yin J, Teuscher KB, Zhang M, Ji H (2016). Structure-based design of 1,4-dibenzoylpiperazines as β-catenin/B-cell lymphoma 9 protein–protein interaction inhibitors. ACS Med Chem Lett 7: 508–513.

Yamanaka H (2002). JNK functions in the non-canonical Wnt pathway to regulate convergent extension movements in vertebrates. EMBO Rep 3: 69–75.

Yang P-T, Anastas JN, Toroni RA, Shinohara MM, Goodson JM, Bosserhoff AK *et al.* (2012). WLS inhibits melanoma cell proliferation through the β-catenin signalling pathway and induces spontaneous metastasis: WNTLESS/WLS in melanoma tumourigenesis. EMBO Mol Med 4: 1294–1307.

Yuzugullu H, Benhaj K, Ozturk N, Senturk S, Celik E, Toylu A *et al.* (2009). Canonical Wnt signaling is antagonized by noncanonical Wnt5a in hepatocellular carcinoma cells. Mol Cancer 8: 90.

Zito G, Saotome I, Liu Z, Ferro EG, Sun TY, Nguyen DX *et al.* (2014). Spontaneous tumour regression in keratoacanthomas is driven by Wnt/retinoic acid signalling cross-talk. Nat Commun 5: 3543.

Manuscripts

WNT ligands control initiation and progression of human papilloma-virus-driven squamous cell carcinoma

Dario Zimmerli[1]*, Virginia Cecconi[2]*, Tomas Valenta[1]*, George Hausmann[1], Claudio Cantù[1], Gaetana Restivo[3], Jürg Hafner[3], Konrad Basler[1], Maries van den Broek[2]

[1] Institute of Molecular Life Sciences, University of Zürich, 8057 Zurich, Switzerland
[2] Institute of Experimental Immunology, University of Zürich, 8057 Zurich, Switzerland
[3] University Hospital Zürich, Department of Dermatology, 8091 Zürich, Switzerland
* These authors contributed equally to this work
Correspondence to: kb@imls.uzh.ch, vandenbroek@immunology.uzh.ch

ABSTRACT

Human papilloma virus (HPV)-driven cutaneous squamous cell carcinoma (cSCC) is the most common cancer in immunosuppressed patients. Despite indications suggesting that HPV promotes genomic instability during cSCC development, the molecular pathways underpinning HPV-driven cSCC development remain unknown. We compared the transcriptome of HPV-driven mouse cSCC with normal skin and observed higher amounts of transcripts for Porcupine and WNT ligands in cSCC, suggesting a role for WNT-signaling in cSCC progression. We confirmed increased Porcupine expression in human cSCC samples. Blocking the secretion of WNT-ligands by the Porcupine inhibitor LGK974 significantly diminished initiation and progression of HPV-driven cSCC. Administration of LGK974 to mice with established cSCC resulted in differentiation of cancer cells and significant reduction of the cancer stem cell compartment. Thus, WNT/β-catenin signaling is essential for HPV-driven cSCC initiation and progression as well as for maintaining the cancer stem cell niche. Interference with WNT-secretion may thus represent a promising approach for therapeutic intervention.

INTRODUCTION

cSCC develops from basal keratinocytes in sunlight-exposed skin and is the second most frequent cancer in fair-skinned individuals. HPV-driven cSCC is the most common cancer in immunosuppressed organ transplant recipients (OTR), up to 50% of those patients develop cSCCs within 10 years after transplantation (Connolly et al., 2014). Thus, immunosuppression increases the risk to develop cSCC by 250-fold (Chockalingam et al., 2015) (Hofbauer et al., 2010). In addition, 80% of cSCC in OTR are positive for HPV compared to 40% in non-OTR (Accardi and Gheit, 2014), suggesting a role for HPV in the initiation and/or progression of cSCC particularly in immunosuppressed individuals. This is underscored by a recent report showing that vaccination against HPV protects against keratinocyte-derived cancers (Nichols et al., 2017). While the main driver mutations of HPV-negative cSCCs are found in the RAS-MAPK signaling pathway (Nassar et al., 2015), a role for WNT/β-catenin signaling has been reported as well (Malanchi et al., 2008a).

The WNT/β-catenin signaling cascade is essential in many developmental processes but is also involved in initiation and progression of many cancer types. Signaling is initiated by the binding of secreted WNT-ligands (WNTs) to the Frizzled/LRP receptor complexes. Secretion

of WNT ligands fully depends on their acylation by the acyl-transferase Porcupine (PORCN) (Herr and Basler, 2012), (Zimmerli et al., 2017a). Binding of WNTs to Frizzled/LRP triggers a cascade of events, which culminates in cytoplasmic stabilization and subsequent nuclear translocation of β-catenin. In the nucleus, β-catenin associates with TCF/LEF transcription factors to drive expression of WNT-target genes (Nusse and Clevers, 2017). WNTs also initiate various β-catenin independent outputs, some of which may play a role in cSCC (Pourreyron et al., 2012).

To investigate the molecular mechanisms underlying the initiation and progression of HPV-driven cSCC, we used a mouse model in which UV-induced overexpression of the HPV8-derived E6 oncogene in keratinocytes drives the development of a progressive cSCC (*Krt14*-HPV8(*E6*); (Schaper, 2005), (Marcuzzi et al., 2009a)). We found increased expression of WNTs and PORCN in cSCCs. Furthermore, blocking WNT secretion by a small-molecule inhibitor of PORCN, LGK974 decreased the cSCC stem cell compartment and inhibited induction and progression of cSCC.

RESULTS AND DISCUSSION

Increased expression of WNT ligands and elevated WNT/β-catenin signaling are hallmarks of HPV8-E6 driven cSCC

Aberrantly active WNT/β-catenin drives various epithelial cancers, including non-viral cSCC (Malanchi et al., 2008b), (Powell et al., 1992), (Zimmerli et al., 2017b). The importance of WNT/β-catenin signaling in HPV-driven tumors is unknown. To investigate this, we used the *Krt14*-HPV8(*E6*) transgenic mouse model for cSCC in which tumor induction can be triggered by UV-irradiation (Marcuzzi et al., 2009b). We observed nuclear localization of β-catenin, a hallmark for active WNT/β-catenin signaling, in established cSCC (Fig 1A, left panels) and confirmed elevated WNT/β-catenin signaling by in situ hybridization for the WNT/β-catenin target gene *Axin2* (Jho et al., 2002) (Fig 1A, right panels).

In non-viral cSCCs, CSC reside at the tumor-stroma interface in close proximity to the vasculature (Beck et al., 2011) and express, besides EpCAM, several integrins including integrin β1 (CD29), α6 (CD49f) (Schober and Fuchs, 2011), as well as CD34 (Schober and Fuchs, 2011), (Malanchi et al., 2008b), (Lapouge et al., 2012). We found a population of $EpCAM^+$, $CD34^+$, $CD49f^+$ cells at the tumor-stroma interface in HPV-driven cSCCs (supplementary Figure 1A), which are putative CSCs. Importantly, these $EpCAM^+$ $CD34^+$

CSCs expressed a higher amount of the WNT/β-catenin target gene and stem cell marker *Lgr5* (Haegebarth and Clevers, 2009), when compared to non-stem cell tumor cells ($EpCAM^+$ $CD34^-$) or stromal cells ($EpCAM^-$ $CD34^-$) (Fig 1B). Thus as in non-viral cSCC and colorectal cancer (Malanchi et al., 2008b), (de Sousa e Melo and Vermeulen, 2016) elevated WNT signaling and expression of LGR5 seem to mark the CSC pool.

To better understand the involvement of WNT/β-catenin signaling in HPV-driven cSCCs, we compared the transcriptome of established cSCC to that of healthy skin. Gene ontology analysis (The Gene Ontology Consortium, 2015) suggested that differentially expressed genes are associated with increased cell motility, altered cell-matrix adhesion and inflammation (supplementary Figure 1B). Several transcripts that have previously been associated with non-viral cSCC, such as *Fosl1* (encoding Fos-like antigen 1), *Ptprz1* (encoding protein tyrosine phosphatase, receptor type Z1) (Schober and Fuchs, 2011), (Latil et al., 2017) as well as transcripts encoding for metalloproteases (*Mmp*), were also upregulated in HPV-driven cSCC (supplementary Figure 1C), suggesting the existence of common pathways in cSCC that are independent of its etiology.

Although no mutations in *Hras* were reported in the *Krt14*-HPV8(*E6*) cSCC tumor model (Marcuzzi et al., 2009a), we found a significant upregulation of the RAS-MAPK-ERK signaling pathway (supplementary Figure 1B and supplementary Figure 1E). Therefore, RAS-MAPK-ERK activation seems to represent a common mechanism associated with cSCC progression together with elevated WNT/β-catenin signaling.

We did not detect an increase of expression of WNT/β-catenin signaling target genes. This was not unexpected because of the very high activity of the WNT pathway in hair follicles, especially during the hair growth (anagen) phase (Huelsken et al., 2001b).

However, consistent with the presence of activated WNT/β-catenin signaling in HPV-driven cSCCs, we observed decreased expression of extracellular WNT-inhibitory factors, including members of the *Sfrp* (encoding secreted frizzled-like protein)-family, *Notum* and *Dkk* (encoding Dickkopf). We also observed increased expression of transcripts of some *Wnt*s and *Porcn,* whose product is essential for WNT-secretion (supplementary Figure 1D). We found significantly increased expression of *Wnt16* transcripts in HPV-induced cSCCs. Using in situ hybridization, we confirmed the increased *Wnt16* expression in tumor tissue compared to healthy skin (Fig 1E). This is interesting because in prostate cancer elevated WNT16 expression correlated with enhanced WNT/β-catenin signaling, leading to cell survival and therapy resistance (Sun et al., 2016), (Sun et al., 2012).

Recent studies have highlighted the importance of PORCN for establishment and maintenance of a CSC niche (Tammela et al., 2017). We found that cells at the tumor-stroma interface strongly expressed PORCN (Fig. 1C). The $PORCN^{+}$ cells included $CD34^{+}$ and $CD34^{-}$ cells (Fig. 1D). Thus, PORCN expression may mark the niche rich in WNTs needed by CSCs as was described recently for lung adenocarcinomas (Tammela et al., 2017).

The clinical relevance of these findings is underscored by the enhanced expression of PORCN along the invasive front also in human cSCC samples (Fig. 1F).

Figure 1

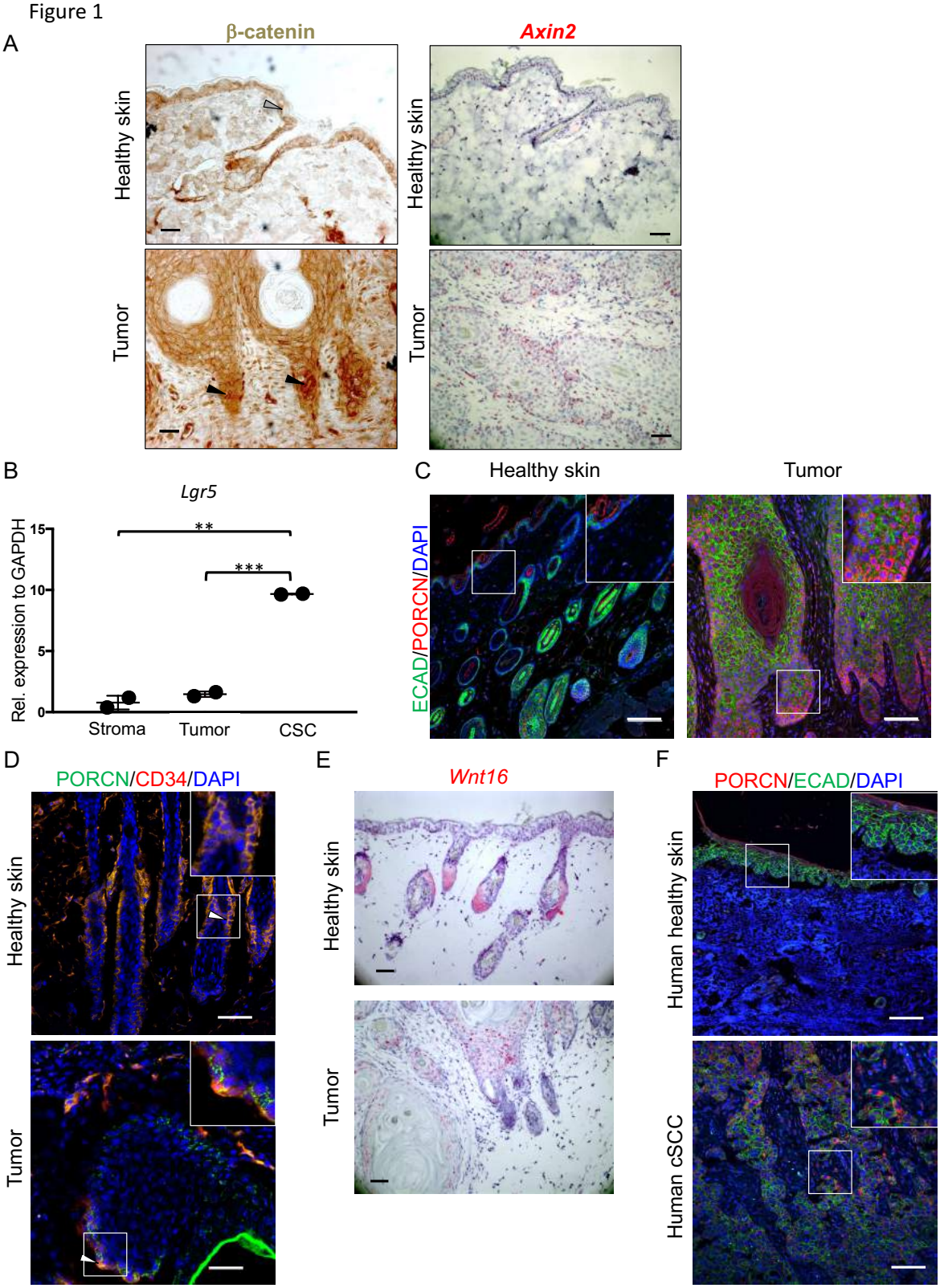
A
β-catenin
Axin2
Healthy skin
Tumor
B
Lgr5
Rel. expression to GAPDH
15
10
5
0
**
***
Stroma
Tumor
CSC
C
Healthy skin
Tumor
ECAD/PORCN/DAPI
D
PORCN/CD34/DAPI
Healthy skin
Tumor
E
Wnt16
Healthy skin
Tumor
F
PORCN/ECAD/DAPI
Human healthy skin
Human cSCC

Figure 1: Elevated WNT/β-catenin signaling and increased expression of WNT ligands are hallmarks of HPV8-E6 driven cSCC.

(A) Left panel: Nuclear accumulation of β-catenin in the invasive front of HPV-driven cSCCs (black arrowheads). Healthy skin shows membranous expression of β-catenin (gray arrowhead). Scale bar = 50 μm. Right panel: In situ hybridization for *Axin2* (red stain) shows increased expression of this WNT/β-catenin signaling target in tumors in comparison to healthy skin. Nuclei are counterstained with hematoxylin (blue stain). Scale bar = 100μm.

(B) Enhanced amount of *Lgr5* transcripts in CSCs ($EpCAM^+$ $CD34^+$ $CD49f^+$) compared to non-CSC tumor cells ($EpCAM^+$ $CD34^-$) (unpaired Student's t-test, ***p<0.001) and stromal cells ($EpCAM^-$ $CD34^-$ $CD49f^-$) (unpaired Student's t-test, **p<0.01). Cells from 2 HPV-driven cSCC from different mice were sorted and expression was quantified by qRT-PCR.

(C) PORCN (red) staining in healthy skin and HPV-driven cSCC. E-cadherin (green) marks epithelial cells, DAPI (blue) marks nuclei. Scale bar = 100μm. PORCN is mostly expressed along the tumor-stroma interphase of the tumor, while it is absent in healthy epidermis. Insets show a larger magnification of the region marked by the white square.

(D) Overlapping expression of PORCN (green) and CD34 (red) in healthy skin with hair follicles and tumor tissue is indicated by arrowheads. Scale bar = 50 μm. Insets show a larger magnification of the region marked by the white square.

(E) In situ hybridization of healthy skin and HPV-driven cSCC for *Wnt16* (red), shows higher expression of *Wnt16* in tumors compared to healthy skin. The section is counterstained with hematoxylin. Scale bar = 50 μm.

(F) Increased expression of PORCN (red) in human cSCC in comparison to healthy human skin. E-cadherin (green) marks epithelial tissue, nuclei are counterstained in blue. Scale bar = 100 μm. Insets show a larger magnification of the region marked by a white square.

Krt14-HPV8*(E6)* mice were described previously (Marcuzzi et al., 2009b) and were bred to FVB mice (Harlan Laboratories, Envigo) in house. Mice were kept under specific pathogen-free conditions at the Laboratory Animal Services Center at the University of Zurich.

To induce cSCC, approximately 4 cm^2 of shaved dorsal skin was irradiated with UVA (5 J/cm^2) plus UVB (1 J/cm^2) using the UV 802 L Waldmann device.

Murine tumor samples were collected 4 weeks after tumor induction. Representative samples from at least 3 biologically independent replicas are shown in the immunohistochemistry, immunofluorescence and in situ hybridization.

Experiments were performed in accordance with the Swiss federal and cantonal regulations on animal protection and were approved by the Cantonal Veterinary Office Zurich.

Human SCC samples were obtained from biobanks managed by the University Research Priority Project "Translational Cancer Research" and the research project "Skintegrity". All material were surplus biopsies from patients who had signed an informed consent that was approved by the cantonal ethics commission Zurich (EK647 and EK800).

For flow cytometry and sorting, tumors were collected in PBS and digested for 2 h at 37°C in 2.4 mg/ml Dispase (Roche), cut into pieces and digested again for one hour at 37°C in 1 mg/ml collagenase Type IV

(Worthington Biochemical Corporation) and 0.1 mg/ml DNase (Sigma-Aldrich). Antibodies against the following proteins were used: CD45.1 (clone A20, BioLegend), CD31 (clone MEC13.3, BioLegend), EpCAM (clone GoH3, BioLegend), CD34 (clone RAM34, eBioscience). Dead cells were excluded using Zombie Violet Fixable Viability Kit (BioLegend). Doublets were excluded by FSC-A versus FSC-H and SSC-A versus SSC-H gating.

Immunohistochemistry on frozen sections was performed on tissue fixed in 4% PFA for 1 h, left to sink in 30% sucrose and embedded in OCT. Ten-µm thick cryosections were blocked for 1h at RT with 2.5% Hings and 2.5% BSA in 0.1% Tween in PBS (PBST) (blocking buffer), and then stained with biotin-conjugated anti-CD34 (clone RAM34, eBioscience) and unconjugated rabbit anti-PORCN (clone ab105543, Abcam) over night at 4°C in blocking buffer. Secondary antibodies (see below) were added for 1 h in blocking buffer at RT, then samples were mounted in fluor save (CalBiochem).

Standard protocols were used for embedding and cutting Formalin-fixed paraffin-embedded (FFPE) tissue. After deparaffinization, on both mouse and human samples, antigen retrieval was performed in 10mM Trisodium citrate buffer pH 6. Staining was performed as described above for frozen sections.

The following antibodies were used for mouse and human FFPE samples: Mouse-anti-β-catenin (clone14, BD transduction labs), mouse-anti-E-cadherin (BD transduction labs), rabbit-anti-PORCN (Abcam ab105543), rabbit-anti-Ki67 (Abcam), rabbit-anti-HMGA2 (SantaCruz), rabbit-anti-MMP13 (clone 3H13L17, ThermoFisher) and rabbit-anti-phospho-ERK (Cell Signaling).

Secondary antibodies used were goat-anti-mouse AlexaFluor 488 and goat-anti-rabbit AlexaFluor 555. For the PORCN staining a biotin-labeled goat-anti-rabbit secondary antibody was used, followed by the ABC kit (VectaShield), and the Cy3 tyramide amplification kit (PerkinElmer).

Stainings for nuclear β-catenin were performed with biotin-labeled secondary antibodies, followed by DAB staining (VectorLabs).

When mouse primary antibodies were used on murine tissues, VectorLabs MOM kit was used to block endogenous antigens.

In situ hybridization was performed using the RNAscope kit (Advanced Cell Diagnostics) according to the manufacturer's instructions. Probes for *Axin2* and *Wnt16* were obtained from the same company.

For qRT-PCR, RNA was isolated from sorted cells using the NucleoSpin RNA XS kit (Machery-Nagel) according to the manufacturer's instructions. qRT-PCRs using SybrGreen were performed on cDNA synthesized with the Roche Transcriptor High Fidelity cDNA Synthesis Kit after RNA isolation by standard TRI-Reagent protocols. Reactions were performed in triplicates and monitored with the ABI Prism 7900HT system (Applied Biosystems). The following 5'-3' primers (Microsynth) were used for qRT-PCR. *Gapdh*, fwd AACTTTGGCATTGTGGAAGG, rev ATCCACAGTCTTCTGGGTGG; *Lgr5*, fwd CTCCACACTTCGGACTCAACAG, rev AACCAAGCTAAATGCACCGAAT.

Supplementary Figure 1

A

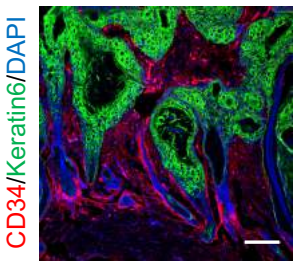

B

Selected GO terms of first 1500 hits skin vs tumor

GO biological process complete	Gene number	Expected number	Fold Enrichment	P value
positive regulation of MAPK cascade	66	29.91	2.21	4.54E-05
regulation of cell migration	98	47.94	2.04	5.45E-07
inflammatory response	63	27.09	2.33	1.74E-05

C

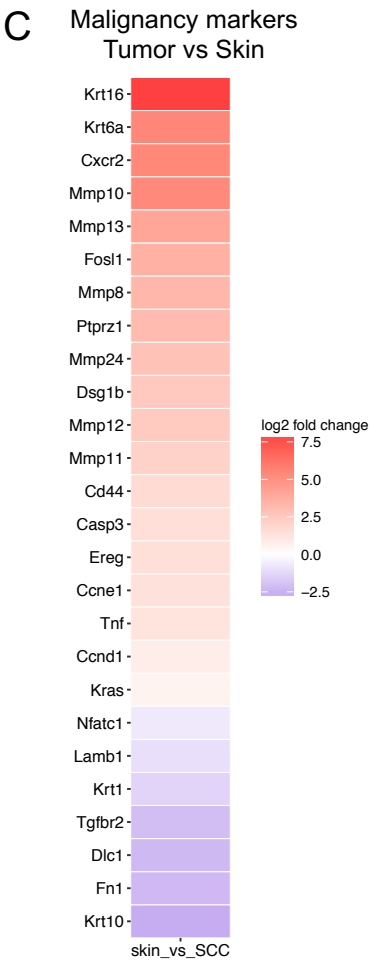

D

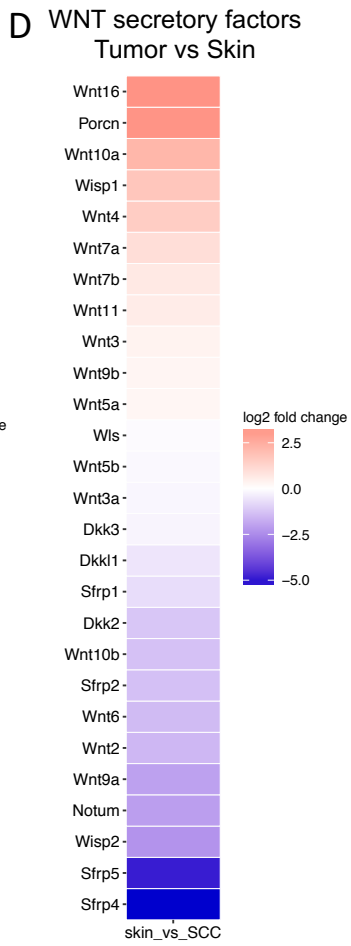

E

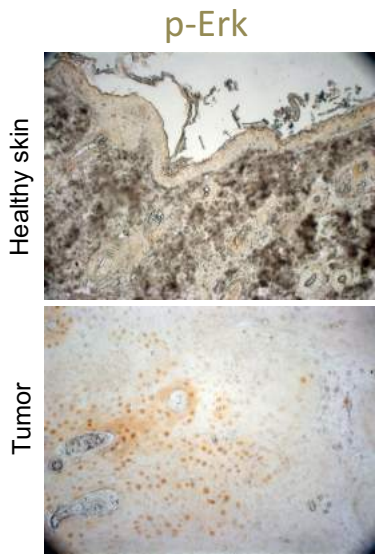

Supplementary Figure 1: Secretion of WNTs is elevated in HPV-driven cSCCs in comparison to healthy skin, leading to active WNT/β-catenin signaling. Relates to Figure 1.

(A) Gene ontology analysis of RNA-sequencing data comparing HPV-driven cSCCs with healthy skin. Four independent samples for each condition were sequenced and analyzed.

(B) Heatmap showing expression of selected malignancy-associated genes in cSCC compared to healthy skin. Malignancy markers are upregulated, while differentiation markers are downregulated in cSCC.

(C) Heatmap showing expression of transcripts for *Wnts* and factors implicated in WNT secretion or availability in cSCC compared to healthy skin; tumor tissue shows increased expression of transcripts associated with WNT production and decreased expression of transcripts for WNT inhibitory factors.

(D) Staining for phosphorylated ERK (p-ERK, brown) in HPV-driven cSCC four weeks after tumor induction. P-ERK was not detected in healthy skin.

(E) Staining for CD34 (red) in HPV-driven cSCC shows expression at tumor-stroma interphase in the invasive front of the tumors. Cells are counterstained with DAPI, Keratin6 marks epithelial tumor cells. Scale bar = 100μm.

Protocols were as described for the main figures.

For RNA-sequencing, RNA was isolated from healthy skin (n=4) and tumors from LGK974-treated (n=4) and vehicle-treated (n=4) mice using TRI-Reagent combined with the Ambion PureLink RNA mini Kit. Each sample was obtained from an individual mouse. Single-stranded 100-bp read sequencing was performed on an Illumina HiSeq2500 machine at the Genomics Platform of the University of Geneva. The reads were mapped with the TopHat v.2 software to the Ensembl GRCm38.p4 reference on new junctions and known junction annotations. Biological quality control and summarization were performed with PicardTools1.141. EdgeR was used for normalization and differential expression testing.

Clustering analysis was performed using the online tool described in (Babicki et al., 2016), other heatmaps were generated in R-studio. The top-ranked genes for the clustering analysis and other heatmaps were chosen according to $p<0.05$ (general linear model with negative binomial distribution, (quasi-likelyhood F-test)). False discovery rate was too stringent due to the high variability between different tumors and low number of changing transcripts. qRT-PCR and immunohistochemistry was used to confirm the findings.

Inhibition of WNT secretion impairs the initiation of HPV-driven cSCC

To address whether WNT-secretion and -signaling are essential for the initiation of HPV-driven cSCC, we administered a small-molecule inhibitor of PORCN (LGK974), which blocks the secretion of all WNTs (Liu et al., 2013a). LGK974 (or vehicle) was administered daily *per os*, starting one week prior to tumor induction (Fig. 2A). Administration of LGK974 or vehicle did not affect the general wellbeing of mice and the dose used here did not affect the intestinal stem cell compartment, which is most sensitive to perturbations of WNT/β-catenin signaling (Valenta et al., 2016), (data not shown).

Treatment with LGK974 prior to the tumor induction resulted in a significant reduction in tumor size in comparison to the vehicle-treated control mice (Fig 2B), suggesting an essential

role of PORCN and by extension WNTs for the initiation of HPV-driven cSCC. Analysis of haematoxylin and eosin (H&E) stained sections confirmed that UV-induced skin inflammation failed to progress to carcinoma in LGK974-treated mice, whereas characteristic cSCC lesions were observed in vehicle-treated mice (Fig 2C). In contrast, the lesions in LGK974-treated mice (Fig 2B) consisted mainly of keratin whorls reminiscent of differentiation and in some cases of hair follicles with normal morphology (supplementary Figure 2).

Expression of CSC markers is indicative for malignancy and loss of stem cells often results in differentiation and ultimately regression of tumors (Singh and Settleman, 2010). WNT/β-catenin signaling is one of the key pathways defining the stem cell niche in many epithelial tissues and cancers of epithelial origin (de Sousa e Melo and Vermeulen, 2016), (Shiokawa et al., 2017). As a next step we therefore investigated whether inhibition of WNT-secretion has an impact on CSCs in HPV-driven cSCCs. Thus, we quantified transcripts by qRT-PCR that are expressed in cSCC stem cells (Schober and Fuchs, 2011), (Malanchi et al., 2008b), (Lapouge et al., 2012). We focused on *Pthlh* (encoding parathyroid hormone-like hormone), *Ptprz1* and *Cd44* because of their association with CSC in a chemically induced model of cSCC (Schober and Fuchs, 2011), (Oshimori et al., 2015). Blocking WNT-secretion via LGK974 administration resulted in significantly reduced expression of all these cancer stem cell markers (Fig 2D). Therefore, WNT-ligands are presumably essential for the stem cell niche in HPV-driven cSCCs. In support of these findings, inhibition of PORCN inhibited also basal cell carcinoma (BCC) (Larsimont et al., 2015) as well as keratoacanthoma development (Zito et al., 2014).

Figure 2

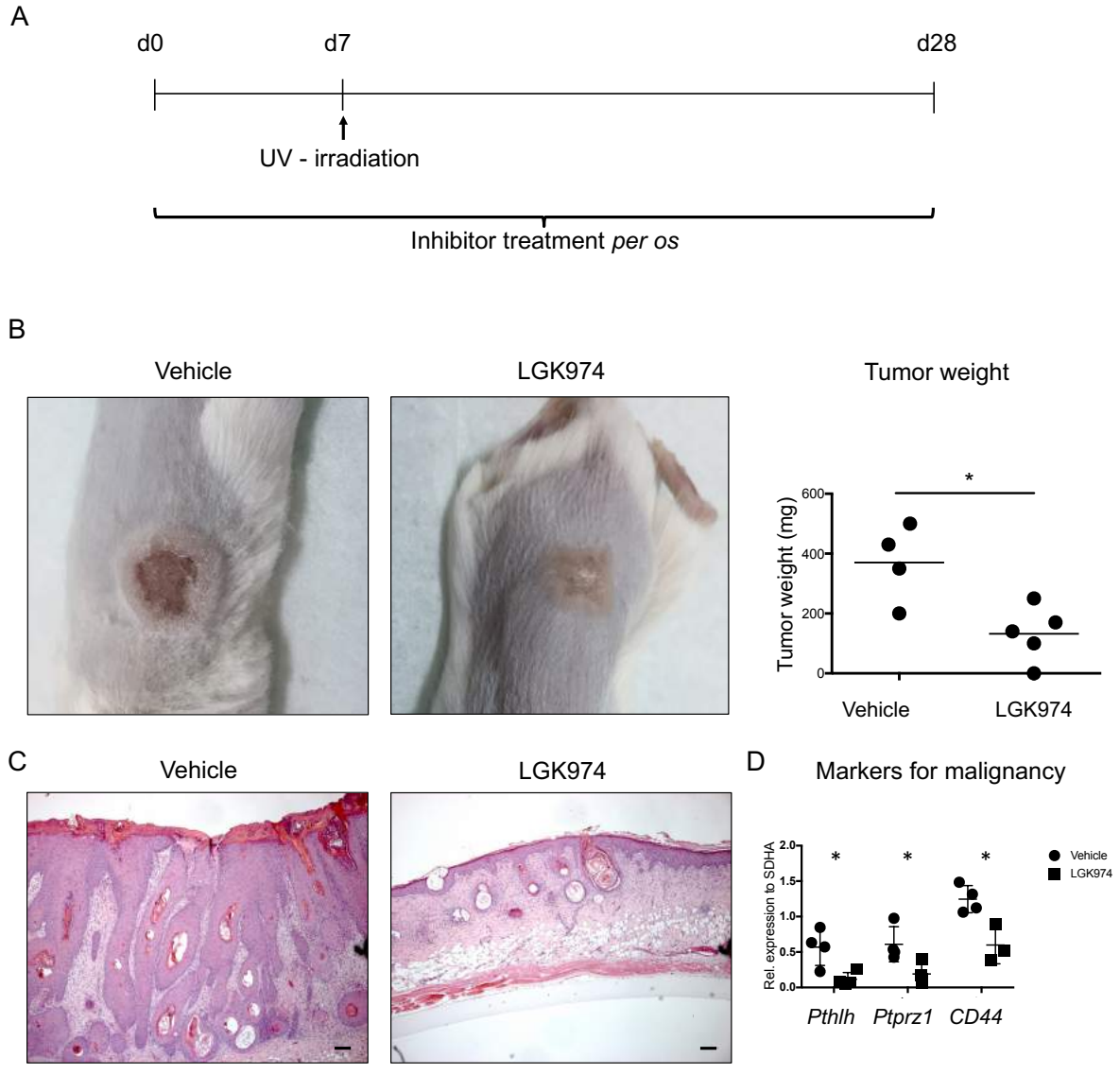

Figure 2: Inhibition of WNT secretion by the PORCN-inhibitor LGK974 impairs the initiation of HPV-driven cSCC.

(A) Experimental design. Treatment with LGK974 (6 mg/kg) or vehicle was started 7 days prior to tumor induction by UV-irradiation. Mice were treated daily until the endpoint at day 28. Control mice were treated with vehicle.

(B) Representative macroscopic display of a control (left panel) and LGK974-treated (middle panel) tumor. Tumor weight at endpoint (right panel). Unpaired Student's t-test, *p<0.05.

(C) H&E staining of control (left panel) and LGK974-treated (right panel) tumors. Scale bar = 100 µm.

(D) Quantification of transcripts for *Pthlh*, *Ptprz1* and *Cd44* in vehicle- and LGK974-treated tumors shows significant reduction of markers for tumor malignancy upon treatment. Unpaired Student's t-test, *p<0.05.

The Porcupine-inhibitor LGK974 was applied as described in (Liu et al., 2013b). Briefly, LGK974 was dissolved in DMSO and diluted in citrate buffer pH 3 to a final concentration of 1mg/ml. Mice were treated

daily with 6 mg/kg LGK974 or vehicle (20% DMSO in citrate buffer pH 3) *per os*.

This experiment was performed once with groups consisting of 4 untreated and 5 treated mice, representative images are shown.

Staining and qPCR Protocols were as described above. The primers used were *Pthlh*, fwd ATCCCCGACGCCTATGTAA, rev GGGGAAAAAGCAATCAGAGA; *Ptprz1*, fwd GCCAGTTGTTGTCCACTGC, rev CCTTTGAGAACGAATGTGCTT; *Cd44*, fwd CTCCTTCTTTATCCGGAGCAC, rev TGGCTTTTTGAGTGCACAGT.

Supplementary Figure 2

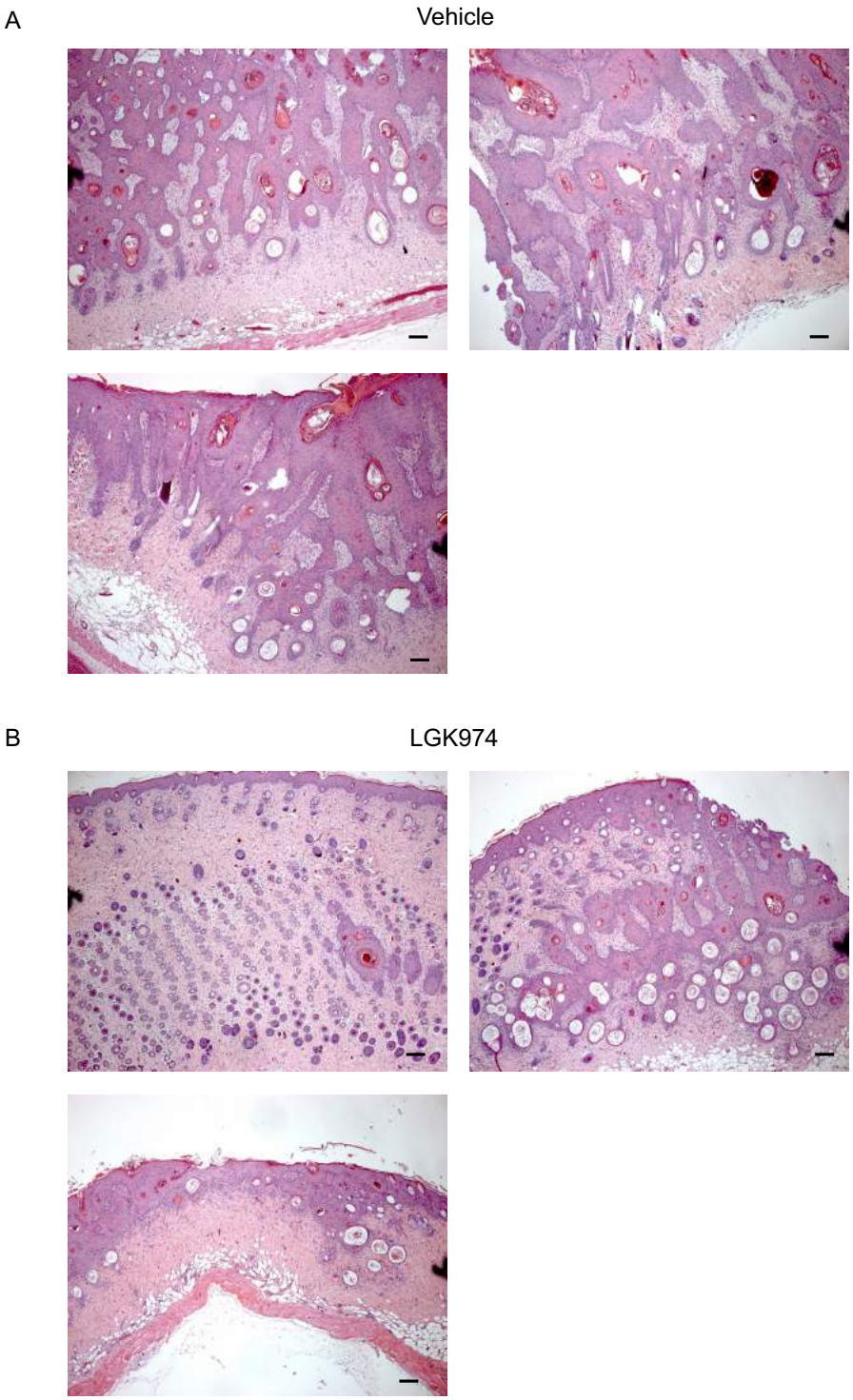

Supplementary figure 2: Tumors are replaced by hair follicles and keratin in mice treated with pre-emptive LGK974. Relates to Figure 2.

(A) H&E stained sections from 3 different tumors of mice treated with vehicle previous to UV-irradiation to induce tumors (see Figure 2A).

(B) H&E stained sections from 3 different UV-irradiated patches from mice treated with LGK974 previous to UV-irradiation (see Figure 2A).

This experiment was performed once with groups consisting of 4 untreated and 5 treated mice, representative images are shown.

Protocols were as described for the main figures.

WNTs promote progression of HPV-driven cSCC

Since preemptive inhibition of WNT secretion significantly reduced the development of HPV-driven cSCC, we investigated whether blocking WNT-secretion also interferes with tumor progression in established tumors (Fig 3A). We observed a marked reduction of nuclear staining for β-catenin in response to LGK974 treatment, indicative of reduced WNT/β-catenin signaling. This finding was corroborated by a reduction in *Axin2* expression, especially at the tumor-stroma interphase (Fig. 3B).

Although LGK974-treament did not macroscopically reduce tumor size, analysis of H&E-stained sections revealed that LGK974-treated tumors displayed a more differentiated morphology than vehicle-treated tumors (Fig. 3C). A good indicator of reduced malignancy and the differentiation status of cSCCs is the increased presence of keratin whorls (Yanofsky et al., 2011) and a reduced density of invasive cones (Wicki and Christofori, 2007). LGK974-treated tumors showed both: an increased density of keratin whorls and a loss of invasive cones (Fig. 3C). Furthermore, and in line with increased differentiation, LGK974-treated tumor cells proliferated less than control tumors as visualized by significantly reduced staining for Ki67 (Fig. 3D and supplementary Figure 3A). Together, our findings indicate that blocking WNT secretion promotes differentiation, and reduces proliferation as well as invasive potential of established HPV-driven cSCC.

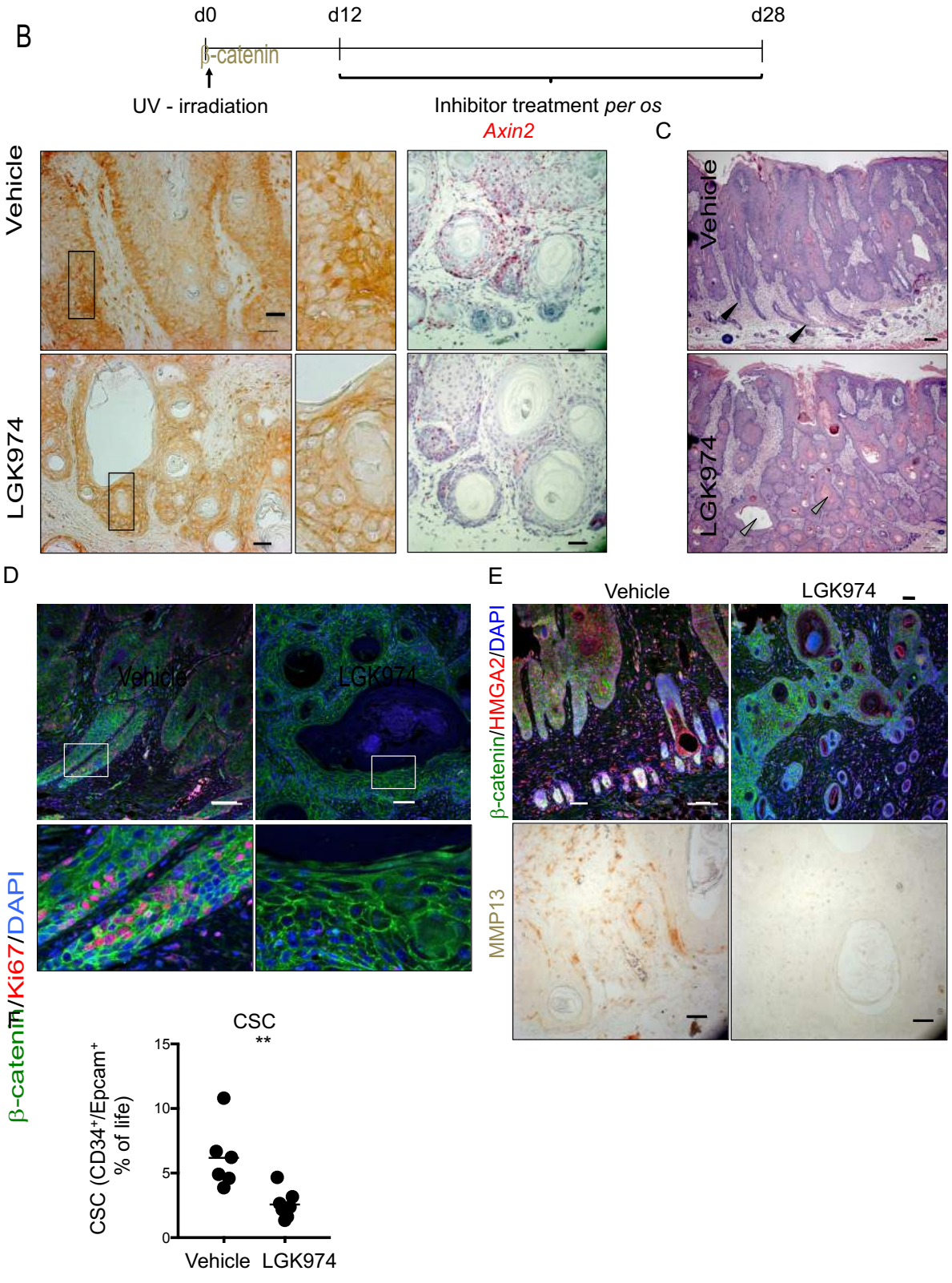
B
d0
d12
d28
β-catenin
UV - irradiation
Inhibitor treatment per os
Axin2
C
Vehicle
LGK974
D
E
β-catenin/Ki67/DAPI
β-catenin/HMGA2/DAPI
MMP13
CSC
**
CSC (CD34+/Epcam+ % of life)
15
10
5
0
Vehicle
LGK974

Figure 3: WNTs promote HPV-driven cSCC progression.

(A) Experimental design. Treatment with LGK974 (6 mg/kg) was started 12 days after tumor induction by UV-irradiation. Mice were treated daily until the endpoint at day 28. Control mice were treated with vehicle.

(B) β-catenin staining of vehicle- and LGK974-treated tumors. Nuclear β-catenin is reduced upon treatment. Middle panels show a magnification of the boxed area. Right panels show an in situ hybridization for *Axin2* (red), indicating a reduction of its expression upon treatment, nuclei are counterstained with hematoxylin (blue). Scale bars = 50 μm.

(C) Keratin whorls (grey arrowheads in lower panel) and loss of invading cones (black arrowheads in upper panel) indicate differentiation in H&E stained sections of vehicle- and LGK974-treated cSCC. Scale bar = 100 μm.

(D) Sections stained for Ki67 (red) as marker for proliferation and β-catenin (green) to outline the cells, nuclei are counterstained by DAPI. The staining shows a clear reduction of proliferating Ki67 positive cells upon treatment. Lower panels show a magnification of the boxed area. Scale bar = 100 μm.

(E) HMGA2 (red) is strongly reduced upon treatment in the tumors. β-catenin in green marks the cells, DAPI counterstains the nuclei in blue. Scale bar = 100 μm.

MMP13 expression is lost upon LGK974 treatment. Scale bar = 50 μm.

(F) Flow cytometric analysis of the percentage of CSC in comparison to live cells ($EpCAM^+$ $CD34^+$ $CD31^-$) in vehicle- and LGK974-treated cSCC. Unpaired Student's t-test, $^{**}p<0.01$. Groups consisted of 5 vehicle treated and 6 LGK974 treated mice. This experiment was performed twice with similar results.

Protocols were as described for Figure 1. For HMGA2 staining, the same protocol as for PORCN was used, for the MMP13 staining, the protocol for nuclear β-catenin staining was used.

PORCN inhibition decreases the malignant potential of HPV-driven cSCCs

To clarify the downstream effects of PORCN inhibition in HPV-driven cSCCs, we performed RNA-sequencing of LGK974- and vehicle-treated tumors (supplementary Figure 3B). Gene ontology analysis (The Gene Ontology Consortium, 2015) of the top deregulated transcripts ($p<0.05$) showed "regulation of keratinocyte migration" as the primary hit, which confirms our findings of reduced invasiveness and malignancy of the tumors upon LGK974 treatment (supplementary Figure 3D). In particular, we observed a significant downregulation of transcripts for matrix metalloproteinases (*Mmp9*, *Mmp10*, *Mmp13*) and upregulation of *Timp4*, which is an inhibitor of them (Wang et al., 1997), (supplementary Figure 3C).

Because we performed RNA sequencing on whole tumor tissues, we cannot draw conclusions about whether LGK974-treatment affects tumor cells, tumor infiltrating cells or both. To confirm some findings from the RNA-sequencing, as well as to clarify the cell type in which the changes occur, we used immunohistochemistry. Our observation that LGK974-treatment reduced the expression of HMGA2 in tumor cells suggested a tumor-intrinsic effect of PORCN-inhibition (Fig. 3E) but does not exclude that tumor-extrinsic effects occur. This was

demonstrated by the stark reduction of MMP13 in tumor as well as stromal tissue upon LGK974 administration (Fig. 3E). On the other hand, WNT secreted by PORCN positive cells may affect the expression of WNT target genes in the stromal compartment and the stromal MMP13 could of course be secreted from the tumor cells.

To check the effects of PORCN inhibition on CSCs in control and LGK974-treated tumors, we analyzed the cellular composition of tumors by flow cytometry. Blocking WNT-secretion resulted in the reduction of the $CD34^{+}$ $EpCAM^{+}$ $CD31^{-}$ CSC population (Schober and Fuchs, 2011), (Fig. 3F, supplementary Figure 3F). This was confirmed by antibody stainings for CD34 on tumor sections (supplementary Figure 3E), again underscoring the importance of WNT-secretion for CSC maintenance and thus tumor growth and malignancy.

Supplementary Figure 3

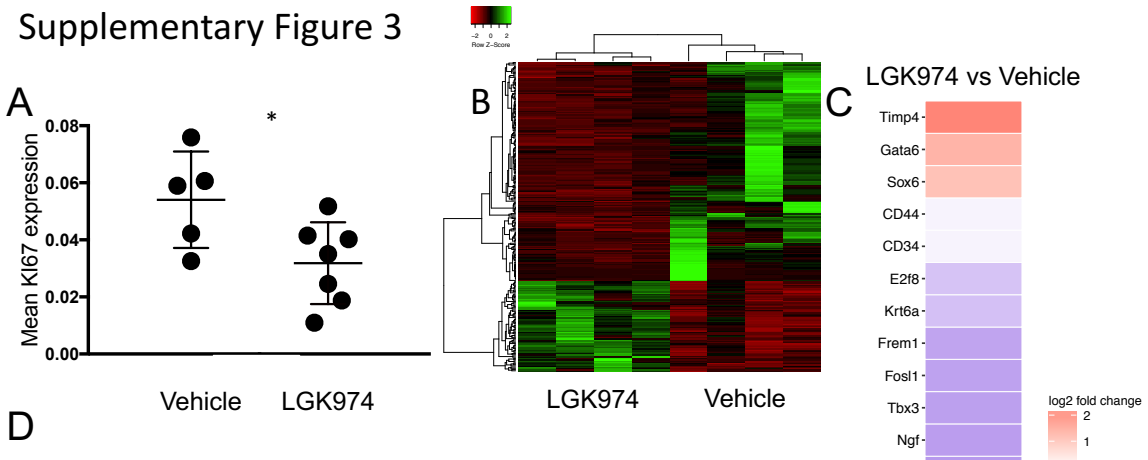

D

GO biological process complete: p<0.05 vehicle vs Lgk974	Gene number	Expected number	Fold Enrichment	P value
positive regulation of keratinocyte migration	4	0.09	45.74	1.78E-02
positive regulation of cell proliferation	28	9.36	2.99	2.48E-03

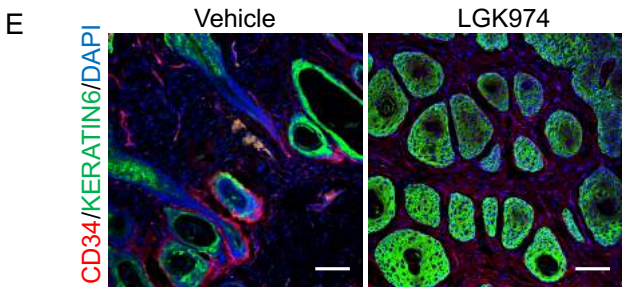

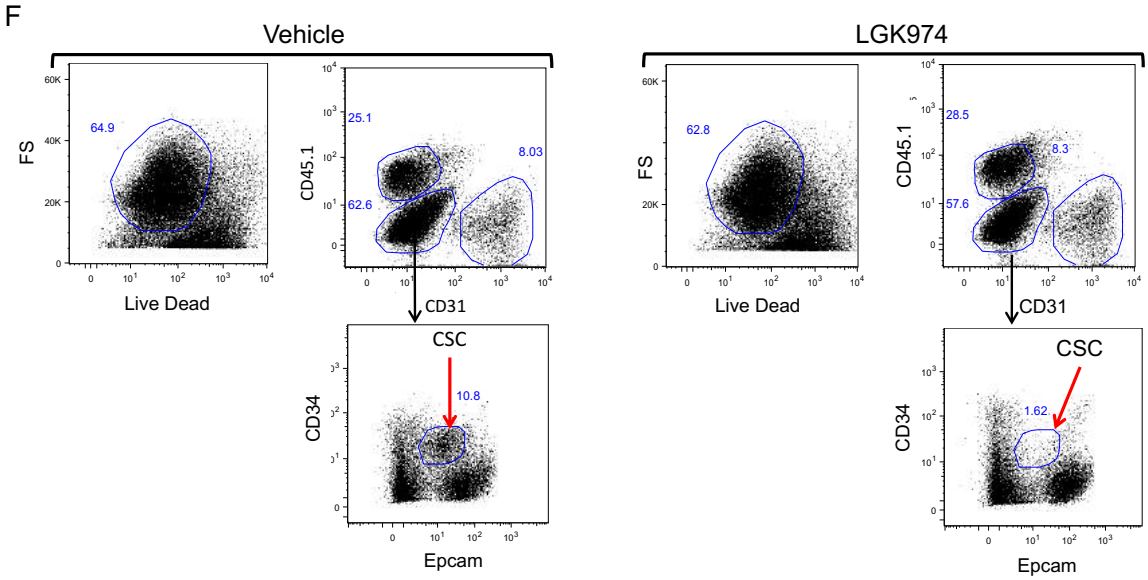

Supplementary figure 3: Treatment of HPV-driven cSCC with LGK974 reduces proliferative and invasive capacity of the tumors. Relates to Figure 3.

(A) Proliferation in epithelial areas of five LGK974- and four vehicle-treated tumors indicated by Ki67 staining (Figure 3D) and quantified using the Vectra 3.0 system (PerkinElmer). Unpaired Student's t-test, *$p<0.05$.

(B) Clustering analysis (average linkage, Pearson distance measurement) showing the differentially expressed genes (general linear model with negative binomial distribution, (quasi-likelyhood F-test) *$p<0.05$) from an RNA-sequencing experiment comparing four LGK974- with four vehicle-treated tumors.

(C) Heatmap showing selected differentially expressed genes associated with SCC malignancy in RNA-sequencing of four LGK974- and four vehicle-treated tumors.

(D) Gene ontology analysis of RNA-sequencing data comparing vehicle- and LGK974-treated HPV-driven cSCCs. Four independent samples for each condition were sequenced and analyzed.

(E) Staining for CD34 (red) and Keratin-6 (green) in LGK974- and vehicle- treated tumors. CD34 staining is lost upon treatment along the tumor-stroma interphase. Sections are counterstained with DAPI (blue). Scale bar = 100μm.

(F) FACS analysis of 6 LGK974- and 5 vehicle-treated tumors. Cells were stained for live/dead, CD45.1 (leukocytes), EpCAM (epithelial cells including tumor), CD31 (vascular endothelial cells) and CD34 (CSC). The $EpCAM^+$ $CD34^+$ CSC population is clearly reduced upon treatment (see also Figure 3G).

This experiment was performed twice with similar results.

The protocols used were as described for the main figures.

Conclusion

We investigated the pathways involved in tumorigenesis and growth of cSCCs that are driven by HPV. Our finding, that WNT-signaling is crucial for tumorigenesis is in line with work on cSCCs induced by chemical carcinogenesis (Malanchi et al., 2008b). Of note, in the case of cSCCs, no prominent activating mutations downstream of the WNT/β-catenin pathway components were found (Nassar et al., 2015), in contrast to classical WNT/β-catenin-dependent cancers like colon carcinomas (Nusse and Clevers, 2017). WNT/β-catenin activation in HPV-driven cSCC seems rather to be reached by upregulation of WNTs and factors such as PORCN that are required for their secretion. The combination is apparently crucial to maintain a proper CSC niche. Compelling evidence in support of this theory comes from a study by (Tammela et al., 2017), where they show that the CSC niche of lung adenocarcinomas is maintained by cells expressing high levels of PORCN. By using PORCN inhibitor on HPV-driven cSCCs, we show the addiction of these cancers for WNT secretion. Since inhibiting WNT secretion severely hampers tumorigenesis, PORCN inhibition might thus be a valuable preventive measure against cSCCs after organ transplantation and subsequent immunosuppression. The fact that not only cSCCs, but also lung

adenocarcinomas seem to upregulate PORCN to maintain a CSC niche asks for further investigation into this matter in further epithelial tumor types. It also draws attention towards the necessity to not only check the mutational landscape in tumors but also to carefully check changes in the transcriptome.

In conclusion, our results provide novel insights into the molecular details of HPV-driven cSCCs. They also reveal a possible therapeutic approach to prevent and treat this type of cancers.

ACKNOWLEDGEMENTS

We thank Karina Silina and Michal Beffinger (Institute of Experimental Immunology, UZH) for help with some experiments, Lukas Sommer (Institute of Anatomy, UZH) for reagents and discussions, Sabine Werner (Institute for Molecular Health Sciences, ETHZ) for discussions, sharing reagents and mouse strains *(Krt14*-HPV8-*E6*), Alexandra Franz for help with R and Martin Moser and Eliane Escher for technical support (Institute of Molecular Life Sciences, UZH). We thank the personnel of the Laboratory Animal Service Center from the University of Zurich for expert animal care. This work was supported by the Swiss National Science Foundation (SNF) (K.B., M.v.d.B), Swiss Cancer League (K.B.), the Promedica Foundation Zurich (M.v.d.B.), University of Zurich Research Priority Program "Translational Cancer Research" and the Kanton of Zürich (K.B., M.v.d.B.). V.C and T.V. are fellows in the URPP Translational Cancer Research Program.

AUTHOR CONTRIBUTIONS

T.V. and M.v.d.B. conceived the research. T.V. D.Z. and V.C. planned experiments and analyzed the data. D.Z. and V.C. performed experiments. G.R. and J.H. provided material. K.B, G.H. and C.C. discussed the data and gave scientific input. K.B. and M.v.d.B. initiated the project and secured funding. D.Z, T.V, G.H. and M.v.d.B wrote the manuscript.

CONFLICT OF INTEREST

The authors declare no conflict of interest.

Supplementary Information accompanies this paper on the Oncogene website (http://www.nature.com/onc).

REFERENCES

Accardi, R., and Gheit, T. (2014). Cutaneous HPV and skin cancer. Presse Médicale *43*: e435–e443.

Appelman-Dijkstra, N.M., and Papapoulos, S.E. (2016). Sclerostin Inhibition in the Management of Osteoporosis. Calcif. Tissue Int. *98*: 370–380.

Babicki, S., Arndt, D., Marcu, A., Liang, Y., Grant, J.R., Maciejewski, A., et al. (2016). Heatmapper: web-enabled heat mapping for all. Nucleic Acids Res. *44*: W147–W153.

Bänziger, C., Soldini, D., Schütt, C., Zipperlen, P., Hausmann, G., and Basler, K. (2006). Wntless, a Conserved Membrane Protein Dedicated to the Secretion of Wnt Proteins from Signaling Cells. Cell *125*: 509–522.

Beck, B., Driessens, G., Goossens, S., Youssef, K.K., Kuchnio, A., Caauwe, A., et al. (2011). A vascular niche and a VEGF–Nrp1 loop regulate the initiation and stemness of skin tumours. Nature *478*: 399–403.

Cantù, C., Pagella, P., Shajiei, T.D., Zimmerli, D., Valenta, T., Hausmann, G., et al. (2017). A cytoplasmic role of Wnt/β-catenin transcriptional cofactors Bcl9, Bcl9l, and Pygopus in tooth enamel formation. Sci. Signal. *10*: eaah4598.

Cantù, C., Zimmerli, D., Hausmann, G., Valenta, T., Moor, A., Aguet, M., et al. (2014). Pax6-dependent, but β-catenin-independent, function of Bcl9 proteins in mouse lens development. Genes Dev. *28*: 1879–1884.

Chockalingam, R., Downing, C., and Tyring, S. (2015). Cutaneous Squamous Cell Carcinomas in Organ Transplant Recipients. J. Clin. Med. *4*: 1229–1239.

Connolly, K., Manders, P., Earls, P., and Epstein, R.J. (2014). Papillomavirus-associated squamous skin cancers following transplant immunosuppression: one Notch closer to control. Cancer Treat. Rev. *40*: 205–214.

Deka, J., Wiedemann, N., Anderle, P., Murphy-Seiler, F., Bultinck, J., Eyckerman, S., et al. (2010). Bcl9/Bcl9l are critical for Wnt-mediated regulation of stem cell traits in colon epithelium and adenocarcinomas. Cancer Res. *70*: 6619–6628.

Haegebarth, A., and Clevers, H. (2009). Wnt Signaling, Lgr5, and Stem Cells in the Intestine and Skin. Am. J. Pathol. *174*: 715–721.

Herr, P., and Basler, K. (2012). Porcupine-mediated lipidation is required for Wnt recognition by Wls. Dev. Biol. *361*: 392–402.

Hofbauer, G.F.L., Bavinck, J.N.B., and Euvrard, S. (2010). Organ transplantation and skin cancer: basic problems and new perspectives: Organ transplantation and skin cancer. Exp. Dermatol. *19*: 473–482.

Huelsken, J., Vogel, R., Erdmann, B., Cotsarelis, G., and Birchmeier, W. (2001a). beta-Catenin controls hair follicle morphogenesis and stem cell differentiation in the skin. Cell *105*: 533–545.

Huelsken, J., Vogel, R., Erdmann, B., Cotsarelis, G., and Birchmeier, W. (2001b). ?-Catenin Controls Hair Follicle Morphogenesis and Stem Cell Differentiation in the Skin. Cell *105*: 533–545.

Jho, E., Zhang, T., Domon, C., Joo, C.-K., Freund, J.-N., and Costantini, F. (2002). Wnt/beta-catenin/Tcf signaling induces the transcription of Axin2, a negative regulator of the signaling pathway. Mol. Cell. Biol. *22*: 1172–1183.

Kahn, M. (2014). Can we safely target the WNT pathway? Nat. Rev. Drug Discov. *13*: 513–532.

Kasper, M., Jaks, V., Are, A., Bergström, Å., Schwäger, A., Svärd, J., et al. (2011). Wounding enhances epidermal tumorigenesis by recruiting hair follicle keratinocytes. Proc. Natl. Acad. Sci. U. S. A. *108*: 4099–4104.

Kramps, T., Peter, O., Brunner, E., Nellen, D., Froesch, B., Chatterjee, S., et al. (2002). Wnt/wingless signaling requires BCL9/legless-mediated recruitment of pygopus to the nuclear beta-catenin-TCF complex. Cell *109*: 47–60.

Lapouge, G., Beck, B., Nassar, D., Dubois, C., Dekoninck, S., and Blanpain, C. (2012). Skin squamous cell carcinoma propagating cells increase with tumour progression and invasiveness: Tumour propagating cells in skin cancers. EMBO J. *31*: 4563–4575.

Larsimont, J.-C., Youssef, K.K., Sánchez-Danés, A., Sukumaran, V., Defrance, M., Delatte, B., et al. (2015). Sox9 Controls Self-Renewal of Oncogene Targeted Cells and Links Tumor Initiation and Invasion. Cell Stem Cell *17*: 60–73.

Latil, M., Nassar, D., Beck, B., Boumahdi, S., Wang, L., Brisebarre, A., et al. (2017). Cell-Type-Specific Chromatin States Differentially Prime Squamous Cell Carcinoma Tumor-Initiating Cells for Epithelial to Mesenchymal Transition. Cell Stem Cell *20*: 191–204.e5.

Lim, X., and Nusse, R. (2013). Wnt Signaling in Skin Development, Homeostasis, and Disease. Cold Spring Harb. Perspect. Biol. *5*: a008029–a008029.

Liu, J., Pan, S., Hsieh, M.H., Ng, N., Sun, F., Wang, T., et al. (2013a). Targeting Wnt-driven cancer through the inhibition of Porcupine by LGK974. Proc. Natl. Acad. Sci. *110*: 20224–20229.

Liu, J., Pan, S., Hsieh, M.H., Ng, N., Sun, F., Wang, T., et al. (2013b). Targeting Wnt-driven cancer through the inhibition of Porcupine by LGK974. Proc. Natl. Acad. Sci. *110*: 20224–20229.

Malanchi, I., Peinado, H., Kassen, D., Hussenet, T., Metzger, D., Chambon, P., et al. (2008a). Cutaneous cancer stem cell maintenance is dependent on beta-catenin signalling. Nature *452*: 650–653.

Malanchi, I., Peinado, H., Kassen, D., Hussenet, T., Metzger, D., Chambon, P., et al. (2008b). Cutaneous cancer stem cell maintenance is dependent on β-catenin signalling. Nature *452*: 650–653.

Marcuzzi, G.P., Hufbauer, M., Kasper, H.U., Weissenborn, S.J., Smola, S., and Pfister, H. (2009a). Spontaneous tumour development in human papillomavirus type 8 E6 transgenic mice and rapid induction by UV-light exposure and wounding. J. Gen. Virol. *90*: 2855–2864.

Marcuzzi, G.P., Hufbauer, M., Kasper, H.U., Weissenborn, S.J., Smola, S., and Pfister, H. (2009b). Spontaneous tumour development in human papillomavirus type 8 E6 transgenic mice and rapid induction by UV-light exposure and wounding. J. Gen. Virol. *90*: 2855–2864.

Moor, A.E., Anderle, P., Cantù, C., Rodriguez, P., Wiedemann, N., Baruthio, F., et al. (2015). BCL9/9L-β-catenin Signaling is Associated With Poor Outcome in Colorectal Cancer. EBioMedicine *2*: 1932–1943.

Nassar, D., Latil, M., Boeckx, B., Lambrechts, D., and Blanpain, C. (2015). Genomic landscape of carcinogen-induced and genetically induced mouse skin squamous cell carcinoma. Nat. Med. *21*: 946–954.

Nichols, A.J., Allen, A.H., Shareef, S., Badiavas, E.V., Kirsner, R.S., and Ioannides, T. (2017). Association of Human Papillomavirus Vaccine With the Development of Keratinocyte Carcinomas. JAMA Dermatol.

Nusse, R., and Clevers, H. (2017). Wnt/β-Catenin Signaling, Disease, and Emerging Therapeutic Modalities. Cell *169*: 985–999.

Oshimori, N., Oristian, D., and Fuchs, E. (2015). TGF-β Promotes Heterogeneity and Drug Resistance in Squamous Cell Carcinoma. Cell *160*: 963–976.

Pourreyron, C., Reilly, L., Proby, C., Panteleyev, A., Fleming, C., McLean, K., et al. (2012). Wnt5a Is Strongly Expressed at the Leading Edge in Non-Melanoma Skin Cancer, Forming Active Gradients, while Canonical Wnt Signalling Is Repressed. PLoS ONE *7*: e31827.

Powell, S.M., Zilz, N., Beazer-Barclay, Y., Bryan, T.M., Hamilton, S.R., Thibodeau, S.N., et al. (1992). APC mutations occur early during colorectal tumorigenesis. Nature *359*: 235–237.

Schaper, I.D. (2005). Development of Skin Tumors in Mice Transgenic for Early Genes of Human Papillomavirus Type 8. Cancer Res. *65*: 1394–1400.

Schilling, S., Steiner, S., Zimmerli, D., and Basler, K. (2014). A regulatory receptor network directs the range and output of the Wingless signal. Development *141*: 2483–2493.

Schober, M., and Fuchs, E. (2011). Tumor-initiating stem cells of squamous cell carcinomas and their control by TGF- and integrin/focal adhesion kinase (FAK) signaling. Proc. Natl. Acad. Sci. *108*: 10544–10549.

Shiokawa, D., Sato, A., Ohata, H., Mutoh, M., Sekine, S., Kato, M., et al. (2017). The Induction of Selected Wnt Target Genes by Tcf1 Mediates Generation of Tumorigenic Colon Stem Cells. Cell Rep. *19*: 981–994.

Singh, A., and Settleman, J. (2010). EMT, cancer stem cells and drug resistance: an emerging axis of evil in the war on cancer. Oncogene *29*: 4741–4751.

Sousa e Melo, F. de, and Vermeulen, L. (2016). Wnt Signaling in Cancer Stem Cell Biology. Cancers *8*: 60.

Sun, P., Watanabe, K., Fallahi, M., Lee, B., Afetian, M.E., Rheaume, C., et al. (2014). Pygo2 regulates -catenin-induced activation of hair follicle stem/progenitor cells and skin hyperplasia. Proc. Natl. Acad. Sci. *111*: 10215–10220.

Sun, Y., Campisi, J., Higano, C., Beer, T.M., Porter, P., Coleman, I., et al. (2012). Treatment-induced damage to the tumor microenvironment promotes prostate cancer therapy resistance through WNT16B. Nat. Med. *18*: 1359–1368.

Sun, Y., Zhu, D., Chen, F., Qian, M., Wei, H., Chen, W., et al. (2016). SFRP2 augments WNT16B signaling to promote therapeutic resistance in the damaged tumor microenvironment. Oncogene *35*: 4321–4334.

Tammela, T., Sanchez-Rivera, F.J., Cetinbas, N.M., Wu, K., Joshi, N.S., Helenius, K., et al. (2017). A Wnt-producing niche drives proliferative potential and progression in lung adenocarcinoma. Nature *545*: 355–359.

The Gene Ontology Consortium (2015). Gene Ontology Consortium: going forward. Nucleic Acids Res. *43*: D1049–D1056.

Valenta, T., Degirmenci, B., Moor, A.E., Herr, P., Zimmerli, D., Moor, M.B., et al. (2016). Wnt Ligands Secreted by Subepithelial Mesenchymal Cells Are Essential for the Survival of Intestinal Stem Cells and Gut Homeostasis. Cell Rep. *15*: 911–918.

Valenta, T., Gay, M., Steiner, S., Draganova, K., Zemke, M., Hoffmans, R., et al. (2011). Probing transcription-specific outputs of -catenin in vivo. Genes Dev. *25*: 2631–2643.

Wang, M., Liu, Y.E., Greene, J., Sheng, S., Fuchs, A., Rosen, E.M., et al. (1997). Inhibition of tumor growth and metastasis of human breast cancer cells transfected with tissue inhibitor of metalloproteinase 4. Oncogene *14*: 2767–2774.

Washington Smoak, I., Byrd, N.A., Abu-Issa, R., Goddeeris, M.M., Anderson, R., Morris, J., et al. (2005). Sonic hedgehog is required for cardiac outflow tract and neural crest cell development. Dev. Biol. *283*: 357–372.

Wicki, A., and Christofori, G. (2007). The potential role of podoplanin in tumour invasion. Br. J. Cancer *96*: 1–5.

Yanofsky, V.R., Mercer, S.E., and Phelps, R.G. (2011). Histopathological Variants of Cutaneous Squamous Cell Carcinoma: A Review. J. Skin Cancer *2011*: 1–13.

Zimmerli, D., Hausmann, G., Cant?, C., and Basler, K. (2017a). Pharmacological interventions in the Wnt pathway: inhibition of Wnt secretion versus disrupting the protein-protein interfaces of nuclear factors: Inhibition of the Wnt pathway. Br. J. Pharmacol.

Zimmerli, D., Hausmann, G., Cantù, C., and Basler, K. (2017b). Pharmacological interventions in the Wnt pathway: Inhibition of Wnt secretion versus disrupting the protein-protein interfaces of nuclear factors: Inhibition of the Wnt pathway. Br. J. Pharmacol.

Zito, G., Saotome, I., Liu, Z., Ferro, E.G., Sun, T.Y., Nguyen, D.X., et al. (2014). Spontaneous tumour regression in keratoacanthomas is driven by Wnt/retinoic acid signalling cross-talk. Nat. Commun. *5*:.

Pax6-dependent, but β-catenin-independent, function of Bcl9 proteins in mouse lens development

Claudio Cantù [1], Dario Zimmerli [1], George Hausmann [1], Tomas Valenta [1], Andreas Moor [2], Michel Aguet [2], Konrad Basler [1]

[1)] Institute of Molecular Life Sciences, University of Zurich, Winterthurerstrasse 190, 8057 Zurich, Switzerland

[2)] Swiss Institute for Experimental Cancer Research, Ecole Polytechnique Fédérale de Lausanne, School of Life Sciences, Lausanne, Switzerland

Running title: β-catenin independent function of Bcl9/9l

Correspondence: basler@imls.uzh.ch

RESEARCH COMMUNICATION

Pax6-dependent, but β-catenin-independent, function of Bcl9 proteins in mouse lens development

Claudio Cantù,[1] Dario Zimmerli,[1] George Hausmann,[1] Tomas Valenta,[1] Andreas Moor,[2] Michel Aguet,[2] and Konrad Basler[1]

[1]Institute of Molecular Life Sciences, University of Zurich, 8057 Zurich, Switzerland; [2]Swiss Institute for Experimental Cancer Research, Ecole Polytechnique Fédérale de Lausanne, School of Life Sciences, 1011 Lausanne, Switzerland

***Bcl9* and *Bcl9l* (*Bcl9/9l*) encode Wnt signaling components that mediate the interaction between β-catenin and Pygopus (Pygo) via two evolutionarily conserved domains, HD1 and HD2, respectively. We generated mouse strains lacking these domains to probe the β-catenin-dependent and β-catenin-independent roles of Bcl9/9l and Pygo during mouse development. While lens development is critically dependent on the presence of the HD1 domain, it is not affected by the lack of the HD2 domain, indicating that Bcl9/9l act in this context in a β-catenin-independent manner. Furthermore, we uncover a new regulatory circuit in which Pax6, the master regulator of eye development, directly activates *Bcl9/9l* transcription.**

Supplemental material is available for this article.

Received May 26, 2014; revised version accepted August 8, 2014.

Pygopus (Pygo) and Legless (Lgs) were discovered as dedicated Wnt signaling components in *Drosophila* (Kramps et al. 2002; Parker et al. 2002; Thompson et al. 2002) and *Xenopus* (Belenkaya et al. 2002). In *Drosophila*, *pygo* and *lgs* are classified as segment polarity genes, and mutations in their coding sequences lead to a dramatic developmental arrest, reminiscent of *wingless* mutations (Kramps et al. 2002; Parker et al. 2002; Thompson et al. 2002). They are considered to serve as dedicated and essential β-catenin transcriptional coactivators. Lgs simultaneously binds Pygo and Arm/β-catenin via two evolutionarily conserved homology domains, HD1 and HD2, respectively (Kramps et al. 2002). The prevailing model is that Pan/TCF > Arm/β-catenin > Lgs > Pygo serially recruit each other to the DNA in order to efficiently activate Wnt target gene expression, forming a "chain of adaptors." In this model, the sole function of Lgs is to recruit Pygo to β-catenin (Städeli and Basler 2005).

Vertebrates feature two *pygo* genes, *PYGO1* and *PYGO2*, and two *lgs* homologs, *BCL9* and *BCL9l* (*BCL9/9l*). In contrast to β-catenin loss-of-function mutants, *Pygo1/Pygo2* double-knockout mice proceed normally throughout gastrulation and die later during embryonic development from a series of tissue-specific defects. *Pygo1* knockout mice are viable and fertile, with no apparent phenotype. Compound *Pygo1/Pygo2* knockout mutants are indistinguishable from *Pygo2* knockout, suggesting that Pygo2 plays the more important role during development (Li et al. 2007; Schwab et al. 2007; M Aguet, unpubl.). Unlike in *Drosophila*, in mice, Pygo1 and Pygo2 are now considered to be tissue-specific Wnt pathway components.

Bcl9/9l are necessary for the expression of Wnt targets in normal intestinal epithelia (Deka et al. 2010) and the myogenic progenitors during muscle regeneration, where a reduction of Bcl9/9l inhibits the Wnt-driven myogenic differentiation (Brack et al. 2009): This indicates that Bcl9/9l are required for the expression of key subsets of β-catenin target genes. Consistent with this, mutating β-catenin such that it cannot bind Bcl9/9l (β-catenin-D164A) results in embryonic lethality at mid-gestation, around embryonic day 10.5 (Valenta et al. 2011). In addition, a growing body of evidence indicates that Bcl9/9l and their interaction with β-catenin are important not only for normal cell functions but also in different types of tumors (Mani et al. 2009; Deka et al. 2010; Brembeck et al. 2011; Takada et al. 2012). When their interaction is abrogated in these tumors, an attenuated migratory potential is observed, accompanied by a decrease in the expression of the $Lgr5^+$-associated stem cell genes (de la Roche et al. 2012; Kawamoto et al. 2012; A Moor, P Anderle, C Cantù, N Wiedemann, F Baruthio, P Rodriguez, J Deka, S André, T Valenta, B Györffy, et al., in prep.). The conclusion from these studies was that, in mammals, Bcl9/9l retains a critical global function for β-catenin-mediated target gene control, at least in a tissue-specific manner. Based on comparison with the Pygo2 knockout situation, this role can be considered, at least in part, Pygo-independent. However, the molecular function of Bcl9/9l during mammalian development and tissue homeostasis remains largely unexplored.

Here we present an analysis of a series of *Bcl9/9l* knock-in mouse strains in which, via the deletion of the HD1 or HD2 domains, Bcl9/9l lose the ability to bind Pygo or β-catenin, respectively. We found that both interactions are relevant for development, and their individual disruption leads to embryonic lethality. Unexpectedly, however, we found that Bcl9/9l contribute in a Pygo-dependent, but β-catenin-independent, fashion to eye lens formation, revealing for the first time that Bcl9/9l have functions that are separate from canonical Wnt signaling. Moreover, we provide molecular evidence for a novel genetic circuit containing Bcl9/9l and Pygo that does not involve β-catenin: Pax6, the master regulator of eye differentiation, directly activates *Bcl9* and *Bcl9l* transcription. Pygo2 is required for the function of Bcl9/9l, and the Bcl9/9l–Pygo2 complex appears to sustain Pax6 expression. This reveals that, independently of canonical Wnt signaling, Bcl9/9l and Pygo2 constitute a critical molecular unit that responds to tissue-specific regulators, such as, in the lens, the Pax6 transcription factor.

[*Keywords*: Wnt; mouse; Bcl9; Pygopus; lens induction; Pax6]
Corresponding author: basler@imls.uzh.ch
Article is online at http://www.genesdev.org/cgi/doi/10.1101/gad.246140.114.

Results and Discussion

Pygo2 is assumed to be recruited by Bcl9/9l to promote the output of the Wnt signaling pathway. However, clear evidence that the Bcl9/9l–Pygo2 interaction is relevant during mammalian development is lacking. To specifically investigate this, we generated constitutive knock-in *Bcl9* and *Bcl9l* alleles that carry an in-frame deletion of the conserved HD1 (Fig. 1A; Supplemental Fig. S1), the domain responsible for binding to Pygo proteins (Kramps et al. 2002; Städeli and Basler 2005; Fiedler et al. 2008). This deletion abrogates the recruitment of Pygo proteins to the β-catenin transcriptional complex (Fig. 1A; Mosimann et al. 2009). Indeed, via GST pull-down assays, we confirmed that a Bcl9 protein lacking the HD1, when incubated with total protein extracts obtained from 12.5-d post-coitum (dpc) embryos, fails to bind Pygo2 but still binds β-catenin (Fig. 1B), supporting the validity of the rationale and indicating that a deletion of this domain does not lead to improper folding of the protein. Pygo1 was not detectable in our experiments, consistent with the previous finding that it is only weakly expressed later during embryonic development (Li et al. 2004). For this reason, in our study, we only considered the contribution of Pygo2.

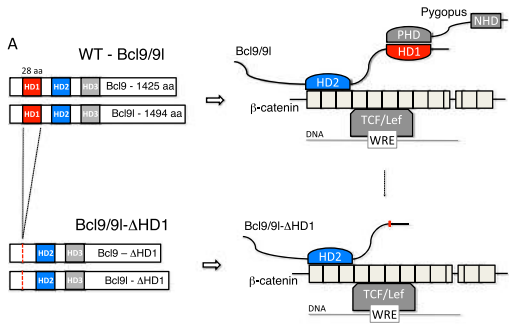

Bcl9/9l wt copies	Expected ratio	13.5 dpc (TOTAL=51)	14-15.5 dpc (TOTAL=75)	Adult (TOTAL=60)
4/4	1/16	4	4	5
3/4	4/16	13	18	23
2/4	6/16	16	39	26
1/4	4/16	15	14	4
0/4	1/16	3	0	0

Figure 1. The Bcl9/9l–Pygo2 interaction is necessary during mouse embryonic development. (*A*) Wild-type and ΔHD1 mutant Bcl9 and Bcl9l proteins; at the *right* is presented the variation in the "chain of adaptors" induced by the deletion of the HD1 domain. (WRE) Wnt-responsive element; (PHD) plant homeodomain; (NHD) N-terminal homology domain. (*B*) A GST-Bcl9-ΔHD1 protein, when incubated with protein extracts obtained from 12.5-dpc wild-type embryos, loses the ability to interact with Pygo2 but maintains the ability to pull down β-catenin; nonspecific signal (n.s.), obtained with Pygo2 antibody, was used as a loading control. (*C*) Crossings between double-heterozygous mice: All of the possible genetic combinations are grouped based on the number of wild-type alleles of *Bcl9/9l*, from four out of four to zero out of four. Double-homozygous ΔHD1 mutant mice (*Bcl9/9l*-ΔHD1) are never found after 13.5 dpc, indicating embryonic lethality. (*D*) *Bcl9/9l*-ΔHD1 mice at 13.5 dpc appear slightly smaller but do not display any obvious developmental defect, apart from an eye malformation (see Fig. 2), when compared with control littermates (wild type [WT]).

Double-heterozygous knock-in mice ($Bcl9^{\Delta HD1/+}$; $Bcl9l^{\Delta HD1/+}$) develop normally and do not display any obvious defect. Interestingly, mice homozygous mutant only in either *Bcl9* or *Bcl9l* (that is, $Bcl9^{\Delta HD1/\Delta HD1}$; $Bcl9l^{+/+}$ and $Bcl9^{+/+}$; $Bcl9l^{\Delta HD1/\Delta HD1}$) are born in ~50% of the expected Mendelian ratios. This indicates a substantial redundancy between Bcl9 and Bcl9l, at least concerning the functions mediated by the HD1. In contrast, no double-homozygous mutants ($Bcl9^{\Delta HD1/\Delta HD1}$; $Bcl9l^{\Delta HD1/\Delta HD1}$) were ever found later than 13.5 dpc (Fig. 1D), indicating embryonic lethality at this stage. Throughout the study, to simplify the analysis and strengthen the validity of the conclusion drawn, we investigate the effects of the simultaneous deletion in both genes and refer to these mice as *Bcl9/9l*-ΔHD1.

Of note, the complete loss of Bcl9/9l (*Bcl9/9l* knockout) causes an earlier lethality, occurring between 9.5 and 10.5 dpc (Supplemental Fig. S2; M Aguet, unpubl.); this suggests the interesting notion that, between 9.5 and 13.5 dpc, Bcl9/9l have Pygo-independent functions. *Bcl9/9l*-ΔHD1 mutant embryos at 13.5 dpc are slightly smaller than the control embryos (Fig. 1C); the cause of the lethality is currently under investigation. Remarkably, the timing of the embryonic lethality of *Bcl9/9l*-ΔHD1 mice is similar to that of *Pygo1/Pygo2* knockout embryos (Supplemental Fig. S3). The time point differs slightly from that previously reported (Li et al. 2007; Schwab et al. 2007). This minor difference may be due to an influence of the genetic background or a difference between the independently generated genomic manipulations. These results indicate that an important aspect of Bcl9/9l function is mediated by the HD1 domain. With the caveat that other, so far unrecognized proteins may also interact with Bcl9/9l via the HD1 domain, the results show that the Pygo2–Bcl9/9l interaction is required for mouse development as of 13.5 dpc.

An aspect in which the *Bcl9/9l*-ΔHD1 embryos are identical to the *Pygo2* knockout ones is that they display an obvious eye defect: The lens is absent (Fig. 2). Of note, the developing eye is one of the head structures displaying a marked expression of both Bcl9 and Bcl9l (Supplemental Fig. S4). The lens defect also often appears in triple-mutant mice, which retain only one wild-type allele of *Bcl9* or *Bcl9l* (that is $Bcl9^{+/\Delta HD1}$; $Bcl9l^{\Delta HD1/\Delta HD1}$ and $Bcl9^{\Delta HD1/\Delta HD1}$; $Bcl9l^{+/\Delta HD1}$). Interestingly, such genetic combinations most often lead only to a unilateral lens loss, a further indication that Bcl9 and Bcl9l are highly redundant with respect to the functions mediated by Pygo2 binding.

During eye development, the surface head ectoderm thickens to form the lens placode and at 10.5 dpc invaginates to generate the lens pit (Lang 2004). In *Bcl9/9l*-ΔHD1 embryos, lens development is blocked at this stage: The surface head ectoderm does not form the eye placode, the first morphological sign of lens development (Fig. 2, bottom panels), indicating that the Bcl9/9l–Pygo2 complex is required early at the onset of lens formation. Also, in *Bcl9/9l* knockout embryos, lens development is arrested at this stage (Supplemental Fig. S2E,F).

Interestingly, a positive role of Bcl9/9l in lens formation is in contradiction with the notion that Wnt signaling must be turned off during lens development (Smith et al. 2005; Machon et al. 2010). Therefore, we reasoned

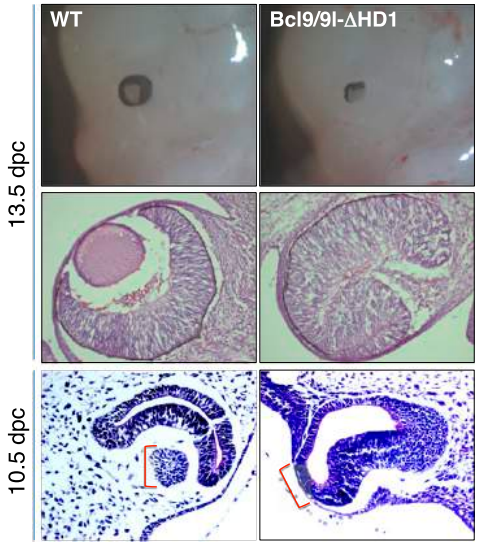

Figure 2. Bcl9/9l has a role in early lens development. (*Top* panels) *Bcl9/9l*-ΔHD1 double-mutant embryos display an eye defect highly reminiscent of the one previously described for Pygo2 loss of function (Song et al. 2007). (*Middle* panels) The dissection of the eye structure at this stage (i.e., 13.5 dpc) shows a complete absence of the lens accompanied by an enlarged developing retina, a feature that resembles the lens-specific conditional loss of Pax6 (Ashery-Padan 2000). (*Bottom* panels) *Bcl9/9l*-ΔHD1 mutant embryos at 10.5 dpc fail to induce eye placode thickening and subsequent lens pit formation. A square bracket indicates the lens vesicle in the wild-type (WT) eye and the region of the surface head ectoderm that, in *Bcl9/9l*-ΔHD1 mutants, despite lying close to the optic vesicle, fails to form a lens placode.

that Bcl9/9l might not act as Wnt signaling components in this tissue. This hypothesis predicts that, if Bcl9/9l can still bind Pygo2 but not β-catenin, the lens will develop correctly. To assess this possibility, we created a knock-in mouse strain carrying an in-frame deletion of HD2 (ΔHD2) in *Bcl9* and *Bcl9l* (Fig. 3A; Supplemental Fig. S5): We and others have previously shown that, in the absence of the HD2 domain, Bcl9/9l can still bind to Pygo2 but not to β-catenin (Fig. 3B; Kramps et al. 2002; Städeli and Basler 2005).

Of note, double-mutant embryos ($Bcl9^{\Delta HD2/\Delta HD2}$; $Bcl9l^{\Delta HD2/\Delta HD2}$, referred to as *Bcl9/9l*-ΔHD2), die at ~10.5 dpc, earlier than *Bcl9/9l*-ΔHD1 mutants (Fig. 3C). This is consistent with the lethality caused by the β-catenin-D164A mutation, which also abrogates the Bcl9/9l–β-catenin interaction (Valenta et al. 2011). A corollary of this is that early Bcl9/9l functions are independent of Pygo2 but are mediated by β-catenin; in other words, a truncated "chain of adaptors" lacking Pygo2 can sustain mouse development until at least embryonic day 13.5.

In order to investigate whether the loss of the Bcl9/9l–β-catenin interaction also blocks lens formation at 10.5 dpc, we compared eye development in *Bcl9/9l* wild-type, *Bcl9/9l*-ΔHD1, and *Bcl9/9l*-ΔHD2 embryos (Fig. 3E). In wild-type embryos at 10.5 dpc, the lens pit is clearly distinguishable. In *Bcl9/9l*-ΔHD1 mutants, the lens pit is not forming. Importantly, in *Bcl9/9l*-ΔHD2 embryos, the lens pit is developing normally (Fig. 3E, right panel). This result indicates that, during lens formation, the Bcl9/9l–Pygo2 complex functions independently of the physical interaction with β-catenin.

In addition, we incorporated the *lens-cre* transgene, a widely used lens-specific Cre recombinase driver (Ashery-Padan et al. 2000), to generate $Bcl9^{\Delta HD1/flox}$; $Bcl9l^{\Delta HD1/flox}$; $lens\text{-}cre^{Tg/+}$ (lens-ΔHD1) and $Bcl9^{\Delta HD2/flox}$; $Bcl9l^{\Delta HD2/flox}$; $lens\text{-}cre^{Tg/+}$ (lens-ΔHD2) mice. Compared with control animals, at birth, lens-ΔHD1 mice have smaller lenses. The same effect is obtained upon the complete loss of Bcl9/9l in the lens in $Bcl9^{flox/flox}$; $Bcl9l^{flox/flox}$; $lens\text{-}cre^{Tg/+}$. This is in agreement with data from Song et al. (2007), who found that *lens-cre*-driven Pygo2 deletion does not entirely recapitulate the lens loss induced by constitutive deletion of Pygo2. Importantly, however, lens-ΔHD2 pups have normally shaped lenses and are in all cases indistinguishable from control littermates (Supplemental Fig. S6). This indicates that the Bcl9/9l–Pygo2 complex does not require β-catenin to mediate its role during lens development.

To our knowledge, this is the first report demonstrating that Bcl9/9l act outside the canonical Wnt signaling cascade. A growing body of evidence indicates that, in

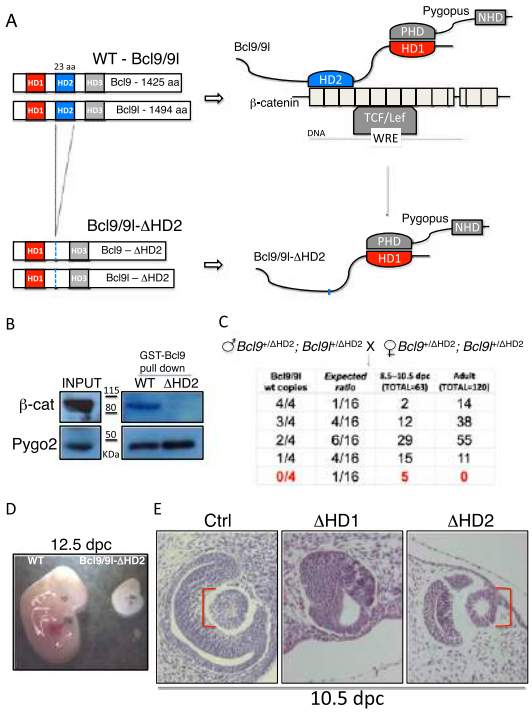

Figure 3. Bcl9/9l act independently from β-catenin during lens development. (*A*) Wild-type (WT) and ΔHD2 mutant Bcl9 and Bcl9l proteins; at the *right* is presented the variation in the "chain of adaptors" induced by deleting the HD2 domain: The interaction between Bcl9/9l and β-catenin is abrogated, and the complex Bcl9/9l–Pygo2 can act independently from canonical Wnt signaling. (*B*) A GST-Bcl9-ΔHD2 protein loses the ability to interact with β-catenin but maintains the ability to pull down Pygo2. (*C*) No double-homozygous ΔHD2 mutant mice are ever scored after birth, suggesting embryonic lethality. (*D*) The few embryos found at 12.5 dpc displayed an evident developmental block at 10.5 dpc. (*E*) At 10.5 dpc, wild-type surface head ectoderm invaginates to form the lens pit; in *Bcl9/9l*-ΔHD1 embryos, this process is arrested (cf. the *middle* and *left* panels). At the same stage, *Bcl9/9l*-ΔHD2 embryos have a correctly shaped lens pit, demonstrating that, in this process, Bcl9/9l function is independent from β-catenin.

mice, Pygo2 has tissue-specific, Wnt-independent functions in the testis (Nair et al. 2008; Cantù et al. 2013) and lens (Song et al. 2007). Also, in *Drosophila*, Pygo was recently reported to act in a β-catenin-independent manner during heart development (Tang et al. 2013, 2014). It will be critical to establish whether other Wnt-independent functions of Pygo2 require the interaction with Bcl9/9l and whether these functions are conserved among species.

Our finding that the Bcl9/9l–Pygo2 complex functions independently of β-catenin in eye development implies that, in this tissue, these factors also act independently from upstream canonical Wnt signals. The abrogation of the Bcl9/9l–Pygo2 interaction causes a lens arrest very reminiscent of Pax6 loss in this tissue (Ashery-Padan et al. 2000). Therefore, we reasoned that Pax6 might lie upstream of Bcl9/9l function. To test whether Pax6 controls *Bcl9*, *Bcl9l*, and *Pygo2* expression, we exploited the mouse-derived lens cell line αTN4, a widely used model for lens cell differentiation. This cell line expresses Pax6 and its direct transcriptional target, αA-crystallin, encoded by the *Cryaa* gene (Yang and Cvekl 2005); importantly, Bcl9/9l and Pygo2 are also expressed (Fig. 4A), making this cell line a suitable model for studying their regulation.

We identified in silico Pax6 consensus sequences between −5 kb and +1 kb of the transcriptional start site (TSS) of *Bcl9*, *Bcl9l*, and *Pygo2*. To determine whether any of these serve as bona fide Pax6-binding sites, we performed chromatin immunoprecipitation (ChIP) experiments. We designed PCR primers to amplify the Pax6-binding sites located within evolutionarily conserved regions (Supplemental Fig. S7). Indicative of Pax6 binding, we found that specific regions upstream of *Bcl9* and *Bcl9l* are enriched in our ChIP assay when using an anti-Pax6 antibody (Fig. 4B). Note that the *Cryaa* promoter, our positive control, displays a comparable enrichment, while no enrichment is observed in several other genomic regions (e.g., *Prm2* promoter) (Fig. 4B). To probe the relevance of Pax6 binding within these regions, we treated αTN4 cells with siRNA against *Pax6* (*siPax6*): *Pax6* mRNA levels were reduced to <5% of normal expression, causing a down-regulation of its target αA-crystallin (Fig. 4C). Of note, Pax6 depletion also resulted in the down-regulation of both Bcl9 and Bcl9l transcripts.

To test whether Pax6 also affected Bcl9/9l expression in vivo, we monitored *Bcl9/9l* expression in the developing eye in the absence of Pax6 function. To this end, we exploited *Small eye* (*Sey*) mice that bear a Pax6-truncating mutation, a good model to investigate Pax6 loss of function in vivo (Hogan et al. 1986; Hill et al. 1991). Homozygous $Pax6^{Sey/Sey}$ embryos can be distinguished as early as 10.5 dpc by the phenotype that, at this stage, the ectoderm does not invaginate to form a lens pit (Hogan et al. 1986). In wild-type mice, we found Bcl9l (Fig. 4D) and Bcl9 (Supplemental Fig. S4) proteins to be highly expressed in the invaginating surface head ectoderm, overlapping with the Pax6 expression domain (Callaerts et al. 1997). In $Pax6^{Sey/Sey}$ embryos, the ectodermal Bcl9l expression appears to be strongly reduced compared with wild-type controls (Fig. 4D, cf. top and

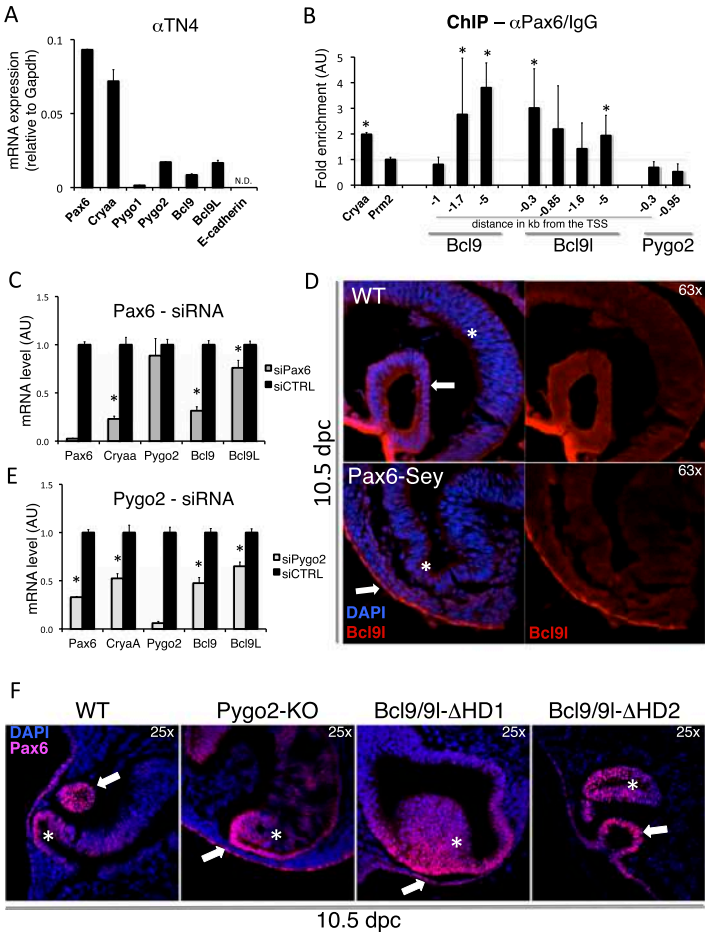

Figure 4. *Bcl9* and *Bcl9l* are direct transcriptional targets of Pax6. (*A*) The mouse-derived lens cell line αTN4 expresses *Bcl9*, *Bcl9l*, and *Pygo2* together with lens-specific genes such as *Pax6* and *Cryaa*. (*B*) ChIP performed on the chromatin extracted from αTN4: Specific regions upstream of *Bcl9* and *Bcl9l* are enriched when the chromatin is immunoprecipitated with an anti-Pax6 antibody, indicative of Pax6-binding events. No such enrichment was scored within the Pygo2 promoter. *Cryaa* and *Prm2* promoters constitute the positive and the negative controls, respectively. The enrichment is expressed as a ratio between anti-Pax6 and control IgG immunoprecipitation reactions. (TTS) Transcriptional start site. (*C*) When αTN4 is treated with siRNA against Pax6, Pax6 mRNA is reduced to <5% of the control. As its direct target, *Cryaa*, *Bcl9* and *Bcl9l* levels are also reduced upon Pax6 depletion. Of note, *Pygo2* transcription is not altered. (*D*) A loss-of-function mutation of Pax6 in vivo leads to a diminished Bcl9l expression in the surface head ectoderm at the onset of lens pit formation. Arrows mark the surface head ectoderm (already forming the lens pit in the wild-type [WT] embryo); the asterisks indicate the diencephalic protrusion that constitutes the presumptive retina. DAPI is in blue and marks cell nuclei; Bcl9l is in red. (*E*) If αTN4 cells are treated with siRNA against Pygo2, *Pax6* is down-regulated. In such experiments, *Bcl9* and *Bcl9l*, together with *Cryaa*, are also affected, very likely due to a secondary effect of Pax6 down-regulation. (AU) Arbitrary units. (*F*, *left* panel) At 10.5 dpc, the surface head ectoderm that forms the lens pit expresses high levels of Pax6; at this stage in wild-type embryos, Pax6 appears to be stronger in the surface ectoderm (white arrows) than in the presumptive retina (asterisks). In *Pygo2* knockout (*Pygo2*-KO) and *Bcl9/9l*-ΔHD1 embryos, this ratio is inverted. Please note that to detect the scant Pax6 within the surface head ectoderm, the signal must be enhanced; this explains the apparent brighter signal in mutant retinas. In *Bcl9/9l*-ΔHD2 embryos, the developing lens pit displays a Pax6 expression comparable with the wild type. Statistically significant values are evidenced by asterisks, which indicate a *P*-value < 0.05 calculated using an unpaired one-tail *t*-test.

bottom panels). The same is true for Bcl9 (data not shown). Taken together, our in vitro and in vivo results strongly suggest that Pax6 is required for *Bcl9* and *Bcl9l* transcription in developing lens cells, making them downstream effectors in this cascade. Of note, *Bcl9l* was also reported as a putative Pax6 target based on ChIP experiments from lenses of newborn mice combined with high-density oligonucleotide array hybridizations (ChIP–chip) (Xie et al. 2013); this is an independent validation of our findings.

In Pygo2-null mice, Pax6 levels are reduced in the surface head ectoderm at 10.5 dpc; on the other hand, when Pax6 function is lacking, Pygo2 expression is unaffected (Fig. 4C; Song et al. 2007, N Vilain and M Aguet, unpubl.). Therefore, Pygo2 appears to be genetically upstream of Pax6. We observed that abrogating the interaction between Bcl9/9l and Pygo2 leads to a very similar decrease of Pax6 expression in the surface head ectoderm at 10.5 dpc (Fig. 4F), indicating that *Bcl9/9l* not only are Pax6 targets but also act together with Pygo2 upstream of *Pax6*. The effect on Pax6 expression is not observed in the Bcl9/9l-ΔHD2 developing lens, lending further support to the notion that, in this context, Bcl9/9l act in a β-catenin-independent fashion. The epistatic hierarchy between Bcl9/9l–Pygo2, Pax6, and Bcl9/9l raises the prediction that, if Pygo2 expression was altered in lens cells, Pax6 and Bcl9/9l expression would be affected accordingly. To test this, we treated αTN4 cells with siRNA targeting Pygo2 (siPygo2): Consistently, Pygo2 down-regulation causes a decrease in *Pax6* mRNA level and diminished levels of its target genes, *Cryaa*, *Bcl9*, and *Bcl9l* (Fig. 4E). Taken together, our results reveal the existence of a novel genetic regulatory circuit in which Bcl9/9l–Pygo2 act upstream of Pax6, which in turn activates *Bcl9* and *Bcl9l*. Thus, in a β-catenin-independent manner, a Bcl9/9l–Pygo2 complex sustains correct lens formation during mouse development (Fig. 5).

Bcl9 and Bcl9l, in a manner requiring Pygo2 binding, thus emerge as new downstream effectors of Pax6 during lens development. In this context, their action does not appear to be modulated by upstream canonical Wnt signals but by a tissue-specific transcription factor, Pax6, the master regulator of the lens-specific differentiation program. The molecular mechanism by which the Bcl9/9l–Pygo2 complex achieves its tissue-specific function in lens differentiation is an interesting line of future investigation. One possibility is that the main function of the Bcl9/9l–Pygo2 complex is to sustain Pax6 expression. Consequently, by activating *Bcl9/9l*, Pax6 would buttress its own expression, creating a positive feedback loop, a very common mechanism in biological systems, instrumental to produce an all-or-none response to a signal (Brandman et al. 2005).

It is currently widely accepted that, in the lens, the Wnt pathway must be turned off (Smith et al. 2005), and a recent study discovered that this inhibition is mediated at least in part by Pax6 (Machon et al. 2010). It is therefore tantalizing to speculate that Bcl9/9l and Pygo2 not only act independently from β-catenin but, together with Pax6, are involved in the inhibition of the Wnt-induced genetic program, thus ensuring that lens development proceeds correctly. To test this speculation, a more detailed understanding of the timing and nature of Wnt signaling and its targets in the developing lens is needed. Our results provide a novel circuit and a novel paradigm (a β-catenin-independent Bcl9/9l–Pygo2 module) that need to be integrated into the emergent picture.

Materials and methods

Generation of Bcl9/9l knock-in mouse strain

Knock-in mutants in *Bcl9* and *Bcl9l* were generated by standard techniques (inGenious Targeting Laboratory). Briefly, the targeting vector was electroporated into BA1 (C57BL/6 × 129/SvEv) hybrid embryonic stem cells. After selection with the antibiotic G418, surviving clones were expanded for PCR and Southern blotting analyses to confirm recombinant embryonic stem cell clones. Mouse embryonic stem cells harboring the knock-in allele were microinjected into C57BL/6 blastocysts. Resulting chimeras were bred to wild-type C57BL/6N mice to generate F1 heterozygous offspring. Neo cassette excision was obtained by crossing heterozygous knock-in animals with mice expressing Flp recombinase. All mouse experiments were performed in accordance with Swiss guidelines and approved by the Veterinarian Office of the Kanton of Zurich, Switzerland.

Cell culture and quantitative RT–PCR

The αTN4 cell line was cultured in DMEM supplemented with 10% FBS at 37°C. Total RNA was extracted using TRIzol (Invitrogen). Quantitative real-time SYBR Green-based PCR reactions were performed in triplicate and monitored with the ABI Prism 7900HT system (Applied Biosystem). All primers are listed in the Supplemental Material.

ChIP

αTN4 were fixed with 1% formaldehyde for 10 min at room temperature and lysed in a nuclei lysis buffer (1% SDS, 50 mM Tris, 10 mM EDTA, protease inhibitors). Chromatin was sonicated to a size between 200 and 1000 base pairs using a Covaris focused ultrasonicator (10 times for 1 min, 10% duty cycle, 5% intensity, 100 cycles per burst). The antibodies and the primers used are listed in the Supplemental Material.

Immunofluorescence

Previously fixed cryosections were blocked with 10% goat serum and 0.3% Triton-X-100 in PBS and incubated overnight at 4°C with the following antibodies: α-Pax6 (Millipore), α-Bcl9 (Abcam), α-Bcl9l (Abnova), and α-β-catenin (Cl. 14, BD Transduction Laboratories). Slides were then incubated with a fluorescently labeled secondary antibody (Alexa 488 goat anti-mouse or Alexa 555 goat anti-rabbit; 1:500). Nuclei were stained with DAPI (1:1000; Sigma).

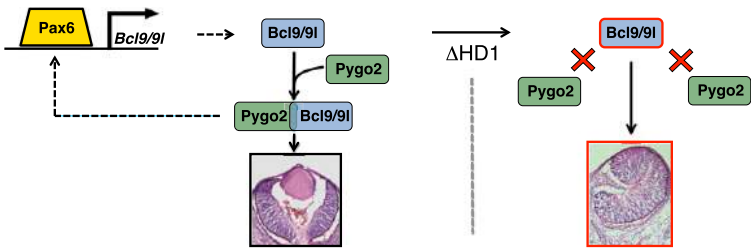

Figure 5. Our data indicate that Pax6 is required for the transcription of *Bcl9/9l*. Bcl9/9l then assemble with Pygo2 to ensure a correct lens development; the lens development is arrested when the Bcl9/9l–Pygo2 interaction is abolished. The complex Bcl9/9l–Pygo2 also lies genetically upstream of Pax6, possibly with the function of sustaining its expression.

Acknowledgments

We are much indebted to Gabriel Cavalheiro and Fabienne Murphy-Seiler for experimental help; Qing Xie, Christian Mosimann, and Bahar Degirmenci for precious inputs and discussion; Lukas Sommer, Peter Gruss, Christian Grimm, Richard Lang, Anastassia Stoykova, and Ales Cvekl for sharing reagents and mouse strains; and Martin Moser, Eliane Escher, and Charlotte Burger for technical support. This work was supported by the Swiss National Science Foundation (SNF) and grants from the Forschungskredit of the University of Zurich (to C.C.).

References

Ashery-Padan R, Marquardt T, Zhou X, Gruss P. 2000. Pax6 activity in the lens primordium is required for lens formation and for correct placement of a single retina in the eye. *Genes Dev* **14:** 2701–2711.

Belenkaya TY, Han C, Standley HJ, Lin X, Houston DW, Heasman J, Lin X. 2002. pygopus encodes a nuclear protein essential for wingless/Wnt signaling. *Development* **129:** 4089–4101.

Brack AS, Murphy-Seiler F, Hanifi J, Deka J, Eyckerman S, Keller C, Aguet M, Rando TA. 2009. BCL9 is an essential component of canonical Wnt signaling that mediates the differentiation of myogenic progenitors during muscle regeneration. *Dev Biol* **335:** 93–105.

Brandman O, Ferrell JE, Li R, Meyer T. 2005. Interlinked fast and slow positive feedback loops drive reliable cell decisions. *Science* **310:** 496–498.

Brembeck FH, Wiese M, Zatula N, Grigoryan T, Dai Y, Fritzmann J, Birchmeier W. 2011. BCL9-2 promotes early stages of intestinal tumor progression. *Gastroenterology* **141:** 1359–1370.e3.

Callaerts P, Halder G, Gehring WJ. 1997. PAX-6 in development and evolution. *Annu Rev Neurosci* **20:** 483–532.

Cantù C, Valenta T, Hausmann G, Vilain N, Aguet M, Basler K. 2013. The Pygo2–H3K4me2/3 interaction is dispensable for mouse development and Wnt signaling-dependent transcription. *Development* **140:** 2377–2386.

Deka J, Wiedemann N, Anderle P, Murphy-Seiler F, Bultinck J, Eyckerman S, Stehle J-C, André S, Vilain N, Zilian O, et al. 2010. Bcl9/Bcl9l are critical for Wnt-mediated regulation of stem cell traits in colon epithelium and adenocarcinomas. *Cancer Res* **70:** 6619–6628.

de la Roche M, Rutherford TJ, Gupta D, Veprintsev DB, Saxty B, Freund SM, Bienz M. 2012. An intrinsically labile α-helix abutting the BCL9-binding site of β-catenin is required for its inhibition by carnosic acid. *Nat Commun* **3:** 680.

Fiedler M, Sánchez-Barrena MJ, Nekrasov M, Mieszczanek J, Rybin V, Müller J, Evans P, Bienz M. 2008. Decoding of methylated histone H3 tail by the Pygo-BCL9 Wnt signaling complex. *Mol Cell* **30:** 507–518.

Hill RE, Favor J, Hogan BL, Ton CC, Saunders GF, Hanson IM, Prosser J, Jordan T, Hastie ND, van Heyningen V. 1991. Mouse small eye results from mutations in a paired-like homeobox-containing gene. *Nature* **354:** 522–525.

Hogan BL, Horsburgh G, Cohen J, Hetherington CM, Fisher G, Lyon MF. 1986. Small eyes (Sey): a homozygous lethal mutation on chromosome 2 which affects the differentiation of both lens and nasal placodes in the mouse. *J Embryol Exp Morphol* **97:** 95–110.

Kawamoto SA, Coleska A, Ran X, Yi H, Yang C-Y, Wang S. 2012. Design of triazole-stapled BCL9 α-helical peptides to target the β-catenin/B-cell CLL/lymphoma 9 (BCL9) protein-protein interaction. *J Med Chem* **55:** 1137–1146.

Kramps T, Peter O, Brunner E, Nellen D, Froesch B, Chatterjee S, Murone M, Züllig S, Basler K. 2002. Wnt/wingless signaling requires BCL9/legless-mediated recruitment of pygopus to the nuclear β-catenin–TCF complex. *Cell* **109:** 47–60.

Lang RA. 2004. Pathways regulating lens induction in the mouse. *Int J Dev Biol* **48:** 783–791.

Li B, Mackay DR, Ma J, Dai X. 2004. Cloning and developmental expression of mouse pygopus 2, a putative Wnt signaling component. *Genomics* **84:** 398–405.

Li B, Rhe C, Teng A, Bilanchone V, Munguia JE, Hu M, Jessen S, Piccolo S, Waterman ML, Dai X. 2007. Developmental phenotypes and reduced Wnt signaling in mice deficient for pygopus 2. *Genesis* **45:** 318–325.

Machon O, Kreslova J, Ruzickova J, Vacik T, Klimova L, Fujimura N, Lachova J, Kozmik Z. 2010. Lens morphogenesis is dependent on Pax6-mediated inhibition of the canonical Wnt/β-catenin signaling in the lens surface ectoderm. *Genesis* **48:** 86–95.

Mani M, Carrasco DE, Zhang Y, Takada K, Gatt ME, Dutta-Simmons J, Ikeda H, Diaz-Griffero F, Pena-Cruz V, Bertagnolli M, et al. 2009. BCL9 promotes tumor progression by conferring enhanced proliferative, metastatic, and angiogenic properties to cancer cells. *Cancer Res* **69:** 7577–7586.

Mosimann C, Hausmann G, Basler K. 2009. β-Catenin hits chromatin: regulation of Wnt target gene activation. *Nat Rev Mol Cell Biol* **10:** 276–286.

Nair M, Nagamori I, Sun P, Mishra DP, Rhéaume C, Li B, Sassone-Corsi P, Dai X. 2008. Nuclear regulator Pygo2 controls spermiogenesis and histone H3 acetylation. *Dev Biol* **320:** 446–455.

Parker DS, Jemison J, Cadigan KM. 2002. Pygopus, a nuclear PHD-finger protein required for Wingless signaling in *Drosophila*. *Development* **129:** 2565–2576.

Schwab KR, Patterson LT, Hartman HA, Song N, Lang RA, Lin X, Potter SS. 2007. Pygo1 and Pygo2 roles in Wnt signaling in mammalian kidney development. *BMC Biol* **5:** 15.

Smith AN, Miller L-AD, Song N, Taketo MM, Lang RA. 2005. The duality of β-catenin function: a requirement in lens morphogenesis and signaling suppression of lens fate in periocular ectoderm. *Dev Biol* **285:** 477–489.

Song N, Schwab KR, Patterson LT, Yamaguchi T, Lin X, Potter SS, Lang RA. 2007. pygopus 2 has a crucial, Wnt pathway-independent function in lens induction. *Development* **134:** 1873–1885.

Städeli R, Basler K. 2005. Dissecting nuclear Wingless signalling: recruitment of the transcriptional co-activator Pygopus by a chain of adaptor proteins. *Mech Dev* **122:** 1171–1182.

Takada K, Zhu D, Bird GH, Sukhdeo K, Zhao J-J, Mani M, Lemieux M, Carrasco DE, Ryan J, Horst D, et al. 2012. Targeted disruption of the BCL9/β-catenin complex inhibits oncogenic Wnt signaling. *Sci Transl Med* **4:** 148ra117.

Tang M, Yuan W, Fan X, Liu M, Bodmer R, Ocorr K, Wu X. 2013. Pygopus maintains heart function in aging *Drosophila* independently of canonical Wnt signaling. *Circ Cardiovasc Genet* **6:** 472–480.

Tang M, Yuan W, Bodmer R, Wu X, Ocorr K. 2014. The role of pygopus in the differentiation of intracardiac valves in *Drosophila*. *Genesis* **52:** 19–28.

Thompson B, Townsley F, Rosin-Arbesfeld R, Musisi H, Bienz M. 2002. A new nuclear component of the Wnt signalling pathway. *Nat Cell Biol* **4:** 367–373.

Valenta T, Gay M, Steiner S, Draganova K, Zemke M, Hoffmans R, Cinelli P, Aguet M, Sommer L, Basler K. 2011. Probing transcription-specific outputs of β-catenin in vivo. *Genes Dev* **25:** 2631–2643.

Xie Q, Yang Y, Huang J, Ninkovic J, Walcher T, Wolf L, Vitenzon A, Zheng D, Götz M, Beebe DC, et al. 2013. Pax6 interactions with chromatin and identification of its novel direct target genes in lens and forebrain. *PLoS ONE* **8:** e54507.

Yang Y, Cvekl A. 2005. Tissue-specific regulation of the mouse αA-crystallin gene in lens via recruitment of Pax6 and c-Maf to its promoter. *J Mol Biol* **351:** 453–469.

Footnote:

Supplemental material for the article:

Pax6-dependent, but β-catenin-independent, function of Bcl9 proteins in mouse lens development

Can be found online at: http://genesdev.cshlp.org/content/28/17/1879/suppl/DC1

The files in this Data Supplement are:

- Supplemental Figures S1-S7.ppt
- Supplemental Experimental Procedures.docx

Mutations in the Wnt/β-catenin cofactors *Bcl9* and *Pygo* Cause Congenital Heart Malformations

Claudio Cantù[1,†], Anastasia Felker[1,†], Dario Zimmerli[1,†], Elena Chiavacci[1], Lucia Kirchgeorg[1], Tomas Valenta[1], George Hausmann[1], Jorge Ripoll[3], Natalie Vilain[2], Michel Aguet[2], Konrad Basler[1,*], Christian Mosimann[1,*]

[1]Institute of Molecular Life Sciences, University of Zürich, Winterthurerstrasse 190, 8057 Zürich, Switzerland
[2]Swiss Institute for Experimental Cancer Research (ISREC), Ecole Polytechnique Fédérale de Lausanne (EPFL), School of Life Sciences, 1015 Lausanne, Switzerland.
[3]Department of Bioengineering and Aerospace Engineering, Universidad Carlos III de Madrid, 28911 Madrid, Spain.

† contributed equally to this work
* correspondence to: kb@imls.uzh.ch; christian.mosimann@imls.uzh.ch

Highlights

- Mutations in the genes encoding for Bcl9, Bcl9l, Pygo1 and Pygo2 lead to severe cardiac malformations both in zebrafish and in the mouse
- Bcl9 and Pygo drive the Wnt signaling-dependent transcription in heart progenitor cells
- The β-catenin-Bcl9-Pygo module directly controls the expression of important regulators of cardiac and neural crest development
- The zebrafish and mouse mutants we generated constitute powerful models to study human congenital heart conditions

Summary (147 words)

Congenital heart diseases are the most frequent defects at birth, often lethal even after surgical intervention. Discovering novel mechanisms of heart development is the prerequisite to generate new diagnostic and therapeutic strategies. Here, via a CRISPR/Cas9 genetic screen in zebrafish, we identified a role for the Wnt//β-catenin cofactors Bcl9, Bcl9l and the histone code-reader Pygo2 during cardiac development. We show that loss-of-function of these proteins, or the sole abrogation of their interaction with β-catenin via in vivo small-domain deletion, induce heart malformations, both in fish and in mouse, that recapitulate human CHDs. We find that the Bcl9-Pygo complex acts in specific cell populations of the developing heart, where it directly activates a previously unrecognized tissue-specific transcriptional program. Collectively, our results uncover a new role of Wnt/β-catenin signaling during heart development, and implicate mutations in *BCL9* and *PYGO* as potentially causative in the formation of human CHDs.

Introduction

Understanding heart development at the molecular level is imperative for discovering the causes of congenital heart diseases (CHDs). CHDs are the most frequent birth defects, affecting ca. 0.8% of live births, and often result in perinatal lethality or life-long complications, even after sophisticated surgical interventions (Zaidi et al., 2013). A number of mutations in cardiac transcription factors have been linked to genetic forms of congenital heart disease (Andersen et al., 2014), but the developmental pathways that drive the onset of specific cardiac phenotypes remain unclear.

Wnt signaling is a key determinant of several developmental processes in metazoans, including heart formation (Nusse and Clevers, 2017; Woudstra et al., 2017). Studies on the role of Wnt signaling in cardiac development have been challenging to interpret, with reports supporting both promoting and restricting functions on cardiac progenitor specification, depending on the developmental stage (Gessert and Kühl, 2010). Canonical, β-catenin-mediated Wnt signaling has been shown to play a role in mesodermal cardiac progenitor expansion (Buikema et al., 2013) and in the proliferation of cardiac neural crest (CNC) cells (Kioussi et al., 2002). Defects in these cell populations are associated with malformations such as outflow tract (OFT) defects, persistent truncus arteriosus (PTA), double outlet right ventricle (DORV), commonly present in patients with tetralogy of Fallot and genetic syndromes, such as DiGeorge syndrome (Neeb et al., 2013). How defects in Wnt/β-catenin signaling contributes to these disease conditions is currently unknown.

Nuclear β-catenin orchestrates target gene expression by recruiting a host of co-factors to *cis*-regulatory elements occupied by the TCF/LEF transcription factors (Mosimann et al., 2009; Nusse and Clevers, 2017). In *Drosophila*, the coupling of the histone code-reader plant homology domain (PHD) finger protein Pygopus (Pygo) via the adaptor protein Legless (Lgs) to the β-catenin N-terminal Armadillo repeats was shown to be necessary for virtually all canonical Wnt signaling-dependent processes (Kramps et al., 2002a; van Tienen et al., 2017; Townsley et al., 2004a). The genomes of common vertebrate model organisms encode for two paralogs of *lgs*, *Bcl9* and *Bcl9l* (*Bcl9/9l*), and two of *pygo*, *Pygo1* and *Pygo2* (*Pygo1/2*). In vertebrates their relevance has been debated, and they appear to participate in the β-catenin-mediated transcription in a context-dependent manner (Brembeck et al., 2004a; Kennedy et al., 2010; Schwab et al., 2007). Additionally, they have evolved tissue-specific β-catenin-independent functions (Cantù et al., 2013, 2014a, 2017; Li et al., 2007).

Here, via a CRISPR/Cas9-mediated genetic screen in zebrafish, we identify mutations in *bcl9* as being potentially causative of developmental heart malformations. Subsequently, we generated a series of zebrafish and mouse loss-of-function mutants for *Bcl9, Bcl9l,* as well as for *Pygo1* and *Pygo2* (the only known Bcl9/9l-interacting proteins), and present genetic and molecular evidence for an evolutionarily conserved role of the β-catenin-Bcl9/9l-Pygo1/2 transcriptional module during vertebrate heart development. In both model organisms, when the β-catenin>Bcl9/9l>Pygo1/2 complex formation is abrogated, the resulting embryos display severe heart defects reminiscent of human CHDs, associated with forelimb and cartilage defects. The heart phenotype is recapitulated, in the mouse, by both constitutive and heart-specific conditional loss of Bcl9/9l or Pygo1/2, or by simultaneous impairment of the Bcl9/9l-β-catenin and Bcl9/9l-Pygo2 interactions achieved via in vivo small domain deletions. Transcriptomics studies (RNA-seq) and chromatin immunoprecipitation followed by deep sequencing (ChIP-seq) revealed that the β-catenin>Bcl9>Pygo complex lies functionally upstream of a heart-specific genetic program that includes several important regulators of cardiac and neural crest development. Collectively, our results suggest a causative link between mutations in *BCL9, BCL9L*, and perhaps in *PYGO1* and *PYGO2*, and human CHDs, as result of a tissue-specific perturbation of canonical Wnt signaling.

Results

CRISPR/Cas9-mediated genetic screen in zebrafish reveals a potential role for Bcl9 during heart development

With the aim of identifying novel genes involved in heart formation, we developed a genetic screen in zebrafish in which, via Cas9 RNP-mediated mutagenesis (Burger et al., 2016), we introduced specific loss-of-function mutations in a series of genes that have not previously been functionally implicated in heart development. We injected Cas9 protein together with target-specific guideRNAs (gRNA) into zebrafish embryos, and screened for impaired heart development between 56-72 hours post fertilization (hpf). Among other candidates, we identified specific heart defects upon mutations in *bcl9*, a gene encoding for a Wnt/β-catenin signaling cofactor. Mutations in *bcl9* lead to highly penetrant pericardial edema appearing before 72 hpf. To validate this observation, and to exclude possible off-target effects, we generated a new set of gRNAs targeting the 5' region of its coding sequence. We established heterozygous mutant strains carrying frameshift 5' deletions within the region encoding for the HD1 and HD2, the domains of Bcl9 that allow functional interaction with the only known interactors, Pygo and β-catenin, respectively. We refer to this new allele as

bcl9$^{\Delta 29}$ (Figure 1A, B). Homozygous mutant embryos for *bcl9*$^{\Delta 29}$, despite growing normally until 48 hpf, develop a pericardiac edema between 56-72 hpf (with an incidence of 25-90%), (Supplementary Figure 2 A-C), and mis-expression of the cardiac valve marker *vcana* (Supplementary Figure 2 F,G). At 5 days post fertilization (dpf), lightsheet imaging of homozygous *bcl9*$^{\Delta 29}$; *drl:EGFP*$^{+}$ [that marks cardiovascular lineages (Mosimann et al., 2015)] larvae, revealed an underdeveloped cardiopharyngeal vasculature, vascular defects at the cardiac inflow tract, and a miss-looped heart with miss-aligned atria and ventricles, when compared to wildtype or heterozygous sibling mutants (Figure 1F-I). *bcl9*$^{\Delta 29}$ mutants also displayed other selective phenotypes with high penetrance, such as cartilaginous craniofacial defects consisting of deformed pharyngeal skeletons with abnormal Meckel's and palatoquadrate cartilage development, and fusion defects of the ceratohyal and ceratobranchial 1 cartilage (Figure 1 J-M). Importantly, homozygous *bcl9*$^{\Delta 29}$-mutant larvae die at around 11 dpf, possibly due to a failure in properly inflating the swim bladder already apparent at 5dpf (Figure 1 C-E).

To assess for a potential redundant role between Bcl9 and the paralog protein Bcl9l, we generated mutant alleles also for the latter (we refer to this allele as *bcl9l*$^{\Delta 4}$, Supplementary Figure 2 A, B). Interestingly, and contrary to previous conclusions based on morpholino-mediated knockdowns (Brembeck et al., 2004b), homozygous *bcl9l*$^{\Delta 4}$ mutants were viable and fertile with no obvious phenotypes (observed for at least 4 generations) (Supplementary Figure 2 C-G). In addition, *bcl9/9l* double-mutant embryos (i.e. homozygous for the *bcl9*$^{\Delta 29}$ and *bcl9l*$^{\Delta 4}$ alleles) look indistinguishable from *bcl9*$^{\Delta 29}$ (Figure 1 E), corroborating the non-essential function of *bcl9l* and establishing that no significant compensation (Rossi et al., 2015) by the paralog *bcl9l* occurs upon *bcl9* perturbation in *bcl9*$^{\Delta 29}$;*bcl9l*$^{\Delta 4}$ mutants.

Supplementary Figure 1

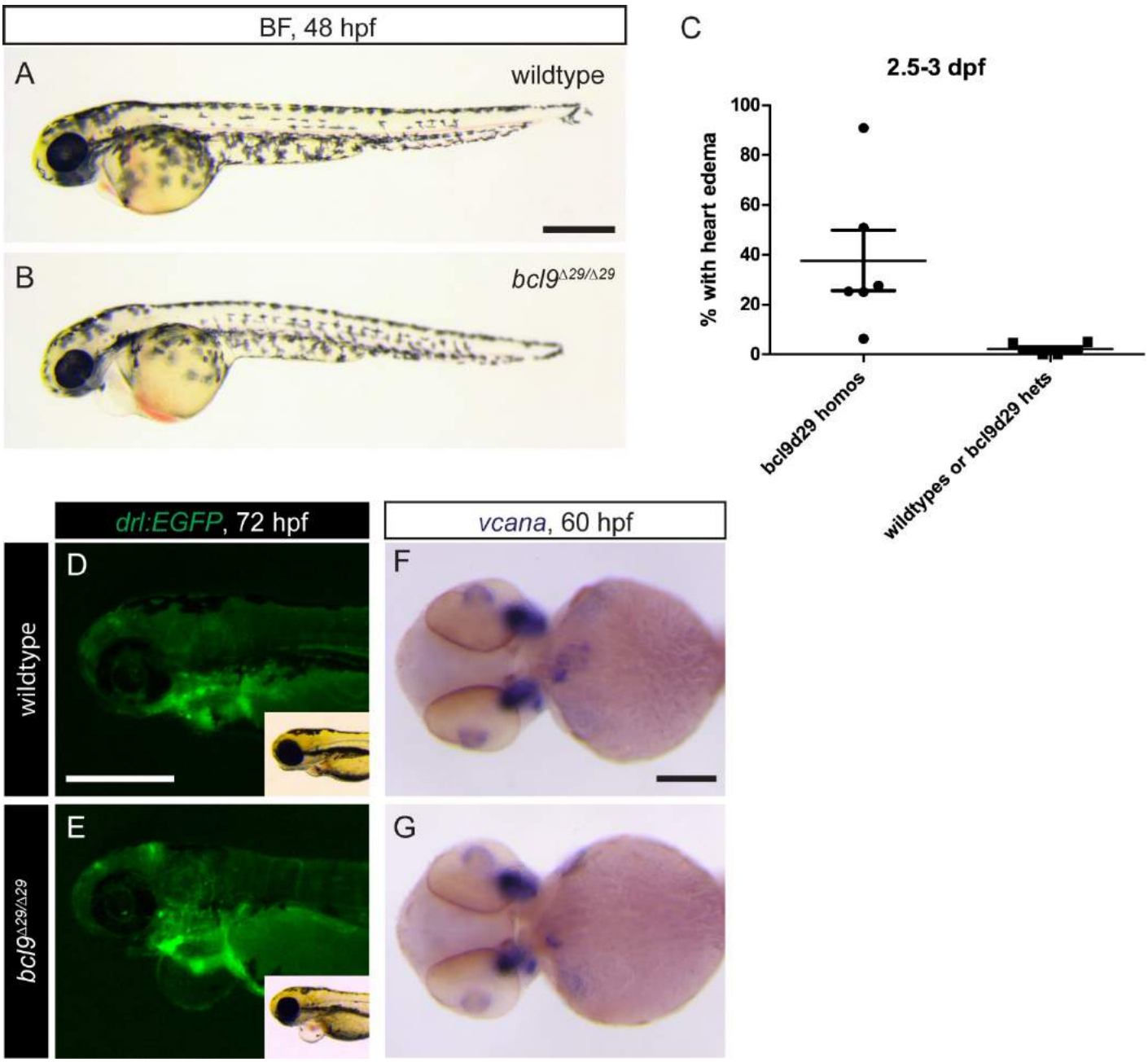

Supplementary Figure 1: Variable cardiac phenotypes in *bcl9*$^{\Delta 29}$ mutants between 2-3 dpf. (**A,-C**) At 48 hpf, *bcl9*$^{\Delta 29}$ develop pericardiac edema with a variable penetrance. Scale bar 500 µm. (**D,E**) The hearts of *bcl9*$^{\Delta 29}$ are patterned into atria and ventricle as visualized by *drl:EGFP*. The two chambers are, however, miss-aligned revealing a looping defect caused by the *bcl9* mutation. Scale bar 500 µm. (**F,G**) Whole mount ISH for *vcana* reveals reduced expression specifically in the heart suggesting a defect in valve formation. Scale bar 200 µm.

Figure 1

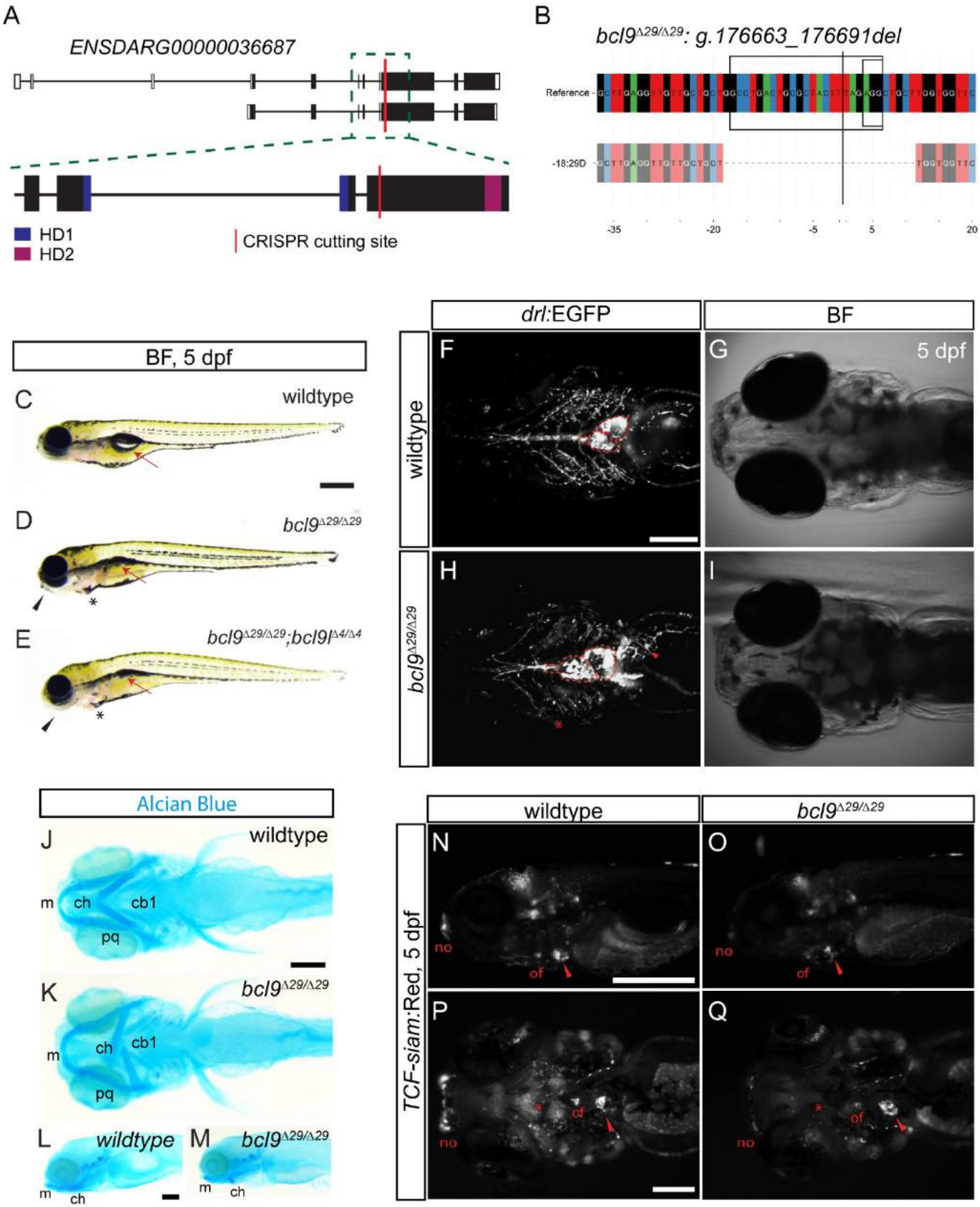
A
ENSDARG00000036687
HD1
HD2
CRISPR cutting site
B
bcl9Δ29/Δ29: g.176663_176691del
Reference
-18:29D
-35
-20
-5
5
20
BF, 5 dpf
C
wildtype
D
bcl9Δ29/Δ29
E
bcl9Δ29/Δ29;bcl9lΔ4/Δ4
drl:EGFP
BF
F
G
5 dpf
wildtype
H
I
bcl9Δ29/Δ29
Alcian Blue
J
wildtype
m
ch
cb1
pq
K
bcl9Δ29/Δ29
L
wildtype
M
bcl9Δ29/Δ29
wildtype
bcl9Δ29/Δ29
N
O
P
Q
TCF-siam:Red, 5 dpf
no
of

Figure 1: A homozygous 29 bp deletion between HD1 and HD2 leads to severe cardiac and craniofacial defects in zebrafish. (**A**) CRISPR-Cas9-mediated mutagenesis via NHEJ in coding exon 6 between HD1 and HD2 of the zebrafish *bcl9* gene. Gene locus represented as per genome annotation Zv10 with two isoforms that differ in the first coding exon and the untranslated regions (UTRs). The green dotted box represents a zoomed region of the gene locus, with the red line representing the location of the sgRNA used for mutagenesis; black boxes mark coding exons (CDS), white boxes mark UTRs, the blue boxes represent the part of the CDS that will contribute to HD1 and purple boxes to HD2. Note that the schematic is not to scale. (**B**) CrispRVariants panel plot depiction of the germline allele with a 29 bp deletion at the CRISPR cutting site. Top shows genomic reference with the *bcl9:g.176663_176691* (*bcl9Δ29*) allele shown below. *bcl9Δ29* results in an out-of-frame deletion introducing a frameshift in the CDS. The black box over genomic reference sequence indicates sgRNA sequence, the smaller box the 5'-NGG-3' PAM sequence, and the black line the predicted Cas9-induced double-strand break position. (**C-E**) Brightfield images of 5 dpf homozygous *bcl9*$^{\Delta 29}$ and *bcl9*$^{\Delta 29}$*;bcl9l*$^{\Delta 4}$ larvae and their wildtype siblings. Mutant larvae do not inflate their swim bladder (arrows) presumably due to a failure to gasp air because of craniofacial malformations (black arrow heas). Moreover, mutant larvae show heart looping defects (asterisks). Scale bar 500 µm. (**F-I**) SPIM images of *drl:EGFP*+ wildtype and *bcl9*$^{\Delta 29}$ larvae. Mutant larvae show craniofacial vasculature (asterisks and arrow head) and heart looping (dotted line outlines the atrium and ventricle) defects. Scale bar 200 µm. (**J-M**) Alcian blue stainings of the pharyngeal cartilage of 5 dpf wildtype and *bcl9*$^{\Delta 29}$ larvae shown in ventral (**J,K**) and lateral (**L,M**) view. *bcl9*$^{\Delta 29}$ larvae show malformations of the pharyngeal apparatus with fusions defect of the ceratohyal (ch) and ceratobranchial 1 (cb1) arches and miss-shaped Meckel's (m) and palatoquadrate (pq) cartilage. Scale bars 100 µm. (**N-Q**) Fluorescent images of *TCF-siam:Red bcl9*$^{\Delta 29}$ and wildtype larvae. *TCF* reporter activity is severely reduced in the cardiac outflow tract (of), nose (no), and craniofacial apparatus (asterisks **P,Q**) and altered in the atrio-ventricular valve (arrow heads **N-Q**). Scale bars **N,O** 500 µm; **P,Q** 200 µm.

Supplementary Figure 2

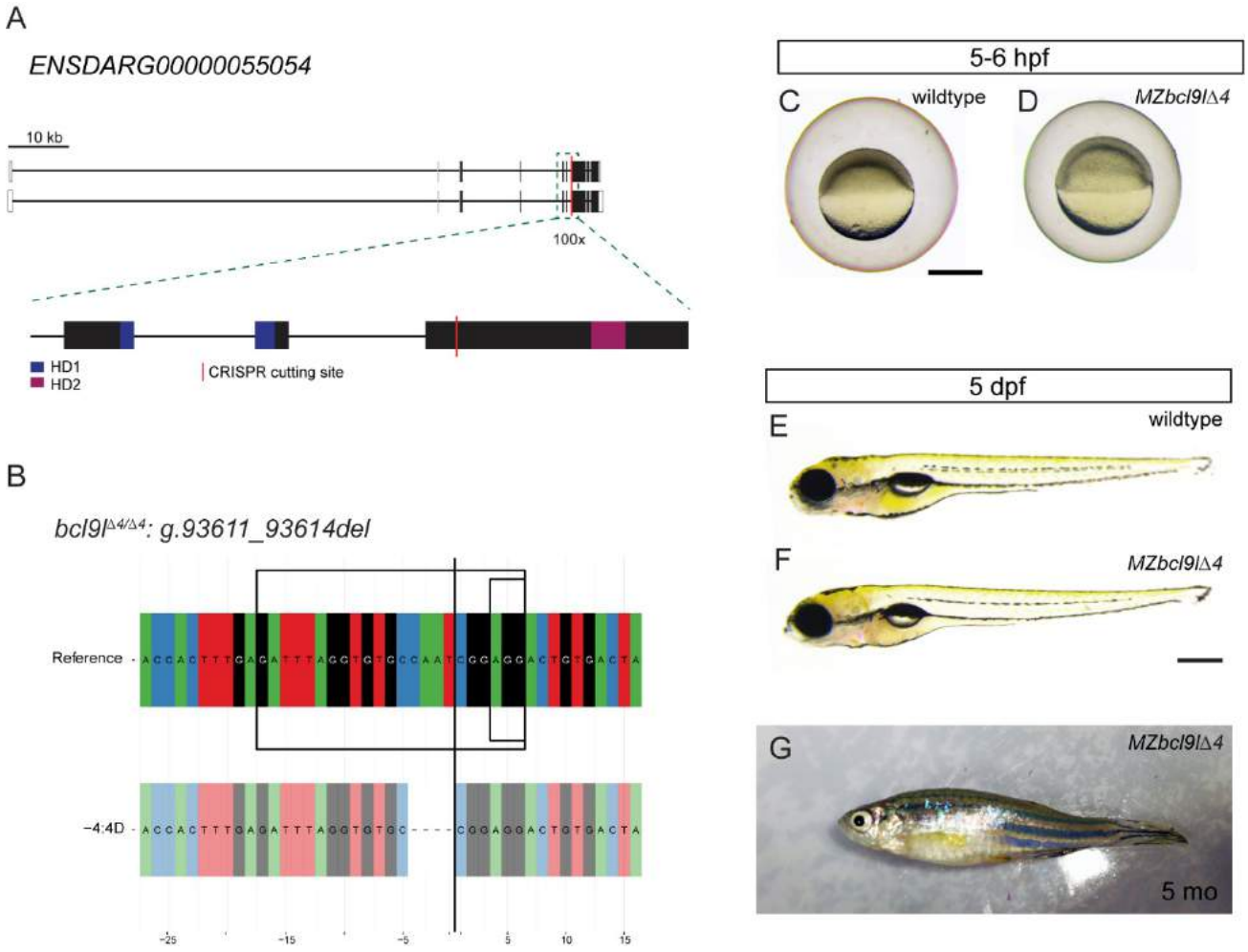

Supplementary Figure 2: *MZbcl9lΔ4* mutants are viable and fertile. (**A,B**) Schematics showing the mutation induced in *bcl9Δ4* mutants. Analogous to *bcl9* mutants (see Figure 1 A, B), we designed a sgRNA that binds between the HD1 and HD2 domain. (**A**) Gene locus represented as per genome annotation Zv10 with two isoforms that differ in the first coding exon and the untranslated regions (UTRs). The green dotted box represents a zoomed region of the gene locus, with the red line representing the location of the sgRNA used for mutagenesis; black boxes mark coding exons (CDS), white boxes mark UTRs, the blue boxes represent the part of the CDS that will contribute to HD1 and purple boxes to HD2. (**B**) A 4 pb deletion at the CRISPR cutting side leads to a frame-shift allele with a premature *STOP* codon before HD2. (**C-G**) Homozygous *bcl9l*$^{\Delta4}$ mutants were viable and fertile. Thus, we could analyze maternal zygotic mutants (*MZbcl9lΔ4*) by crossing two adult homozygous bcl9l mutants. (**C**) *MZbcl9lΔ4* mutants did not show any gastrulation defects in contrast to bcl9l morphant phenotypes reported in the literature, lateral views. Scale bar 500 µm. (**E,F**) At 5 dpf we could not detect any cardiac and craniofacial phenotypes as observed in zygotic *bcl9*$^{\Delta29}$ mutants (see Figure 1), lateral views, anterior to the left. Scale bar 500 µm. (**G**) Representative image of a five month old (5 mo) *MZbcl9lΔ4* F4 mutant.

***pygo* mutant zebrafish recapitulate *bcl9* loss**

Bcl9 has been shown to act, during Drosophila and vertebrate development, via functional coupling with the histone-code reader Pygopus (Kramps et al., 2002)(Thompson et al., 2002). To test for a potential role of Pygo1 and Pygo2 during zebrafish heart development we generated, with a similar Cas9 RNP-mediated approach, *pygo1* and *pygo2* loss-of-function mutant alleles. These alleles harbor frameshift mutations within the essential NH2-terminal homology domain (NHD) and result in a premature STOP codon before the Bcl9-binding C-terminal PHD domain; we refer to these alleles as $pygo1^{\Delta 5}$ and $pygo2^{\Delta 1}$ (Supplementary figure 3 A-C). Surprisingly, homozygous $pygo1^{\Delta 5}$ and homozygous $pygo2^{\Delta 1}$ mutant strains were indistinguishable from wild-type siblings throughout development, and homozygous $pygo1^{\Delta 5}$ animals were viable and fertile. In contrast, embryos that were homozygous for the $pygo2^{\Delta 1}$ alleles and concomitantly carried a homozygous or heterozygous $pygo1^{\Delta 5}$ mutation displayed cardiac and cartilaginous defects that recapitulated those observed in $bcl9^{\Delta 29}$ homozygous mutants (Supplementary Figure 3 D-F).

Supplementary Figure 3

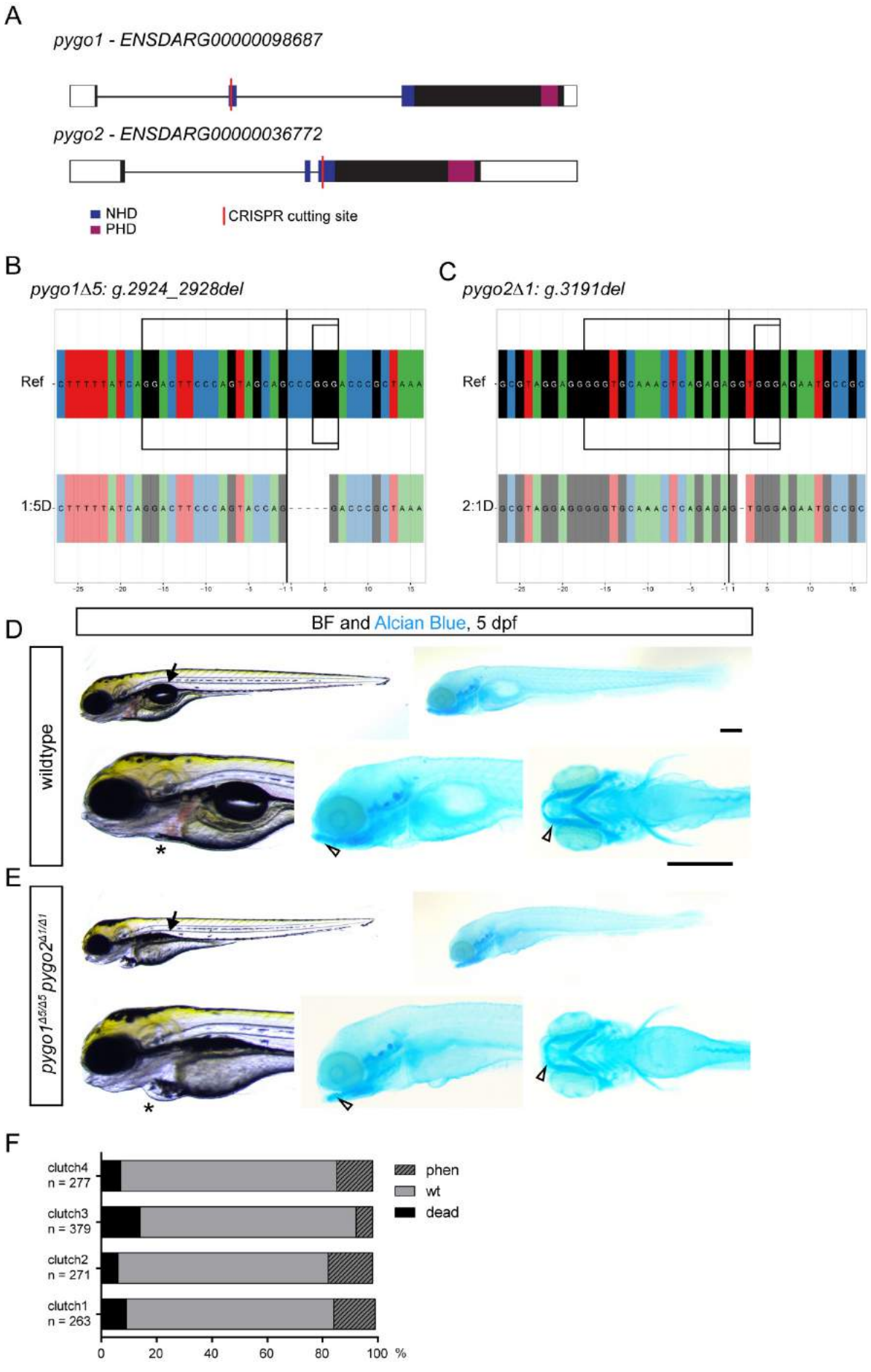

Supplementary Figure 3: Zygotic *pygo1/2* mutants phenocopy *bcl9*$^{\Delta 29}$ zebrafish mutants. (**A**) Schematic representation of the zebrafish pygo1 and pygo2 genes with annotated NHD and PHD domains and the CRISPR cutting site to generate mutants. Gene locus represented as per genome annotation Zv10 with the main isoforms of both genes shown. The red line represents the location of the sgRNA used for mutagenesis; black boxes mark coding exons (CDS), white boxes mark UTRs, the blue boxes represent the part of the CDS that will contribute to NHD and purple boxes to PHD. Note that the schematics are not to scale. (**B,C**) CrispRVariants panel plot depictions of the germline alleles with a 5 bp or 1 bp deletion in *pygo1* and *pygo2*, respectively. Top shows genomic reference with the *pygo1*Δ*5: g.2924_2928del* and *pygo2*Δ*1: g.3191del* alleles shown below. Both alleles result in an out-of-frame deletion introducing a frameshift in the CDS. The black box over genomic reference sequence indicates sgRNA sequence, the smaller box the 5'-NGG-3' PAM sequence, and the black line the predicted Cas9-induced double-strand break position. (**D,E**) Brightfield images of live and Alcian blue stained *pygo1*$^{\Delta 5}$*;pygo2*$^{\Delta 1}$ double mutants reveal cardiac edema (asterisks) and craniofacial defects (arrow heads), and aberrant swim bladder inflation (arrows) as detected in *bcl9*$^{\Delta 29}$ mutants (see Figure 1), lateral or ventral views, anterior to the left. Scale bars 250 µm. (**F**) Quantification of phenotypes in four individual *pygo1*$^{\Delta 5/wt}$ x *pygo2*$^{\Delta 1/wt}$ crosses reveal defects in 7-18% of all larvae. Genotyping of phenotypic larvae revealed phenotype occurrence in homozygous *pygo2*$^{\Delta 1}$ mutants in combination with homozygous or heterozygous *pygo1*$^{\Delta 5}$ mutation.

Bcl9 is required for selective developmental processes

As a next step, we set out to identify the gene expression changes that accompanied the phenotypic defects occurring upon mutations in *bcl9*. To this end, we performed RNA extraction followed by deep sequencing (RNA-seq) on combined zebrafish trunk and head regions - where the ensemble of phenotypic defects was manifest -, including the heart, pharyngeal arches, pectoral fins, and craniofacial structures, and compared homozygous *bcl9*$^{\Delta 29}$ mutants and wild-type siblings derived from heterozygote *bcl9*$^{\Delta 29}$ in-crosses at 54 hpf. Our aim was to capture the gene-expression changes leading to the cardiac and cartilaginous craniofacial defects occurring later at 5 dpf (Figure 1). At 54 hpf, we detected deregulation of 178 genes (124 genes down, cut-off: 2x downregulation, FC <0.5; 54 genes up, cut-off: 2.5x upregulation, FC>2.5) in homozygous *bcl9*$^{\Delta 29}$ mutants compared to the wild-type siblings. Among the deregulated genes, 37 have been associated with zebrafish heart, pharyngeal arches, pectoral fins, and cranial neural crest development (Supplementary Table 1). A number of the downregulated genes (e.g. *vegfa*, *cdh5*) have been linked to epithelial-to-mesenchymal transition (EMT), and to morphogenetic processes occurring during cardiac valve formation (Supplementary Table 1). Considering this set of genes, we performed a *Search Tool for the Retrieval of Interacting Genes/Proteins* (STRING, Szklarczyk et al., 2015) analysis, and found that they assembled in a medium-to-high confidence protein-protein associations cluster that implies their cooperative action during

cardiac valve formation (Supplementary Figure 4). Overall, these data strongly supported the notion that Bcl9, in zebrafish, acts during selective developmental processes, including fin formation, craniofacial cartilage specification likely via a cell-autonomous role in neural crest cells and, most importantly, during cardiac valve morphogenesis.

Supplementary Figure 4

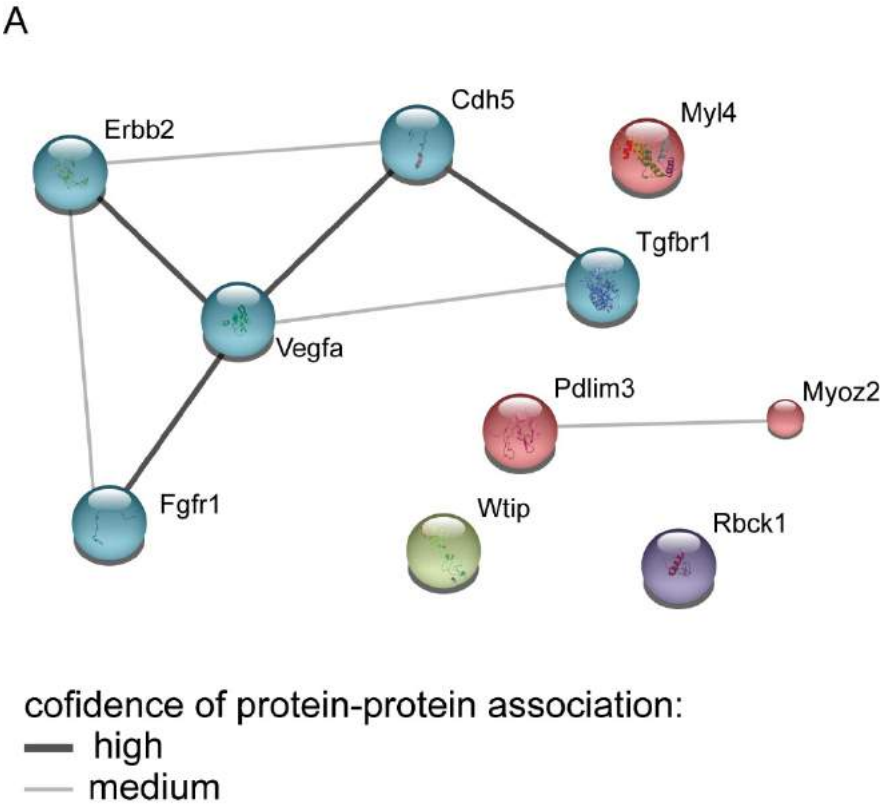

Supplementary Figure 4: Cardiac genes de-regulated in *bcl9*$^{\Delta 29}$ mutants cluster in a network guiding valve development. (**A**) STRING analysis of mouse orthologues of de-regulated genes in *bcl9*$^{\Delta 29}$ zebrafish mutants with kmeans clustering analysis (numbers of clusters 4). Five out of seven down-regulated genes assemble in one cluster with medium to high confidence protein-protein interactions reflecting their interactive involvement in cardiac valve formation as reviewed from the literature. All up-regulated genes assemble a separate cluster reflecting their potential involvement in cardiomyocytes actino-myosin and sarcomere assembly. Permalink to analysis: http://bit.ly/2wmba7z.

Pygo1/2 and *Bcl9/9l* loss in mouse causes lethal heart malformations

The observation that Bcl9 and Pygo proteins have a prominent role during cardiac development in zebrafish, prompted us to test their role in the mouse, a model closer to human physiology.

In the mouse, the compound deletion of *Pygo1* and *Pygo2* (*Pygo1/2*) leads to embryonic lethality at 13.5/14.5 dpc for undetermined reasons (Cantù et al., 2013; Li et al., 2007). We found that *Pygo1/2* mutant embryos, between 13.5 and 14.5 days post coitum (dpc), display

severe heart defects such as malformed atrio-ventricular valves resulting in substantial regurgitate flow and dilated atria, hypoplastic ventricular myocardium and aberrant chamber septation (Figure 2 A-D). In addition, *Pygo1/2* mutant embryos displayed outflow tract (OFT) anomalies such as transposition of the great arteries (TGA, with a penetrance of ca. 80%) (Figure 2 E-F) and a hypotrophic ductus arteriosus, with a penetrance of 90% (Figure 2 G-H). Strikingly, some of these defects are reminiscent of those present in human CHDs such as, for example, Valvular Heart Disease, or DiGeorge syndrome (Racedo et al., 2017). Defects in atrioventricular (AV) valve formation in mice have been found to cause lethality between 13.5 and 16.5 dpc (Combs and Yutzey, 2009; Ranger et al., 1998), suggesting that the cardiac defects likely cause the death of *Pygo1/2*-mutant embryos.

Subsequently, we tested the requirement of Bcl9/9l proteins for this function of Pygo1/2 by making use of *Bcl9/9l* alleles with a deletion in HD1, the domain responsible for Pygo1/2 binding (*Bcl9/9l-ΔHD1*, Cantù et al., 2014). *Bcl9/9l-ΔHD1* homozygous embryos died at the same stage (13.5 - 14.5 dpc), and histological sections revealed heart defects resembling those observed upon *Pygo1/2* loss (Figure 2Q). This suggests that the cardiac defects observed in our mutant mice arise from a cooperative Bcl9-Pygo function. The finding that Bcl9/9l-Pygo1/2 have a role in mouse and zebrafish heart development suggests a conserved tissue-specific function of this complex. Discovered as apparently obligate players in Drosophila Wnt signaling, in vertebrates Bcl9/9l and Pygo1/2 act together in several developmental processes independently of β-catenin (Cantù et al., 2013, 2014a, 2017; Song et al., 2007). As a next step, we therefore sought to establish if the zebrafish and mouse phenotypes described here constitute other examples of β-catenin independent processes or if they are connected to Wnt/β-catenin signaling.

Figure 2

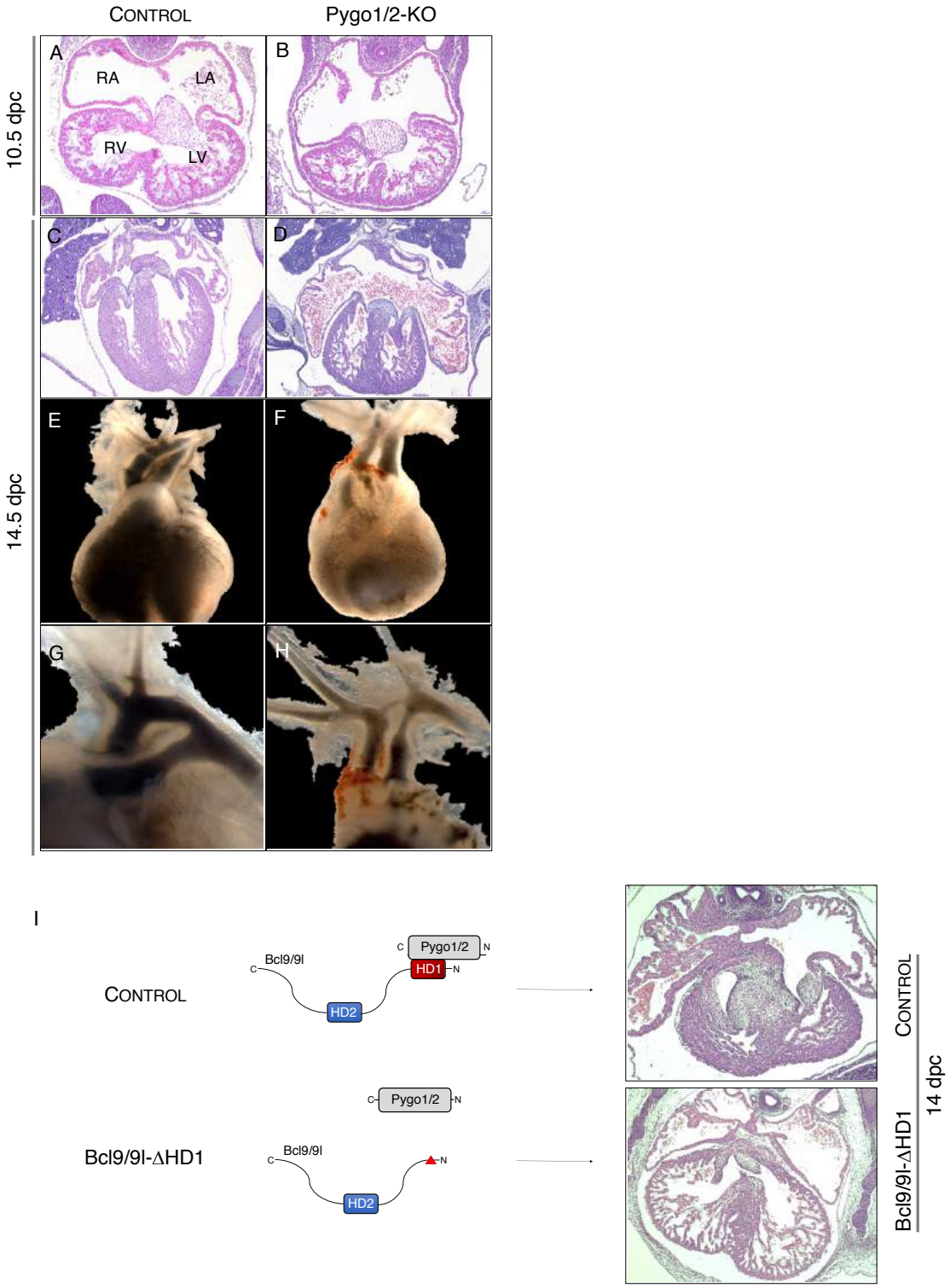
CONTROL
Pygo1/2-KO
10.5 dpc
14.5 dpc
A
B
C
D
E
F
G
H
RA
LA
RV
LV
I
CONTROL
Bcl9/9l
Pygo1/2
HD1
HD2
Bcl9/9l-ΔHD1
CONTROL
Bcl9/9l-ΔHD1
14 dpc

Figure 2: Cardiac defects in *Pygo1/2* and Bcl9/9l$^{\Delta HD1}$ mutant mouse embryos. (**A-D**) Haematoxylin/eosin stained sagittal sections of the heart at 10.5 (**A, B**) and 14.5 dpc (**C,D**). At 10.5 dpc the development of heart and heart cushion was still largely normal in the mutants. At 14.5 dpc the mutants displayed markedly smaller and thinner valves, highly dilated atria, and the atrial septum was missing. (**E,F**) Gross anatomical view of heart and great vessels at 13.5/14.5 dpc as revealed by India ink injection. (**G**) While normally the aorta (Ao) arises from the left (L) and the pulmonary artery (Pa) from the right ventricle (R), mutants had a classic TGA (**H**) in addition to a hypoplastic aortic arch (Aa) and ductus arteriosus (Du). (**I**) Schematic representation of the Bcl9/9l-Pygo1/2 interaction (upper left) and the molecular configuration of this interaction when the HD1 domain in Bcl9/9l is deleted in *Bcl9/9l-ΔHD1* mice (upper right). The abrogation of this interaction leads to a delayed chamber septation, hypoplastic myocardium and velves deficiency.

The Bcl9/9l-Pygo1/2 complex drives Wnt/β-catenin signaling in the developing heart

Wnt signaling is required for the formation of both the AV valves, the OFT (Bosada et al., 2016; Liebner et al., 2004), and the activity of Pax3 and Pitx2 during cardiac neural crest (CNC) migration and expansion (Bang et al., 1999; Kioussi et al., 2002). Since Bcl9/9l function as linker proteins connecting β-catenin and Pygo1/2 (Bienz, 2006), we aimed at specifically testing the concurrent requirement of connecting these two interaction partners for Wnt/β-catenin dependent outputs in the mouse. We combined mouse *Bcl9/9l* alleles in which either the HD1 (Pygo binding) or the HD2 (β-catenin binding) domains are deleted (Figure 3A, B) (Cantù et al., 2014). Double-heterozygous mice for the HD1 (*Bcl9*$^{\Delta HD1/+}$; *Bcl9l*$^{\Delta HD1/+}$, referred to as *Bcl9/9l-ΔHD1/+*) or the HD2 (*Bcl9*$^{\Delta HD2/+}$; *Bcl9l*$^{\Delta HD2/+}$, referred to as *Bcl9/9l-ΔHD2/+*) deletions are viable and fertile. Crosses between *Bcl9/9l-ΔHD1/+* and *Bcl9/9l-ΔHD2/+* must lead to trans-heterozygous embryos (1/16) in which both domain deletions are present (*Bcl9*$^{\Delta HD1/\Delta HD2}$; *Bcl9l*$^{\Delta HD1/\Delta HD2}$, referred to as *Bcl9/9l-Δ1/Δ2*): this allelic composition would not allow for a single molecule of Bcl9/9l to simultaneously bind β-catenin and Pygo. In fact, in *Bcl9/9l-Δ1/Δ2* mice, the resulting protein products can form Bcl9-β-catenin and Bcl9-Pygo complexes, but not the full tripartite transcriptional complex (Figure 3B), thereby enabling us to precisely test the developmental requirement of the β-catenin-Bcl9-Pygo complex.

From such crosses, we never recovered *Bcl9/9l-Δ1/Δ2* pups (Figure 3B), indicating embryonic lethality. *Bcl9/9l-Δ1/Δ2* embryos reached the 13.5-14.5 dpc stage, even though in a smaller proportion than the expected Mendelian ratio (Figure 3B). *Bcl9/9l-Δ1/Δ2* embryos displayed heart defects including ventricular myocardium hypoplasia and aberrant cardiac valves and OFT formation (Figure 3C-F). In addition to cardiac defects, we observed severe underdeveloped limbs (Figure 3I, L), and several skeletal malformations (Figure 3M-R) including shortened radius and ulna bones, incorrect specification of digit number (Figure 3

M,N and P,Q), and bifid ribs (Figure 3M,O and P,R). Suggestive that the observed defects are related to perturbed canonical Wnt signaling. *Bcl9/9l-Δ1/Δ2*-mutant mouse embryos also displayed a reduced expression of the in vivo *BATgal* reporter transgene in the cardiac cushions (Figure 3D, F), craniofacial structures, and limbs (Figure 3G-L).

To confirm that the heart defects induced by the loss of Bcl9 or Pygo function are caused by a tissue-specific perturbation of Wnt signaling also in zebrafish, we treated wild-type embryos with LH-2-40, a recently developed selective inhibitor of the β-catenin/Bcl9 interaction (Wisniewski et al., 2016). LH-2-40 was administered at concentrations ranging from 10 to 25 μM, at different time-points: 4 cell-stage, shield stage, or 18 somite stage. LH-2-40-treated embryos recapitulated the *bcl9*$^{\Delta 29}$-mutant phenotypes at 5 dpf (Figure 4A-H). In addition to the craniofacial and cardiac defects found in *bcl9*$^{\Delta 29}$ mutants, we frequently scored fin defects, characterized by the formation of an aberrant angle between the fin and the trunk, and a deformation of the proximal fin tissue (Figure 4C-H). We monitored the Wnt signaling activation status via *Tg(7xTCF-Xla.Siam:nlsmCherry)*^{ia5} *(Moro et al., Dev Biol 2012) (referred to as TCF-siam:Red* it is a canonical Wnt signaling in vivo reporter). Both in LH-2-40-treated embryos and in *bcl9*$^{\Delta 29}$ mutants (Figure 1N-Q), we could measure a specific alteration of *TCF-siam:Red* expression in the atrio-ventricular valve, in the craniofacial structures, and in the pectoral fins, at 3 and 5 dpf (Figure 4M-T).

While we cannot rule out that Bcl9 and Pygo proteins possess additional functions that are independent of Wnt/β-catenin signaling, these results provide compelling genetic evidence that they are simultaneously required during vertebrate heart development for β-catenin-dependent transcription.

Figure 3

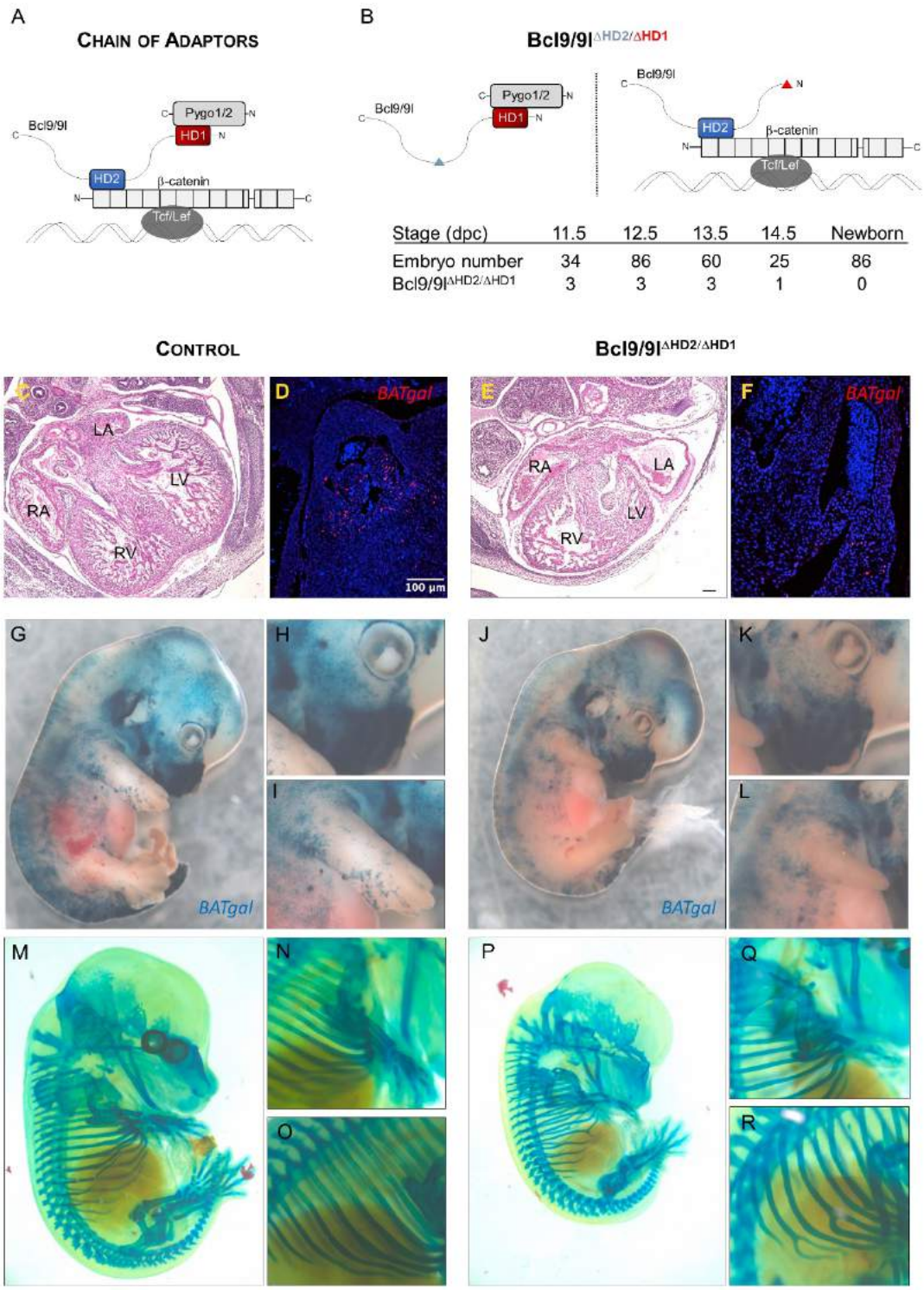
A
CHAIN OF ADAPTORS
Bcl9/9l
Pygo1/2
HD1
HD2
β-catenin
Tcf/Lef
B
Bcl9/9l ΔHD2/ΔHD1
Bcl9/9l
Pygo1/2
HD1
HD2
β-catenin
Tcf/Lef
Stage (dpc) 11.5 12.5 13.5 14.5 Newborn
Embryo number 34 86 60 25 86
Bcl9/9l ΔHD2/ΔHD1 3 3 3 1 0
CONTROL
Bcl9/9l ΔHD2/ΔHD1
LA
LV
RA
RV
D
BATgal
100 µm
E
F
G
H
I
J
K
L
M
N
O
P
Q
R

Figure 3: The abrogation of the tripartite b-catenin-Bcl9-Pygo complex leads to selective heart and skeletal defects.

(**A**) Schematic representation of the β-catenin transcriptional complex. Bcl9/9l simultaneously interact with Pygo1/2 and β-catenin via the domains HD1 and HD2, respectively. (**B**) In the *Bcl9/9l-Δ1/Δ2* mice, no Bcl9/9l molecule can simultaneously bind Pygo1/2 and β-catenin; the deletion of the HD2 or HD1 domains abrogates Bcl9/9l binding to β-catenin (left panel) or Pygo1/2 (right panel), respectively. *Bcl9/9l-Δ1/Δ2* embryos are never found after stage 14.5 dpc (table). (**C-H**) In vivo *BATgal* reporter expression at 13.5 dpc: mutant embryos have a slightly decreased reporter expression, but it is generally retained in most tissues (compare **C** and **F**, or **D** and **G**). *Bcl9/9l-Δ1/Δ2* embryos display severe limb defects accompanied by a complete loss of canonical Wnt signalling activity as reported by the lack of *BATgal* expression (compare **E** with **H**). (**I-N**) Alcian blue cartilage staining reveals loss of digits in *Bcl9/9l-Δ1/Δ2* embryos (compare **I-J** with **L-M**). Other cartilage malformations are present, for example rib bifurcations (**K, N**). (**O, P**) H&E staining of heart sections at 13.5 dpc. *Bcl9/9l-Δ1/Δ2* embryos sport pronounced heart defects, in particular in the ventricle walls, the forming septum, the AV valves and outflow tract. (**X,Y**) The expression of *BATgal* in the outflow tract region is completely lost in *Bcl9/9l-Δ1/Δ2* mutant hearts. RA, right atrium; LA, left atrium; RV, right ventricle; LV, left ventricle.

Figure 4

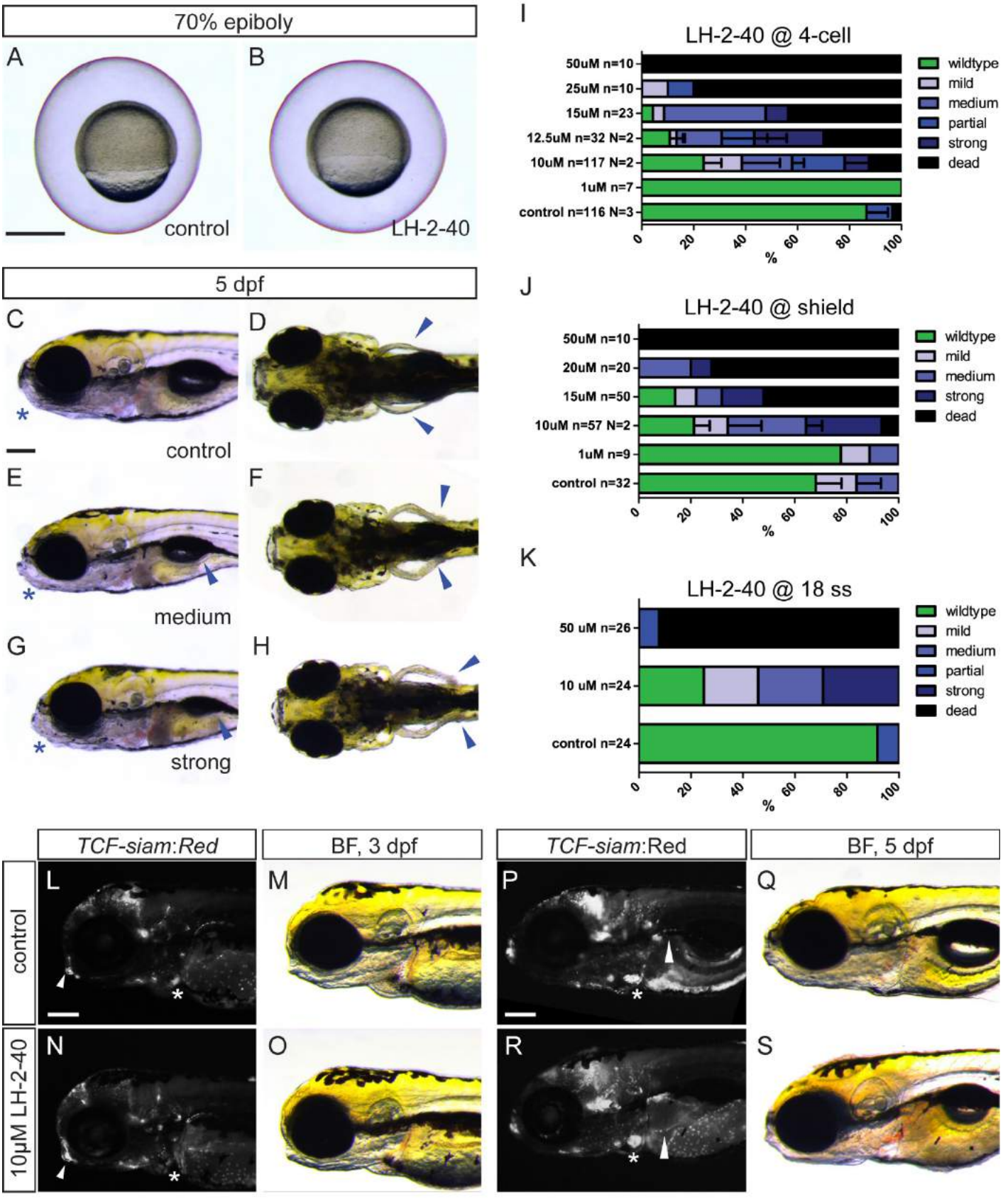
70% epiboly
A
B
control
LH-2-40
5 dpf
C
D
control
E
F
medium
G
H
strong
I
LH-2-40 @ 4-cell
50uM n=10
25uM n=10
15uM n=23
12.5uM n=32 N=2
10uM n=117 N=2
1uM n=7
control n=116 N=3
wildtype
mild
medium
partial
strong
dead
0
20
40
60
80
100
%
J
LH-2-40 @ shield
50uM n=10
20uM n=20
15uM n=50
10uM n=57 N=2
1uM n=9
control n=32
wildtype
mild
medium
strong
dead
0
20
40
60
80
100
%
K
LH-2-40 @ 18 ss
50 uM n=26
10 uM n=24
control n=24
wildtype
mild
medium
partial
strong
dead
0
20
40
60
80
100
%
TCF-siam:Red
BF, 3 dpf
TCF-siam:Red
BF, 5 dpf
control
10μM LH-2-40
L
M
P
Q
N
O
R
S

Figure 4: The Bcl9 inhibitor LH-2-40 induces phenotypes mimicking *bcl9*$^{\Delta 29}$ mutants.
(**A-B**) Treatment with 10 µM LH-2-40 from 2-4 cell stage does not result in gastrulation defects. Scale bar 500 µm. (**C-H**) Phenotypes in LH-2-40 treated embryos become visible at 5 dpf, comparable to phenotypes observed in *bcl9*$^{\Delta 29}$ mutants. LH-2-40 treated embryos show a variable phenotype expressivity with mild to strong swim bladder inflation defects (arrow heads **E,G**) caused variable craniofacial defects (asterisks **C,E,G**). Additionally, Bcl9 inhibited larvae with medium or strong phenotype expressivity are characterized by readily observable fin phenotypes (arrow heads **D,F,H**). Scale bar 200 µm. (**I-K**) Similar dose-dependent phenotype penetrance and expressivity can be observed after Bcl9 inhibition at 4-cells, shield and 18 ss stage suggesting that the observed phenotypes result from Bcl9 function in craniofacial, fin, and heart development after somitogenesis. Mild phenotypes are characterized by mild craniofacial and swim bladder defects without observable fin defects. Partial phenotypes show strong craniofacial defects and a complete failure to inflate the swim bladder, but no fin defects. Medium and strong phenotypes as described in (**E-H**). (**L-S**) Fluorescent and brightfield images of *TCF:siamRed* Bcl9 inhibited and DMSO treated wildtype siblings. *TCF* reporter activity is severely reduced in the atrio-ventricular valve at 3 dpf (asterisks **L,N**) and altered in the craniofacial cartilage (arrow heads **L,N**). At 5 dpf, TCF is miss-expressed in the atrio-ventricular valve (asterisks **P,R**) and fins (arrow heads **P,R**). Scale bars 200 µm.

Bcl9-Pygo act in neural crest cells and cardiac heart progenitors

The zebrafish and mouse phenotypes described above suggest a potential role for the Bcl9-Pygo complex both in neural crest cells as well as in mesodermal cardiac progenitors. We set out to test this by using mouse genetics, and combining conditional alleles of *Pygo1/2* and *Bcl9/9l* with tissue-specific Cre-drivers (Figure 5A,B). When we combined the conditional *Pygo1/2* and Bcl9/9l alleles (*Pygo1*$^{flox/flox}$;*Pygo2*$^{flox/flox}$, referred to as *Pygo-flox; Bcl9* $^{flox/flox}$*;Bcl9l* $^{flox/flox}$*,* referred to as *Bcl9/9l-flox*) with the neural crest-specific Cre-driver *Wnt1-Cre,* we observed embryonic lethality at 13.5/14.5 dpc, and heart malformations that morphologically recapitulated the constitutive loss of *Pygo1/2* (Figure 2Q, Figure 5A).

The transcription factors Pax3 and Pitx2 are required for the migration and expansion of CNC cells at 10.5 dpc (Bang et al., 1999; Kioussi et al., 2002). We observed decreased expression of *Pax3* and *Pitx2* transcripts in migratory CNC cells in *Pygo1/2*-mutant embryos at 10.5 dpc, (Figure 2I-P). In addition, cultured primary neural crest cells, isolated from the pharyngeal arches at 10.5 dpc from *Pygo-flox* embryos, displayed signs of impaired differentiation into smooth muscle actin (SMA)-positive non-neuronal cells (Achilleos and Trainor, 2012), when *Pygo1/2* conditional alleles were recombined via transduction of Adeno-CreEGFP viral particles (Figure 5C). This provided strong evidence that the OFT valves and septation defects we observed might be due to aberrant CNC cell differentiation.

Defective myocardium and cardiac valve formation in *Pygo* and *Bcl9* mutant mice and fish could be a secondary consequence of failed OFT morphogenesis, due to perturbed communication of colonizing extra-cardiac neural crest lineages with cardiac and endocardial progenitors (Neeb et al., 2013). To test for earlier heart field defects contributing to cardiac malformations upon Bcl9/9l-Pygo1/2 perturbation, we combined *Pygo-flox and Bcl9/9l-flox* with a Cre-recombinase driven by the regulatory regions of the cardiac homeobox gene *Nkx2-5*, activated in heart progenitors at early cardiac crescent stages (ca. 7.5 dpc) (Stanley et al., 2010). *Nkx2.5*-Cre-mediated *Bcl9/9l* recombination led to embryonic lethality around 13.5 dpc, with obvious myocardial malformations, such as thinner myocardium and aberrantly enlarged atrio-ventricular valves (Figure 5B), indicating a cardiac mesoderm-specific requirement of the β-catenin-Bcl9-Pygo mediated transcription. Additionally, siRNA-mediated downregulation of *Pygo2* in cultured murine embryonic cardiomyocytes lead to enhanced signs of differentiation (Figure 5D), consistent with the known role of canonical Wnt signaling in preventing cardiomyocyte differentiation (Naito et al., 2006). We conclude that the Bcl9-Pygo complex is required both in migrating CNC cells and the early mesodermal Nkx2.5-expressing cardiac progenitors, whose interplay is crucial during heart development (Brade et al., 2013).

Figure 5

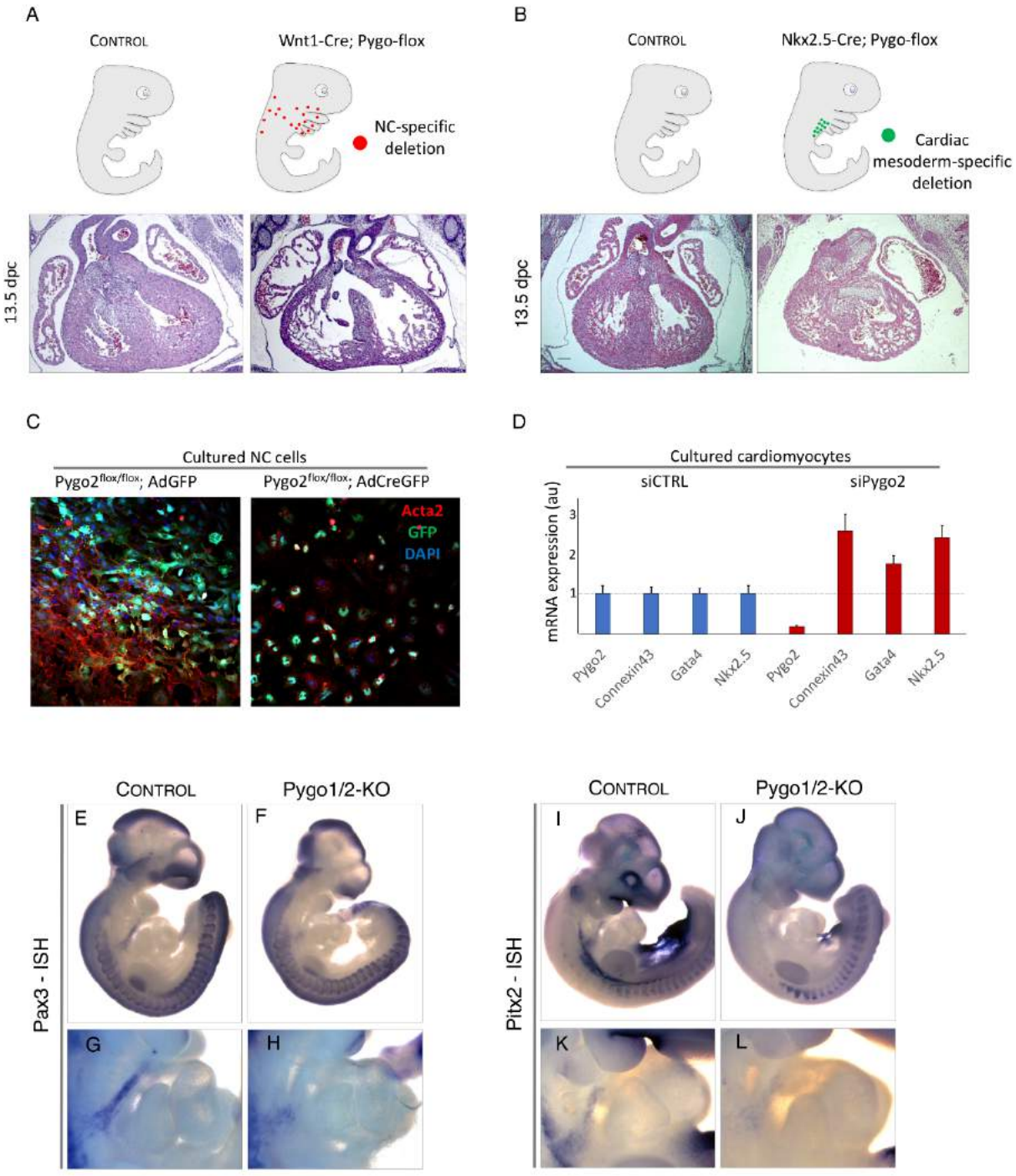
A
CONTROL
Wnt1-Cre; Pygo-flox
NC-specific deletion
13.5 dpc
B
CONTROL
Nkx2.5-Cre; Pygo-flox
Cardiac mesoderm-specific deletion
13.5 dpc
C
Cultured NC cells
Pygo2flox/flox; AdGFP
Pygo2flox/flox; AdCreGFP
Acta2
GFP
DAPI
D
Cultured cardiomyocytes
siCTRL
siPygo2
mRNA expression (au)
Pygo2
Connexin43
Gata4
Nkx2.5
Pygo2
Connexin43
Gata4
Nkx2.5
CONTROL
Pygo1/2-KO
Pax3 - ISH
E
F
G
H
CONTROL
Pygo1/2-KO
Pitx2 - ISH
I
J
K
L

Figure 5: Neural crest specific deletion of Pygo1/2 as well as cardiac mesoderm deletion of the same genes leads to similar defects as total loss of the protein.

(**A**) Schematic of the cells deleted upon Wnt1-Cre mediated recombination (red dots) and Haematoxilin/Eosin staining of heart section from wild-type (left panel) or neural crest-specific conditional *Pygo1/2* mutant mice (right panel). (**B**) Schematic of the cells deleted upon Nkx2.5-Cre mediated recombination (green dots). Akin to neural crest-specific loss of *Pygo1/2*, deletion of *Bcl9/9l* in *Nkx2.5*-expressing ALPM-derived cardiac progenitors disturb heart formation, in particular causing septal and valve defects (arrow) and highlighting important functions of the chain-of-adaptors in both mesodermal and neural crest lineages during cardiac morphogenesis. (**C**) Branchial arch cell explants from *Pygo1/2-flox* mice were treated with *adenoCre* viral particles and TGFβ to induce differentiation. Neural crest differentiation potential was markedly reduced upon treatment as indicated by the loss of smooth muscle actin (Acta2) fibers. (**D**) Cardiomyocyte cultures showed increase of differentiation markers upon siRNA mediated knock-down of Pygo2, consistent with a role for Pygo2 in these cells as well. (**E, F**) Whole mount ISH showing expression of the neural crest cell markers *Pax3* in representative 10.5 dpc wild-type (**E**) and mutant (**F**) embryos. (**G, H**) *Pax3* expression in the region of branchial arches (insets of I and J, respectively). (**I, J**) Whole mount ISH of *Pitx2* expression in 10.5 dpc wild-type (**I**) and mutant (**J**) embryos. *Pitx2* expression was drastically reduced in mutant embryos, particularly in periocular mesoderm, oral ectoderm, branchial arches and anterior somites. (**K, L**) *Pitx2* expression in the region of branchial arches.

The β-catenin-Pygo2 transcriptional complex directly activates a heart-specific genetic program

To get insights into the molecular mechanism that explains the previously described gene expression changes, we set out to discover the full ensemble of target genes directly controlled by the β-catenin-Bcl9-Pygo transcriptional module in the combined mesodermal heart progenitors and CNC cells.

In a first experiment, we dissected embryonic branchial arches 3-6, through which CNC progenitor cells migrate dorso-ventrally toward the heart cushion and OFT structures (Gessert and Kühl, 2010) together with the developing heart tube, from constitutive *Pygo1/2* mutant and control siblings at 10.5 dpc, and performed RNA-seq (N=4, Figure 6A). *Pygo1/2*-mutant embryos featured a reproducible set of 127 deregulated genes (p-value<0.05), 84 of which were downregulated and 53 upregulated (Figure 6B). Gene Ontology (GO) analysis (http://www.geneontology.org/) revealed that deregulated genes were associated with biological processes such as cardiac ventricle development, embryonic limb morphogenesis, skeletal system development and determination of bilateral symmetry, recapitulating the biological processes perturbed upon *bcl9* mutations in zebrafish (Figure 6D). Notably, the down-regulated genes included several genes encoding for transcription factors crucial for heart development, such as *Pitx2*, *Hand2*, *Msx1* and *Prrx1* (Andersen et al., 2014; Chen et

al., 2007; Kioussi et al., 2002; Ocaña et al., 2017), indicating that Wnt/β-catenin lies functionally upstream of a heart-specific genetic program. Although the statistical power of the RNA-seq was low, possibly due to the differences between samples caused by the manual dissection or individual variability, we could confirm the downregulation of the most relevant genes by in situ hybridization (ISH) (Figure 6E). STRING analysis of the differentially expressed genes revealed two Pygo-dependent clusters of important regulators of heart and limb development (Figure 6F). Because some of the differentially expressed genes found before the onset of cardiac defects at 11.5, such as *Pitx2*, *Hand2*, *Msx1* and *Prrx1,* are known important regulators that activate tissue-specific gene regulatory networks (Chen et al., 2007; Kioussi et al., 2002; Laurent et al., 2017; Nadadur et al., 2016; Ocaña et al, 2017), we interpret the phenotypes observed at 13.5 as a consequence of the early perturbation of these genes. These data raised the hypothesis that, at around 10.5 dpc, β-catenin-Bcl9/9l-Pygo1/2 activates several heart-specific effectors, whose combined deregulation produces the complement of heart defects we described at later stages. To test this, we collected ca. 250 wild-type mouse embryos at 10.5 dpc and carefully dissected the looping heart tube and pharyngeal arches 3-6, exactly as carried out for the RNA-seq experiment, and performed chromatin immunoprecipitation for β-catenin and Pygo2, followed by deep DNA sequencing (ChIP-seq, Figure 7A). This assay, performed in duplicate, revealed a total of 982 high-confidence genomic loci occupied by β-catenin, and 5252 by Pygo2 (Figure 7B). Of note, co-occupancy of β-catenin and Pygo2 was observed at a large fraction of the total β-catenin peaks (577/982), implying their in vivo interaction on a substantial number of regulatory genomic locations in developing cardiopharyngeal structures. Of interest, in line with its known role as chromatin code-reader (Bienz, 2006; Fiedler et al., 2015) and its Wnt-independent functions (Cantù et al., 2013), Pygo2 displayed a much broader spectrum of targets than β-catenin (Figure 7B). We focused our attention on the overlapping peaks (i.e. chain-of-adaptors targets): we found binding events in the vicinity of classical Wnt targets such as *Axin2* and *Lef1* (Figure 7D). These correspond to previously described Wnt-regulatory-elements (WRE) at these loci (Hovanes et al., 2001; Jho et al., 2002). Furthermore, we found heart specific genes like Prrx1 and Six1 (Figure 7D, lower panels). This, while constituting a strong validation of our experiment, indicated that mainstream Wnt target genes are mechanistically regulated via the β-catenin-Bcl9-Pygo interaction, in this context. Importantly, and consistent with the phenotypes and the gene expression profile described above, GO analysis of the targets revealed a striking enrichment of genes that control heart development and morphogenesis, cardiac chamber septation, and skeletal development (Figure 7C, E).

Figure 6

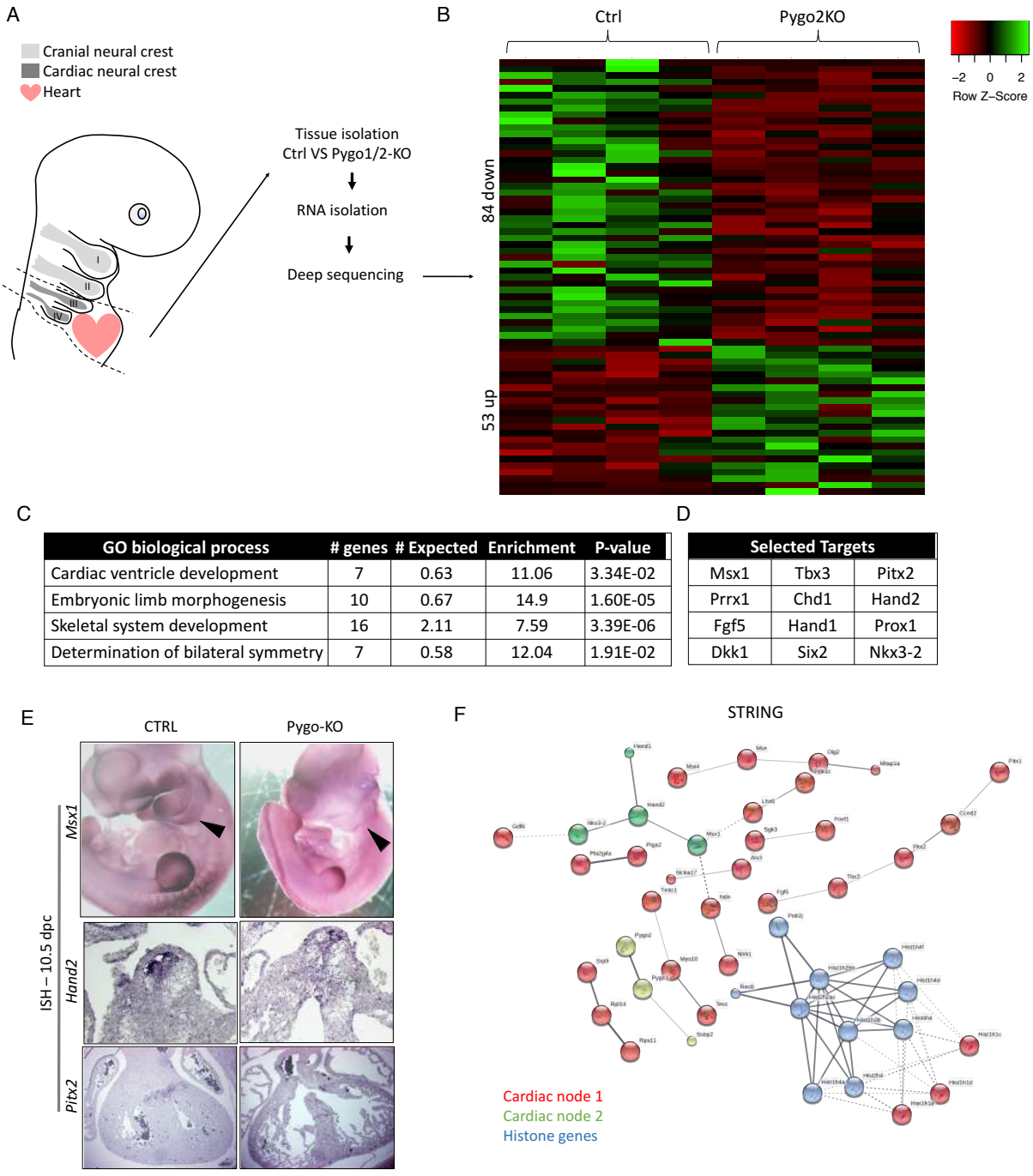

GO biological process	# genes	# Expected	Enrichment	P-value
Cardiac ventricle development	7	0.63	11.06	3.34E-02
Embryonic limb morphogenesis	10	0.67	14.9	1.60E-05
Skeletal system development	16	2.11	7.59	3.39E-06
Determination of bilateral symmetry	7	0.58	12.04	1.91E-02

Selected Targets		
Msx1	Tbx3	Pitx2
Prrx1	Chd1	Hand2
Fgf5	Hand1	Prox1
Dkk1	Six2	Nkx3-2

Figure 6: Pygo1/2 control a set of heart regulator genes, explaining the observed heart malformations.

(**A**) Artificial depiction of the dissected structures to extract the sequenced RNA from. (**B**) Heatmap showing the up- and down- regulated genes in Pygo1/2 mutant versus wilt-type E10.5 branchial arches and hearts. (**C**) Table showing the GO terms associated with the misregulated genes. (**D**) Selected targets that are misregulated upon loss of Pygo1/2. (**E**) Whole mount ISH for *Msx1* in E10.5 embryos shows strong downregulation of the transcript especially in the branchial arches (arrows), as well as parts of the forelimbs in *Bcl9/9l-Δ1/Δ2* mutants (upper 2 panels). Lower 4 panels: ISHs of

sections from E13.5 embryos. *Hand2* expression is reduced upon loss of Pygo2 especially in the valves. *Pitx2* expression is reduced upon ablation of Pygo in the neural crest cells via a Wnt1 Cre driver.
(**F**) STRING analysis network of the differentially expressed genes shows two heart specific cluster as well as a histone cluster of genes.

The intersection between the data deriving from the RNA-seq and the ChIP-seq, revealed that β-catenin, in this context, is an upstream regulator of important cardiac genes. Among these, *Msx1,* that governs CNC cell proliferation and migration, OFT formation, and EMT during AV valves formation (Chen et al., 2008, 2007), and Prrx1, a mesodermal homeobox transcriptional regulator of the neural crest-derived mesenchyme, whose function is highly conserved between fish and mammals (Braasch et al., 2014), and that activates a genetic program required for the formation of the heart asymmetry (Ocaña et al., 2017). Other direct targets include *Nr2f2,* mutations in which are causative of congenital AV septal defects (Al Turki et al., 2014), and Six2, a marker of the SHF progenitors, whose ablation leads to hypoplastic RV and pulmonary atresia (Zhou et al., 2017). Collectively, these data implicate that the β-catenin-dependent transcription, via the action of the transcriptional activators Bcl9/9l and Pygo1/2, is an upstream governor of a heart-specific genetic program, and that it acts by directly regulating a series of important heart-specific transcription factors.

Figure 7

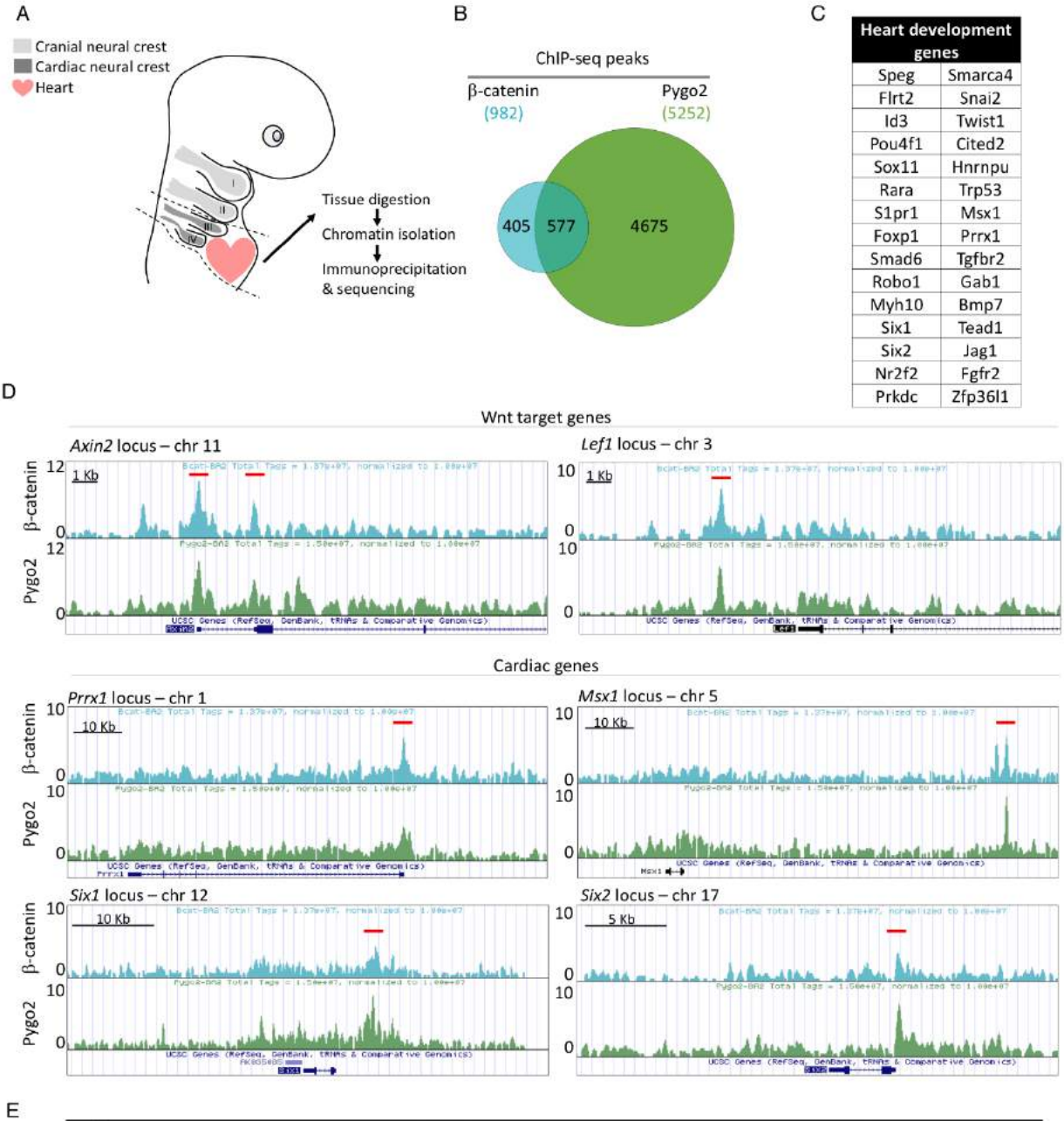

Heart development genes	
Speg	Smarca4
Flrt2	Snai2
Id3	Twist1
Pou4f1	Cited2
Sox11	Hnrnpu
Rara	Trp53
S1pr1	Msx1
Foxp1	Prrx1
Smad6	Tgfbr2
Robo1	Gab1
Myh10	Bmp7
Six1	Tead1
Six2	Jag1
Nr2f2	Fgfr2
Prkdc	Zfp36l1

E

β-catenin-Pygo2 common targets - GO biological process	# genes	# Expected	Enrichment	P-value
cardiac septum development	**14**	**2.53**	**5.54**	**3.40E-03**
heart development	**30**	**11.93**	**2.52**	**4.60E-02**
skeletal system morphogenesis	19	5.19	3.66	1.61E-02
heart morphogenesis	**20**	**5.54**	**3.61**	**1.06E-02**
negative regulation of transcription from RNA pol II	53	17.01	3.12	5.02E-09
negative regulation of transcription, DNA-templated	70	23.88	2.93	1.34E-11
negative regulation of RNA metabolic process	74	25.58	2.89	3.71E-12
negative regulation of nucleic acid-templated transcription	70	24.25	2.89	2.82E-11
negative regulation of RNA biosynthetic process	70	24.57	2.85	5.34E-11
in utero embryonic development	28	9.84	2.85	9.63E-03
negative regulation of cellular macromolecule biosynthesis	78	27.88	2.8	3.21E-12
chromatin organization	37	13.47	2.75	4.44E-04
muscle structure development	28	10.41	2.69	2.79E-02

Figure 7: Pygo and β-catenin co-occupy selective regulatory regions

(**A**) Illustration showing the upper body of a mouse embryo at 10.5 dpc. Dashed lines delineate the region dissected to perform ChIP-seq experiments. (**B**) Venn diagram depicting the peak overlap between β-catenin and Pygo2 occupancy. (**C**) 30 direct β-catenin-Bcl9/9l-Pygo2 target genes have been already implicated in heart development. (**D**) ChIP peaks on the *Axin2* (left panel) and *Lef1* (right panel) loci; these are prototypical Wnt target genes. Red bars indicate the position of previously described WREs. ChIP-seq custom tracks are visualized in the UCSC genome browser (https://genome.ucsc.edu). The lower 4 panels show the same tracks for *Prrx1* and *Six1*, two genes known to be crucial for heart development (**E**) Gene Ontology analysis of the common β-catenin and Pygo2 target genes reveals the direct regulation of processes associated with heart development.

Discussion

Bcl9/9l and Pygo1/2: new players in heart development

A role for Wnt signaling during cardiac morphogenesis was previously established: waves of activation and inhibition of Wnt/β-catenin signaling were shown to be essential for second heart field (SHF) progenitor proliferation (Ai et al., 2007; Cohen et al., 2007; Kwon et al., 2007; Qyang et al., 2007; Tian et al., 2010), for endocardial invagination and EMT and neural crest migration during cardiac valve formation (Liebner et al., 2004; Augustine et al., 1993; Bosada et al., 2016b; Hurlstone et al., 2003; Kirby and Hutson, 2010).

Here, by using genetics, genome engineering, chemical genetics, and biochemical approaches in the mouse and in zebrafish, we identify Bcl9/9l and Pygo1/2 as regulators of Wnt/β-catenin signaling during heart development. Of note, the cardiac defects induced by loss-of-function mutations in these genes include defective aortic arch, truncus arteriosus, incomplete chamber septation and aberrant valvulogenesis. Tantalizingly, *BCL9* and *BCL9L* have been recently connected to human congenital heart defects: *BCL9* has been reported as a frequently *de novo* mutated gene in innate CHD (Andersen et al., 2014; Zaidi et al., 2013), while loss of *BCL9L* has been genetically linked to heterotaxia (HTX), a human syndrome in which left-right asymmetry of various organs, including the heart, is perturbed (Saunders et al., 2012). Our study confirms this hypothesized connection, and shows that the consequence of the mutations in *BCL9* and *BCL9l* are due to perturbed canonical Wnt signaling. This is important, as the heart defects induced by mutations in *Bcl9* and *Pygo* genes resemble those commonly found in patients with different CHDs.

Notably, by combining RNA-seq and ChIP-seq studies, we found that Bcl9 and Pygo orchestrate the correct expression of mesodermal heart and neural crest regulators such as *Msx1, Prrx1, Hand2, Pitx2,* as well as members of the FGF signaling cascade (Lee et al., 2006; Li et al., 2016). We wish to point out that, among these genes, *Msx1* and *Prrx1*, display β-catenin and Pygo2 enrichment in their regulatory regions (Figure 7D) and can therefore be considered as new direct Wnt/β-catenin targets. Importantly, deregulation of these genes per se could lead, in principle, to the series of heart defects we observed: *Msx1* was previously implicated in CNC cell proliferation, OFT formation and EMT during AV valves formation (Chen et al., 2007, 2008), while *Prrx1* encodes for a mesodermal homeobox transcription factor that contributes in establishing the left-right asymmetry in zebrafish, and its downregulation causes heart looping defects (Ocaña et al., 2017). Other master regulators of heart development, such as *Hand2* and *Pitx2*, were found deregulated upon mutations of Bcl9/9l and Pygo1/2, but did not appear to be associated to any ChIP-seq peak, indicating that they are likely secondary targets. Notably, Hand2 controls cardiac development by triggering a gene regulatory network (GRN) of effectors with known functions in EMT processes and AVC cardiac cushion formation (Laurent et al., 2017), while Pitx2 modulates a Tbx5-dependent GRN necessary to proper adult heart function (Nadadur et al., 2016). The perturbation of Hand2 and/or Pitx2 activity is associated with several heart defects accordant with the phenotypes caused by loss of β-catenin-Bcl9-Pygo signaling (Andersen et al., 2014; Gessert and Kühl, 2010; Kioussi et al., 2002; Neeb et al., 2013). The observation that the β-catenin>Bcl9/9l>Pygo1/2 lies upstream of these mechanisms thrusts forward the notion that canonical Wnt/β-catenin signaling triggers a broad heart-specific GRN, via the direct activation of important regulators such as *Msx1* and *Prrx1* that, in turn, leads to the subsequent regulation of a plethora of other genes encoding for crucial heart regulators, among which the relevant Hand2 and Pitx2 transcription factors are included.

Of note, the human diseases DiGeorge Syndrome (DGS) and Holt-Oram Syndrome (HOS) present cardiac features resembling those identified in *Bcl9* and *Pygo* mutant mice. DGS is known to be caused by loss of *TBX1* function (Papangeli and Scambler, 2013; Yagi et al., 2003). Interestingly, it has been recently suggested that perturbation of β-catenin function causes DGS-like defects in murine hearts by affecting Fgf8-Tbx1 pathways activity, and that the unbalance of this mechanism might result in the variable expressivity observed in DGS patients (Racedo et al., 2017). Moreover, the combination of heart and limb defects is remarkably similar to the human genetic condition HOS, caused by mutations in *TBX5* (Al-Qattan and Abou Al-Shaar, 2015; Mori et al., 2006). Intriguingly, our data does not seem to suggest direct regulation of *Tbx1* or *Tbx5* by β-catenin. However, both *Tbx1* and *Tbx5* are

mildly downregulated at 12.5 dpc in the mouse, suggesting that they might be secondary targets, or that the interplay between these factors and the β-catenin transcriptional complex occurs at the protein level. Exploring the role of a Wnt/β-catenin dependent transcriptional network mediated in the context of a TBX factor-guided regulatory network presents a promising avenue of the project, and could potentially uncover new mechanistic insights into the molecular causes of DGS and HOS.

Canonical Wnt signaling is executed, in specific cell populations, via the β-catenin-Bcl9-Pygo chain of adaptors complex

Intriguingly, we found that in zebrafish as in the mouse, mutations in Bcl9 and Pygo lead to a location-specific downregulation of in vivo Wnt signaling reporters, as evidenced by the reduction of *TCF-siam:Red,* in *bcl9*$^{\Delta 29}$ mutants and LH-2-40-treated zebrafish embryos (Figure 1N-Q, Figure 4L,N,P,R), or of the widely used *BatGal* reporter transgene in the mouse (Figure 3D,F,G-L). Of note, the decrease in Wnt signaling was not ubiquitous but occurred in a tissue-specific manner. This is important, as these proteins have been discovered in Drosophila as constitutive transducers of the Wnt/Wg cascade (Kramps et al., 2002a; Townsley et al., 2004b), but their in vivo relevance as general β-catenin cofactors in other organisms has been the matter of a long debate (Cantù et al., 2014b, 2017; Mosimann et al., 2009; van Tienen et al., 2017). To understand the tissue-specific molecular mechanism of action of the Wnt/β-catenin-Bcl9-Pygo complex, we studied the effects of their mutation on the transcriptome (RNA-seq) and their genome-wide physical association to the DNA (ChIP-seq). The combination of these data sets established a new tissue-specific list of direct β-catenin transcriptional targets. Among these, we found not only classical Wnt targets, but also genes associated with tissue-specific differentiation programs, such as that of the heart, limbs and neural crest cells. Therefore, this study indicates that Wnt/β-catenin orchestrate cell fate in a tissue-specific manner, and invite revisiting the precise mechanisms of Wnt signaling-dependent transcription in other tissues.

Methods

Zebrafish husbandry and transgenic strains

All zebrafish embryos were raised and maintained in E3 medium at 28.5°C without light cycle essentially as described (Westerfield, 2007). All experiments were performed on embryos and larvae up to 5 dpf and older larvae only kept for raising mating pairs in agreement with procedures mandated by the veterinary office of UZH and the Canton of Zürich. Embryo staging was done according to morphological characteristics corresponding to hours post fertilization (hpf) or days post fertilization (dpf) as described previously (Kimmel et al., 1995). Previously established transgenic zebrafish lines used for this study include *Tg(-6.35drl:EGFP)* (Mosimann et al., 2015) and *Tg(7xTCF-Xla.Siam:nlsmCherry)*^{ia5} *(Moro et al., 2012).*

CRISPR-Cas9 mutagenesis

CRISPR-Cas9 mutagenesis was essentially performed as described in Burger et al. 2016(Burger et al., 2016). Oligo-based sgRNA templates (Bassett et al., 2013) were generated by PCR amplification using the the invariant reverse primer *5'-AAAAGCACCGACTCGGTGCCACTTTTTCAAGTTGATAACGGACTAGC CTT-3'* and forward primers of the sequence *5'-GAAATATTTAGGTGACACTATA-*(N_{20-22})*-GTTTTAGAGCTAGAAATAGC-3'* with N representing the 20 nucleotides of the *sgRNA* target sequence plus up to 2 *G*s at the 5'-end for successful T7 *in vitro* transcription. sgRNA (plus added 5'Gs in brackets) sequences were: i) *bcl9 5'-(G)GCCTGACTGCGCTACTTTAG-3'*; ii) *bcl9l 5'-(G)GATTTAGGTGTGCCAATCGG-3'*; iii) *pygo1 5'-GGACTTCCCAGTAGCAGCCC-3'* ; iv) *pygo2 5'-(G)GCCGATGGTTGACCACCTGG-3'*.

Crispants were raised to adulthood and crossed to wildtypes to make F1 germline mutants. All analyses and experiments were taken out on F2 mutant generations and beyond. Genotyping primers were designed to either amplify target regions of mutated alleles that were subsequently analyzed via sequencing (for *pygo1*Δ*1*) or high-percentage gel electrophoresis (for *bcl9*$^{\Delta 29}$) or allele-specific primers were designed to bind to mutated vs. wildtype sequences specifically (for *bcl9l*$^{\Delta 4}$ and *pygo1*$^{\Delta 5}$). Primers used were: i) *bcl9 5'-GGTGGAAAGCCCCAACTCC-3'* (fwd), *5'-CGTGTGCCAACTGCTGGTGG-3'* (rev); ii) *bcl9l 5'- CACTTGCAGGTGCTGCATGG-3'* (fwd), *5'- CTTTGAGATTTAGGTGTGCCGG-3'* (rev); iii) *pygo1 5'-CACTTTTACTGACCCCCACAC-3'* (fwd), *5'-GGACTTCCCAGTAGCAGGA-3'* (rev); iv) *pygo2 5'- GCCCAGAGAAAAAGAAGAGG-3'* (fwd), *5'-GCTGTCCACTTCCAGGTCC-3'* (rev). Genotyping results were analyzed and alleles visualized using CrisprVariantsLite as described in Lindsay et al., 2016(Lindsay et al., 2016).

Chemical treatments

Wildtype and *Tg(7xTCF-Xla.Siam:nlsmCherry)*^{ia5} embryos were treated with LH-2-40 to globally perturb Bcl9ΔHD2-β-catenin interaction at the respective developmental stages. LH-2-40 was kindly received from the laboratory of Dr. Haitao Ji at the Moffitt Cancer Center, Tampa/FL, USA. Single-use LH-2-40 stocks were kept at a concentration of 100 mM in DMSO at -80°C and thawed and diluted in E3 to a working concentration indicated in individual experiments directly before administration to the embryos.

Alcian Blue staining

Wildtype*, bcl9*, and *pygo1/2* mutant larvae were fixed in 4% Paraformaldehyde (PFA) overnight at 4°C and after washing in 0.1% PBS-Tween (PBST) stained in Alcian blue staining solution (0.1 g Alcian blue, 70 mL ethanol, 30 mLl glacial acetic acid) overnight at room temperature. Embryos were washed in Ethanol and transferred through an Ethanol series to PBST and subsequently bleached in hydrogen peroxide (3% H2O2 in 1% KOH in PBS) for 1 hour or until pigments of specimens became transparent.

Whole-mount in situ hybridization

Antisense RNA probes were designed for the genes *vcana*. First-strand complementary DNA (cDNA) was generated from pooled zebrafish RNA isolated from different developmental stages using Superscript III First-Strand Synthesis kit (Invitrogen). DNA templates were generated using first-strand cDNA as PCR template and following primers *5'-TTACGTATGCAGCCTTCTCG-3'* and *5'-GGTTCATGGGGTAACTGTGG-3'*). For *in vitro* transcription initiation, the T7 RNA polymerase promoter *5'-TAATACGACTCACTATAGGG-3'* was added to the 5'-end of reverse primers. PCR reactions were performed under standard conditions using Phusion High-Fidelity DNA Polymerase (ThermoFisher Scientific). RNA probes were generated via overnight incubation at 37°C using T7 RNA polymerase (20 U/µl) (Roche) and Digoxigenin (DIG)-labeled dNTPs (Roche). The resulting RNA was precipitated in lithium chloride and Ethanol.

Embryos were fixed in 4% PFA overnight at 4°C, transferred into 100% methanol and stored at -20°C. ISH of whole mount zebrafish embryos was performed essentially according to standard protocols (Thisse and Thisse, 2008).

Microscopy and data processing

Brightfield (BF), basic fluorescence, and ISH imaging was performed using a Leica M205FA equipped with a DFC450 C camera. Detailed fluorescent embryo imaging of *drl*:EGFP-expressing *bcl9* mutants was performed by Single Plane Illumination Microscopy (SPIM) with a Zeiss Lightsheet Z.1 microscope. Prior to imaging, embryos were embedded in a rod of 1% low melting agarose in E3 with 0.016% Ethyl 3-aminobenzoate methanesulfonate salt (Tricaine, Sigma) in a 50 µL glass capillary.

Image processing was done with Leica LAS, Zeiss Zen Black, ImageJ/Fiji and Adobe Photoshop and Illustrator CS6 according to image-preserving guidelines to ensure unbiased editing of the acquired image data. Quantitative data analysis was performed using GraphPad Prism 5.0. Data are presented as mean ± SEM. A lower case "n" denotes the number of embryos, while a capital "N" signifies the number of replicates.

Mouse lines

Knock-in mutants in *Bcl9* and *Bcl9l* were generated by standard techniques (inGenious Targeting Laboratory). Briefly, the targeting vector was electroporated into BA1 (C57BL/6 × 129/SvEv) hybrid embryonic stem cells. After selection with the antibiotic G418, surviving clones were expanded for PCR and Southern blotting analyses to confirm recombinant embryonic stem cell clones. Mouse embryonic stem cells harboring the knock-in allele were microinjected into C57BL/6 blastocysts. Resulting chimeras were bred to wild-type C57BL/6N mice to generate F1 heterozygous offspring. Neo cassette excision was obtained by crossing heterozygous knock-in animals with mice expressing Flp recombinase. All mouse experiments were performed in accordance with Swiss guidelines and approved by the Veterinarian Office of the Kanton of Zurich, Switzerland.

Histological analysis

Embryos between day E9.5 and E14.5 were fixed overnight in 4% paraformaldehyde at 4°C, dehydrated and embedded in paraffin. Sections were stained with haematoxylin and eosin for histological analysis. The same paraffin embedded material was sectioned under RNase free conditions for in situ hybridization.

Mouse in situ hybridization

Whole-mount in situ hybridization was performed as described previously (Piette et al., 2008). Digoxigenin-labeled probes (Roche) were detected by enzymatic color reaction using alkaline phosphatase-conjugated anti-digoxigenin Fab fragments (1:1000, Roche) and BM purple alkaline phosphatase substrate (Roche). In situ hybridization on paraffin sections was performed as described (Gregorieff et al., 2005). Digoxigenin-labeled RNA probes were

detected with peroxidase-conjugated anti-digoxigenin Fab fragments (1:500, Roche) followed by fluorescence detection using Tyramide Signal Amplification (PerkinElmer). Mouse antisense RNA probes were as described in supplementary materials.

Intracardiac injection of India ink

For the analysis of the cardiovascular system, india ink was injected into the left ventricle of mouse embryos at E14.5 using a finely drawn glass pipette. The embryos were fixed in 4% paraformaldehyde and hearts were dissected for the anatomic examination.

RNA sequencing

Zebrafish samples (poly A selection):

Zebrafish embryos from *bcl9*$^{\Delta 29/wt}$ crosses were dissected at 56 hpf: a cut was made between the anterior part of the embryo (containing the head, pharyngeal and cardiac structures) and the posterior part starting from the beginning of the yolk extension. The anterior tissues were directly snap-frozen in liquid nitrogen in single tubes of PCR 8-tube strips. The posterior trunks and tails were transferred in 50 mM NAOH and genomic DNA was extracted. Single embryos were genotypes using the target sequence primers listed above and PCR products were separated through high-percentage gel electrophoresis leading to a separation of the wildtype allele and mutant allele with the following outcome: i) a low running band in *bcl9*$^{\Delta 29}$ mutants; ii) a high running band in wildtypes; iii) two bands in *bcl9*$^{\Delta 29/wt}$ heterozygous mutants. All snap-frozen anterior parts of *bcl9*$^{\Delta 29}$ mutants and of wildtypes were pooled in two separate tubes and RNA isolation performed with the RNeasy Plus Mini Kit (Qiagen). The whole procedure was repeated for a total of three clutches making three independent replicates.

The TruSeq mRNA stranded kit from Illumina was used for the library preparation with 250 ng of total RNA as input. The libraries were 50-bases sequenced on an Illumina HiSeq 2500 sequencer. The quality control of the resulting reads was done with FastQC and the reads mapped to the UCSC Danio rerio danRer10 genome with the TopHat v.2.0.11 software. For differential expression analysis the gene features were counted with HTSeq v.0.6.1 (htseq-count) on the UCSC danRer10 gene annotation. The normalization and differential expression analysis were performed with R/Bioconductor package EdgeR v. 3.14. The p-values of the differentially expressed genes are corrected for multiple testing error with a 5 % false discovery rate (FDR) using Benjamini-Hochberg (BH).

Mouse samples (ribo depletion):

The Illumina TruSeq stranded Total RNA library Prep kit with RiboZero was used for the library preparation with 300 ng of total RNA as input. The libraries were 100-bases

sequenced on an Illumina HiSeq 4000 sequencer. The quality control of the resulting reads was done with FastQC and the reads mapped to the UCSC Mus musculus mm10 genome with the TopHat v.2.0.11 software. For differential expression analysis the gene features were counted with HTSeq v.0.6.1 (htseq-count) on the UCSC mm10 gene annotation. The normalization and differential expression analysis were performed with R/Bioconductor package EdgeR v. 3.14. The p-values of the differentially expressed genes are corrected for multiple testing error with a 5 % false discovery rate (FDR) using Benjamini-Hochberg (BH).

qRT-PCR

Quantitative real-time SYBR Green-based PCR reactions were performed in triplicate and monitored with the ABI Prism 7900HT system (Applied Biosystem).

ChIP

Ca. 200 branchial arches of E10.5 embryos were fixed with EGS (5mM) for 40 minutes, then 1% formaldehyde was added for another 20 min at room temperature. Cells were then lysed in a nuclei lysis buffer (1% SDS, 50 mM Tris, 10 mM EDTA, protease inhibitors). Chromatin was sonicated to a size between 200 and 1000 base pairs using a Covaris focused ultrasonicator (10 times for 1 min, 10% duty cycle, 5% intensity, 100 cycles per burst). The antibodies used were anti IgG (Santa Cruz), anti-Pygo2 (Novus Biological, NBP1-46171) and anti-β-catenin (Cl. 14, BD Transduction Laboratories, 610154).

Immunofluorescence

FFPE sections were blocked with 5% hings, % BSA and 0.1% Tween in PBS and incubated overnight at 4°C with the following antibodies: mouse anti p53 5E2 (NovusBio), rabbit anti Sox9 (Millipore), Troponin type2 (novus biologicals), Acta2 (Sommer lab), GFP (Aves). Slides were then incubated with a fluorescently labeled secondary antibody (Alexa 488 goat anti-mouse or Alexa 555 goat anti-rabbit, Alexa 594 goat anti-chicken; 1:500). Nuclei were stained with DAPI (1:1000; Sigma).

Branchial arch explants

Pharyngeal apparatus was dissected in PBS and resuspended in digestion mix (0.5mg collagenase/ml, 0.1% Trypsin) and incubate at 37 °C for 15min. Digestion was inactivated with 750ul of DMEM 10%FCS and plated in fibronectin coated wells in medium according to (Zhao et al., 2006), medium 2.

References

1. Zaidi, S. *et al.* De novo mutations in histone-modifying genes in congenital heart disease. *Nature* **498,** 220–3 (2013).
2. Andersen, T. A., Troelsen, K. D. L. L. & Larsen, L. A. Of mice and men: Molecular genetics of congenital heart disease. *Cell. Mol. Life Sci.* **71,** 1327–1352 (2014).
3. Nusse, R. & Clevers, H. Review. *Cell* **169,** 985–999 (2017).
4. Woudstra, O. I. *et al.* Origins and consequences of congenital heart defects affecting the right ventricle. *Cardiovasc. Res.* (2017). doi:10.1093/cvr/cvx155
5. Gessert, S. & Kühl, M. The multiple phases and faces of Wnt signaling during cardiac differentiation and development. *Circ. Res.* **107,** 186–199 (2010).
6. Buikema, J. W. *et al.* Wnt/β-catenin signaling directs the regional expansion of first and second heart field-derived ventricular cardiomyocytes. *Development* **140,** 4165–4176 (2013).
7. Kioussi, C. *et al.* Identification of a Wnt/Dvl/β-catenin → Pitx2 pathway mediating cell-type-specific proliferation during development. *Cell* **111,** 673–685 (2002).
8. Neeb, Z., Lajiness, J. D., Bolanis, E. & Conway, S. J. Cardiac outflow tract anomalies. *Wiley Interdiscip. Rev. Dev. Biol.* **2,** 499–530 (2013).
9. Mosimann, C., Hausmann, G. & Basler, K. Beta-catenin hits chromatin: regulation of Wnt target gene activation. *Nat. Rev. Mol. Cell Biol.* **10,** 276–86 (2009).
10. Kramps, T. *et al.* Wnt/wingless signaling requires BCL9/legless-mediated recruitment of pygopus to the nuclear beta-catenin-TCF complex. *Cell* **109,** 47–60 (2002).
11. Townsley, F. M., Cliffe, A. & Bienz, M. Pygopus and Legless target Armadillo/beta-catenin to the nucleus to enable its transcriptional co-activator function. *Nat. Cell Biol.* **6,** 626–33 (2004).
12. van Tienen, L. M. *et al.* Constitutive scaffolding of multiple Wnt enhanceosome components by Legless/BCL9. *Elife* **6,** 477–488 (2017).
13. Kennedy, M. W. *et al.* A co-dependent requirement of xBcl9 and Pygopus for embryonic body axis development in Xenopus. *Dev. Dyn.* **239,** 271–83 (2010).
14. Brembeck, F. H. *et al.* Essential role of BCL9-2 in the switch between NL -catenin ' s adhesive and transcriptional functions. *Genes Dev.* 2225–2230 (2004). doi:10.1101/gad.317604.GENES
15. Schwab, K. R. *et al.* Pygo1 and Pygo2 roles in Wnt signaling in mammalian kidney

development. *BMC Biol.* **5,** 15 (2007).

16. Li, B. *et al.* Developmental Phenotypes and Reduced Wnt Signaling in Mice Deficient for Pygopus 2. **325,** 318–325 (2007).

17. Cantù, C. *et al.* The Pygo2-H3K4me2/3 interaction is dispensable for mouse development and Wnt signaling-dependent transcription. *Development* **140,** 2377–86 (2013).

18. Cantù, C. *et al.* Pax6-dependent , but b -catenin- independent , function of Bcl9 proteins in mouse lens development. 1879–1884 (2014). doi:10.1101/gad.246140.114.double-knockout

19. Cantù, C. *et al.* A cytoplasmic role of Wnt/β-catenin transcriptional cofactors Bcl9, Bcl9l, and Pygopus in tooth enamel formation. *Sci. Signal.* **10,** 1–11 (2017).

20. Burger, A. *et al.* Maximizing mutagenesis with solubilized CRISPR-Cas9 ribonucleoprotein complexes. *Development* **143,** 2025–37 (2016).

21. Mosimann, C. *et al.* Chamber identity programs drive early functional partitioning of the heart. *Nat. Commun.* **6,** 8146 (2015).

22. Brembeck, F. H. *et al.* Essential role of BCL9-2 in the switch between beta-catenin's adhesive and transcriptional functions. *Genes Dev* **18,** 2225–2230 (2004).

23. Rossi, A. *et al.* Genetic compensation induced by deleterious mutations but not gene knockdowns. *Nature* **524,** 230–233 (2015).

24. Kramps, T. *et al.* Wnt/wingless signaling requires {BCL}9/legless-mediated recruitment of pygopus to the nuclear beta-catenin-{TCF} complex. *Cell* **109,** 47–60 (2002).

25. Thompson, B., Townsley, F., Rosin-Arbesfeld, R., Musisi, H. & Bienz, M. A new nuclear component of the {Wnt} signalling pathway. *Nat. Cell Biol.* **4,** 367–373 (2002).

26. Szklarczyk, D. *et al.* STRING v10: Protein-protein interaction networks, integrated over the tree of life. *Nucleic Acids Res.* **43,** D447–D452 (2015).

27. Racedo, S. E. *et al.* Reduced dosage of β-catenin provides significant rescue of cardiac outflow tract anomalies in a Tbx1 conditional null mouse model of 22q11.2 deletion syndrome. *PLoS Genet.* **13,** 1–23 (2017).

28. Ranger, a M. *et al.* The transcription factor NF-ATc is essential for cardiac valve formation. *Nature* **392,** 186–190 (1998).

29. Combs, M. D. & Yutzey, K. E. Heart valve development: Regulatory networks in

development and disease. *Circ. Res.* **105,** 408–421 (2009).

30. Song, N. *et al.* pygopus 2 has a crucial, Wnt pathway-independent function in lens induction. *Development* **134,** 1873–85 (2007).

31. Liebner, S. *et al.* B-Catenin Is Required for Endothelial-Mesenchymal Transformation During Heart Cushion Development in the Mouse. *J. Cell Biol.* **166,** 359–367 (2004).

32. Bosada, F. M., Devasthali, V., Jones, K. A. & Stankunas, K. Wnt/β-catenin signaling enables developmental transitions during valvulogenesis. *Development* **143,** (2016).

33. Bang, A. G., Papalopulu, N., Goulding, M. D. & Kintner, C. Expression of Pax-3 in the Lateral Neural Plate Is Dependent on a Wnt-Mediated Signal from Posterior Nonaxial Mesoderm. *Dev. Biol.* **212,** 366–380 (1999).

34. Bienz, M. The PHD finger, a nuclear protein-interaction domain. *Trends Biochem. Sci.* **31,** 35–40 (2006).

35. Wisniewski, J. A., Yin, J., Teuscher, K. B., Zhang, M. & Ji, H. Structure-Based Design of 1,4-Dibenzoylpiperazines as β-Catenin/B-Cell Lymphoma 9 Protein–Protein Interaction Inhibitors. *ACS Med. Chem. Lett.* acsmedchemlett.5b00284 (2016). doi:10.1021/acsmedchemlett.5b00284

36. Achilleos, A. & Trainor, P. A. Neural crest stem cells: discovery, properties and potential for therapy. *Cell Res.* **22,** 288–304 (2012).

37. Stuhlmiller, T. J. & García-Castro, M. I. Current perspectives of the signaling pathways directing neural crest induction. *Cell. Mol. Life Sci.* **69,** 3715–3737 (2012).

38. Stanley, E. G. *et al.* Efficient cre-mediated deletion in cardiac progenitor cells conferred by a 3 ' UTR-ires-Cre allele of the homeobox gene Nkx2-5. **439,** 431–439 (2010).

39. Naito, A. T. *et al.* Developmental stage-specific biphasic roles of Wnt/beta-catenin signaling in cardiomyogenesis and hematopoiesis. *Proc. Natl. Acad. Sci. U. S. A.* **103,** 19812–7 (2006).

40. Brade, T., Pane, L. S., Moretti, A., Chien, K. R. & Laugwitz, K. L. Embryonic heart progenitors and cardiogenesis. *Cold Spring Harb. Perspect. Med.* **3,** 1–17 (2013).

41. Chen, Y. H., Ishii, M., Sun, J., Sucov, H. M. & Maxson, R. E. Msx1 and Msx2 regulate survival of secondary heart field precursors and post-migratory proliferation of cardiac neural crest in the outflow tract. *Dev. Biol.* **308,** 421–437 (2007).

42. Ocaña, Oscar H.; Coskun, Hakan; Minguillón, Carolina; Murawala, Prayag; Elly M. Tanaka; Galcerán, Joan; Muñoz-Chapuli, Ramón; Nieto, M. Á. A right-handed

signalling pathway drives heart looping in vertebrates. *Nature* **549,** 86–90 (2017).

43. Nadadur, R. D. *et al.* Pitx2 modulates a Tbx5-dependent gene regulatory network to maintain atrial rhythm. *Sci. Transl. Med.* **8,** 354ra115-354ra115 (2016).

44. Laurent, F. *et al.* HAND2 Target Gene Regulatory Networks Control Atrioventricular Canal and Cardiac Valve Development. *Cell Rep.* **19,** 1602–1613 (2017).

45. Fiedler, M. *et al.* An ancient Pygo-dependent Wnt enhanceosome integrated by chip/LDB-SSDP. *Elife* **4,** 1–22 (2015).

46. Jho, E. *et al.* Wnt / β -Catenin / Tcf Signaling Induces the Transcription of Axin2 , a Negative Regulator of the Signaling Pathway Wnt / ß-Catenin / Tcf Signaling Induces the Transcription of Axin2 , a Negative Regulator of the Signaling Pathway. *Mol. Cell. Biol.* **22,** 1172–1183 (2002).

47. Hovanes, K. *et al.* Beta-catenin-sensitive isoforms of lymphoid enhancer factor-1 are selectively expressed in colon cancer. *Nat. Genet.* **28,** 53–7 (2001).

48. Chen, Y.-H., Ishii, M., Sucov, H. M. & Maxson, R. E. Msx1 and Msx2 are required for endothelial-mesenchymal transformation of the atrioventricular cushions and patterning of the atrioventricular myocardium. *BMC Dev. Biol.* **8,** 75 (2008).

49. Braasch I., Guiguen Y., Loker R., Letaw J.H., Ferrara A., Bobe J., and P. J. H. Connectivity of vertebrate genomes: Paired-related homeobox (Prrx) genes in spotted gar, basal teleosts, and tetrapods. **76,** 24–36 (2014).

50. Al Turki, S. *et al.* Rare variants in NR2F2 cause congenital heart defects in humans. *Am. J. Hum. Genet.* **94,** 574–585 (2014).

51. Zhou, Z. *et al.* Temporally Distinct Six2-Positive Second Heart Field Progenitors Regulate Mammalian Heart Development and Disease. *Cell Rep.* **18,** 1019–1032 (2017).

52. Ai, D. *et al.* Canonical Wnt signaling functions in second heart field to promote right ventricular growth. *Proc. Natl. Acad. Sci. U. S. A.* **104,** 9319–24 (2007).

53. Cohen, E. D. *et al.* Wnt/beta-catenin signaling promotes expansion of Isl-1-positive cardiac progenitor cells through regulation of FGF signaling. *J. Clin. Invest.* **117,** 1794–804 (2007).

54. Kwon, C. *et al.* Canonical Wnt signaling is a positive regulator of mammalian cardiac progenitors. *Proc. Natl. Acad. Sci. U. S. A.* **104,** 10894–9 (2007).

55. Qyang, Y. *et al.* The renewal and differentiation of Isl1+ cardiovascular progenitors are controlled by a Wnt/beta-catenin pathway. *Cell Stem Cell* **1,** 165–79 (2007).

56. Tian, Y. *et al.* Characterization and In Vivo Pharmacological Rescue of a Wnt2-Gata6 Pathway Required for Cardiac Inflow Tract Development. *Dev. Cell* **18,** 275–287 (2010).

57. Augustine, K., Liu, E. T. & Sadler, T. W. Antisense attenuation ofWnt-1 andWnt-3a expression in whole embryo culture reveals roles for these genes in craniofacial, spinal cord, and cardiac morphogenesis. *Dev. Genet.* **14,** 500–520 (1993).

58. Hurlstone, A. F. L. *et al.* The Wnt/β-catenin pathway regulates cardiac valve formation. *Nature* **425,** 633–637 (2003).

59. Kirby, M. L. & Hutson, M. R. Factors controlling cardiac neural crest cell migration. *Cell Adh. Migr.* **4,** 609–21 (2010).

60. Saunders, C. J. *et al.* Rapid whole-genome sequencing for genetic disease diagnosis in neonatal intensive care units. *Sci. Transl. Med.* **4,** 154ra135 (2012).

61. Li, J., Yue, Y. & Zhao, Q. Retinoic Acid Signaling Is Essential for Valvulogenesis by Affecting Endocardial Cushions Formation in Zebrafish Embryos. *Zebrafish* **13,** 9–18 (2016).

62. Lee, Y. M. *et al.* Vascular endothelial growth factor receptor signaling is required for cardiac valve formation in zebrafish. *Dev. Dyn.* **235,** 29–37 (2006).

63. Papangeli, I. & Scambler, P. The 22q11 deletion: DiGeorge and velocardiofacial syndromes and the role of *TBX1*. *Wiley Interdiscip. Rev. Dev. Biol.* **2,** 393–403 (2013).

64. Yagi, H. *et al.* Role of TBX1 in human del22q11.2 syndrome. *Lancet (London, England)* **362,** 1366–73 (2003).

65. Al-Qattan, M. M. & Abou Al-Shaar, H. Molecular basis of the clinical features of Holt-Oram syndrome resulting from missense and extended protein mutations of the TBX5 gene as well as TBX5 intragenic duplications. *Gene* **560,** 129–136 (2015).

66. Mori, A. D. *et al.* Tbx5-dependent rheostatic control of cardiac gene expression and morphogenesis. *Dev. Biol.* **297,** 566–586 (2006).

67. Townsley, F. M., Thompson, B. & Bienz, M. Pygopus residues required for its binding to Legless are critical for transcription and development. *J. Biol. Chem.* **279,** 5177–83 (2004).

68. Cantù, C. *et al.* Pax6-dependent, but β-catenin-independent, function of Bcl9 proteins in mouse lens development. *Genes Dev.* **28,** 1879–84 (2014).

69. Westerfield, M. *The Zebrafish Book: a guide for the laboratory use of zebrafish (Danio rerio)*. (University of Oregon Press, 2007).

70. Kimmel, C. B., Ballard, W. W., Kimmel, S. R., Ullmann, B. & Schilling, T. F. Stages of embryonic development of the zebrafish. *Dev Dyn* **203,** 253–310 (1995).

71. Moro, E. *et al.* In vivo Wnt signaling tracing through a transgenic biosensor fish reveals novel activity domains. *Dev. Biol.* **366,** 327–340 (2012).

72. Bassett, A. R., Tibbit, C., Ponting, C. P. & Liu, J.-L. Highly efficient targeted mutagenesis of Drosophila with the CRISPR/Cas9 system. *Cell Rep.* **4,** 220–8 (2013).

73. Lindsay, H. *et al.* CrispRVariants charts the mutation spectrum of genome engineering experiments. *Nat. Biotechnol.* **34,** 701–702 (2016).

74. Thisse, C. & Thisse, B. High-resolution in situ hybridization to whole-mount zebrafish embryos. *Nat. Protoc.* **3,** 59–69 (2008).

75. Piette, D., Hendrickx, M., Willems, E., Kemp, C. R. & Leyns, L. An optimized procedure for whole-mount in situ hybridization on mouse embryos and embryoid bodies. *Nat. Protoc.* **3,** 1194–1201 (2008).

76. Gregorieff, A. *et al.* Expression pattern of Wnt signaling components in the adult intestine. *Gastroenterology* **129,** 626–638 (2005).

77. Zhao, H., Bringas, P. & Chai, Y. An in vitro model for characterizing the post-migratory cranial neural crest cells of the first branchial arch. *Dev. Dyn.* **235,** 1433–1440 (2006).

Supplementary Table 1

Gene name	FC	Zfin ID	Expression
mcu	0.46	ZDB-GENE-061013-24	heart, heart tube
nos2b	0.44	ZDB-GENE-080916-1	mandibular arch skeleton
zgc:56699	0.46	ZDB-GENE-040426-2099	pharyngeal arches, pectoral fin
vegfaa	0.49	ZDB-GENE-990415-273	heart, pharyngeal arch
hoxc1a	0.45	ZDB-GENE-000822-2	pectoral fin bud, pharyngeal arch
plaub	0.36	ZDB-GENE-030619-15	heart
cyp3a65	0.43	ZDB-GENE-050604-1	heart
arhgap17a	0.31	ZDB-GENE-050417-56	pharyngeal arch
cdh5	0.43	ZDB-GENE-040816-1	heart, heart primordium, lateral mesoderm
adora2aa	0.46	ZDB-GENE-080723-28	heart
rspo1	0.50	ZDB-GENE-040718-44	heart
met	0.37	ZDB-GENE-041014-1	liver, pharyngeal arch
wtip	0.36	ZDB-GENE-050419-261	heart
tgfbr1a	0.44	ZDB-GENE-051120-75	pharyngeal arch
hoxb4a	0.41	ZDB-GENE-990415-105	pharyngeal arch
vwf	0.40	ZDB-GENE-070103-1	pharyngeal arch
rbck1	0.51	ZDB-GENE-040704-3	pharyngeal arch
mtf1	0.46	ZDB-GENE-020424-1	heart
mcoln1a	0.42	ZDB-GENE-040426-2704	heart
lepr	0.50	ZDB-GENE-080104-1	heart
fgfr1b	0.48	ZDB-GENE-060503-14	pharyngeal arch, fin bud
sema3ga	0.43	ZDB-GENE-050513-3	pharyngeal arch
cldn15la	0.46	ZDB-GENE-010328-12	heart
ucp3	0.46	ZDB-GENE-040426-1317	heart
cldng	0.48	ZDB-GENE-010328-7	lateral mesoderm, heart
erbb2	0.47	ZDB-GENE-031118-121	neural crest
grhl2b	0.43	ZDB-GENE-060503-719	otic vesicle, pectoral fin
ltk	0.48	ZDB-GENE-030616-115	neural crest
wnt1	0.50	ZDB-GENE-980526-526	neural crest
matn1	2.68	ZDB-GENE-050307-3	pharyngeal arch
gnrh3	8.96	ZDB-GENE-030724-4	heart
slc4a3	3.40	ZDB-GENE-141006-1	fin bud
pdlim3b	3.43	ZDB-GENE-060130-104	heart, heart tube, mandibular arch skeleton
srfb	2.87	ZDB-GENE-040426-1294	heart rudiment, primitive heart tube
fabp10a	3.24	ZDB-GENE-020318-1	heart
optc	2.74	ZDB-GENE-030131-1798	pharyngeal arch
myoz2a	2.92	ZDB-GENE-040426-1880	heart

Supplementary Table 1: De-regulated genes in *bcl9*$^{\Delta 29/\Delta 29}$ mutants with expression in cardiopharyngeal and/or pectoral fin precursors/derivatives as per Zfin annotations and selected publications.

A regulatory receptor network directs range and output of the Wingless signal

Sabine Schilling[1, 2] Sarah Steiner[1], Dario Zimmerli[1] and Konrad Basler

Institute of Molecular Life Sciences, University of Zurich, Switzerland

[1] Co-first authors

[2] Current address: Institute of Molecular Systems Biology, ETH Zurich, Switzerland

© 2014. Published by The Company of Biologists Ltd | Development (2014) 141, 2483-2493 doi:10.1242/dev.108662

RESEARCH ARTICLE

A regulatory receptor network directs the range and output of the Wingless signal

Sabine Schilling*,‡, Sarah Steiner‡, Dario Zimmerli‡ and Konrad Basler§

ABSTRACT

The potent activity of Wnt/Wingless (Wg) signals necessitates sophisticated mechanisms that spatially and temporally regulate their distribution and range of action. The two main receptor components for Wg – Arrow (Arr) and Frizzled 2 (Fz2) – are transcriptionally downregulated by Wg signaling, thus forming gradients that oppose that of Wg. Here, we analyze the relevance of this transcriptional regulation for the formation of the Wg gradient in the *Drosophila* wing disc by combining *in vivo* receptor overexpression with an *in silico* model of Wg receptor interactions. Our experiments show that ubiquitous upregulation of Arr and Fz2 has no significant effects on Wg output, whereas clonal overexpression of these receptors leads to signaling discontinuities that have detrimental phenotypic consequences. These findings are supported by our *in silico* model for Wg diffusion and signal transduction, which suggests that abrupt changes in receptor levels causes discontinuities in Wg signaling. Furthermore, we identify a 200 bp regulatory element in the *arr* locus that can account for the Arr gradient, and we show that this is indirectly negatively controlled by Wg activity. Finally, we analyze the role of Frizzled 3 (Fz3) in this system and find that its expression, which is induced by Wg, contributes to the establishment of the Arr and Fz2 gradients through counteracting canonical signaling. Taken together, our results provide a model in which the regulatory network of Wg and the three receptor components account for the range and shape of this prototypical morphogen system.

KEY WORDS: Wingless receptors, Wnt pathway, Model for Wg diffusion

INTRODUCTION

Communication between the cells in a tissue depends on extracellular signaling molecules. The vast majority of these are produced by defined subsets of cells. This restricted production provides spatial information that is needed for the signals to orchestrate patterning and growth. The signaling output is dependent on the range of action and level of activity of the secreted signaling protein – determinants that depend not only on the biochemical nature of the signal but also on the receptor systems that are employed by the receiving cells. The glycoproteins of the Wnt family serve as an interesting model to understand the interplay between these determinants.

Mechanisms that precisely and tightly control Wnt signal reception and transduction, both spatially and temporally, are absolutely necessary – Wnt signaling is crucial in many developmental processes, and improper activation of the canonical signaling cascade can have severe pathological consequences, such as cancer (Clevers, 2006). Altering receptor levels is often the first step in attenuating the cellular response to a signaling molecule. Receptor downregulation can be achieved on the transcriptional level through repression of the receptor-encoding gene, or on the protein level through internalization and subsequent lysosomal degradation. Both processes lead to a diminution of active receptors from the cell membrane and, thereby, to an attenuation of the signaling output.

Wingless (Wg), the founding member of the highly conserved Wnt family, plays an important role in the primordium of the *Drosophila melanogaster* wing (Zecca et al., 1996; Neumann and Cohen, 1997). In this tissue, Wg is expressed in a thin stripe at the dorsal-ventral boundary from where it spreads to either side, producing a symmetrical concentration gradient. The canonical Wnt/Wg transduction pathway is initiated by the binding of Wnt/Wg ligands to a receptor of the Frizzled family and a co-receptor, the low-density lipoprotein receptor-related LRP5/6 [Arrow (Arr) in *D. melanogaster*]. This binding transduces the extracellular signal into an intracellular cascade that ultimately results in the cytoplasmic stabilization and nuclear localization of β-catenin/Armadillo (Arm) and its subsequent association with TCF/LEF [Pangolin (Pan) in *D. melanogaster*] DNA binding proteins. The activation of Wnt target genes is promoted by the interaction of the bipartite Arm-Pan complex with various auxiliary co-factors (Mosimann et al., 2009).

In *Drosophila*, the genes encoding the Wg receptor Fz2 and the co-receptor Arr are transcriptionally downregulated by Wg signaling (Cadigan et al., 1998; Wehrli et al., 2000). However, the details of the underlying molecular mechanism, and an understanding of its physiological significance, are still lacking. Wnt-induced transcriptional repression could be either direct or indirect; only a detailed analysis of the *cis*-regulatory elements (CREs) and the corresponding transcription factors can distinguish between these modes of repression (Affolter et al., 2008). In addition to signaling-induced transcriptional downregulation, there is evidence for a collateral post-transcriptional layer of regulation of Wg receptors. Both Fz2 and Arr contain endocytosis signals and have been shown to localize to endocytic compartments together with their ligand Wg (Rives et al., 2006), which suggests that both the receptor and co-receptor are internalized upon Wg binding. The contribution of this to Wg internalization, however, is less clear, as it can also occur in their absence (Baeg et al., 2004).

Here, we experimentally address the contribution of the transcriptional regulation of the Wg receptors Arr and Fz2 to wing development and Wg gradient formation. We show that Wg-mediated patterning is, remarkably, unaffected by a ubiquitous upregulation of the levels of the receptor. However, local interruptions of the transcriptional gradient of *arr* and *fz2* lead to detrimental outcomes caused by an imbalance between receptor and ligand levels at the borders of signaling discontinuity. Furthermore, we uncover a second, but less important, layer of control – in high-signaling regions the decoy receptor Fz3 is expressed, dampening the signal. By dissecting

Institute of Molecular Life Sciences, University of Zurich, 8057 Zurich, Switzerland.
*Present address: Institute of Molecular Systems Biology, ETH Zurich, 8093 Zurich, Switzerland.
‡These authors contributed equally to this work

§Author for correspondence (basler@imls.uzh.ch)

Received 7 February 2014; Accepted 24 April 2014

Development (2014) 141, 2483-2493 doi:10.1242/dev.108662

the regulatory control regions that are responsible for *arr* and *fz3* expression, we find *fz3* to be a direct positive, and *arr* an indirect negative, target of the Wg pathway.

RESULTS

Transcriptional downregulation of Arr and Fz2 by Wg signaling

In the *Drosophila melanogaster* wing imaginal disc, the expression pattern of Arr and the inferred Wg protein gradient are inverse (Fig. 1A-C) – low Arr levels close to the Wg source are contrasted by high Arr levels at sites of little or no Wg. We explored the potential relevance of the Arr expression pattern by experimentally perturbing it, by using a heterologous ubiquitously active promoter. Surprisingly, animals that expressed Arr under the control of the *tubulinα1* promoter (*tubArr*) were viable and did not show any wing phenotypes. To monitor Arr expression in *tubArr* animals, we used an antibody against Arr for immunohistochemical analysis. Arr expression was elevated in *tubArr* wing pouches, but still graded, with reduced levels towards the Wg expression domain (Fig. 1D-F). We quantified the fluorescent intensities of Arr in *tubArr* and

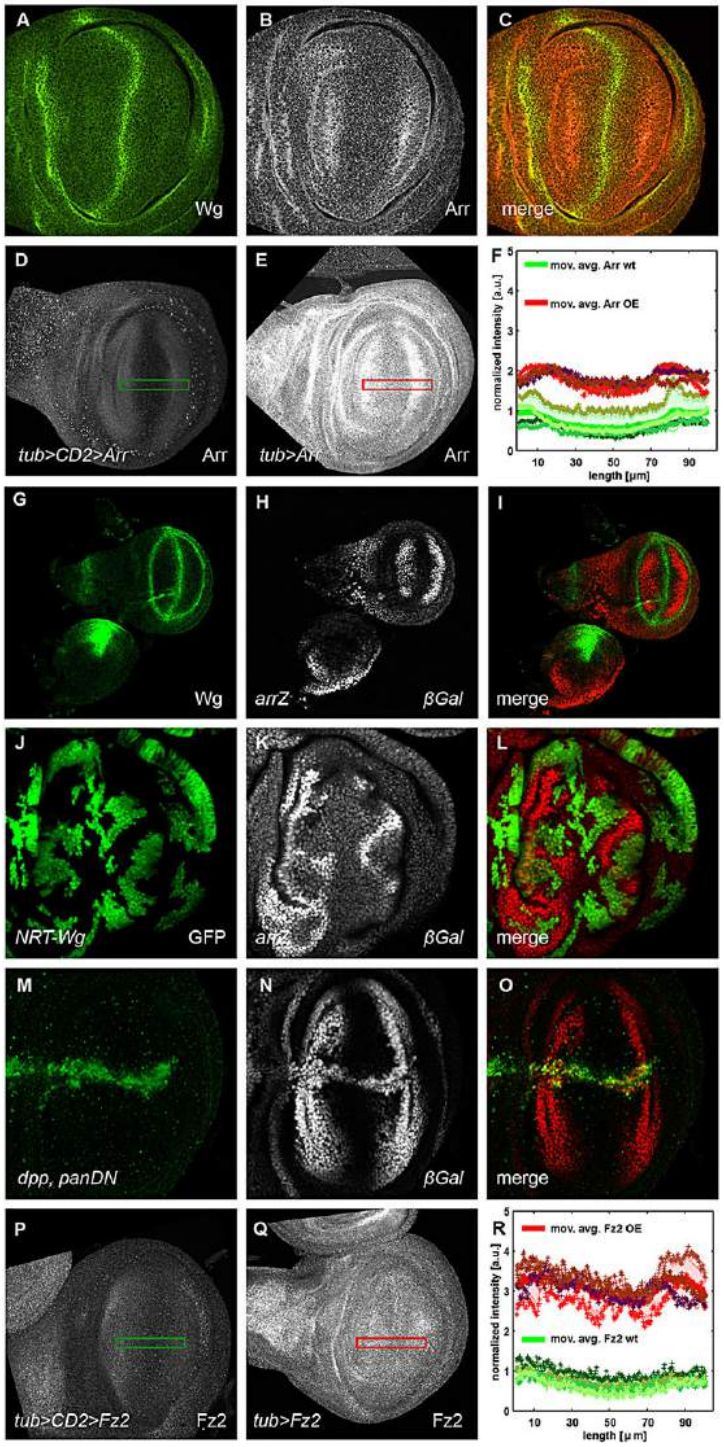

Fig. 1. Wg represses its receptors Arrow and Frizzled 2 – graded expression of the receptors is maintained upon *tubulinα1* promoter-mediated misexpression. In all panels showing imaginal discs, the posterior compartment is oriented towards the top, the anterior compartment is towards the bottom of the image. The green (D,P) and red (E,Q) rectangles displayed on these example discs show the ROI, sized 100 µm×16 µm, that was used to quantify the level of receptor in F and R. (A-C) Wingless (Wg) and Arrow (Arr) exhibit an inverse relationship in their expression levels. Immunofluorescence staining for Wg (green in A and C) and Arr (gray in B and red in C) revealed the inverse expression levels of the two proteins (C). (D,E) Graded Arr expression was maintained in Arr-overexpressing discs. Wild-type wing discs (D), and wing discs that misexpressed Arr, controlled by the *tubulinα1* promoter (tubArr) (E), were stained for Arr. (G-L) Wg represses *arr* transcription. The transcriptional *arr* reporter *arr-lacZ* (*arrZ*) (gray, H) was repressed in Wg-expressing areas of the wing imaginal disc. It was also repressed in randomly induced somatic clones (gray, K), as revealed by immunostaining against β-galactosidase (β-Gal), that overexpressed membrane-attached NRT-Wg [marked by green fluorescent protein (GFP) in J]. (M-O) Dominant-negative pan (panDN) derepresses Arr. Expression of dominant-negative *UAS-panDN* with *dppGAL4* (M), marked by GFP, led to derepression of the *arrZ* reporter (gray, N). (P,Q) Graded Fz2 expression is maintained in Fz2-overexpressing discs. *tubFz2*-expressing wing discs (Q) that were immunostained for Fz2 showed a higher intensity profile of Fz2 than that of wild-type controls (P). Note that the receptor upregulation in *tubFz2* was much stronger than in the corresponding *tubArr* discs. (F,R) Receptor level intensity plots. In both panels, intensities of four wild-type (wt, green-shaded crosses) and four receptor-overexpressing discs (OE, red-shaded crosses) are projected on the longer axis of the ROI, perpendicular to the dorsal-ventral compartment boundary. The corresponding moving averages (defined by a half window size of three micrometer) are denoted by solid green (wt) and red (overexpression) lines. Green- and red-shaded areas denote standard deviations of the mean of the data from wild-type and mutant imaginal discs, respectively. Intensity plots were normalized to the maximum of the moving average of the wild-type discs. a.u., arbitrary units.

Development (2014) 141, 2483-2493 doi:10.1242/dev.108662

control animals. The absolute Arr levels in *tubArr* animals were higher, whereas the shapes of the gradients were similar to those in the wild type (Fig. 1F; supplementary material Table S1).

In order to further analyze the *arr* transcriptional gradient, we used the recessive lethal *lacZ* P-element insertion *l(2)k08131*, which we refer to as *arrZ* (Wehrli et al., 2000) and is uncharacterized at the molecular level. We mapped the insertion site and found that it is positioned in the 5′UTR region of *arr* in the short first untranslated exon (data not shown). Owing to its insertion site and its expression pattern, *arrZ* can be used as a molecular read-out to study the transcription of the *arr* gene. *arrZ* is expressed in a graded manner and is inactive in areas of high Wg signaling (Fig. 1G-I). To investigate this negative regulation of *arr* by Wg, we clonally overexpressed NRT-Wg, which is a membrane-tethered non-diffusible fusion protein of Wg (Zecca et al., 1996). All over the wing imaginal disc, clones that expressed *NRT-Wg* showed repression of *arrZ*, as did adjacent wild-type neighboring cells (Fig. 1J-L). We next asked whether the nuclear mediator of Wg signaling Pan is involved in *arrZ* repression. Overexpression of a dominant-negative form of Pan (*UAS-panDN-HA*), which lacks the Armadillo-binding domain and was tagged with hemagglutinin (HA), resulted in a strong and strictly cell-autonomous derepression of *arrZ* expression (Fig. 1M-O). Hence, *arrZ* is a negative target of Wg signaling in the wing pouch and is repressed as a consequence of signaling events downstream of Pan.

Negative transcriptional regulation by Wg signaling has also been reported for the *fz2* gene, which encodes the main Wg receptor (Cadigan et al., 1998). To study the physiological relevance of this regulation, we misexpressed Fz2 under the control of the *tubulinα1* promoter (*tubFz2*) in the wing imaginal disc. Similar to the case of *tubArr*, *tubFz2* animals had wings that appeared wild type. Also, as observed for Arr, Fz2 protein levels were elevated in *tubFz2* animals, but remained graded with a slightly steeper slope, as observed for that in corresponding wild-type discs (Fig. 1P-R; supplementary material Table S1). Although weaker, a gradient could still be observed in larvae that harbored *tubFz2* but lacked endogenous Fz2 (supplementary material Fig. S1A-D and Table S1). These observations suggest that post-transcriptional regulation plays a rather minor role in gradient formation.

Modeling Wg receptor interactions

To formalize, and systematically study, the mechanisms of Wg-receptor interaction, we developed an *in silico* model that reproduces the negative regulation of Arr and Fz2 by Wg in cells of the wing pouch (Fig. 2). We first reduced the complexity of the system by summarizing the similar biological roles of the receptor Arr and its co-receptor Fz2 into the receptor entity ‘ArrFz2’. Next, we set up a system of coupled ordinary and partial differential equations that described the production and decay of the Wg ligand and its receptors, the reverse complex formation between ligand and the receptor entity, the diffusion of Wg, as well as the transcriptional downregulation of the receptor entity by Wg (Fig. 2).

A simplified analytical model suggests that most Wg is not bound to its receptors

Neglecting the Wg-induced transcriptional receptor repression ($k^t_{Wg-ArrFz2}=0$ in Fig. 2) allowed us to study the effect of receptor upregulation analytically in one dimension (Schwank et al., 2011; details in the supplementary methods). Supplementary material Fig. S2 shows the dependence of the amplitude of total Wg (black) in regions that overexpressed the receptor on the relative amount of ligand that was not bound to the receptor, $a=[Wg]/[Wg_T]$. In such a simplified model, the higher the value of a, the less the amplitude of the total Wg distribution is affected by changes in receptor levels.

To study the consequences of apposing wild-type and receptor-overexpressing cells, as well as to have a direct comparison of the Wg distribution in receptor-overexpressing cells to wild-type cells in the same disc, we generated *tubulinα1>CD2,y*$^+$*>arr* and *tubulinα1>CD2,y*$^+$*>fz2* transgenes that harbored flp-out cassettes between the promoter and coding region. Exposure to Flp recombinase during development leads to clones that overexpress the corresponding receptor. In discs, where the receptor overexpression was compartmental (Fig. 3; supplementary material Fig. S3 and Table S1), we found no significant difference between the Wg amplitudes in wild-type compartments and those that overexpressed the receptor. If the staining revealed the total amount of Wg, then the analytical model (supplementary material Fig. S2 and supplementary methods) suggests that the majority of Wg is not receptor bound.

A simplified analytical model predicts narrowing of Wg distribution upon receptor overexpression

Assuming further that Wg decay occurs only in complex with its receptors (leading to $k_{Wg}=0$), the analytical model predicts a narrowing of the Wg gradient in regions of receptor overexpression – an n-fold upregulation of the receptor would lead to a decrease in the Wg decay length (the distance from the Wg source, where the Wg concentration is reduced by a factor of 1/e from its maximal value) by a factor $1/\sqrt{(n)}$ in the receptor-overexpression (OE) region (supplementary methods). Remarkably, theory and experiment coincided within the measurement error for compartmental Arr

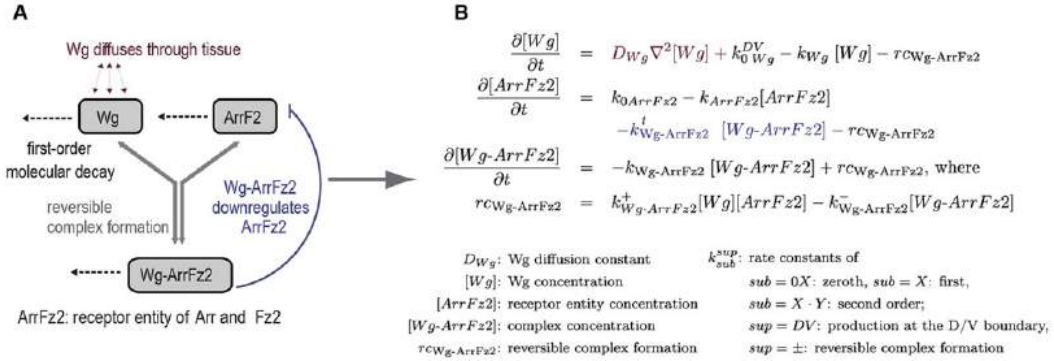

Fig. 2. Model representing Wg-induced negative regulation of Arr and Fz2. (A) Dotted arrows denote the first order decay of either single molecules or complexes of molecules; the reversible formation of complexes is denoted by groups of arrows. This mechanistic model can be translated into a set of differential equations (B).

Development (2014) 141, 2483-2493 doi:10.1242/dev.108662

overexpression experiments; we found $\lambda^{OE,Arr}/\lambda^{wt}=0.7\pm0.1$ (Fig. 3M; supplementary material Table S1), whereas the simple model predicted $\lambda_{th}^{OE,Arr}/\lambda_{th}^{wt}=1/\sqrt{n}=1/\sqrt{2}=0.7$ for the upregulation of Arr by a factor of n=2.

Receptors hinder diffusion of Wg

Extending our Wg receptor interaction model to two dimensions, we numerically solved the corresponding system of differential equations (displayed in Fig. 2) on a mesh, which resembled the cell shapes at the apical side of the wing disc. The vertex model describes cells and their contact surfaces as polygons that are composed from connected vertices with positions that are defined by the local minimum of an energy function (Farhadifar et al., 2007). Using these polygons as local control volumes, we discretized the diffusion of Wg by using the Finite Volume Method. Our modeling approach allowed us to study the consequences of changing receptor levels with cellular resolution in patches of cells, disc compartments or the entire wing pouch.

Simulating receptor overexpression in entire compartments (Fig. 4) led to a narrower Wg distribution than that in the corresponding wild-type compartments (Fig. 4B,C,F; supplementary material Table S1). These findings are also supported by our measurements of the extracellular Wg gradients (Fig. 3J-L; supplementary material Fig. S3). In our model, cells that overexpressed ArrFz2 hindered the spreading of Wg, the only diffusing protein of the model; thus, these cells serve as a 'sink' for Wg if placed next to wild-type cells (Fig. 3) – cells that overexpressed ArrFz2, positioned immediately adjacent to wild-type cells, exhibited pathway activity (simulated by the amount of Wg-ArrFz2 complex formation) further away from the Wg source than the overexpressing cells that were not adjacent to wild-type cells (Fig. 4E). In our model, these cells receive unbound Wg from neighboring wild-type cells (see Discussion).

Abrupt changes in receptor levels lead to detrimental phenotypic effects

The clonal abrupt upregulation of the receptor levels by using *tubulinα1>CD2,y⁺>arr* or *tubulinα1>CD2,y⁺>fz2* transgenes caused detrimental phenotypic defects in the wings and legs of adult flies; in wings, we detected clones that caused typical Wg gain-of-function phenotypes, such as blistering and ectopic sensory-margin

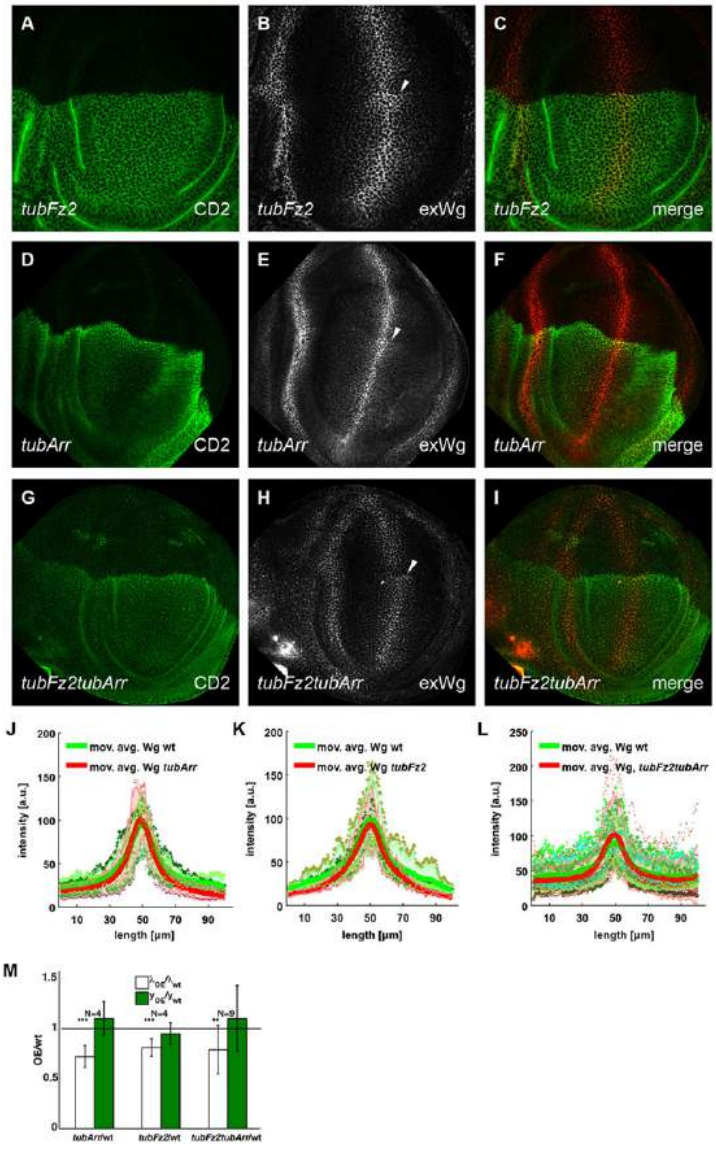

Fig. 3. Compartmental misexpression of Arr and Fz2 leads to accumulation of Wg at the edge that is shared between wild-type and receptor-overexpressing cells and to a slightly decreased distribution of Wg. The posterior (towards the top of the image) and anterior compartments of the wing imaginal discs are marked by the absence and presence of CD2, respectively. Arrowheads indicate the point of Wg accumulation. (A-C) Expression of *tubFz2* in the P compartment led to an accumulation of extracellular Wg, exactly at the boundary between the A and P compartments. (D-I) Expression of *tubArr* in the P compartment, or *tubArr* and *tubFz2* together, led to a similar extracellular Wg accumulation. (J-L) Wg level intensity plots in discs that compartmentally overexpressed Arr (J, n=4), Fz2 (K, n=4) and simultaneous overexpression of Arr and Fz2 (L, n=9), where n denotes the number of discs. Green-shaded crosses denote Wg intensities in the A compartment, red-shaded dots denote Wg intensities in the receptor-overexpressing P compartment. The moving average and standard error are defined as described in Fig. 1. a.u., arbitrary units. (M) Quantification of the change in Wg decay length (λ) and amplitude (y) upon receptor overexpression. Within each disc, we calculated the ratio between the decay length (white) and amplitude (green) in the receptor-overexpression (OE) and wild-type (wt) compartments. The bar charts display the mean and standard deviation for each experimental set up. We tested the null hypothesis, that decay length and amplitude were unchanged upon receptor overexpression, ***P<0.001, **P<0.01.

Development (2014) 141, 2483-2493 doi:10.1242/dev.108662

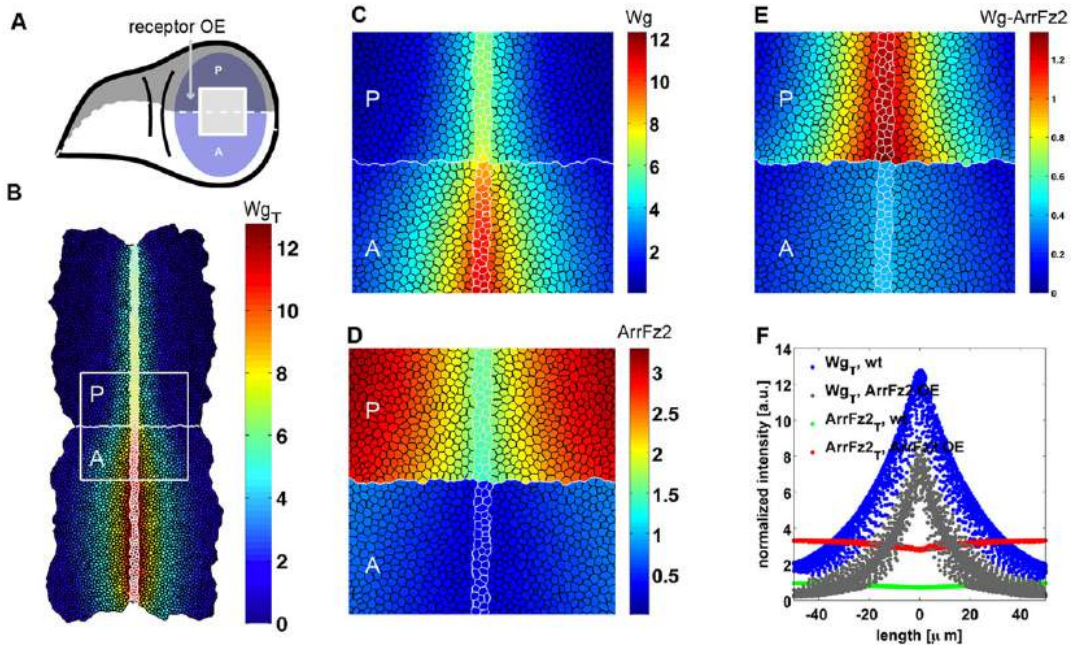

Fig. 4. Modeling reveals ectopic pathway activation in receptor-overexpressing cells juxtaposed with wild-type ells. (A) Schematic view of a wing disc. The posterior (P) compartment of the wing pouch is marked in dark blue, and the anterior (A) compartment is marked in light blue. (B) An example simulation result shows the total Wg concentration of a disc, where the ArrFz2 production rate was increased by a factor *n=3* in all cells of the upper (P) compartment. Concentrations are displayed using Matlab's jet algorithm, where red corresponds to high, and blue corresponds to low concentrations. All concentrations were normalized to the maximum value of the receptor entity ArrFz2 in wild-type discs and are given in arbitrary units. The white square corresponds to a zoomed-in region of 80 μm×80 μm centered around the intersection of the dorsal-ventral and anterior-posterior compartment boundaries. (C-E) Wg (C), ArrFz2 (D) and Wg-ArrFz2 (E) distributions of the zoomed-in region of B. Wg-expressing cells are marked by white cell edges, the anterior-posterior compartment boundary is marked by a white (horizontal) line. Note the narrowing of the total Wg distribution in the receptor-overexpressing compartment. (C) The model predicted reduced levels of diffusible Wg in anterior cells that were adjacent to the compartment boundary. (E) The distribution of Wg-ArrFz2 broadened in posterior cells that were adjacent to the compartment boundary. (F) The total ArrFz2 concentrations (defined as the sum of free and Wg-bound receptor) in a wild-type wing disc (green) and in an ArrFz2-overexpressing wing disc (red) was projected onto the anteroposterior axis. Each cell in the tissue corresponds to one dot in the graphic. Total Wg levels in a wild-type simulation are shown in blue and in an ArrFz2-overexpression simulation in gray. a.u., arbitrary units.

bristles (Fig. 5A). In legs, we found limb bifurcations that created supernumerary appendages (Fig. 5B), or an absence of tarsal segments and claws (Fig. 5C).

As an additional line of experimental validation, and to reach a higher level of reproducibility, we obtained clones that overexpressed Arr and Fz2 simultaneously through the activation of the *tubulinα1>CD2, y$^+$>fz2* and *tubulinα1>CD2,y$^+$>arr* cassettes upon a *hedgehog*-driven Flp recombinase, which was specifically expressed in the posterior compartment. They showed similar defects to the flies described above. Accordingly, when probed with an antibody against the prototypical Wg target gene *Senseless* (*Sens*), cells that co-overexpressed *tub>fz2* and *tub>arr* and were adjacent to wild-type cells displayed ectopic expression of Sens (Fig. 5D-F). We observed a similar phenotype with *tub>fz2* flp-out clones (Fig. 5G-I), but not with *tub>arr* clones (Fig. 5J-L). If we induced clones overexpressing Arr with the stronger GAL4-UAS expression system (Fig. 5M-O), again, we observed upregulation of Sens at the dorsal-ventral compartment border. Thus, we conclude that perturbations of Wg receptor levels cause ectopic pathway activity in cells with high amounts of receptor, if juxtaposed with cells that have lower levels of receptor levels.

Receptor-overexpressing cells neighboring wild-type cells act as a Wg sink

To test our model – that the receptor-overexpressing cells apposed to wild-type cells, indeed, serve as a Wg sink and benefit from this situation by increased signaling – we monitored extracellular Wg in discs that misexpressed the receptors in all posterior (P) compartment cells. Consistent with our model, such discs exhibited an accumulation of extracellular Wg, exactly at the border between wild-type anterior (A) and misexpressing P cells (arrows in Fig. 3A-I). These findings also explain the very restricted upregulation of Sens, noted above, exactly at the border between wild-type cells and cells that overexpressed the receptor.

The dual role of Fz3 – stabilization of Wg, and attenuation of Fz2 and Arr

Although Arr and Fz2 constitute the main Wg receptors, Fz3 has also been implicated in modulating the Wg response. Fz3 is expressed in the wing pouch (Sivasankaran et al., 2000) and has been proposed to serve as a negative-feedback regulator of the Wg pathway (Sato et al., 1999). Unlike Fz2 and Arr, however, the expression of Fz3 seems to be positively regulated by Wg signaling (Sivasankaran et al., 2000; Sato et al., 1999). To clarify the role of Fz3 in Wg gradient formation, we overexpressed Fz3 in the P compartment and monitored Sens levels as a read-out for Wg pathway activity. Indeed, we observed decreased Sens levels in the P territory, suggesting that overexpressed Fz3 attenuates Wg signaling (Fig. 6A-C). Consistent with this finding, Sens levels are enhanced in *fz3* mutant mitotic clones (Fig. 6D-F). We wondered whether the alterations in Sens levels in *fz3* mutant tissue, or tissue that overexpressed *fz3*, were mediated by changes in the levels of Wg, Fz2 or Arr. We first monitored extracellular Wg protein in compartments that overexpressed Fz3 and observed a notably enhanced and broadened extracellular distribution of the Wg protein (Fig. 6G-J). Interestingly, Fz2 and Arr levels were reduced in such

Development (2014) 141, 2483-2493 doi:10.1242/dev.108662

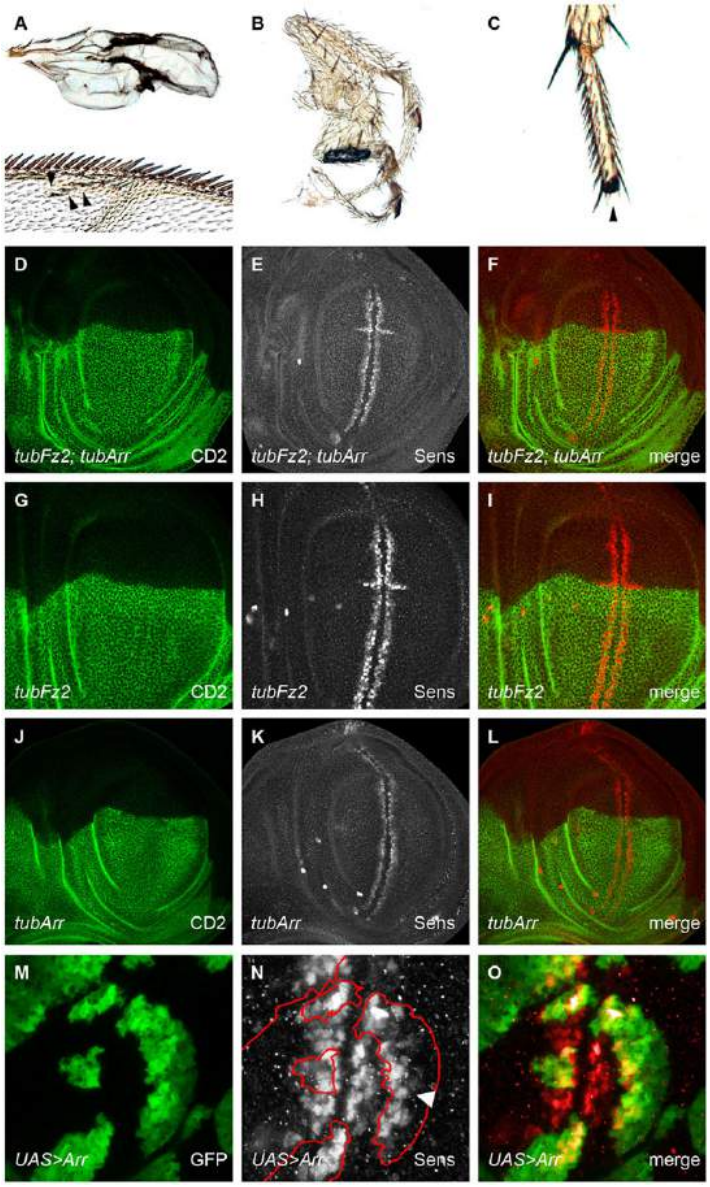

Fig. 5. Clonal overexpression of Arr and Fz2 leads to severe border effects. (A) Adult wing phenotypes that arose from random clones that expressed *tubFz2* or *tubArr* showed Wg gain-of-function defects, such as blistering and ectopic sensory bristles (arrowheads). (B,C) Random *tubFz2*- and *tubArr*-expressing mitotic clones resulted in bifurcations and truncations in legs. (D-F) Third-instar imaginal discs that contained *hhGal4, UAS-Flp, tubFz2, tubArr* clones (D-F) showed ectopic expression of the Wg target Sens (gray in E, red in F), predominantly in cells that were adjacent to wild-type neighbors at the border of the clone, close to the Wg source [*tubFz2*- and *tubArr*-expressing clones were marked by the absence of CD2 (green in D and F)]. (G-I) Similar to cells that expressed both receptor components, cells that only expressed *tubFz2* exhibited ectopic expression of Sens at the border of the clone (gray in H, red in I). CD2 expression is shown in green in G and I. (J-O) *hhGal4, UAS-Flp, tubArr* clones did not show strong Sens upregulation at the border with wild-type cells (J-L); however, in random heatshock-induced *UAS-GFP, UAS-Arr*-expressing clones (M-O), ectopic Sens expression at the border of the clone facing the Wg source was observed (arrowhead). CD2 staining is shown in green in J and L; Sens staining is marked by gray in K and N, and by red in L and O; GFP in M represents the Arr expression domain; the red outline in N marks the clone outline shown in M.

tissue (supplementary material Fig. S4A-F); however, the activity of a transcriptional *arr* reporter (ArrC19, described below and in supplementary material Fig. S7) did show a small increase in the area over which it was expressed (supplementary material Fig. S4G-I), suggesting that Fz3 post-translationally regulates the levels of Fz2 and Arr. By contrast, *fz3* mutant wing discs exhibited increased levels of Fz2 and, to a lesser extent, Arr (supplementary material Fig. S4M-N), but no discernible effect on the distribution of Wg was observed (Fig. 6K). Remarkably, we only observed the downregulation of Arr and Fz2 upon overexpression of Fz3, if the overexpressing cells included the Wg source (supplementary material Fig. S4A-F). In Fz3-overexpressing clones that were distant from the Wg source, Arr levels were higher, as we expected for a negative target, following attenuation of signaling (supplementary material Fig. S4J-L). This also suggests that downregulation of the receptor is not the primary cause for the observed attenuation of Wg signaling. We did not detect any upregulation of Fz2 levels in this situation. We conclude from these findings that the binding of Wg to Fz3 mediates the degradation of Arr and Fz2, presumably lowering receptor levels at the Wg-expressing stripe even further (supplementary material Fig. S4M-N), as well as broadening the area of Wg distribution through stabilizing the protein (Fig. 6G-J). These findings are supported by the observation that compartmental Fz3 overexpression, combined with RNA interference against Wg, reduces the downregulation of Arr in this compartment (data not shown).

To further define and rationalize the above observations, we incorporated Fz3 into our *in silico* model (supplementary material Fig. S5). We modeled Fz3 production to depend on the concentration of the Wg-ArrFz2 complex (our approximation of Wg pathway activity). Furthermore we assumed – as in the case of the receptor entity ArrFz2 – a reversible complex formation between Wg and Fz3. Our experimental data (supplementary material Fig. S4J-L) suggest that the Fz3-induced repression of Arr and Fz2 is mediated by Wg (albeit the exact mechanism still has to be investigated). Therefore, we assume in our model that Fz3 represses Arr and Fz2 expression only when Fz3 is interacting with Wg. The resulting extended set of differential equations is provided in the supplementary methods. Scanning the corresponding parameter

Development (2014) 141, 2483-2493 doi:10.1242/dev.108662

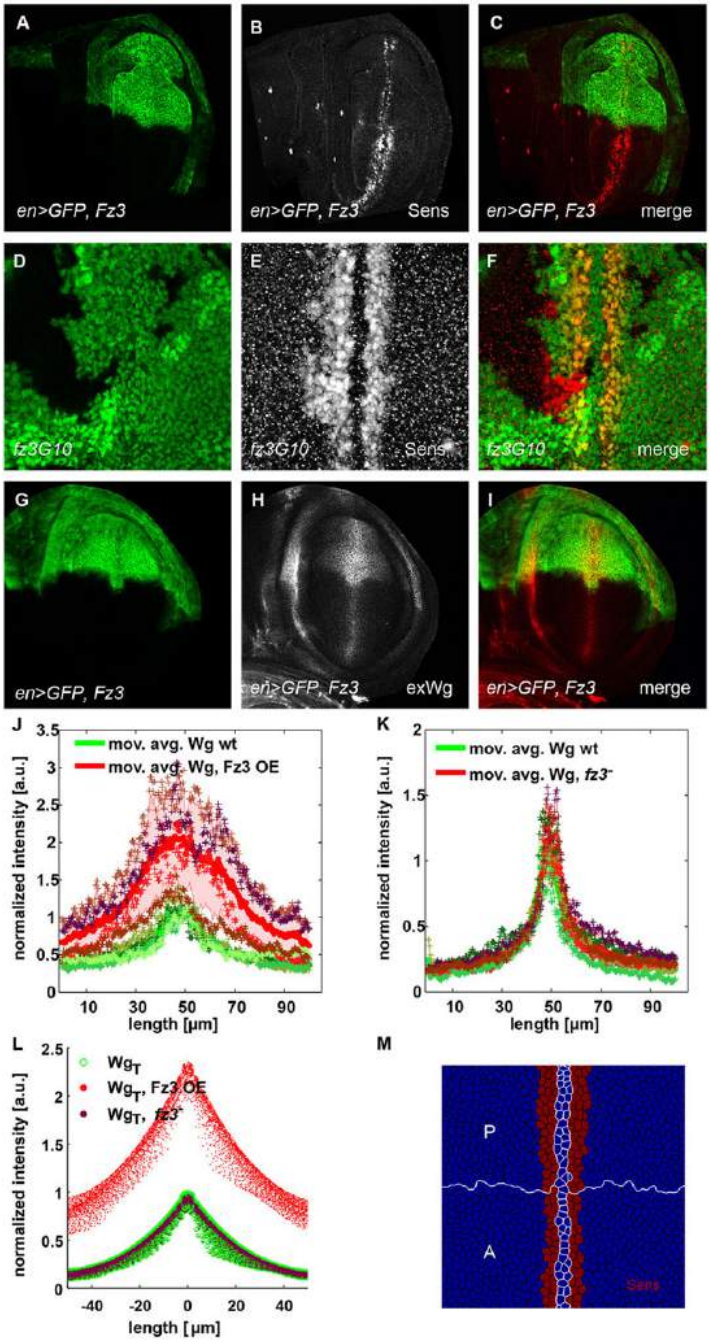

Fig. 6. Fz3 acts as an attenuator of Wg signaling.
(A-C) Overexpression of Fz3 in the P compartment (A), marked with GFP, results in a prominent reduction of Sens levels (gray in B, red in C). (D-F) Fz3 loss-of-function clones (*fz3G10*), marked by the absence of GFP (clones induced with an *FRT19, ubiGFP* chromosome) (D), led to an enhancement of Sens expression at the dorsal-ventral compartment boundary (gray in E, red in F). (G-I) Ectopic expression of Fz3 in the P compartment (G) resulted in an enhancement and broadening of the extracellular Wg gradient, revealed by immunostaining of the extracellular (ex) Wg levels (gray in H, red in I). GFP marks the P compartment. (J) Intensity profile of the Wg gradient in Fz3-overexpressing (OE) P compartments (red) and wild-type (wt) compartments (green) in a ROI of 100 µm×20 µm. *n*=8. Note the higher and broader Wg gradient in Fz3-overexpressing compartments. (K) Intensity profile of the Wg gradient in *fz3* mutant wing discs (red, $fz3^{-}$) and wild-type wing discs (green) in a ROI of 100 µm×20 µm. *n*=8. *fz3* mutant wing discs showed reduced levels of Wg and a narrower Wg distribution. (L) Results of the simulation model showed the total Wg levels (defined as the sum of free and receptor-bound Wg) in a wild-type (green), *fz3* mutant (dark red) and Fz3-overexpression simulation (light red). As in the experimental intensity profiles (J,K), Wg levels were normalized to the maximum of the wild-type expression. The simulation qualitatively reproduced the behavior of the experimental situations (J,K; supplementary material Table S1). a.u., arbitrary units. (M) A simulated profile of Senseless (red) distribution in wild-type (lower compartment) and $fz3^{-}$ cells (upper compartment). The ROI was the same as that described in Fig. 4. Wg-expressing cells are marked by white edges, and the compartment boundary is marked by a white line. We modeled Wg-expressing cells as being deficient for Senseless expression. It was assumed that all other cells with Wg-ArrFz2 concentrations higher than 95% of the maximal Wg-ArFz2 concentration expressed Senseless. A, anterior; P, posterior.

space (supplementary methods), we identified a parameter set that qualitatively reproduced the experimentally observed Wg and receptor distributions in the wild-type and receptor-misexpression conditions (the exact parameters are shown in supplementary material Table S1). Remarkably, the parameter exploration suggested that the complex that was formed by Wg and Fz3 might be more stable than the corresponding Wg-ArrFz2 complex (see supplementary material Table S2 in the supplementary methods), confirming the role of Fz3 in stabilizing Wg.

In summary, we show that Fz3 acts as an attenuator of Wg signaling in the wing pouch. We propose that Fz3 reduces the amount of Arr and Fz2 protein close to the Wg source and mediates a broader distribution of Wg.

Wg signaling indirectly represses *arr* and directly activates *fz3*

The existence of the transcriptional gradients of Arr and Fz2 prompted us to analyze by which mechanism(s) Wg signaling represses the transcription of their genes. Many feedback regulatory mechanisms of signaling pathways use direct transcriptional regulation. However, signaling-mediated transcriptional repression (as opposed to activation) has rarely been described (Affolter et al., 2008). Thus, we sought to isolate and characterize the regulatory DNA elements of *arr* and *fz2* that are responsible for the Wg input. The similar expression patterns and regulatory roles of *arr* and *fz2* led us to speculate that both genes might be transcriptionally controlled by the same molecular mechanism. Hence, we chose the *arr* locus as a case study and

Development (2014) 141, 2483-2493 doi:10.1242/dev.108662

systematically dissected its regulatory region. Seven overlapping fragments (*A* to *G*) covering 25 kb were cloned into a p*lacZ-attB* reporter vector, 5′ to an *hsp70* minimal promoter. Each construct was integrated into the same *attP* landing site on the second chromosome (Bischof et al., 2007) and the expression of lacZ in imaginal discs was analyzed. Fragment *arrC* recapitulated the endogenous *arr* expression pattern (Fig. 7A) and also properly reacted to experimentally increased and decreased Wg pathway activity, as assessed in clones that expressed *NRT-Wg* and pan^{DN}, respectively (data not shown). We next narrowed down the regulatory activity of *arrC* by using an extensive series of reporter constructs (supplementary material Fig. S7), resulting in a 200 bp fragment termed *arrC19*, which could not be shortened further without compromising activity. Clones that expressed a constitutively active version of Arm (Arm^{act}) repressed *arrC19* reporter expression, confirming that it retained the element(s) responsible for the negative Wg input (Fig. 7B-D). To check if this regulatory Wg input was mediated directly by Pan, we mutated the four highly conserved Pan binding sites in the *arrC19* enhancer. The expression pattern of the resulting *arrC19_Tcf_mut* transgene was not derepressed, suggesting that Pan is not directly involved in regulating *arrC19* (Fig. 7I). Thus, we conclude that Wg-mediated repression of *arrC19* occurs independently of the direct binding of Pan.

Furthermore, we analyzed the nature of the Wg input on *fz3* by using a similar approach – dissecting the *fz3* locus into seven overlapping fragments, *A* to *G*. The expression pattern of fragment Fz3G was the only one that was reminiscent of the pattern of *fz3*. Further dissection yielded *fz3G5*, a fragment of approximately 290 bp that retained *fz3*-like expression (Fig. 7E). Clones that expressed Arm^{act} (Fig. 7F-H) caused upregulation of *fz3G5* reporter gene activity. This regulation seems to be directly exerted by the canonical Wg pathway because it was completely abrogated upon mutation of the Pan-binding site (Fig. 7I).

We conclude that Wg signaling indirectly regulates *arr* (and presumably *fz2*), whereas *fz3* is a direct positive-target gene of the pathway. Thus, the sign of regulation by Wg of *arr* and *fz2* differs from that of *fz3* (to impact negatively and positively on their expression, respectively), as well as the mode of regulation (indirect versus direct).

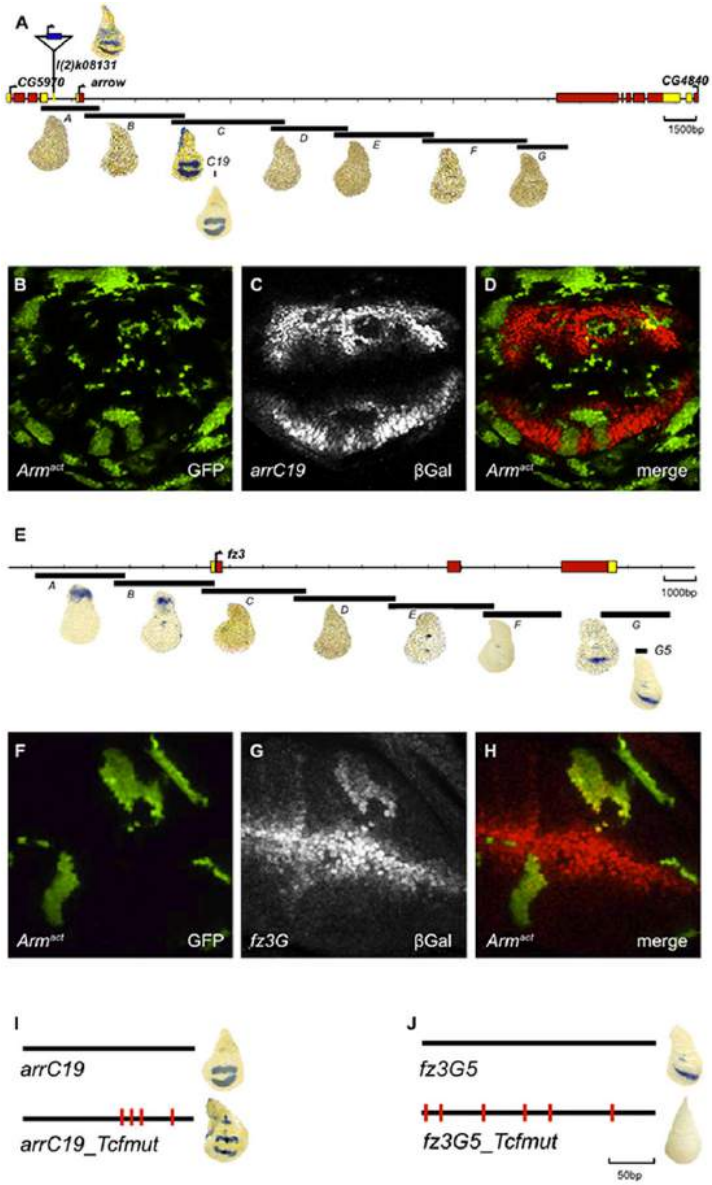

Fig. 7. *arr* is an indirect negative Wg target, and *fz3* is a direct positive Wg target. A map of the genomic region of *arr* (A). Translated exons are shown in red, untranslated regions in yellow. Fragments *A-G* were tested for their ability to activate a heterologous promoter driving *lacZ* expression (blue stain). Only fragment *C* recapitulated the *arr* expression pattern in the wing imaginal disc. Insertion of the P-element *arrZ* is shown on top. Further dissection of fragment *C* revealed the minimal enhancer fragment *arrC19* (see supplementary material Fig. S4 for further details). (B-D) Randomly induced clones that overexpressed the constitutively active *UAS-*Arm^{act}, marked with GFP in (B), led to a cell-autonomous repression of *arrC19* expression, revealed by immunostaining of β-galactosidase (gray in C, red in D) (C,D). (E) A map of the genomic *fz3* locus. Fragments *A-G* were tested for their ability to activate a heterologous promoter driving *lacZ* expression. Only fragment *G* recapitulated the *fz3* expression pattern in the wing pouch. (F-H) Overexpression of *UAS-*Arm^{act} (green) (F) results in a cell-autonomous derepression of *fz3G*, as shown by by immunostaining of β-galactosidase (gray in G, red in H) (G,H). (I) Mutation of TCF sites in conserved regions of *arrC19* did not affect the expression of the reporter. By contrast, mutation of TCF sites in the *fz3G5* reporter completely abolished reporter expression (J).

Development (2014) 141, 2483-2493 doi:10.1242/dev.108662

DISCUSSION

During the development of a metazoan organism, signaling events are precisely regulated. One frequently employed mode of regulation is feedback loops. Here, we analyzed a network of feedback loops in the *Drosophila* wing pouch that regulate receptor abundance, and thus the range of distribution and signaling output of Wg.

Receptors sequester their ligands and, thereby, impact upon the range of the signal (supplementary material Fig. S6). A transcriptional regulatory link between receptor expression and signaling activity, causing up- or downregulation of receptor levels in cells in response to the signal, can thus restrict or extend the signaling range. For example, the Hedghog (Hh) signal induces the expression of its receptor Patched (Ptc), a regulatory link which severely narrows the Hh activity gradient (Chen and Struhl, 1996). In the case of Wg, we observed the opposite – Wg signaling appeared to extend the range of Wg distribution by transcriptionally downregulating expression of *arr* and *fz2*; downregulation of the receptors hinders the formation of Wg-Arr-Fz2 complexes. This allows superfluous Wg to diffuse further away from the source without being immobilized by its receptors. In agreement with this notion, we observed a slightly narrower distribution of extracellular Wg in discs that expressed Fz2 or Arr under the *tubulinα1* promoter (Fig. 3; supplementary material Fig. S2). Quantifying these observations in discs that compartmentally overexpressed the receptor (Fig. 3; supplementary material Fig. S2 and Table S1), we observed a subtle reduction of the decay length (corresponding to a slightly steeper Wg distribution) in compartments that overexpressed the receptor compared with that in wild-type compartments.

In apparent contradiction, a previous study (Cadigan et al., 1998) has shown that high levels of Fz2 can stabilize Wg and promote Wg spreading; accordingly, we observed an accumulation of Wg when repeating this experiment by overexpressing Fz2 using the GAL4-UAS system. These contradictory findings can be reconciled by taking into account the different strength of Fz2 upregulation in the two experimental setups – Fz2 expression that is driven by the *tubulinα1* promoter leads to a relatively mild upregulation of the receptor by, approximately, a factor of 2 (Fig. 1; supplementary material Table S1), whereas overexpression by using the GAL4-UAS system causes a much stronger overexpression. Presumably, Arr becomes the limiting factor in *UAS-Fz2*-overexpressing cells, a situation that might prevent the surplus Wg-Fz2 complexes from being internalized, thus causing an extracellular accumulation of Wg (Marois et al., 2006). If Fz2 is only moderately overexpressed, sufficient Arr protein might be available to allow this extra Fz2 to form Wg-Arr-Fz2 complexes, which are subsequently internalized, leading to a slight narrowing of the gradient because there is less free and diffusible Wg. Consistent with this notion, simultaneous strong overexpression of both of the receptors Fz2 and Arr, by means of Gal4, leads to a reduction of extracellular Wg levels (Piddini et al., 2005).

Receptors act as a Wg sink

Although Wg signaling transcriptionally represses both Arr and Fz2, ubiquitous overexpression of Arr, or Fz2, had no phenotypic consequences. Unexpectedly, however, severe phenotypes arose upon mosaic expression of the *tub>arr* or *tub>fz2* transgenes. Theoretical modeling (Fig. 4) and reporter gene analysis indicated that cells that had elevated receptor levels ectopically activated the pathway when situated close to wild-type cells. Apparently, the 'high-receptor-level state' allows *tub-fz2* or *tub-arr* cells to engage in ligand-receptor interactions that depend on the 'low-receptor-level state' of their neighbors. One plausible explanation might be that *tub-fz2*, or *tub-arr*, cells bind to Wg that diffuses in from neighboring wild-type cells.

The different outcome of clonal versus uniform alteration of the Wg pathway is reminiscent of observations that have been reported by Piddini and Vincent (Piddini and Vincent, 2009), where loss of Wg signaling in the entire P compartment had no impact on the expression of low-threshold target genes but resulted in their repression, and in patterning defects, when Wg signaling was only clonally abolished. Piddini and Vincent also used different patterns of Wg receptor expression for their experiments, and they explained their findings by postulating that there is a Wg-induced, still to be identified, inhibitory signal that negatively regulates target gene expression in surrounding cells.

The negative feedback regulator Fz3

In an additional layer of negative-feedback regulation in the wing pouch, Wg signaling activates the expression of the Frizzled family member Fz3 (this work; Sato et al., 1999; Sivasankaran et al., 2000). Fz3 seems to act as a negative regulator of Wg signaling by repressing Wg signaling readouts and downregulating Wg receptor levels. Various models could be envisaged of how Fz3 acts as an inhibitor of Wg signaling. As it has been demonstrated that Fz3 is able to bind Wg (Wu and Nusse, 2002), Fz3 could work as a decoy receptor that acts as a molecular trap by binding to Wg without eliciting a signal. Decoy receptors are often part of negative-feedback mechanisms. In the *Drosophila* epidermal growth factor (EGF) system, the pathway inhibitor Argos is a target of EGF signaling and functions as a decoy receptor (Klein et al., 2004). In vertebrates, decoy Frizzled receptors have been identified that modulate Wnt signaling – secreted Frizzled-related molecules (sFRPs) have strong homology to the Frizzled extracellular domains. sFRPs inhibit signaling by directly binding to the Wnt ligands (Mii and Taira, 2011). No sFRP gene has been identified in the *Drosophila* genome.

In another scenario, Fz3 could work as a negative regulator of Wg receptors. Its function could be analogous to that of ZNRF3 and RNF43 in crypt base columnar intestinal stem cells. These related E3 ubiquitin ligases have been shown to regulate the stability and levels of cell-surface Fz and LRP5/6, through internalization and lysosomal degradation of the receptor components in the presence of Wnt signaling (Hao et al., 2012; Koo et al., 2012). Several of our experimental findings indicate that Fz3 might work as an inhibitor of Wg feedback at the receptor level – firstly, we observed decreased Arr and Fz2 levels in compartments that overexpressed Fz3 (supplementary material Fig. S2B,E), and secondly, Arr and Fz2 levels were increased in *fz3* mutant wing discs (supplementary material Fig. S4M,N). Most probably, Fz3 acts by more than one mechanism – cells that overexpressed Fz3 in the Wg stripe lead to Arr downregulation, whereas cells that overexpressed Fz3 outside of the Wg stripe lead to Arr upregulation (supplementary material Fig. S4J-L). Furthermore, extracellular Wg was stabilized upon Fz3 overexpression (Fig. 6G-I). In a wild-type situation, this stabilization of Wg might contribute to a broader Wg gradient and promote signaling in the outskirts of the wing pouch. Taken together, these findings suggest that only Wg-bound Fz3 causes inhibition of the pathway.

The role of transcriptional Wg receptor regulation

The post-translational regulation of Wg receptor levels was not the focus of this study, but we undertook substantial efforts to further characterize the transcriptional regulation of the receptor genes. In particular, we sought to identify the regulatory elements of these genes that mediated the feedback loops. The isolation of a 200 bp

Development (2014) 141, 2483-2493 doi:10.1242/dev.108662

fragment of the *arr* locus and a 300 bp fragment of the *fz3* gene – each of which was responsive to Wg signaling and drove reporter gene expression in a pattern that was reminiscent of the endogenous expression pattern – allowed us to investigate whether the Wg pathway controls these genes directly or indirectly; *fz3* appeared to be a direct target of canonical Wg signaling, whereas *arr* did not. Pan-binding sites were dispensable in the minimal *arr* enhancer, indicating that either Arm regulates the transcriptional activity of *arr* through another DNA-binding protein, or that Arm and/or Pan transcriptionally induce one (or more) negative regulators that, in turn, regulate *arr* expression. Hence, although the Wg pathway has been reported to possess the capacity to directly negatively regulate transcription (Blauwkamp et al., 2008; Affolter et al., 2008), it apparently does not use this mechanism to attenuate *arr* expression.

Including transcriptional Wg receptor downregulation in our model led to a broader distribution of Wg (supplementary material Fig. S6A) – receptor downregulation by ligand-induced endocytosis consumes the ligand, this was not the case for transcriptional repression (supplementary material Fig. S6B). The broadening of the Wg distribution area under a mechanism of transcriptional receptor repression might facilitate a robust signaling readout for high-threshold Wg target genes.

A recent study indicates that the long-range Wg gradient might be less important for imaginal disc patterning than assumed previously (Alexandre et al., 2014). Hence, it is also conceivable that the receptor gradients are not essential, a notion supported by our finding that uniform misexpression of Arr or Fz2 in the wing imaginal disc had no phenotypic consequences. Nevertheless, it remains to be determined whether the Arr and Fz2 gradients are dispensable; our *tubArr* transgene is not able to rescue *arr* loss-of-function mutants.

A cell-based ligand-receptor model

So far, most quantitative models of the Wnt-Wg pathway have focused on intracellular events (reviewed in Kofahl and Wolf, 2010), and only a few models have taken into account the spatial aspects of this signaling system (Sick et al., 2006; Ramis-Conde et al., 2008; van Leeuwen et al., 2009; Zhu, 2011). Our model is the first to systematically study the roles of Wg-receptor complexes – Wg-ArrFz2 and Wg-Fz3 – in the spatial profile of Wg signaling, as well as being the first to be challenged experimentally by manipulations of the receptor levels. Our cell-based modeling approach of ligand receptor interactions allowed us to vary all parameters in a cell-autonomous manner, which has not been done in previous studies (Eldar and Barkai, 2005; Dalessi et al., 2012; Schwank et al., 2011). This technique is, thus, an ideal tool to predict the impact of clonal conditions with cellular precision, which have historically formed the basis of experimental approaches in *Drosophila* but have also become increasingly available in vertebrates.

MATERIALS AND METHODS

Quantifying the shape of Wg and receptor distributions

We quantified the Wg intensity projections of each disc, i, by fitting an exponential decay $y_{is}=y_{0is}\times exp(-x/\lambda_{is})$, where y_{0is} is the corresponding Wg amplitude and λ_{is} the decay length, from the center of the region of interest to both sides ($s\in[left,right]$) up to 30 µm, omitting the Wg-producing source region (approximately 4 µm in width).

How well the data fitted to each curve was estimated by calculating the coefficient of determination, R^2_{is}, from the intensity projections and the fit of the curve. For the two fits, to the left and right within each region of interest (ROI), of disc number i, we calculated the mean R^2_i and the mean of the absolute values of the two decay lengths, $\lambda_i=(|\lambda_{i\,left}|+|\lambda_{i\,right}|)/2$.

We quantified the receptor intensity projections of each disc i by fitting exponential functions, linear (data not shown) and second order polynomials $y_i(x)=a_ix^2+b_ix+c_i$, where the latter showed the best overall coefficients of determination. The slope of the receptor distributions was then defined as the derivation of the second order polynomial with respect to x. Supplementary material Table S1 displays the mean fit coefficients of n measurements.

Fly stocks

Transgenic flies were generated by using the PhiC31 transgenesis system and integrated on the landing sites ZH-51D or ZH-86Fb (Bischof et al., 2007).

The following stocks were used for genetic and clonal analysis:
Sp/CyO; hhGAL4, UAS-Flp/TM6B (Pérez-Garijo et al., 2009);
yw hsp-flp; UAS-HA-NRT-Wg/SM5^; MKRS/TM6B (Zecca et al., 1996);
yw hsp-flp; UAS-ΔPan-HA/TM6B (van de Wetering et al., 1997);
yw hsp-flp; UAS-Armact (Zecca et al., 1996);
yw hsp-flp; Sp/CyO; dpp-GAL4/TM6B (Entchev et al., 2000);
yw hsp-flp; enGAL4, UAS-GFP, tubGal80ts/CyO; MKRS/TM6B (individual components are from Bloomington);
yw hsp-flp; act>CD2, y+>GAL4, UAS-GFP (Pignoni et al., 1997);
UAS-Fz3, UAS-Arr, UAS-Fz2 and UAS-PanHA (Bischof et al., 2013);
yw hsp-flp; C765-GAL4 (Nellen et al., 1996);
Tub-flp (Struhl et al., 1993);
P(lacZ) arrk08131 (Bloomington stock 665);
FRT19 (Bloomington stock 1709), *Fz3G10* (Sato et al., 1999);
fz2(c1) (Chen and Struhl, 1999);
Df(3L)fz2 (Bloomington stock 6754).

Vectors

For cloning, standard molecular biology cloning methods were used.

To generate hybrid *tubArr* and *tubFz2* constructs, the coding regions of Arr and Fz2, respectively, were cloned 3′ in-frame of the *tubulinα1* promoter and a *FRT*-flanked *>CD2,y+>* flp-out cassette in a plasmid that contained the *tubulinα1* 3′UTR and an *attB* site for phage-mediated transgenesis.

To generate *lacZ* reporter constructs, fragments of the genomic *arr* and the *fz3* locus were amplified from *yw* genomic DNA by using PCR with primers that harbored suitable restriction enzymes for subsequent cloning into p*lacZattB*. A detailed list of the primers and constructs that were used is available upon request.

The sequences of *arrC19* and *fz3G5* containing mutated TCF sites (mutated from ttt to ccc, the site is in bold) were synthesized by Entelechon GmbH as follows: arrC19, 5′-CCAACAGCCAGCAGTCTCCCCGTT-CGACGAATTGCTAATTTATTTCACTCTTGTACCTCGGAACACGCT-TCCTATCTAGACGTTG**GAAAgggA**CCAATTTAAAGTTTATTTATGG-**CgggTATTAgggTATA**CCCTCTCTATATTTGGCATTTTTCCTGTTGC-TCTTTTTTTTTTTGCCTTTTGCAGCTGCCTCTTCGACTGGCGTTTG-TCAA**TgggTAAC**CTGTTGTGCATACTAATTTG-3′; fz3G5, 5′;-GGTAC-CCTTTCCCTGCTCTCTGGAT**GgggGGGC**TGCGTCAGAACACGGG-TAATTGGTATCAACCGAGGCACAATTA**AgggGAT**TGAAGCTGCC-ACACCGCATGCCGCTCCAACGAACAACGAATCCATC**CTACcccT**T-GCCGGCCGTCGTGGCAGGCAACAAG**CCGcccc**CACTGCGGCAACA-TCGGCACAATAGCAACAGCAACTGTGCAGCAAGCGTGCAATTA-ACTCTTGTGCGCCAA**GATCcccG**CGATTAATGCGGCCCCAAGTT-CCCAGACGAAGGGACTCTAGA-3′.

Clone induction

tubArr- and *tubFz2*-expressing clones were generated by heat-shocking the larvae for 1 h at 37°C 72 h (±12 h) after egg-laying and dissected 2-3 days after clone induction. P compartments that expressed UAS constructs were generated by shifting the crosses to 29°C for 2-3 days before dissection. *NRT-Wg*-expressing clones were induced 4 days after egg-laying for 15 min at 37°C.

Immunohistochemistry

Immunostainings were performed using standard protocols. Images were taken by using a Zeiss LSM710 confocal microscope using 40× and 63× oil objectives and analyzed with the ImageJ software. Maximum z projections

of ROI were performed for the individual micrographs: Discs were oriented and processed in Adobe Photoshop, intensities were projected on the longer axis of the ROI, perpendicular to the dorsal-ventral compartment boundary. For each condition, we measured at least four independent discs.

The following antibodies were used against the indicated proteins: β-galactosidase (mouse, 1:2000, Promega); Arrow (rabbit, 1:15,000, a generous gift from Steve DiNardo, University of Pennsylvania, USA; Senseless (guinea pig, 1:800, a generous gift from Hugo Bellen, Baylor College of Medicine, Houston, TX, USA; Wg [mouse, 1:3 (for extracellular stainings, see Baeg et al., 2001), Developmental Studies Hybridoma Bank]; Fz2 (mouse, 1:30, Developmental Studies Hybridoma Bank); CD2 (rat, Alexa Fluor 488-conjugated, 1:25, Serotec); HA (rabbit, 1:200, Santa Cruz Biotechnology).

To detect β-galactosidase activity of the *arr* reporters, third-instar larvae were subjected to standard X-Gal reactions. For color detection, we used standard conditions.

The secondary antibodies used were Alexa Fluor 594-conjugated goat against mouse IgG, Alexa Fluor 488-conjugated goat against mouse IgG, Alexa Fluor 594-conjugated against rabbit IgG, Alexa Fluor 488-conjugated against rabbit IgG, Alexa Fluor 568-conjugated against guinea pig IgG. All were obtained from Molecular Probes and were used 1:400.

Acknowledgements
We thank S. DiNardo and H. Bellen for antibodies; G. Morata, G. Struhl and T. Kojima for fly stocks; F. Meyer and P. Herr for help with injections; and G. Hausmann, T. Valenta, M. Hödl and C. Cantù for critically reading the manuscript.

Competing interests
The authors declare no competing financial interests.

Author contributions
All authors developed the presented concepts and prepared the manuscript. S. Steiner and D.Z. performed the experiments; S. Schilling, S. Steiner and D.Z. performed the data analysis. S. Schilling developed the *in silico* model of Wg receptor interactions and wrote the supplementary methods.

Funding
The European Research Council, the Swiss National Science Foundation and the Canton of Zurich supported this work.

Supplementary material
Supplementary material available online at
http://dev.biologists.org/lookup/suppl/doi:10.1242/dev.108662/-/DC1

References
Affolter, M., Pyrowolakis, G., Weiss, A. and Basler, K. (2008). Signal-induced repression: the exception or the rule in developmental signaling? *Dev. Cell* **15**, 11-22.
Alexandre, C., Baena-Lopez, A. and Vincent, J.-P. (2014). Patterning and growth control by membrane-tethered Wingless. *Nature* **505**, 180-185.
Baeg, G. H., Lin, X., Khare, N., Baumgartner, S. and Perrimon, N. (2001). Heparan sulfate proteoglycans are critical for the organization of the extracellular distribution of Wingless. *Development* **128**, 87-94.
Baeg, G.-H., Selva, E. M., Goodman, R. M., Dasgupta, R. and Perrimon, N. (2004). The Wingless morphogen gradient is established by the cooperative action of Frizzled and Heparan Sulfate Proteoglycan receptors. *Dev. Biol.* **276**, 89-100.
Bischof, J., Maeda, R. K., Hediger, M., Karch, F. and Basler, K. (2007). An optimized transgenesis system for Drosophila using germ-line-specific phiC31 integrases. *Proc. Natl. Acad. Sci. U.S.A.* **104**, 3312-3317.
Bischof, J., Björklund, M., Furger, E., Schertel, C., Taipale, J. and Basler, K. (2013). A versatile platform for creating a comprehensive UAS-ORFeome library in Drosophila. *Development* **140**, 2434-2442.
Blauwkamp, T. A., Chang, M. V. and Cadigan, K. M. (2008). Novel TCF-binding sites specify transcriptional repression by Wnt signalling. *EMBO J.* **27**, 1436-1446.
Cadigan, K. M., Fish, M. P., Rulifson, E. J. and Nusse, R. (1998). Wingless repression of Drosophila frizzled 2 expression shapes the wingless morphogen gradient in the wing. *Cell* **93**, 767-777.
Chen, Y. and Struhl, G. (1996). Dual roles for patched in sequestering and transducing hedgehog. *Cell* **87**, 553-563.
Chen, C. M. and Struhl, G. (1999). Wingless transduction by the Frizzled and Frizzled2 proteins of Drosophila. *Development* **126**, 5441-5452.
Clevers, H. (2006). Wnt/β-catenin signaling in development and disease. *Cell* **127**, 469-480.
Dalessi, S., Neves, A. and Bergmann, S. (2012). Modeling morphogen gradient formation from arbitrary realistically shaped sources. *J. Theor. Biol.* **294**, 130-138.
Eldar, A. and Barkai, N. (2005). Interpreting clone-mediated perturbations of morphogen profiles. *Dev. Biol.* **278**, 203-207.
Entchev, E. V., Schwabedissen, A. and González-Gaitán, M. (2000). Gradient formation of the TGF-beta homolog Dpp. *Cell* **103**, 981-991.
Farhadifar, R., Roper, J.-C., Aigouy, B., Eaton, S. and Julicher, F. (2007). The influence of cell mechanics, cell-cell interactions, and proliferation on epithelial packing. *Curr. Biol.* **17**, 2095-2104.
Hao, H.-X., Xie, Y., Zhang, Y., Charlat, O., Oster, E., Avello, M., Lei, H., Mickanin, C., Liu, D., Ruffner, H. et al. (2012). ZNRF3 promotes Wnt receptor turnover in an R-spondin-sensitive manner. *Nature* **485**, 195-200.
Klein, D. E., Nappi, V. M., Reeves, G. T., Shvartsman, S. Y. and Lemmon, M. A. (2004). Argos inhibits epidermal growth factor receptor signalling by ligand sequestration. *Nature* **430**, 1040-1044.
Kofahl, B. and Wolf, J. (2010). Mathematical modelling of Wnt/β-catenin signalling. *Biochem. Soc. Trans.* **38**, 1281-1285.
Koo, B.-K., Spit, M., Jordens, I., Low, T. Y., Stange, D. E., van de Wetering, M., van Es, J. H., Mohammed, S., Heck, A. J. R., Maurice, M. M. et al. (2012). Tumour suppressor RNF43 is a stem-cell E3 ligase that induces endocytosis of Wnt receptors. *Nature* **488**, 665-669.
Marois, E., Mahmoud, A. and Eaton, S. (2006). The endocytic pathway and formation of the Wingless morphogen gradient. *Development* **133**, 307-317.
Mii, Y. and Taira, M. (2011). Secreted Wnt "inhibitors" are not just inhibitors: regulation of extracellular Wnt by secreted Frizzled-related proteins. *Dev. Growth Differ.* **53**, 911-923.
Mosimann, C., Hausmann, G. and Basler, K. (2009). [beta]-Catenin hits chromatin: regulation of Wnt target gene activation. *Nat. Rev. Mol. Cell Biol.* **10**, 276-286.
Nellen, D., Burke, R., Struhl, G. and Basler, K. (1996). Direct and long-range action of a DPP morphogen gradient. *Cell* **85**, 357-368.
Neumann, C. J. and Cohen, S. M. (1997). Long-range action of Wingless organizes the dorsal-ventral axis of the Drosophila wing. *Development* **124**, 871-880.
Pérez-Garijo, A., Shlevkov, E. and Morata, G. (2009). The role of Dpp and Wg in compensatory proliferation and in the formation of hyperplastic overgrowths caused by apoptotic cells in the Drosophila wing disc. *Development* **136**, 1169-1177.
Piddini, E. and Vincent, J.-P. (2009). Interpretation of the wingless gradient requires signaling-induced self-inhibition. *Cell* **136**, 296-307.
Piddini, E., Marshall, F., Dubois, L., Hirst, E. and Vincent, J.-P. (2005). Arrow (LRP6) and Frizzled2 cooperate to degrade Wingless in Drosophila imaginal discs. *Development* **132**, 5479-5489.
Pignoni, F. and Zipursky, S. L. (1997). Induction of Drosophila eye development by decapentaplegic. *Development* **124**, 271-278.
Ramis-Conde, I., Drasdo, D., Anderson, A. R. A. and Chaplain, M. A. J. (2008). Modeling the influence of the e-cadherin-β-catenin pathway in cancer cell invasion: a multiscale approach. *Biophys. J.* **95**, 155-165.
Rives, A. F., Rochlin, K. M., Wehrli, M., Schwartz, S. L. and DiNardo, S. (2006). Endocytic trafficking of Wingless and its receptors, Arrow and DFrizzled-2, in the Drosophila wing. *Dev. Biol.* **293**, 268-283.
Sato, A., Kojima, T., Ui-Tei, K., Miyata, Y. and Saigo, K. (1999). Dfrizzled-3, a new Drosophila Wnt receptor, acting as an attenuator of Wingless signaling in wingless hypomorphic mutants. *Development* **126**, 4421-4430.
Schwank, G., Dalessi, S., Yang, S.-F., Yagi, R., de Lachapelle, A. M., Affolter, M., Bergmann, S. and Basler, K. (2011). Formation of the long range Dpp morphogen gradient. *PLoS Biol.* **9**, e1001111.
Sick, S., Reinker, S., Timmer, J. and Schlake, T. (2006). WNT and DKK determine hair follicle spacing through a reaction-diffusion mechanism. *Science* **314**, 1447-1450.
Sivasankaran, R., Calleja, M., Morata, G. and Basler, K. (2000). The Wingless target gene Dfz3 encodes a new member of the Drosophila Frizzled family. *Mech. Dev.* **91**, 427-431.
Struhl, G., Fitzgerald, K. and Greenwald, I. (1993). Intrinsic activity of the lin-12 and Notch intracellular domains in vivo. *Cell* **74**, 331-345.
van de Wetering, M., Cavallo, R., Dooijes, D., van Beest, M., van Es, J., Loureiro, J., Ypma, A., Hursh, D., Jones, T., Bejsovec, A. et al. (1997). Armadillo coactivates transcription driven by the product of the Drosophila segment polarity gene dTCF. *Cell* **88**, 789-799.
van Leeuwen, I. M. M., Mirams, G. R., Walter, A., Fletcher, A., Murray, P., Osborne, J., Varma, S., Young, S. J., Cooper, J., Doyle, B. et al. (2009). An integrative computational model for intestinal tissue renewal. *Cell Prolif.* **42**, 617-636.
Wehrli, M., Dougan, S. T., Caldwell, K., O'Keefe, L., Schwartz, S., Vaizel-Ohayon, D., Schejter, E., Tomlinson, A. and DiNardo, S. (2000). arrow encodes an LDL-receptor-related protein essential for Wingless signalling. *Nature* **407**, 527-530.
Wu, C.-h. and Nusse, R. (2002). Ligand receptor interactions in the Wnt signaling pathway in Drosophila. *J. Biol. Chem.* **277**, 41762-41769.
Zecca, M., Basler, K. and Struhl, G. (1996). Direct and long-range action of a Wingless morphogen gradient. *Cell* **87**, 833-844.
Zhu, H. (2011). Spatiotemporally modulated Vestigial gradient by Wingless signaling adaptively regulates cell division for precise wing size control. *J. Theor. Biol.* **268**, 131-140.

Brief summaries, discussions and outlooks

WNT ligands control initiation and progression of human papilloma-virus-driven squamous cell carcinoma

Summary

Human papilloma virus (HPV)-driven cutaneous squamous cell carcinoma (cSCC) is the most common cancer in immunosuppressed patients. Despite indications suggesting that HPV promotes genomic instability during cSCC development, the molecular pathways underpinning HPV-driven cSCC development remain unknown. We compared the transcriptome of HPV-driven mouse cSCC with normal skin and observed higher amounts of transcripts for Porcupine and WNT ligands in cSCC, suggesting a role for WNT-signaling in cSCC progression. We confirmed increased Porcupine expression in human cSCC samples. Blocking the secretion of WNT-ligands by the Porcupine inhibitor LGK974 significantly diminished initiation and progression of HPV-driven cSCC. Administration of LGK974 to mice with established cSCC resulted in differentiation of cancer cells and significant reduction of the cancer stem cell compartment. Thus, WNT/β-catenin signaling is essential for HPV-driven cSCC initiation and progression as well as for maintaining the cancer stem cell niche. Interference with WNT-secretion may thus represent a promising approach for therapeutic intervention.

Outlook

These experiments in mouse models raise the question, if treating human SCC patients with Porcn inhibitors might be a suitable therapeutic approach. The fact, that Porcn is also upregulated in human tumors suggests that it could have clinical value. Another question remaining to be answered is, if Porcn levels/expression, have predictive value towards the aggressiveness of the cancer. Further experimental validation would be needed for Porcn

inhibitor treatments to be ready for clinical trials in SCC. An interesting line of future investigation is to test if one combines Wnt/β-catenin inhibitors together with the MAPK inhibitors. Are there synergies between the two? Furthermore, an alternative approach might be to apply the inhibitors directly into the tumor instead of giving them systemically. Thereby, much higher doses could be used, which might be able to kill an established tumor instead of just slowing its growth.

Further confirmation for the feasibility of such a therapy might be the use of human primary cSCC cell lines in combination with xeno-transplantation. This would enable us to check the ability of the inhibitor to block human tumor cell growth. In such cell lines, it might also be possible to use the Crispr/Cas9 technology to test some possible downstream effector candidates we retrieved from the RNA-sequencing experiment, such as Procr or Mmp13.

Pax6-dependent, but β-catenin-independent function of Bcl9 proteins in mouse lens development

Summary

Bcl9 and Bcl9l (Bcl9/9l) encode Wnt/β-catenin signaling components that mediate the interaction between β-catenin and Pygopus (Pygo) via two evolutionarily conserved domains, HD1 and HD2, respectively. We generated mouse strains lacking these domains to probe the β-catenin-dependent and β-catenin-independent roles of Bcl9/9l and Pygo during mouse development. While lens development is critically dependent on the presence of the HD1 domain, it is not affected by the lack of the HD2 domain, indicating that Bcl9/9l act in this context in a β-catenin-independent manner. Furthermore, we uncover a new regulatory circuit in which Pax6, the master regulator of eye development, directly activates Bcl9/9l transcription.

What this work neglected, was the cause of lethality in these embryos, which cannot be due to the observed eye defect and led to the next project vide infra.

Mutations in the Wnt/β-catenin cofactors *Bcl9* and *Pygo* Cause Congenital Heart Malformations

Summary

Congenital heart diseases (CHDs) cause life-threatening conditions that often cannot be resolved by surgical correction of the structural defects. Inspired by reports that mutations in the Wnt/β-catenin cofactors *BCL9* and *BCL9L* were associated with human CHDs, we sought to determine the role of these proteins in the onset of cardiac malformations. We show that mutations in *Bcl9*, *Bcl9l* and in the histone code-reader *Pygo* (a Bcl9-interacting protein), as well as abrogation of their interaction with β-catenin via small-domain deletion

induce dramatic heart malformations, from fish to mammals, that recapitulate human CHDs. We find that the Bcl9>Pygo complex transduces the Wnt/β-catenin-dependent transcription in cardiac neural crest and mesodermal heart progenitor cells, and lies upstream of heart-specific master genes, such as Prrx1 and Msx1. Collectively, our results indicate that Wnt/β-catenin orchestrates a heart-specific gene regulatory network, and implicate mutations in *BCL9* and *PYGO* as potentially causative in the formation of human CHDs.

Outlook

While the need for the "chain of adaptors" in heart development is clear, there are several indications that Bcl9/9l also has Pygo-independent functions. For instance, while Bcl9/9l KO animals die at around 10.5 dpc, Pygo1/2 KO mice survive until 13.5 dpc. Furthermore, we observe severe limb defects (missing digits) in Bcl9/9l$^{\Delta HD1/\Delta HD2}$ mice, which we never see in Pygo mutants. From this, we must conclude that Bcl9/9l may associate with another partner in certain circumstances. Certainly, the fact that the phenotypes occur upon deletions in the HD1 and HD2 domains suggests protein-protein interactions are needed and makes a case against a direct interaction of Bcl9 with the DNA. The existence of another partner of Bcl9/9l is further supported by findings from Andreas Moor and Claudio Cantu (personal communication), that the deletion of the HD1 domain in Bcl9/9l decreases the invasiveness of a mouse colon carcinoma model, while the deletion of Pygo1/2 has no influence on the tumors. Possible candidates for this alternate Bcl9 interaction partner are Tbx factors. Not only are they associated with the Di George syndrome, which is a human congenital disease reminiscent of our murine phenotype, but they are also crucial for limb development. These two properties would perfectly explain a role for them in facilitating β-catenin-Bcl9 dependent transcription in the heart and limbs. To confirm this theory, we plan to perform mass spectrometry on limb as well as colon carcinoma samples after an immunoprecipitation with Bcl9 as a bait.

Another interesting aspect of the limb defects we observed in the Bcl9 mutants was their resemblance to Hedgehog loss of function phenotypes, in fact, there is a report showing very similar heart phenotypes upon Hedgehog signaling disturbances (Washington Smoak et

al., 2005). It would be very interesting to check the interplay between Wnt and Hedgehog signaling in limb and heart development and to elucidate if Wnt signaling is upstream of Hedgehog signaling or if they merely have similar targets in this specific context.

A regulatory receptor network directs the range and output of the Wingless signal

Summary

The potent activity of Wnt/Wingless (Wg) signals necessitates sophisticated mechanisms that spatially and temporally regulate their distribution and range of action. The two main receptor components for Wg – Arrow (Arr) and Frizzled 2 (Fz2) – are transcriptionally downregulated by Wg signaling, thus forming gradients that oppose that of Wg. Here, we analyze the relevance of this transcriptional regulation for the formation of the Wg gradient in the *Drosophila* wing disc by combining *in vivo* receptor overexpression with an *in silico* model of Wg receptor interactions. Our experiments show that ubiquitous upregulation of Arr and Fz2 has no significant effects on Wg output, whereas clonal overexpression of these receptors leads to signaling discontinuities that have detrimental phenotypic consequences. These findings are supported by our *in silico* model for Wg diffusion and signal transduction, which suggests that abrupt changes in receptor levels causes discontinuities in Wg signaling. Furthermore, we identify a 200 bp regulatory element in the *arr* locus that can account for the Arr gradient, and we show that this is indirectly negatively controlled by Wg activity. Finally, we analyze the role of Frizzled 3 (Fz3) in this system and find that its expression, which is induced by Wg, contributes to the establishment of the Arr and Fz2 gradients through counteracting canonical signaling. Taken together, our results provide a model in which the regulatory network of Wg and the three receptor components account for the range and shape of this prototypical morphogen system.

Outlook

While in mammalian systems, the SFRPs have long been known as so-called decoy receptors, dampening signaling peaks, their existence in Drosophila was never shown. In this work, we showed that Fz3 might take up this function in the fly. Curiously, the loss of Fz3 has no apparent phenotype in *D. melanogaster*. Therefore, it would be interesting to test if its loss might make flies more prone to Wg induced tumor development.

A further unanswered question from this manuscript is, which transcription factors are responsible for the negative regulation of Arrow upon Wg-signaling. Since careful dissection

of the Arrow promoter and enhancer showed that Pangolin does not work as a repressor to achieve the described expression pattern, other factors need to be responsible. Since the exact DNA sequences where these factors bind are known, immunoprecipitation with this stretch of DNA as bait followed by mass spectrometry might yield interesting results.

Conclusion

N-terminal β-catenin interactors have been largely neglected in recent year's research due to the relatively weak phenotype in comparison to the full β-catenin KO in mammals. Further adding to the confusion is the fact, that while Bcl9 and Pygo do have an important function in Wnt/β-catenin signaling early in fly development, it is not known if they have other functions later in development, as well as if these functions might even be tissue specific during these later stages. This is quite in contrast to the mouse, where they have Wnt-signaling dependent and independent, tissue specific functions. With this work, we tried to clarify the role of these proteins as Wnt signaling effectors in the mammalian kingdom. Specifically, we wanted to answer the question, if these components are ever needed in mammalian development as a tripartite unit of Pygo, Bcl9 and β-catenin, as was described in the fly. The intriguing concept suggested by the data described in this thesis is that this is indeed the case, but in a very specific way. These proteins add an additional layer of tissue/cell specific transcriptional control, that has presumably the function to regulate the Wnt signal in a subset of cells. While most cells seem to be able to activate Wnt/β-catenin signaling without the need for the co-factors Bcl9 and Pygo, some cells undergoing EMT and interactions with different tissues need these factors. A next step should be to elucidate the mechanism why these cells need those co-factors, while other cells can activate the Wnt signal to sufficient levels without them. One possibility that comes to mind is, that it is just a problem of the level of activation, but our data indicate that this cannot be the only issue, since the downregulation of Wnt/β-catenin reporters upon loss of Pygo and Bcl9 is stronger specifically in the tissues where we also see a phenotype.

The discovery that co-factors for a general pathway act specifically in certain cell types is also of interest for the development of inhibitors (e.g. Sclerostin, (Appelman-Dijkstra and Papapoulos, 2016)) since one can inhibit the pathway in a specific set of cells without affecting the well-being of the whole organism.

In the case of Wnt signaling, inhibitors targeting tissue specific components might be a more efficient approach than targeting universal components, such as Porcn. To avoid lethality,

Porcn inhibitors are used at levels where the pathway is not completely abrogated. This seems to work well in certain cancers, but it stands to reason that where the normal cells find a way to survive the inhibition, cancer cells will find such a way as well at some point.

Appendix

β-catenin binding to either C- or N-terminal co-factors alone is sufficient to drive Wnt/β-catenin signaling in hair follicle regeneration

To investigate the specific transcriptional outputs of the different β-catenin interaction partners in the skin, we used β-catenin alleles where β-catenin binding to either the Bcl9/Pygo-axis or all C-terminal partners was abrogated. This was achieved by i) a point mutation at amino acid position 164 mutating a D to an A, thus abrogating β-catenin binding to Bcl9 (β-catenin^{D164A}) and ii) a deletion in the C-terminus of β-catenin abrogated binding from all the factors of the transcriptional machinery binding there (β-catenin$^{\Delta C}$). A combination of these two mutations was also generated, which abrogates all transcriptional output of β-catenin, while retaining the adherens junction function of β-catenin (β-catenin^{dm}) (Valenta et al., 2011).

By crossing these different β-catenin alleles to β-catenin^{flox} mice with a Keratin14^{CreERT} driver (active in keratinocytes mostly of the skin), we could study the effect of specifically abrogating the binding of β-catenin to its C- or N-terminal co-factors, as well as the contribution of transcription and adherens junction function of β-catenin in the epidermis of the skin. We could confirm that β-catenin's adherens junction function is negligible in the epidermis, as well as Wnt/β-catenin mediated transcription (Huelsken et al., 2001). This contrasts to the role of B-catenin in hair follicle regeneration. Upon loss of β-catenin, mice slowly started to lose hair, primarily at sites with high exposure to mechanical stress like the throat/belly and around the snout. Of note, they did not lose the complete hair coat, as would be expected from loss of Wnt/β-catenin signaling (Huelsken et al., 2001), what can be attributed to incomplete recombination, as was confirmed by staining for β-catenin in skin sections from such mice (Appendix Figure 4a). H+E sections revealed the loss of hair to be accompanied by thickening of the epidermis on the belly (Appendix Figure 1a) as well as a stark increase in size of sebaceous glands at the cost of hair follicles (Appendix Figure 1a, b).

These findings are in agreement with previous work where β-catenin was deleted in the skin (Huelsken et al., 2001)(Lim and Nusse, 2013).

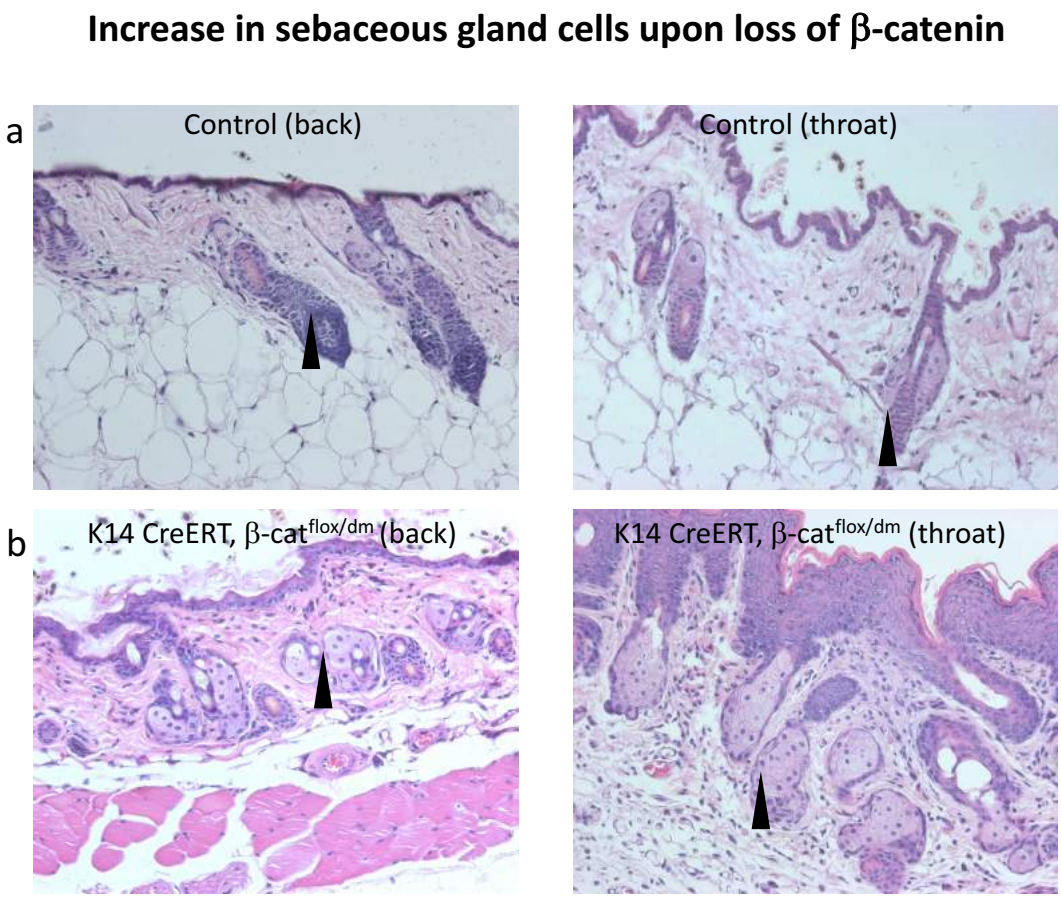

Appendix Figure 1: A) Hair follicles in anagen on the back skin of a mouse (left panel, arrow) and catagen (right panel, arrow) on the throat of a mouse. B) shows the increase in sebaceous gland cells (arrows) upon loss of β-cateninenin signaling function, as well as the thickening of the epidermis on the throat (right panel).

The abrogation of β-catenin's binding to N-terminal interaction partners had no discernible effect on the mice. The hair coat looked normal and also hair regeneration after plucking did not seem to be affected in our hands. This is contradictory to findings, where it was shown that loss of Pygo leads to a slowed down hair regeneration after plucking, which was attributed to canonical Wnt signaling (Sun et al., 2014). One explanation for the divergent results could be recombination issues, especially since we could also not reproduce the results from the mentioned paper with our Pygo mutants. A possible solution might be the use of a different Cre driver, or even the combination of two drivers.

Interestingly, also the loss of the C-terminal co-activators did not have dramatic effects. The mice still had a quite complete hair coat, only around the eyes was some bald skin observed. This was somewhat surprising because it was shown that in the gut, loss of C-terminal co-factors mimicked the complete loss of transcription (personal communication, Tomas Valenta). H+E staining on skin sections after hair plucking indicated a reduction in hair follicle numbers upon loss of C-terminal co-activators (Appendix Figure 2). To further investigate this, we used immunohistochemistry against β-catenin (antibody against β-catenin's C-term) to check recombination efficiency, which was around 60-80%. The incomplete recombination had the unintended advantage of giving us a nice tool to analyze and compare clones of cells with wild type β-catenin to β-catenin^{dm} or β-catenin$^{\Delta C}$ in the same mouse (Appendix Figure 4a, b). Loss of β-catenin N-terminal co-factors in the skin had no significant effect.

After anaphase induction, hair follicle regeneration is severely hampered upon β-catenin loss

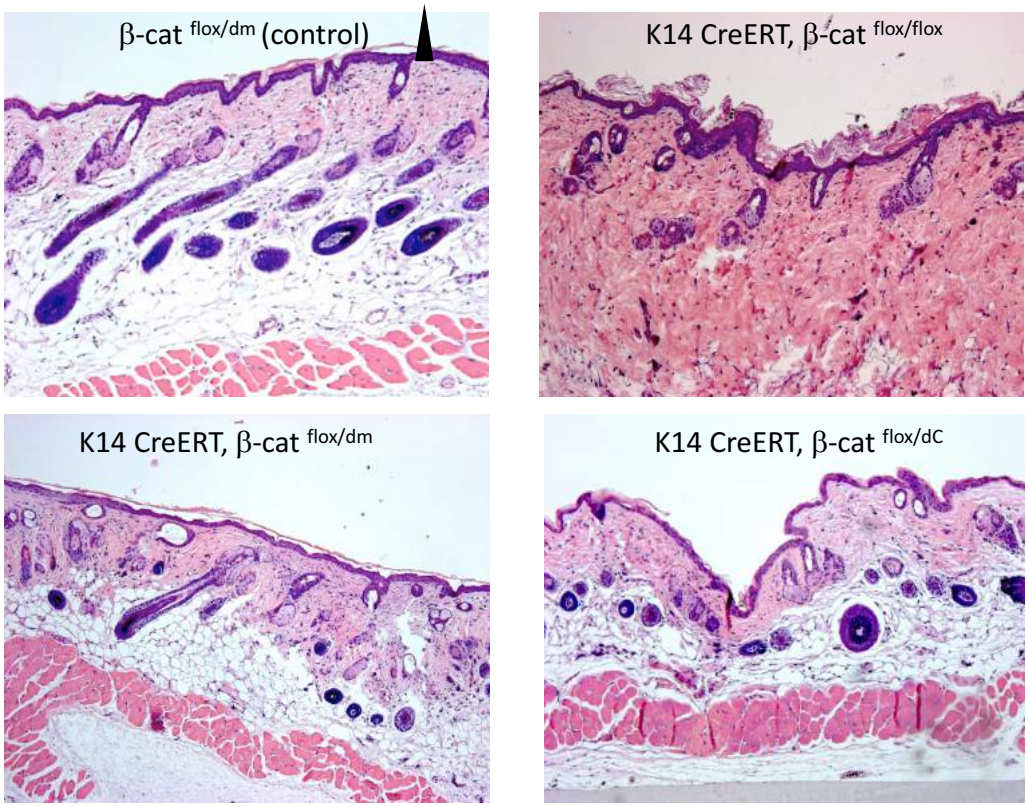

Appendix Figure 2: Stark reduction of hair follicle numbers in anagen upon total loss of β-cateninenin (upper right panel) or its signaling function (lower left panel) after hair plucking in comparison to a control (upper left panel, arrow). The loss of C-terminal binding partners (lower right panel) has a much weaker effect on the reduction of hair follicle numbers.

While we scored telogen stage hair follicles where only β-catenin^{dm}, but no wild type allele was expressed quite readily, we could never find such hair follicles in anagen stage, which is the proliferative phase (Appendix Figure 4a). These findings are in line with previous findings that Wnt/β-catenin signaling is essential for hair follicle stem cells and thus renewal of the hair cycle (Huelsken et al., 2001). Surprisingly though, we did find hair follicles in anagen, where only β-catenin^{DC} was expressed and even some where half the follicle was recombined while the other half was not (Appendix Figure 4a). These results suggest, that N-terminal β-catenin co-activators can be sufficient to carry out most functions of β-catenin mediated transcription in hair follicle regeneration. Interestingly, cells with a wild type allele of β-catenin also do not have a stark advantage in proliferation, since they seem not to be able to out-compete the mutated cells.

Since β-catenin^{DC} cells were also still able to induce strong expression of Lef1, which is a bona fide Wnt/β-catenin target gene in hair follicles, we can conclude that this isoform of β-catenin is indeed still able to activate Wnt/β-catenin signaling in this context (Appendix Figure 4b). A confirmation, that recombination issues were responsible for the only partial hair loss upon Tamoxifen administration to β-catenin$^{flox/flox}$ or β-catenin$^{dm/flox}$ mice, was the finding that upon Wls deletion (Bänziger et al., 2006), hair regeneration was completely abrogated (Appendix Figure 3).

Complete loss of hair follicles upon deletion of Wntless with an ubiquitous Cre driver

Control

Rosa26Cre, $Wls^{flox/flox}$

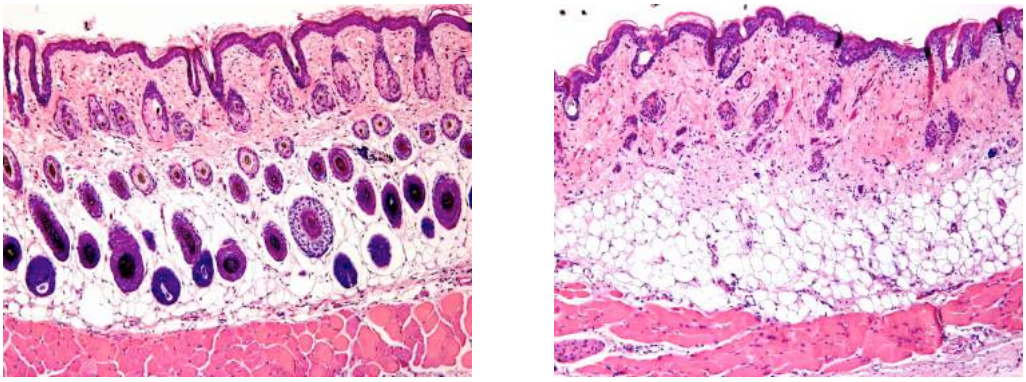

Appendix Figure 3: The left panel shows hair follicles in anagen induced by hair plucking, the right panel the same situation upon deletion of Wls and thus inhibition of Wnt signaling.

Hair regeneration is possible without C-terminal β-catenin co-activators

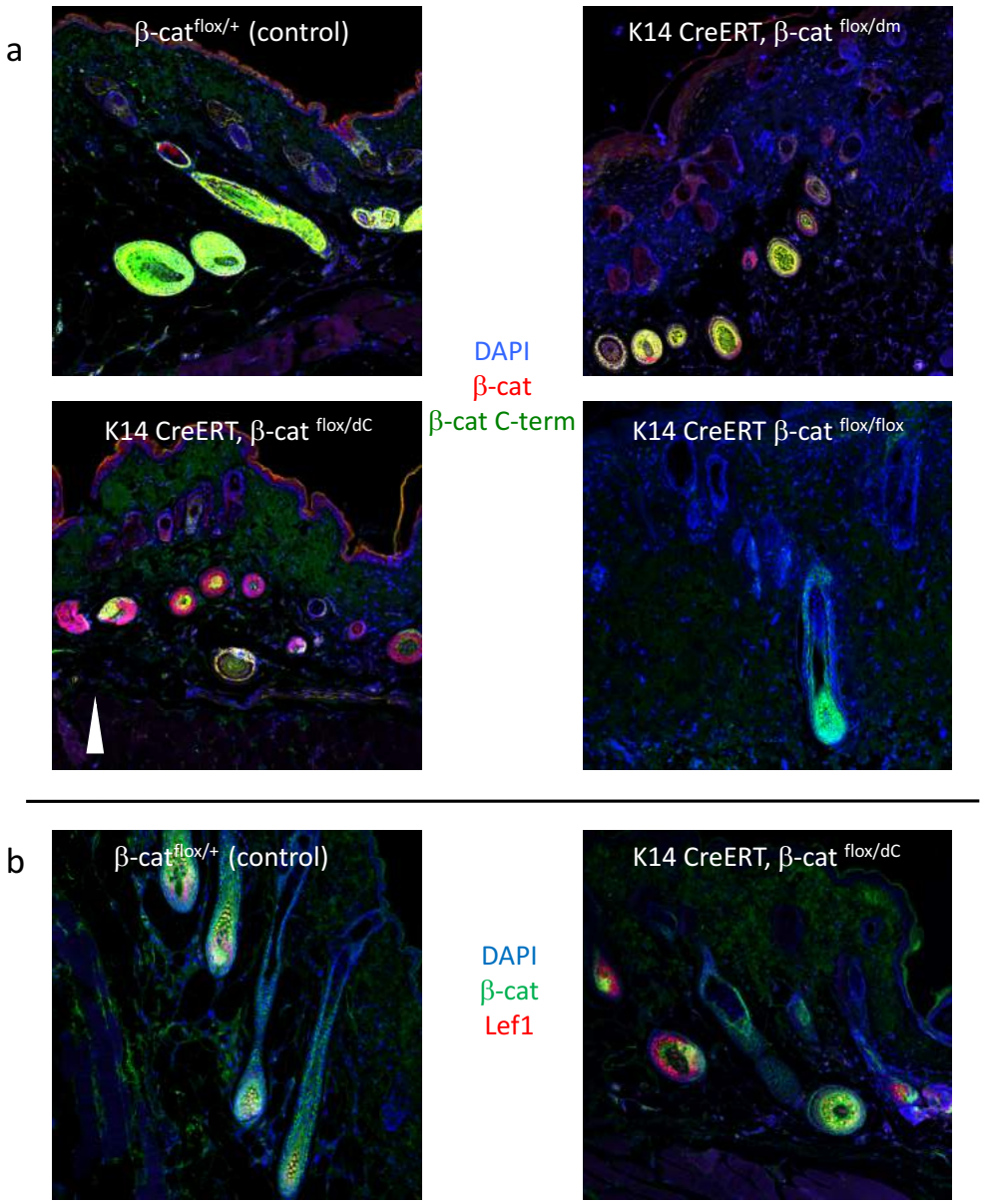

Appendix Figure 4: A) shows the incapability of hair follicles to enter anagen upon loss of β-cateninenin's signaling function (upper and lower right panels), the only hair follicles in anagen are those not recombined for β-cateninenin (green and red staining). The lower left panel shows that hair follicles, that only miss the C-terminus but still have the rest of β-cateninenin intact (red staining only) can survive. These cells are also not outcompeted by unrecombined cells since hair follicles consisting of red and green stained cells exist (arrow). B) shows that hair follicle cells without C-terminal β-cateninenin interactor binding can still express the Wnt-target gene Lef1.

β-catenin's signaling function is necessary for HPV-induced cSCC growth

Experiments with chemically induced cSCCs revealed the crucial role that β-catenin plays in the establishment of these tumors due to the necessity of Wnt/β-catenin signaling in cSCC CSCs (Malanchi et al., 2008).

What was largely neglected so far was the question, what specific outputs of β-catenin signaling was necessary for cSCC establishment and survival and if the adherens junction function of β-catenin plays any role in these tumors. Therefore, we used the above described alleles of β-catenin (Valenta et al., 2011), to shed light on the specific transcriptional changes, mediated by Wnt/β-catenin signaling, that ultimately block tumor growth.

To study this, we used a UV inducible K14-HPV8-E6 SCC tumor model (Marcuzzi et al., 2009), since tumor induction is much faster (around 2-3 weeks) in comparison to chemical induction. We crossed the mice harboring the K14-HPV8-E6 transgene to mice with an inducible skin driver (Keratin5-CrePR, inducible by a synthetic steroid) (Kasper et al., 2011) and crossed in the β-catenin alleles (flox, dm, ΔC and D164A).

Tumor induction after deletion of β-catenin or abrogating its transcriptional outputs (via β-catenin^{dm}) completely failed. This was somewhat surprising, since immunohistochemistry confirmed the incomplete β-catenin recombination (ca. 50%) we observed already in the experiments on hair follicles and skin (Appendix Figure 5a). This argues for the hypothesis, that in this cancer model, there might be a non-cell autonomous need for Wnt/β-catenin signaling or at least a crucial number of cells need to be able to transduce the Wnt/β-catenin signal. A ligand, important for tumor induction, might be needed to be secreted by most of the cells in high enough amounts, or the immune system recognizes recombined cells and then blocks tumor induction. These findings also suggest that tumor induction is most likely not from a single cell in this model, otherwise the non-recombined cells could still readily be tumorigenic.

We could also show that Sox9 as well as the MAPK cascade do not seem to be affected by this loss of Wnt signaling (Appendix Figure 5b, c). This is especially surprising in the case of

Sox9, since it was recently shown to be a Wnt target gene in Basal Cell Carcinoma (Larsimont et al., 2015).

The experiments using β-catenin alleles which lack the ability to bind C- or N-terminal co-factors are currently being analyzed.

cSCCs do not grow without β-catenin

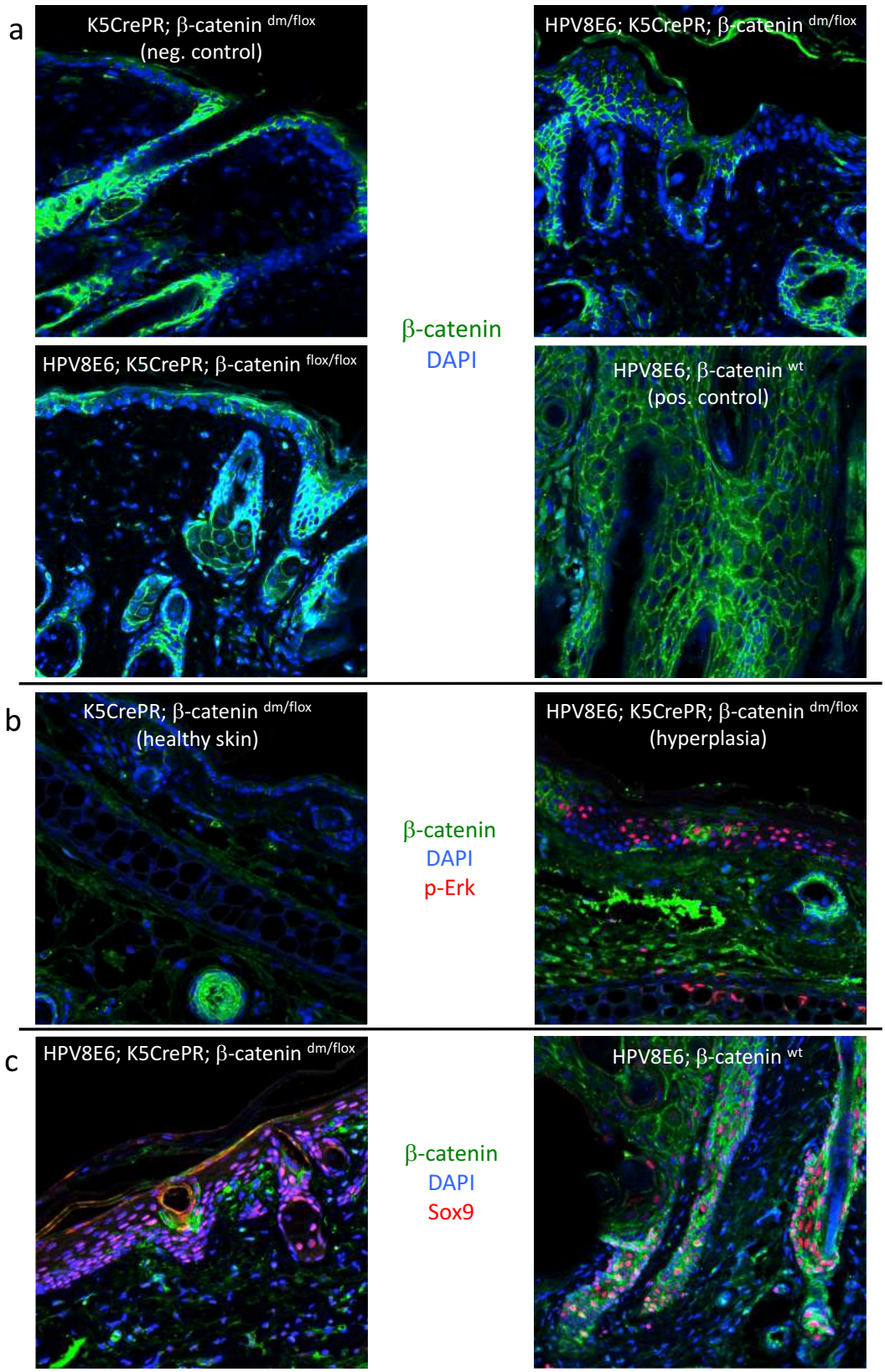

Appendix Figure 5: A) shows the inability of cSCCs to develop without β-cateninenin's signaling function. The lower right panel shows a tumor 3 weeks after UV-irradiation, the upper left panel shows skin from a mouse without the E6 transgene 3 weeks after UV-irradiation. The upper right panel shows that loss of β-cateninenin's signaling function still allows some hyperplasia of keratinocytes upon UV-irradiation, but no proper tumor growth. This despite the fact, that β-catenin recombination is incomplete (green staining). The same holds true for complete loss of β-catenin (lower left panel).

B) clarifies that the MAPK signaling cascade is still activated upon UV-irradiation in E6 positive mice (right panel), despite the absence of β-catenin signaling. This is not sufficient to allow tumor development.

C) Sox9 expression is not β-catenin in dependent (left panel).

Appendix Materials and Methods

Mice experimental procedures: Tumors were induced by UVA ($10\ \mathrm{J/cm^2}$) and UVB ($1.5\ \mathrm{J/cm^2}$) irradiation. The higher doses in comparison to the above described procedures was necessary because C57BL/6 mice were used instead of FVB mice. Genotyping was done with primers according to the Jackson lab and (Valenta et al., 2011).

Hair plucking to induce anagen was done by plucking hair in a $1\mathrm{cm^2}$ square with forceps under isoflurane anesthesia. Mice were sacrificed between 5 and 8 days after plucking.

Recombination of β-catenin alleles with the Keratin14 driver was induced by 10 times 2mg Tamoxifen applications intraperitoneal (Tamoxifen diluted in corn oil, volume of injection was 200ul).

The conditional Keratin5 driver was induced by intraperitoneal Ru486 injection (5 times 2mg).

Stainings were done as described in the included manuscripts.

Bibliography

Appelman-Dijkstra, N.M., and Papapoulos, S.E. (2016). Sclerostin Inhibition in the Management of Osteoporosis. Calcif. Tissue Int. *98*: 370–380.

Bänziger, C., Soldini, D., Schütt, C., Zipperlen, P., Hausmann, G., and Basler, K. (2006). Wntless, a Conserved Membrane Protein Dedicated to the Secretion of Wnt Proteins from Signaling Cells. Cell *125*: 509–522.

Cantù, C., Pagella, P., Shajiei, T.D., Zimmerli, D., Valenta, T., Hausmann, G., et al. (2017). A cytoplasmic role of Wnt/β-catenin transcriptional cofactors Bcl9, Bcl9l, and Pygopus in tooth enamel formation. Sci. Signal. *10*: eaah4598.

Cantù, C., Zimmerli, D., Hausmann, G., Valenta, T., Moor, A., Aguet, M., et al. (2014). Pax6-dependent, but β-catenin-independent, function of Bcl9 proteins in mouse lens development. Genes Dev. *28*: 1879–1884.

Deka, J., Wiedemann, N., Anderle, P., Murphy-Seiler, F., Bultinck, J., Eyckerman, S., et al. (2010). Bcl9/Bcl9l are critical for Wnt-mediated regulation of stem cell traits in colon epithelium and adenocarcinomas. Cancer Res. *70*: 6619–6628.

Herr, P., Hausmann, G., and Basler, K. (2012). WNT secretion and signalling in human disease. Trends Mol. Med. *18*: 483–493.

Huelsken, J., Vogel, R., Erdmann, B., Cotsarelis, G., and Birchmeier, W. (2001). beta-Catenin controls hair follicle morphogenesis and stem cell differentiation in the skin. Cell *105*: 533–545.

Kahn, M. (2014). Can we safely target the WNT pathway? Nat. Rev. Drug Discov. *13*: 513–532.

Kasper, M., Jaks, V., Are, A., Bergström, Å., Schwäger, A., Svärd, J., et al. (2011). Wounding enhances epidermal tumorigenesis by recruiting hair follicle keratinocytes. Proc. Natl. Acad. Sci. U. S. A. *108*: 4099–4104.

Kramps, T., Peter, O., Brunner, E., Nellen, D., Froesch, B., Chatterjee, S., et al. (2002). Wnt/wingless signaling requires BCL9/legless-mediated recruitment of pygopus to the nuclear beta-catenin-TCF complex. Cell *109*: 47–60.

Larsimont, J.-C., Youssef, K.K., Sánchez-Danés, A., Sukumaran, V., Defrance, M., Delatte, B., et al. (2015). Sox9 Controls Self-Renewal of Oncogene Targeted Cells and Links Tumor Initiation and Invasion. Cell Stem Cell *17*: 60–73.

Lim, X., and Nusse, R. (2013). Wnt Signaling in Skin Development, Homeostasis, and Disease. Cold Spring Harb. Perspect. Biol. *5*: a008029–a008029.

Malanchi, I., Peinado, H., Kassen, D., Hussenet, T., Metzger, D., Chambon, P., et al. (2008). Cutaneous cancer stem cell maintenance is dependent on beta-catenin signalling. Nature *452*: 650–653.

Marcuzzi, G.P., Hufbauer, M., Kasper, H.U., Weissenborn, S.J., Smola, S., and Pfister, H. (2009). Spontaneous tumour development in human papillomavirus type 8 E6 transgenic mice and rapid induction by UV-light exposure and wounding. J. Gen. Virol. *90*: 2855–2864.

Moor, A.E., Anderle, P., Cantù, C., Rodriguez, P., Wiedemann, N., Baruthio, F., et al. (2015). BCL9/9L-β-catenin Signaling is Associated With Poor Outcome in Colorectal Cancer. EBioMedicine *2*: 1932–1943.

Schilling, S., Steiner, S., Zimmerli, D., and Basler, K. (2014). A regulatory receptor network directs the range and output of the Wingless signal. Development *141*: 2483–2493.

Sun, P., Watanabe, K., Fallahi, M., Lee, B., Afetian, M.E., Rheaume, C., et al. (2014). Pygo2 regulates -catenin-induced activation of hair follicle stem/progenitor cells and skin hyperplasia. Proc. Natl. Acad. Sci. *111*: 10215–10220.

Valenta, T., Gay, M., Steiner, S., Draganova, K., Zemke, M., Hoffmans, R., et al. (2011). Probing transcription-specific outputs of -catenin in vivo. Genes Dev. *25*: 2631–2643.

Valenta, T., Hausmann, G., and Basler, K. (2012). The many faces and functions of β-catenin. EMBO J. *31*: 2714–2736.

Washington Smoak, I., Byrd, N.A., Abu-Issa, R., Goddeeris, M.M., Anderson, R., Morris, J., et al. (2005). Sonic hedgehog is required for cardiac outflow tract and neural crest cell development. Dev. Biol. *283*: 357–372.

Zimmerli, D., Hausmann, G., Cantu, C., and Basler, K. (2017). Pharmacological interventions in the Wnt pathway: inhibition of Wnt secretion versus disrupting the protein-protein interfaces of nuclear factors: Inhibition of the Wnt pathway. Br. J. Pharmacol.

Acknowledgments

First of all, I want to thank Konrad Basler for giving me the opportunity to work in his lab. I had a fantastic time in a very inspiring atmosphere with great people and scientists. Furthermore, It was a pleasure to work with him, especially due to his uncanny ability to always immediately spot any weak point in a story, but also for his unending curiosity and excitement about research data, even when I myself was rather depressed about an experimental outcome.

I also want to thank Sarah Steiner for teaching me how to do science, when I was her master student.

Furthermore, I want to thank Claudio Cantu for teaching me the trade of mouse genetics and honing my edge in critical thinking in countless discussions about science and other matters, apart from just being a great person to work and drink beer with.

I also want to thank George Hausmann for always having time to discuss scientific results and problems, as well as trying to teach me how to write a decent scientific text with unending patience. Luckily, his efforts to introduce me into the art of bouldering were slightly more successful.

I want to thank Tomas Valenta and Virginia Cecconi for being great collaborators and colleagues, always ready with good advice.

My thanks also go to Maries van den Broek for profound scientific advice and valuable suggestions during countless meetings (and committee meetings), besides her invaluable help with the whole SCC project in general.

Additionally, I want to thank Sabine Werner for valuable inputs and ideas during my committee meetings.

Thanks go also to Christian Mosimann and Anastasia Felker for a very fruitful collaboration in heart development.

Then I want to thank all the people in the lab for creating such a brilliant atmosphere and generally being great friends and colleagues. I specifically have to mention Janine Toggweiler on this instance for on the one hand helping to organize the skiing weekend, as

well as never giving up eating her delicious pastries in the lab despite my countless admonitions. This had the very desirable side effect of me getting pastries as well as a bribe. Special laudation should also go to Nick Doumpas for recognizing my ingenuity in opening boxes.

I further am deeply grateful to Sarah Wyck for just always being there when I needed someone for whatever (even scientific!) reason, besides her of course being the greatest person I ever met (although even she failed at teaching me how to properly fold clothes).

Then I want to thank my family for their unending support of my studies, even though they turned out to take a little bit longer.

Finally I want to thank my friends for always being up to join for the one or other adventure or just having a nice time, thereby never forgetting to remind me that I apparently still have not worked properly for a second in my whole life.